NASA Contractor Report 182105
MTI 87TR72

Advanced Helium Purge Seals for Liquid Oxygen (LOX) Turbopumps

W. Shapiro and C. C. Lee
Mechanical Technology Incorporated
Latham, New York

March 1989

Prepared for
Lewis Research Center
Under Contract NAS3-24645

National Aeronautics and
Space Administration

1. Report No.	2. Government Accession No.	3. Recipient's Catalog No.
NASA CR-182105		

4. Title and Subtitle
Advanced Helium Purge Seals for Liquid Oxygen (LOX) Turbopumps

5. Report Date
17 March 1989

6. Performing Organization Code

7. Author(s)
Wilbur Shapiro
Dr. Chester Lee

8. Performing Organization Report No.
87TR72

10. Work Unit No.

9. Performing Organization Name and Address
Mechanical Technology Incorporated
Research and Development Division
968 Albany-Shaker Road
Latham, New York 12110

11. Contract or Grant No.
NAS3-24645

13. Type of Report and Period Covered
Final - 9/85 through 8/87

12. Sponsoring Agency Name and Address
National Aeronautics and Space Administration
Lewis Research Center
Cleveland, OH 44135

14. Sponsoring Agency Code

15. Supplementary Notes
Project Manager: J.A. Hemminger
NASA Lewis Research Center
Cleveland, OH 44135

16. Abstract

Program objectives were to determine three advanced configurations of helium buffer seals capable of providing improved performance in a space shuttle main engine (SSME), high-pressure liquid oxygen (LOX) turbopump environment, and to provide NASA with the analytical tools to determine performance of a variety of seal configurations.

The three seal designs included solid-ring fluid-film seals often referred to as floating ring seals, back-to-back fluid-film face seals, and a circumferential sectored seal that incorporated inherent clearance adjustment capabilities. Of the three seals designed, the sectored seal is favored because the self-adjusting clearance features accommodate the variations in clearance that will occur because of thermal and centrifugal distortions without compromising performance. Moreover, leakage can be contained well below the maximum target values; minimizing leakage is important on the SSME since helium is provided by an external tank. A reduction in tank size translates to an increase in payload that can be carried on board the shuttle.

The computer codes supplied under this program included a code for analyzing a variety of gas-lubricated, floating ring, and sector seals; a code for analyzing gas-lubricated face seals; a code for optimizing and analyzing gas-lubricated spiral-groove face seals; and a code for determining fluid-film face seal response to runner excitations in as many as five degrees of freedom. These codes proved invaluable for optimizing designs and estimating final performance of the seals described in this report.

17. Key Words (Suggested by Author(s))	18. Distribution Statement
Rotating Shaft Seals Fluid-Film Seals Sectored Seals Ring Seals Helium Buffer Seals Face Seals LOX Turbopumps	Unclassified - Unlimited

19. Security Classif. (of this report)	20. Security Classif. (of this page)	21. No. of Pages	22. Price*
Unclassified	Unclassified	182	

* For sale by the National Technical Information Service, Springfield, Virginia 22151

MTI-17983

NASA-C-168 (Rev. 6-71)

TABLE OF CONTENTS

TABLE OF CONTENTS (Continued)

LIST OF FIGURES

LIST OF FIGURES (Continued)

LIST OF FIGURES (Continued)

LIST OF TABLES

NOMENCLATURE

A_a	Ambient pressure area
A_s	Supply pressure area
AT	Axial taper ring seal
AS	Axial step ring seal
RS	Rayleigh-step ring seal or radial step face seal
C	Reference clearance (concentric radial clearance)
CT	Taper or step clearance
d_o	Orifice diameter
D	Diameter
e	Shaft displacement from concentric position
EY	Eccentricity ratio in y direction
EX	Eccentricity ratio in x direction
ES	Vibration amplitude of shaft
F_f	Viscous friction force
F_a	Total applied force to sector
F_{ax}	Axial film force
F_c	Hydraulic closing force
F_p	Closing spring preload
F_r	Coulomb friction force
F_R	Radial film force
GANGLE	Groove angle, spiral groove seal
GD	Groove depth, spiral groove seal
h	Local film thickness
h_m	Minimum film thickness
k_f	Fluid film stiffness
k_s	Closing spring stiffness
K_{xx}	Direct concentric stiffness
K_{xy}	Cross coupled concentric stiffness
L	Length
LT	Taper or step length
N	Rotating speed
p	Pressure
P_a	Ambient Pressure
P_{fr}	Face seal (secondary seal) recess pressure
P_{CR}	Critical pressure ratio

NOMENCLATURE (Continued)

P_R	Orifice downstream pressure
P_S	Helium buffer pressure
q	Mass Flow
R	Journal radius
R_i	Inside radius of spiral groove seal
R_m	Dam radius of spiral groove seal
R_o	Outside radius of spiral groove seal
RT	Radial taper face seal
SE	Self-energized hydrostatic seal
t	Time
T	Temperature
W_s	Sector weight
Wl	OD width of sector
x	Shaft displacement
x_o	Amplitude of sector radial displacement
x_s	Sector displacement
X-DISP	x displacement of face seal shaft
X-FRICT	Face seal friction force in x direction
XX-DISP	Angular displacement of face seal shaft about x-axis
XX-FRICT	Face seal friction moment about x-axis
XS-DISP	x displacement of face seal ring
XXS-DISP	Angular displacement of face seal ring about x-axis
Y-DISP	y displacement of face seal shaft
Y-FRICT	Face seal friction force in y direction
YY-DISP	Angular displacement of face seal shaft about y-axis
YY-FRICT	Face seal friction moment about y-axis
YS-DISP	y displacement of face seal ring
YYS-DISP	Angular displacement of face seal ring about y-axis
z	Axial direction coordinate
Z_{cg}	Axial distance from origin to center of gravity of face seal ring
Z_{sc}	Axial distance from origin to secondary seal of face seal ring

NOMENCLATURE (Continued)

Z_{sp}	Axial distance from origin to closing spring of face seal ring
Z-DISP	z displacement of face seal shaft
Z-FRICT	Face seal friction force in z direction
ZS-DISP	z displacement of face seal ring
δ_a	Axial displacement of face seal
ε	Dimensionless shaft displacement (eccentricity ratio) = e/C
εx	Dimensionless x displacement = x/C
εy	Dimensionless y displacement = y/C
μ	Absolute viscosity

1.0 SUMMARY

The program described in this report concerns advanced development of helium buffer seals that are used in liquid oxygen (LOX) pumps of the space shuttle main engine (SSME). The objectives of the program were to provide computer codes to NASA for analyzing a wide variety of seal types and to consummate the design of three different advanced configurations.

The three seal designs completed included solid-ring fluid-film seals often referred to as floating-ring seals, back-to-back fluid-film face seals, and a circumferential sectored seal that incorporated inherent clearance adjustment capabilities. Of the three seals designed, the sectored seal is favored because the self-adjusting clearance features accommodate the variations in clearance that will occur because of thermal and centrifugal distortions without compromising performance. Moreover, leakage can be contained well below the maximum target values; minimizing leakage is important on the SSME since helium is provided by an external tank. A reduction in tank size translates to an increase in payload that can be carried on board the shuttle.

Performance of solid-ring seals are very sensitive to clearance variations, which are difficult to control or accurately predict. Studies indicated that face seals are subjected to detrimental thermal distortions because of the high thermal gradient across the hydrogen side ring, which would obviate their use in the present SSME environment. The face seals would be excellent candidates for LOX turbopumps that are not subject to the high thermal gradients occurring in the present SSME.

The computer codes supplied under this program included a code for analyzing a variety of gas-lubricated, floating-ring, and sector seals; a code for analyzing gas-lubricated face seals; a code for optimizing and analyzing gas-lubricated spiral-groove face seals; and a code for determining fluid-film face seal response to runner excitations in as many as five degrees of freedom. These codes proved invaluable for optimizing designs and estimating final performance of the seals described in this report.

2.0 INTRODUCTION

Helium buffer seals are used on high-pressure LOX turbopumps to separate the hydrogen-enriched steam used to drive the turbine from the oxygen liquid being pumped. Low helium leakage is desirable to reduce the amount of storable helium required and, thus, enable greater space vehicle payload. Mechanical Technology Incorporated (MTI) previously conducted a combined design and test program of helium buffer seals of a configuration designated by NASA [1]*. The prior program (Contract NAS3-23260) concentrated on back-to-back floating-ring seals with a Rayleigh-step hydrodynamic geometry on the inside diameter of the rings.

The program described in this report was a continuation of the original effort with the following objectives:

1. Extend the capability for analyzing seal performance to a wide variety of hydrodynamic/hydrostatic configurations and provide this capability to NASA in the form of computer codes

2. Complete analysis and design of three different purge seal configurations that show promise for significantly reduced leakage and improved dynamic and structural response in the SSME LOX turbopump environment.

Typical operating conditions and general requirements for the SSME purge seals are [2,3]:

- Shaft diameter at seal location: 68 mm (2.68 in.)
- Shaft speed: 2000 to 3400 rad/sec (19,000 to 32,500 rpm)
- Cryogen temperature: 0 to -60°C (32 to -76°F)
- Steam temperature: 60 to 250°C (140 to 482°F)
- Helium temperature: 0 to 50°C (32 to 122°F)
- Helium pressure: 240 to 700 kPa (35 to 102 psig)
- Oxygen side pressure: 0 to 345 kPa (0 to 50 psig)
- Steam side pressure: 0 to 345 kPa (0 to 50 psig)
- Vibration amplitude (peak to peak): 0.0137 mm (0.0005 in.)
- Vibration frequency: synchronous
- Maximum helium leakage: 0.0039 kg/s (0.0086 lb/sec)
- Operating life: 10 hr
- Number of starts: 130.

Note the wide temperature fluctuations on the cryogen and steam sides of the buffer seal.

The accomplishments of this program included:

1. Analysis and design of a sectored floating-ring seal with self-adjusting clearance capability to maintain a small operating clearance over a wide range of centrifugal and thermal distortions.

*Numbers in brackets indicate references, which can be found in Section 8.0.

2. Examination of various configurations of opposed ring seals and selection of a self-energized hydrostatic ring seal that was subjected to detail analysis and design.

3. Examination of various configurations of opposed face seals and selection of a self-energized hydrostatic face seal that was subjected to detail analysis and design.

4. Supplying computer codes for determining steady-state and dynamic response of a wide variety of seal configurations. The codes supplied are identified as follows:

   a. GJOURN - Produces steady-state performance of cylindrical gas seal configurations

   b. GFACE - Produces steady-state performance of gas-lubricated face seal configurations

   c. FACEDY - Determines dynamic response of gas-lubricated face seals

   d. SPIRALP - Determines optimum geometric parameters and steady-state performance of gas-lubricated spiral-groove face seals.

Further descriptions of these programs are provided in Section 7.0 of this report.

3.0 SIGNIFICANT RESULTS AND CONCLUSIONS

Comparative performance of the various purge seal designs is shown in Table 3-1.* MTI favors the sectored seal for the following reasons.

- The seal satisfies the targeted leakage values with a significant margin. The flow is a factor of 4 less than specified.
- The seal sectors will dynamically track rotor excursions without difficulty.
- Although complex, the sectored seal incorporates the capability of operating with low film thickness and, thus, low leakage over a wide range of operating conditions.
- The adjustable clearance capabilities of the sectored seal provides an excellent safety margin against potentially hazardous rubs.
- The sectored seal represents a significant advancement in the state of the art of fluid-film seal technology, but there are risks associated with it. For example, hydrostatic lift-off is required to overcome a reasonably heavy preload of the secondary seal. Also, joint sealing may pose unforeseen problems. It is therefore recommended that a static test rig be constructed to check out a complete seal or individual sectors before the seal is exposed to high-speed rotation. The static test rig will facilitate observing seal behavior much more readily than a dynamic rig and can be used to correct any problems that may have been overlooked. The chances are very good that successful static operation will result in successful dynamic operation.

Of the various ring seals (nonsectored) examined, the self-energized hydrostatic ring seal was best. It has significantly greater stiffness than the other types with little compromise in flow and power loss.

- To provide proper operating clearances in the present SSME environment, the ring seals must be installed with very tight clearances. This imposes difficult manufacturing requirements on the ID of the seal rings and the OD of the mating sleeve. Satisfactory performance would occur even if the rings were installed line to line without clearance. Thus, it might be appropriate to match set the rings and sleeve and use the sleeve itself to obtain the final bore dimensions of the rings.

Of the face seals examined, the self-energized hydrostatic face seal was chosen because it has slightly better leakage and stiffness characteristics than the spiral-groove seal has.

- Thermoelastic studies indicate that excessive and detrimental distortions will occur in the hydrogen side face seal ring when exposed to the high-temperature differentials that presently exist in the SSME oxidizer pump. A divergent clearance distribution in the direction of flow is produced to a degree that would incapacitate operation. The

*Tables and figures are located at the end of each section.

problem is due to the very large temperature gradient that occurs across the seal ring 239°C (430°F). If this high-temperature gradient could be eliminated in future pumps, the face seals become attractive candidates.

For each of the types of seals examined, the helium buffer pressure is 1379 kPa (200 psig), which is higher than on the present SSME. The pressure is necessary to activate the hydrostatic features of the seal with adequate stiffness. It is noted that even for the higher supply pressure requirements, the total flow of the seal configurations is less than targeted values.

The computer codes provided to NASA under this program proved invaluable as screening tools and for determining final geometry and performance of the various types of seals considered.

TABLE 3-1

COMPARATIVE PURGE SEAL PERFORMANCE

	Sectored	Ring	Face
Minimum Film Thickness, mm (in.)	0.0241 (0.0009)	0.0145 (0.0006)	0.0141 (0.0006)
Total Leakage, kg/s (lb/sec)	0.0011 (0.0024)	0.0028 (0.0062)	0.0014 (0.0031)
Power Loss, W (hp)	81 (0.109)	56 (0.075)	260 (0.349)
Buffer Gas Supply Pressure, kPa (psig)	1379 (200)	1379 (200)	1379 (200)
Ambient Pressure, kPa (psig)	0 0	0 0	0 0

4.0 ANALYSIS AND DESIGN OF THE SECTORED, FLOATING-RING SEAL

Floating-ring seals are commonly employed as helium purge seals with two opposite rings, one sealing against the cryogen and the other sealing against the steam. The buffer fluid is introduced between the rings. Design and testing of advanced solid-ring configurations are described in References [1,4,5]. There are several problem areas associated with solid-ring seal geometries.

1. For a solid ring, large variations in clearance will occur because of centrifugal growths and thermal distortions. Since flow is proportional to approximately the third power of clearance, large flow variations will result. Uncertainties in predicting operating conditions generally lead to high clearance designs with high leakage.

2. The film capacity of the seal should be sufficient to overcome the wall friction between the seal ring and stationary housing to allow the rings to track shaft excursions.

3. Mass and inertia properties of the seal ring should be such to prevent against excessive vibrations of the rings induced by shaft excursions transmitted through the fluid film.

A design that incorporates a self-adjusting clearance that can accommodate thermal and centrifugal distortions and shaft dynamic excursions avoids many of the problems associated with captured clearance designs. The sectored ring seal design provides the desired self-adjusting clearance features.

4.1 Sectored Seal Configuration

The general configuration of the sectored seal is shown in Figure 4-1. The sectors consist of T-shaped sections mated to each other at each end with sealed joints. The sectors can move relative to one another circumferentially, and that is the way the seal accommodates variations in the sleeve dimensions due to thermal expansions and contractions and centrifugal growths. The T-shaped sector was chosen because it is a symmetrical shape and the various fluid and friction forces can be designed to avoid upsetting moments on the individual sectors. An overlapping V joint prevents a direct clearance path between the hydrogen and oxygen ends of the seal. Each sector is supported by a hydrostatic fluid film on its inner circumference and along the sidewalls, forming a friction-free secondary seal to permit free movement of the sectors in response to sleeve movements. The fluid films are predominantly hydrostatic to avoid any pitching tendencies introduced by hydrodynamic effects. The hydrostatic bearings are fed by the buffer pressure on the outside diameter of the seal. Figure 4-2 shows the pressure distribution and force balance on the individual sectors.

4.2 Analytical Approach

Conventional steady-state gas bearing theory was applied to perform the fluid-film analysis, utilizing Newton-Raphson iteration in conjunction with the column method. This approach was used in the programs GJOURN and GFACE, which analyzed the cylindrical primary seal and secondary face seals, respectively. Similar analysis was applied except that for the radial secondary seals polar coordinates were used in lieu of cylindrical coordinates.

Figure 4-3 shows the joint configuration for both the ID joint and the radial joint. The ID joint is exposed mostly to ambient pressure along its length, which was the analytical boundary condition assumed. For the radial joint, the top half is at maximum pressure while the bottom half circuits to the low-pressure ambient, which was the assumed analytical boundary condition.

Inherent compensation was selected for the circumferential element to avoid pneumatic hammer and limit flow. Inherent compensation occurs when the flow through the orifice discharges directly into the film rather than into a recess. The restrictor area is considered to be the curtain area of the orifice hole in the clearance space and is equal to πdh, where d is the orifice diameter and h is the film thickness. Inherent compensation provides improved stability characeristics over straight orifice compensation for which the restrictor area is independent of film thickness. A central row of holes is drilled through the ID. To avoid analytical problems with source points, each feed orifice was transferred to a line source with a length equal to one circumferential element and an area equal to the hole area. A subsequent source correction factor was applied to correct for the line source assumption. The higher the correction factor, the closer the discrete source points approximated the line source assumed. A correction factor of 70% and above was considered satisfactory. The theoretical basis for the line source correction is included in the GJOURN documentation [7,8].

4.3 Analysis and Performance of Primary Seal

The radial force applied to the sector is the buffer fluid pressure multiplied by the surface area of the outer periphery of the sector plus the ambient pressure multiplied by the radial area to which it is exposed. Radial load increases with ambient pressure. This applied force must be balanced by the fluid-film force on the ID of the sector. The parameters that are used to adjust the applied force are the width and diameter of the sector, both of which are constrained by the available envelope. A radial displacement of a sector will cause a variation in the fluid-film force until equilibrium is achieved with the applied force. The primary circumferential seal consists of three sectors with inherently compensated feeding holes. Principal dimensions and operating conditions are identified in Table 4-1.

Several factors were considered for selecting the number of orifices and the hole size. These were:

1. Maintain a 70% line source correction factor
2. Ensure that the hole size is large enough to prevent clogging
3. Obtain sufficient fluid-film stiffness to ensure against a lockup condition.

Lockup occurs when the downstream orifice pressure approaches the supply pressure and the fluid-film stiffness reverses and goes negative. Three sectors were selected, and six feed holes of 0.381 mm (0.015 in.) in diameter were incorporated into each sector. The computed source correction factor was 70%.

Figure 4-4 shows sector forces versus the nondimensional displacement of the sector from the concentric position for two ambient pressures at the axial boundaries of the seal. The helium supply pressure was 690 kPa (100 psig), the radial clearance of the seal was 0.03175 mm (0.00125 in.), and the outer

seal width, W1, was 12.7 mm (0.5 in). The equilibrium positions of the sector are indicated by the intersection of the applied load line and the fluid-film force curves. At the high ambient pressure condition, the film force response curve is quite flat, indicative of poor stiffness characteristics. At the high ambient pressure, the sector displacement is large enough to increase the downstream orifice pressure near the point of lockup. Attempts to vary clearance did not alleviate the situation because the hole size became too small, leakage too large, or the stiffness deteriorated further.

An increase in gas supply pressure to 1379 kPa (200 psig) produced acceptable performance. Figure 4-5 shows results for a reduced radial clearance of 0.0254 mm (0.001 in.), which provided performance superior to the original 0.03175 mm (0.00125 in.) clearance. For both ambient pressure conditions, the slope of the curves is greater than for the lower supply pressure condition, indicating greater stiffness. Higher stiffness reduces sector displacements and provides reduced pressure ratios of orifice downstream/supply pressure, thus providing greater insurance against lockup. The maximum nondimensional displacement is slightly greater than 0.3.

Figure 4-6 shows sector radial stiffness versus displacement for the two ambient pressure conditions. The superimposed dashed line is the predicted operating position, which varies with the ambient pressure. For the high ambient pressure condition, the slope of the stiffness curve becomes negative for the higher values of displacement and, although the stiffness still remains positive, a negative slope is approaching the lockup condition and should be avoided. The stiffness at 0 ambient pressure is approximately 34×10^6 N/m (19.4×10^4 lb/in.) and reduces to 30.5×10^6 N/m (17.4×10^4 lb/in.) at the 345-kPa (50-psig) ambient condition.

Total primary seal leakage as a function of sector displacement is shown in Figure 4-7. The higher displacement and lower pressure drop at the high ambient condition results in lower flow than for 0 ambient pressure. The flow through the circumferential seal is 0.0006 kg/sec (0.00132 lb/sec) at 0 ambient and 0.00038 kg/sec (0.00084 lb/sec) at 345-Pa (50-psig) ambient pressure.

Pressure ratio as a function of sector displacement is shown in Figure 4-8. The pressure ratio is the pressure downstream of the orifice divided by the supply pressure. Choking will occur if this ratio is below a value of 0.497. Through the operating range, the ratio is above that value so that choking is not anticipated across the orifice restriction.

Power loss is indicated in Figure 4-9. It is a function of rotating speed, viscosity, and displacement. Since displacements vary as ambient pressure, the power loss will vary as ambient pressure. For an ambient pressure of 0 kPa, the power loss is 81 W (0.11 hp), and for an ambient pressure of 345 kPa (50 psig), the power loss is approximately 99 W (0.13 hp).

4.4 Analysis and Performance of Secondary Seal

The secondary seal is a hydrostatic thrust face seal that is spring loaded against the T-shaped seal rings, as shown in Figures 4-1 and 4-2.

Several configurations were explored, and the configuration selected consisted of a recess in each sector fed by a single orifice. Since the thrust

faces do not rotate relative to one another, very small clearance operation is practical so that leakage can be minimized. The secondary seal was designed to operate with clearances of 0.0076 to 0.0102 mm (0.0003 to 0.0004 in.). The ID and OD of the seal ring are 80 and 100 mm (3.15 and 3.94 in.) respectively. The recess in each sector is near the low-pressure ID region and is 2 mm (0.078 in.) in width and 90° in circumference. It was not practical to use line source inherent compensation for these secondary seals because the hole size becomes impractically small. Pneumatic hammer is avoided by a small recess depth so that the ratio of recess to clearance volume is small. A recess depth of approximately 0.0127 mm (0.0005 in.) was selected. Since the outer periphery of the secondary seal is at high pressure, it was necessary to move the recess toward the low-pressure end to obtain a reasonable pressure ratio for stiffness purposes. An orifice diameter of 0.0254 mm (0.010 in.) was computed to be optimum and also the minimum acceptable. A larger orifice diameter would require larger clearances and higher leakage flows.

Figure 4-10 shows force versus film thickness at the two extremes of ambient pressure. Superimposed on these curves is the spring force that maintains axial equilibrium. The spring preload is 2990 N (672 lb) and will remain constant over the small displacement range corresponding to the two ambient pressure conditions. The variation in film thickness is from 0.0076 mm (0.0003 in.) to 0.0092 mm (0.00036 in.). A spring was designed for 17.5×10^6 N/m (100,000 lb/in.) that would be displaced 0.17 mm (0.00672 in.) to produce the desired preload.

The leakages for the total of both sides of the secondary seal (six sectors) are shown for the two ambient pressure conditions in Figure 4-11; Figure 4-12 indicates the stiffness variations. The secondary seal leakage varies from 0.00045 to 0.00055 kg/sec (0.001 to 0.0012 lb/sec), and the stiffness range is from 115×10^6 to 70×10^6 N/m (65.2×10^4 to 39.7×10^4 lb/in.) for ambient pressure of 0 kPa an 345 kPa (50 psi), respectively.

4.5 Sectored Seal Dynamics

It is important that the seal sectors follow dynamic excursions of the rotor without contact. A single-degree-of-freedom dynamics model in the radial direction was assumed, and the Coulomb friction occurring between sectors and viscous friction occurring along the secondary seal faces was accounted for. A time transient analysis was conducted and the algorithm and governing equations are indicated in Figure 4-13.

The shaft was given a harmonic vibration of 0.020 mm (0.00079 in.) double (peak-to-peak) amplitude at the synchronous frequency of 3142 rad/sec (30,000 rpm), and a conservatively low value of 22.78×10^6 N/m (0.13×10^6 lb/in.) was used to represent the sector fluid film stiffness. Various computer runs were made to determine response as a function of the friction force. The sector response was well behaved for all cases investigated. Figure 4-14 shows response with a friction force of 88.96 N (20 lb), a conservatively high value, which was the worst case considered. The response is in phase with the forcing function having little amplitude degradation indicating excellent tracking capability of the sector.

4.6 Sectored Seal Design

An assembly of the sectored seal design is shown in Figure 4-15. It shows all components assembled in the SSME pump with variations in the housing construction as required. Details have been completed for all of the flagged items identified. Installation requires preloading of the secondary seals, item 3, against the carbon elements with a total force of 2990 N (672 lb). To accomplish this, a preload spring compression, item 2, of 0.171 mm (0.0067 in.) is required. In the absence of external pressure, the sectors are held together by a garter spring, item 5.

Details of the T-shaped carbon elements are shown in Figure 4-16. The sectors are complicated pieces because of the orifice holes on the ID, the recesses on the faces, and joint configurations. Also, accurate tolerances and finishes are required. The preloading member of the secondary seal is shown in Figure 4-17. This member is axially forced into the sectored surface by the preload spring, item 2. A piston ring, item 4, is used to seal this member. The mating surface of the secondary seal preload member is coated with Teflon in case rubbing occurs with the sectors. The piston ring is shown in Figure 4-18. The OD of the ring is also coated with Teflon to improve sliding characteristics. The garter spring is shown in Figure 4-19. The shaft sleeve, item 7, is shown in Figure 4-20. The mating surface of the sleeve is coated with chrome carbide for sliding compatability with the carbon elements of the seal ring sectors. The sleeve fits over the shaft and is shrink fitted to the slinger elements at the right-hand end of the sleeve, as shown in Figure 4-15. The sleeve is held in place in the left end by the labyrinth seal, which is also shown in Figure 4-15. The preload spring is shown in Figure 4-21. It is an Inconel ring with pad supports that provides a beam-type flexure between supports.

Appendix A contains the MTI specification for applying a chrome-carbide coating to the surfaces of bearings and shafts.

4.7 Sectored Seal Conclusions

Table 4-2 summarizes performance results. General conclusions are as follows.

- Adequate stiffness could not be obtained with a supply pressure of 690 kPa (100 psi); it was necessary to double this value to 1379 kPa (200 psi).

- The seal meets the targeted leakage values with a significant margin. The flow is a factor of 4 less than the targeted value, even though it was necessary to double the supply pressure. Figure 4-22 shows total leakage through the primary and secondary seals as a function of ambient pressure.

- The seal sectors will dynamically track rotor excursions without difficulty.

- Although complex, the sectored seal can satisfy the principal requirement of operating with low film thickness and produce excellent performance over a wide range of operating conditions.

TABLE 4-1

PRINCIPAL DIMENSIONS AND OPERATING CONDITIONS
SECTORED PRIMARY SEAL

Shaft Diameter (D)	68 mm (2.68 in.)
Length (L)	41.275 mm (1.625 in.)
Radial Clearance (C)	0.0254 mm (0.001 in.)
Pad Angle	120°
Viscosity	0.00002 Pa-s (2.9×10^{-9} reyns)
Speed (N)	3141 rad/sec (30,000 rpm)
Temperature (T)	+20°C (68°F)
Feed Holes Per Sector	6
Feed Hole Diameter	0.381 mm (0.015 in.)

TABLE 4-2

SUMMARY OF SECTORED SEAL PERFORMANCE

Ambient Pressure	0 kPa	345 kPa
Radial Load on Sector, N (lb)	1010 (227)	1600 (360)
Primary Seal		
Minimum Film Thickness, mm (in.)	0.0241 (0.0009)	0.0173 (0.0007)
Stiffness, N/m × 10^{-6} (lb/in. × 10^{-4})	35 (20)	30.5 (17.4)
Leakage, kg/s (lb/sec)	0.0006 (0.0013)	0.00038 (0.0008)
Pressure Ratio	0.5	0.69
Seal Power Loss, W (hp)	81 (0.11)	99 (0.13)
Secondary Seal		
Axial Force, N (lb)	2990 (672)	2990 (672)
Leakage, kg/s (lb/sec)	0.00045 (0.001)	0.00055 (0.0012)
Stiffness, N/m × 10^{-6} (lb/in. × 10^{-4})	115 (65.7)	72 (41.1)
Total Seal Leakage, kg/s (lb/sec)	0.00105 (0.0023)	0.00093 (0.0020)
Buffer Gas Supply Pressure, kPa (psig)	1379 (200)	1379 (200)
Buffer Gas Temperature, °C (°F)	20 (68)	20 (68)
Primary Seal Orifice Size, mm (in.)	0.381 (0.015)	0.381 (0.015)
Primary Seal, Number of Orifices/Sectors	6	6
Secondary Seal Orifice Size, mm (in.)	0.254 (0.010)	0.254 (0.010)

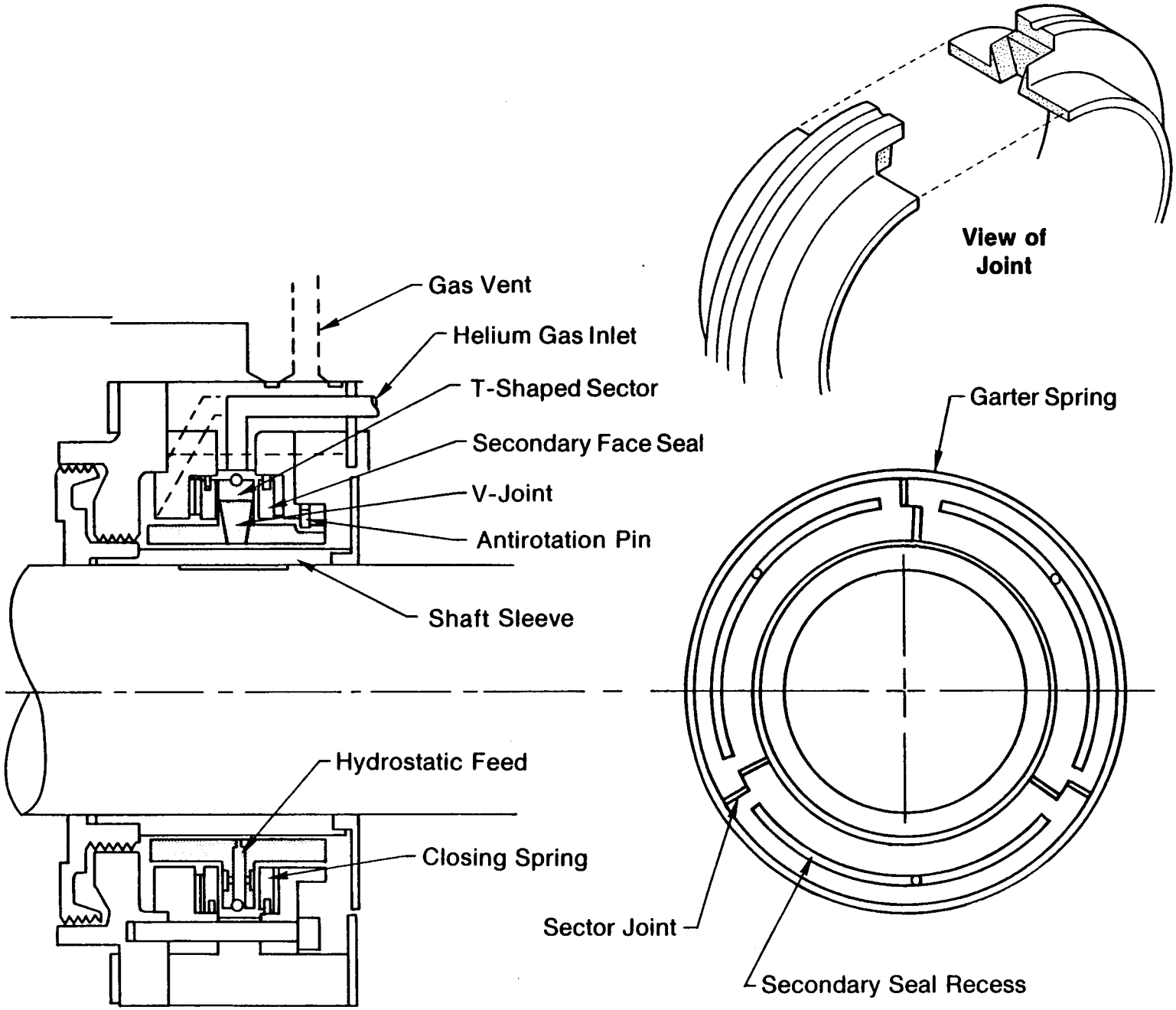

Figure 4-1. Sector Seal Configuration

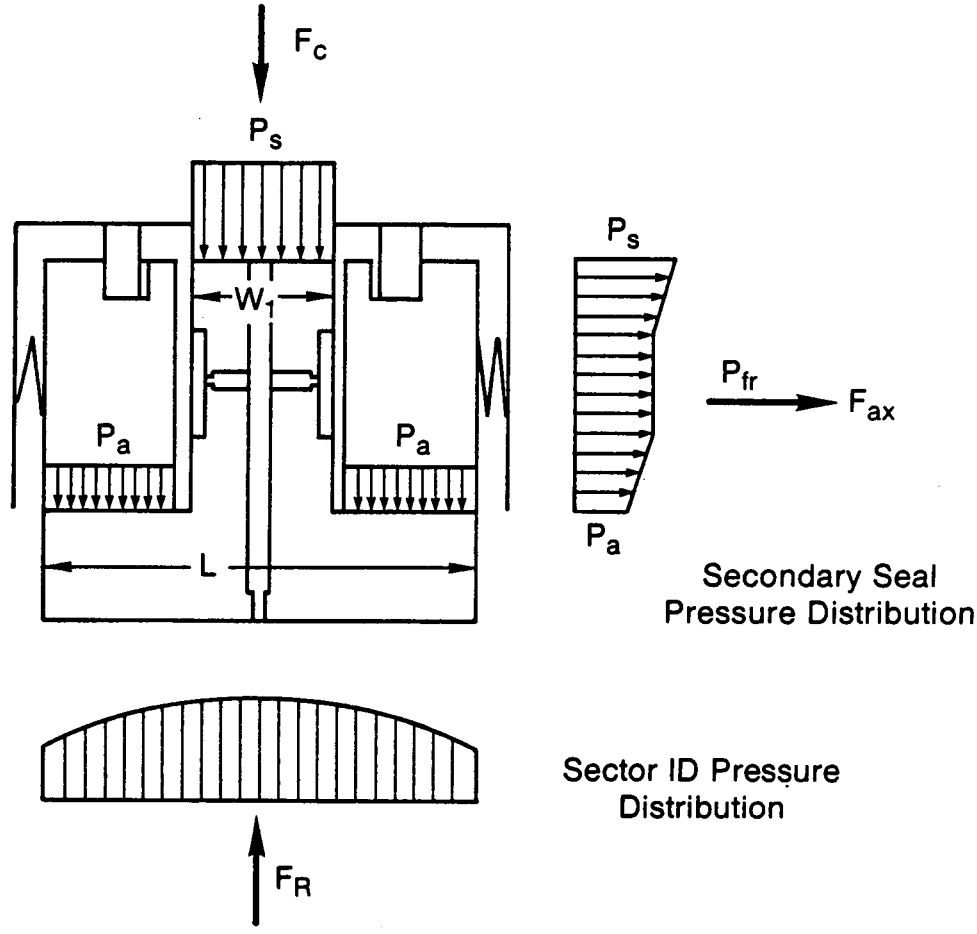

$$F_c = P_s A_s + P_a A_a$$

Radial Force Balance

$$F_R - F_c \pm F_f \pm F_r = 0$$

Axial Force Balance

$$F_{ax} - F_p - k_s \delta_a = 0$$

Figure 4-2. Sector Pressure Distribution and Force Balance

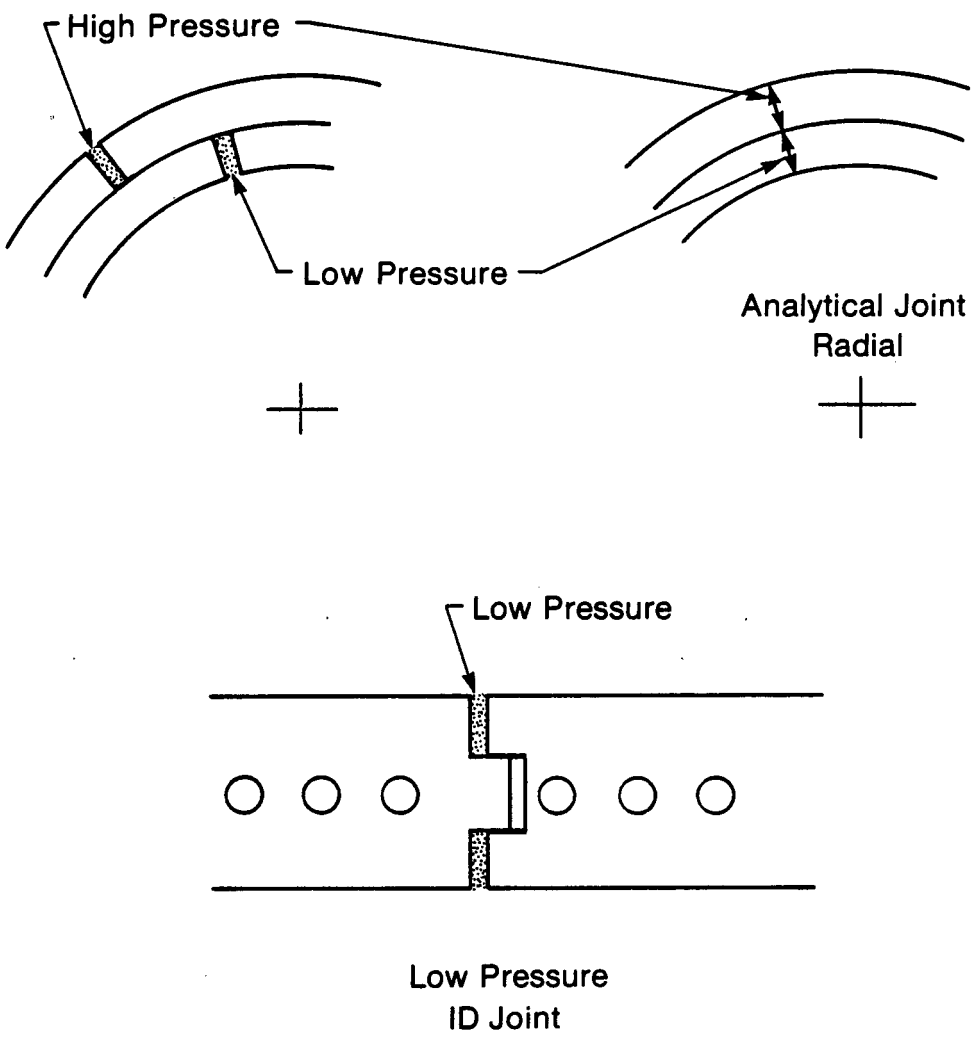

Figure 4-3. Joint Boundary Conditions

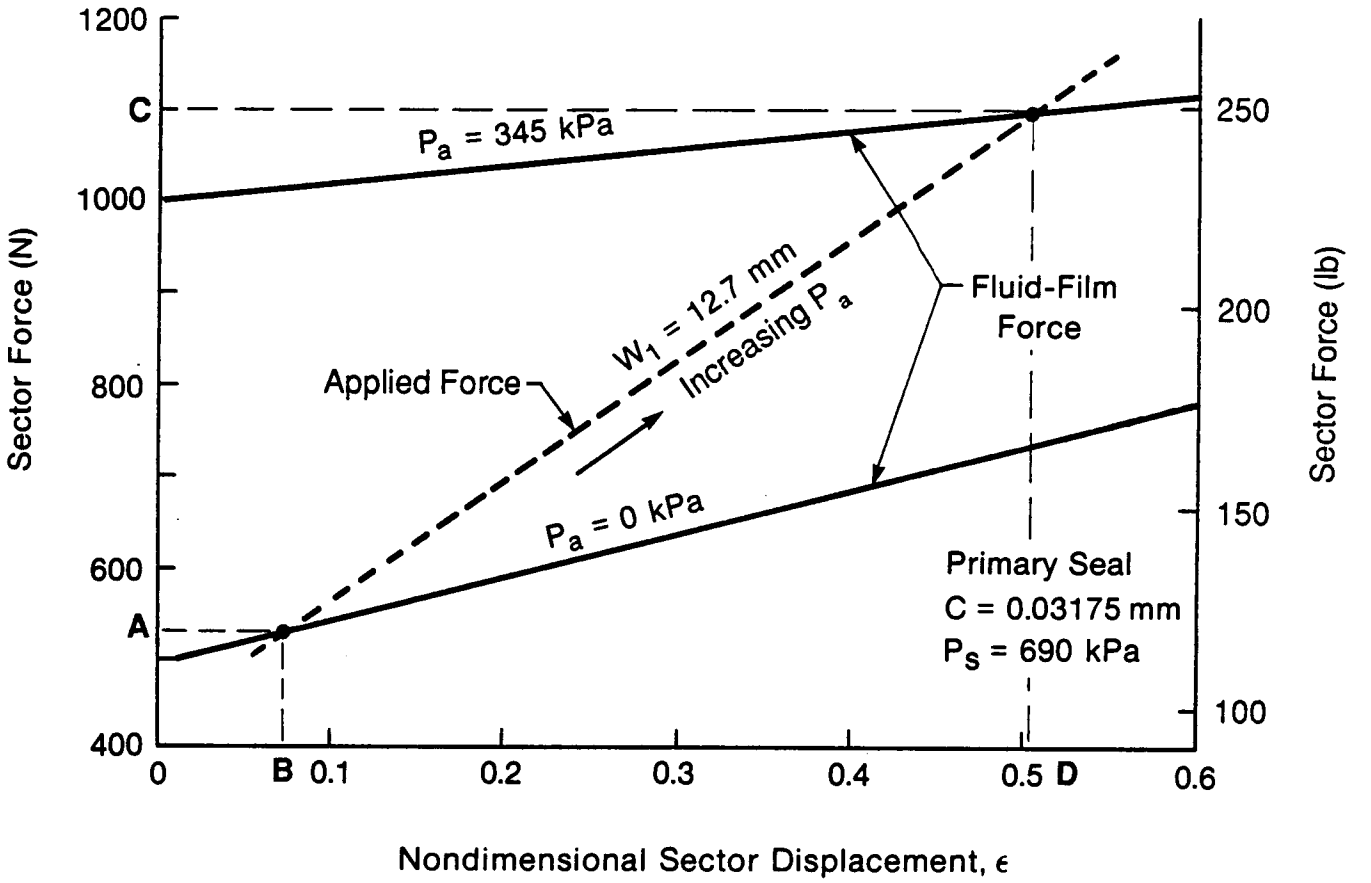

A = sector load at P_a = 0 kPa (0 psig)
B = nondimensional sector displacement at P_a = 0 kPa (0 psig)
C = sector load at P_a = 345 kPa (50 psig)
D = nondimensional sector displacement at P_a = 345 kPa (50 psig)

Notes

1. Applied (closing) force increases with ambient pressure P_a (see Figure 4-2).
2. Loads were computed using dimensions on Figure 4-16.

Figure 4-4 Sector Force vs. Displacement, P_S = 690 kPa

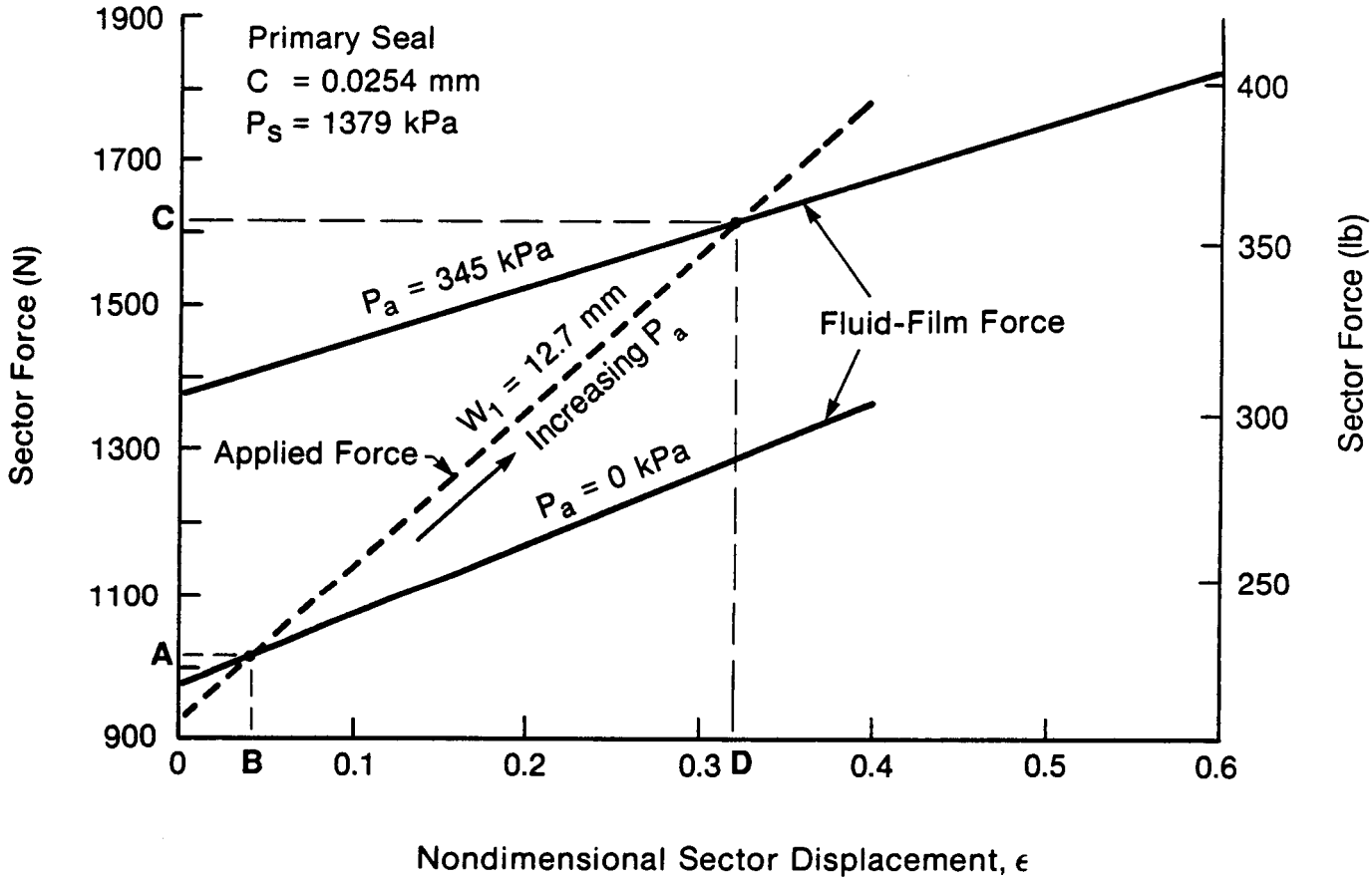

A = sector load at P_a = 0 kPa (0 psig)
B = nondimensional sector displacement at P_a = 0 kPa (0 psig)
C = sector load at P_a = 345 kPa (50 psig)
D = nondimensional sector displacement at P_a = 345 kPa (50 psig)

Notes

1. Applied (closing) force increases with ambient pressure P_a (see Figure 4-2).
2. Loads were computed using dimensions on Figure 4-16.

Figure 4-5 Sector Force vs. Displacement, P_s = 1379 kPa

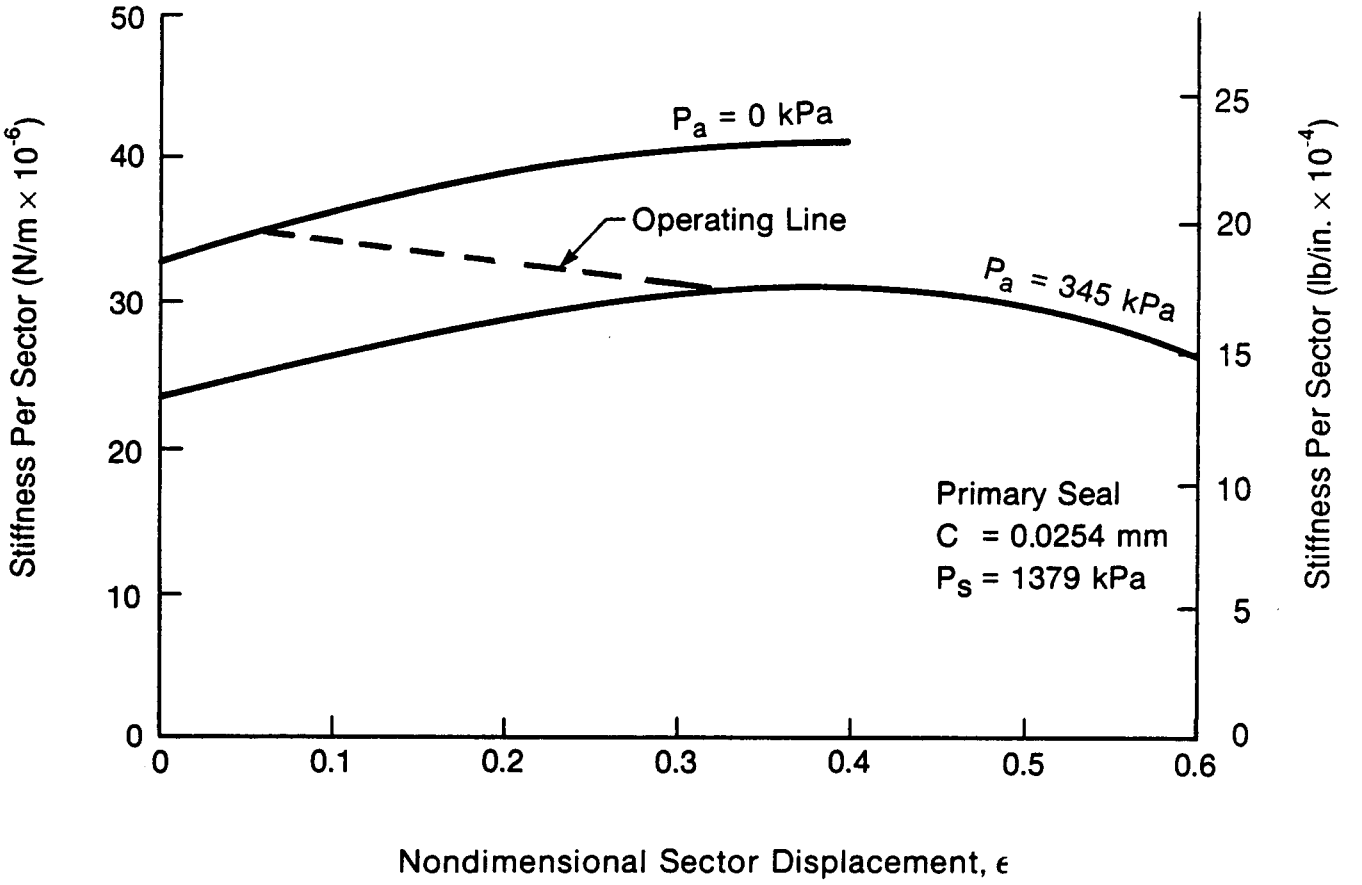

Figure 4-6 Sector Stiffness vs. Displacement

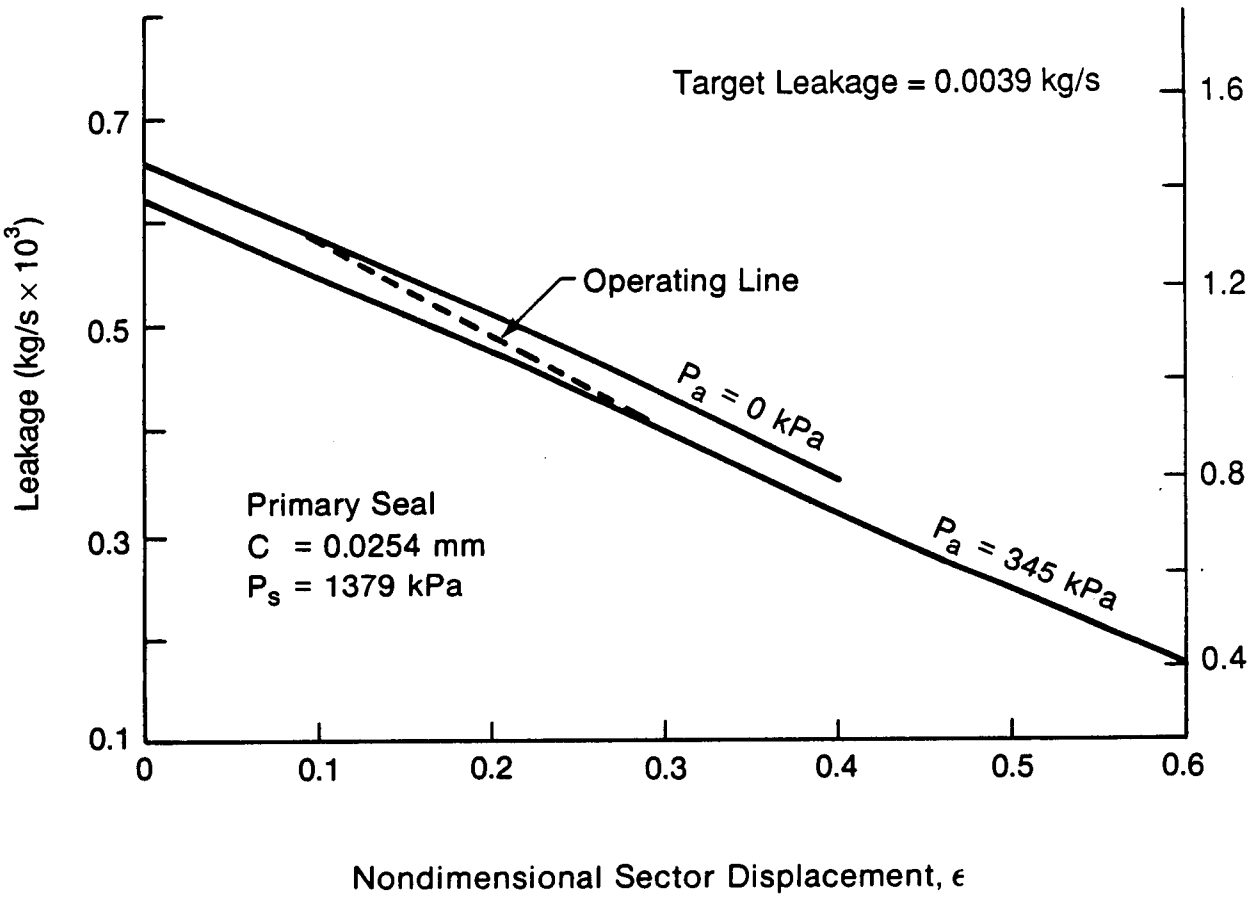

Figure 4-7 Total Primary Seal Leakage vs. Sector Displacement

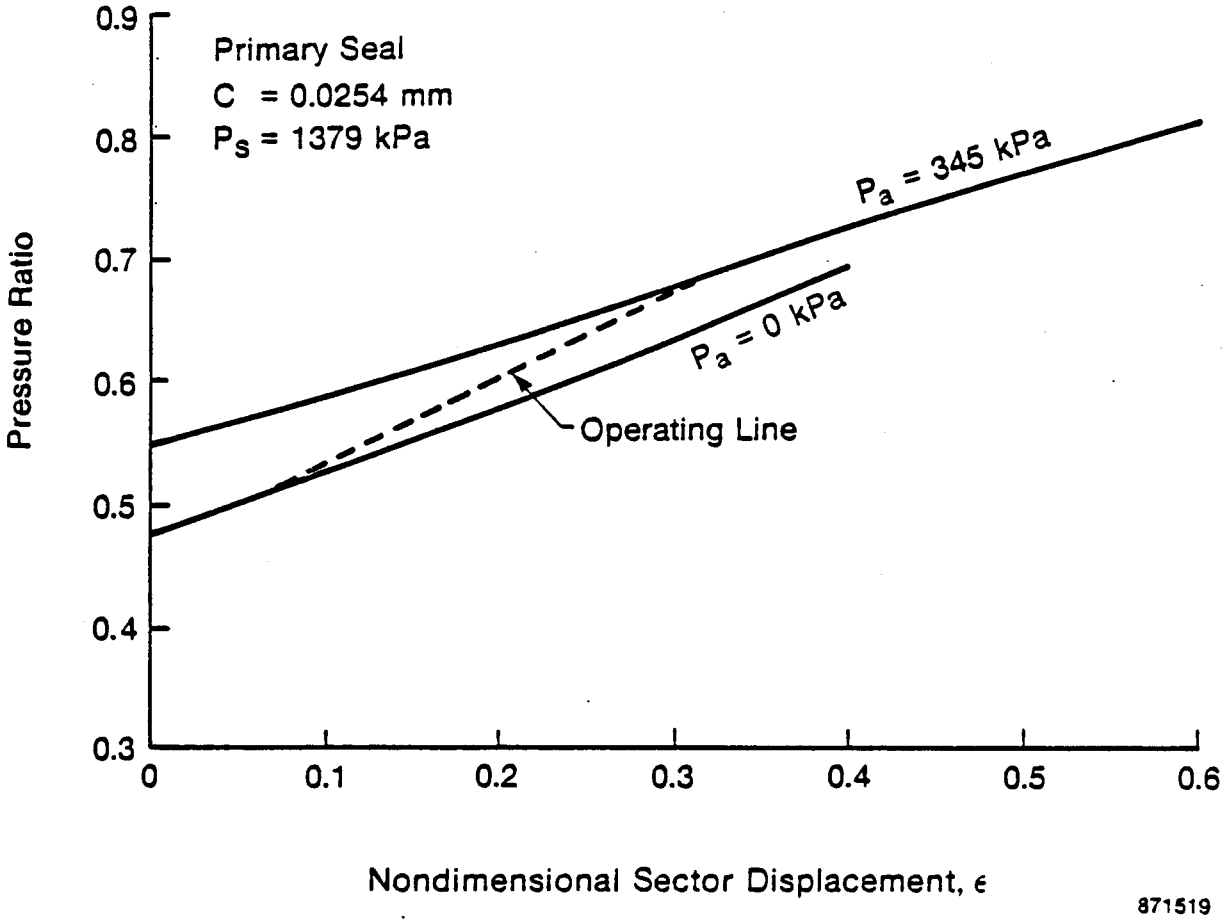

Figure 8 Pressure Ratio vs. Sector Displacement

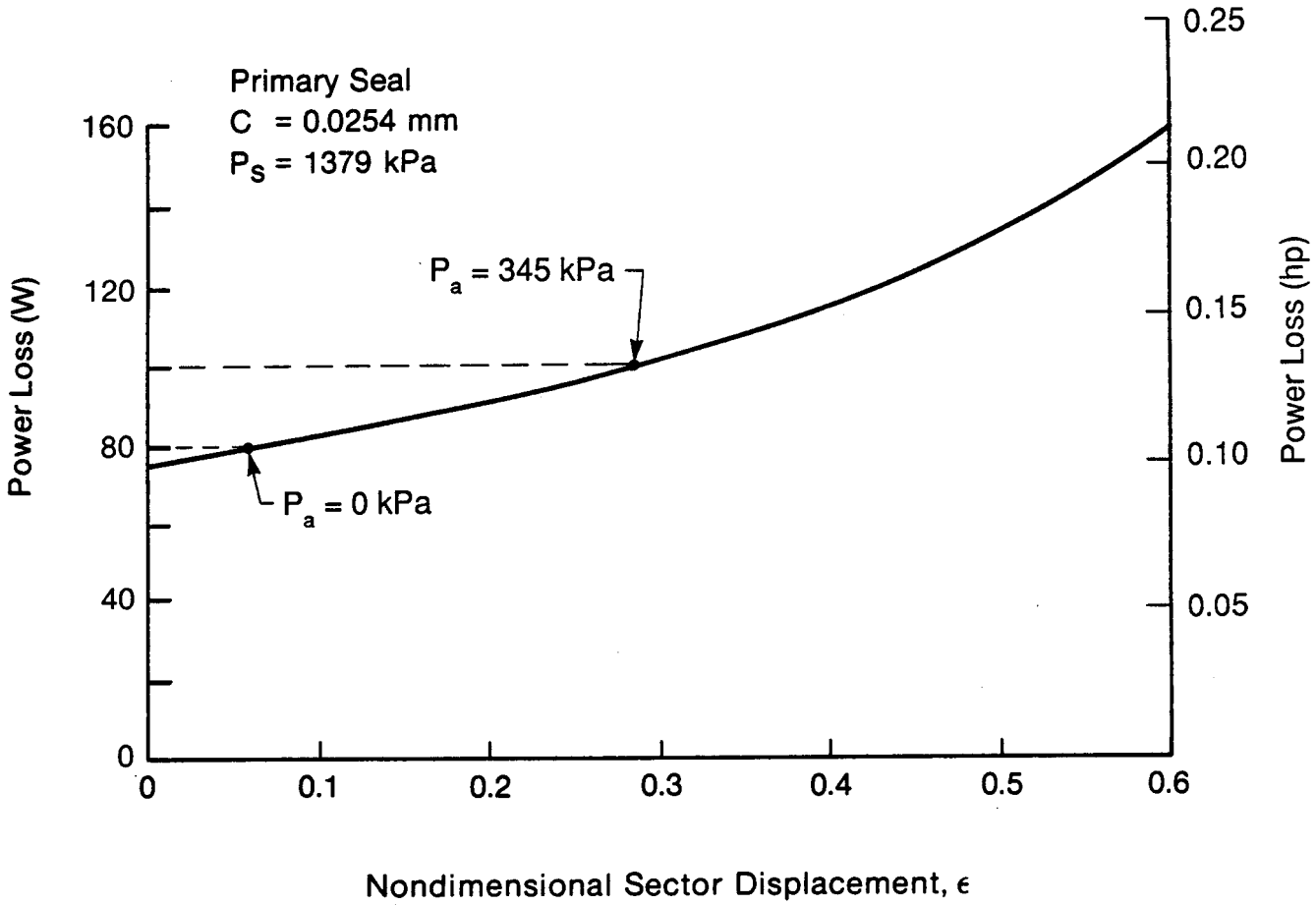

Figure 4-9 Primary Seal Power Loss vs. Displacement

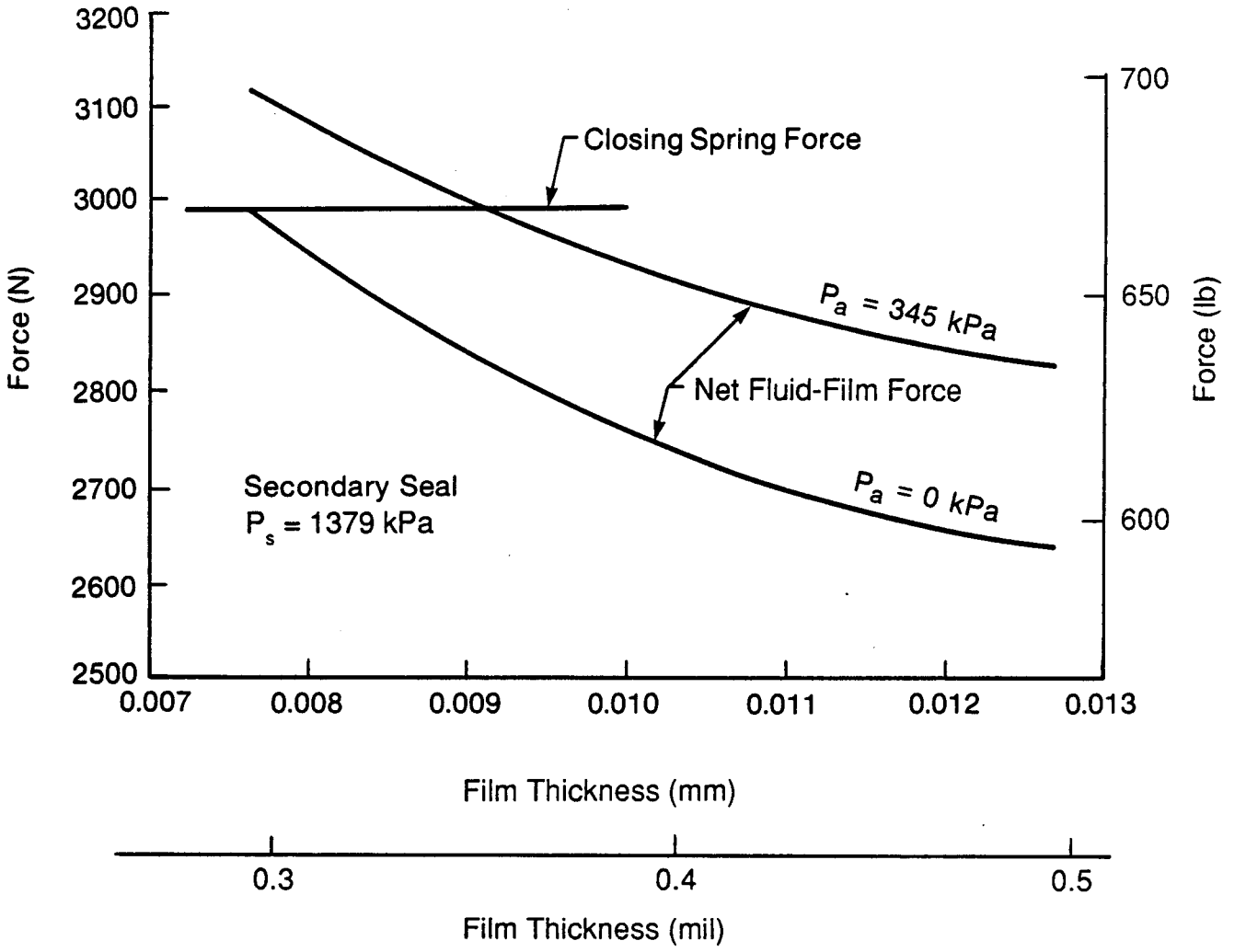

Figure 4-10 Force vs. Film Thickness Secondary Seal
(One side, three sectors)

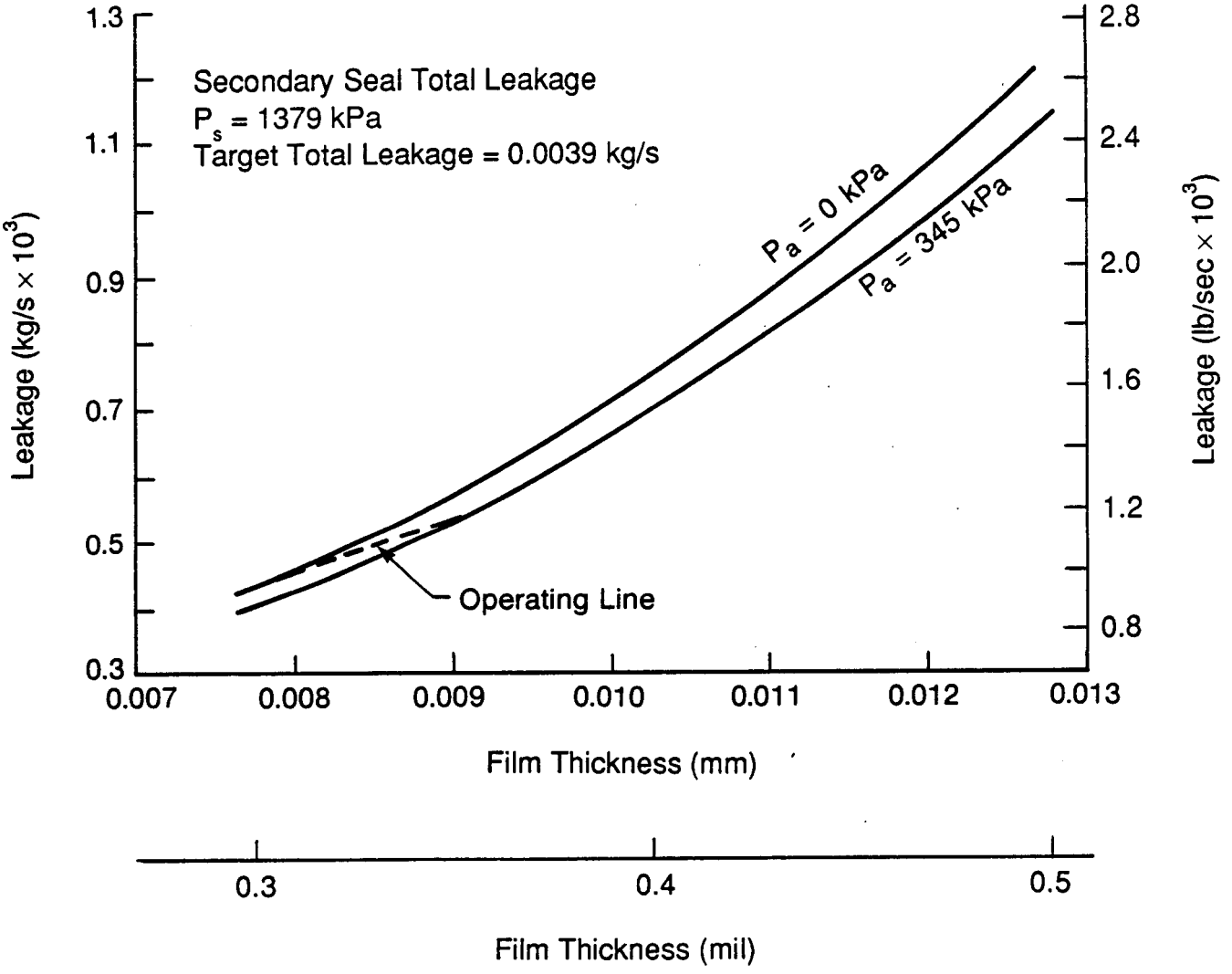

Figure 4-11 Total Secondary Seal Leakage vs. Film Thickness (Two sides, six sectors)

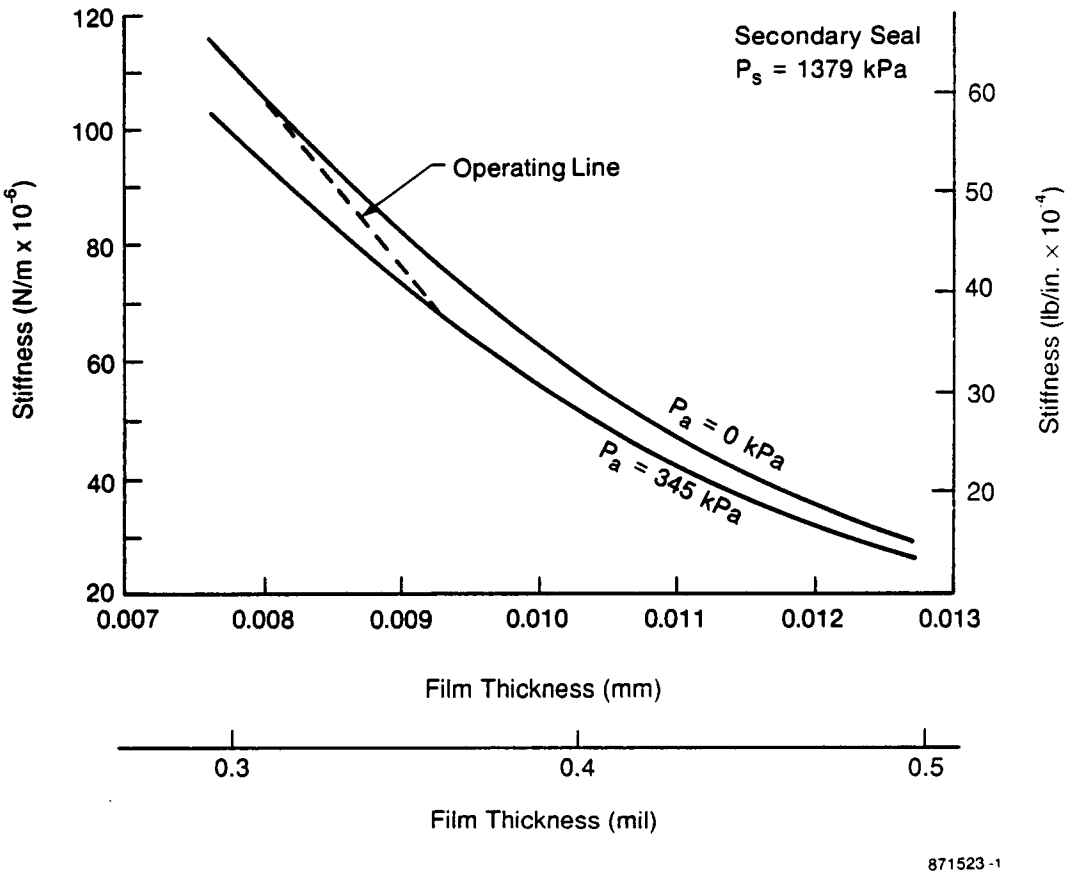

Figure 4-12 Secondary Seal Stiffness vs. Film Thickness

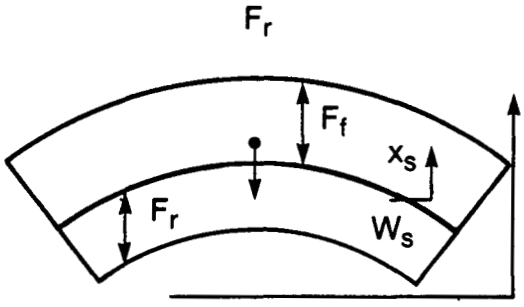

$$x = \ddot{x}_o \sin \omega t$$

$$mx_s = - k_f (x_s - x) \pm F_f \pm F_r - w_s$$

$$\text{Sign } F_f = - \text{ sign } \dot{x}_s$$

$$F_a = - k_f (x_s - x) \pm F_f - w_s$$

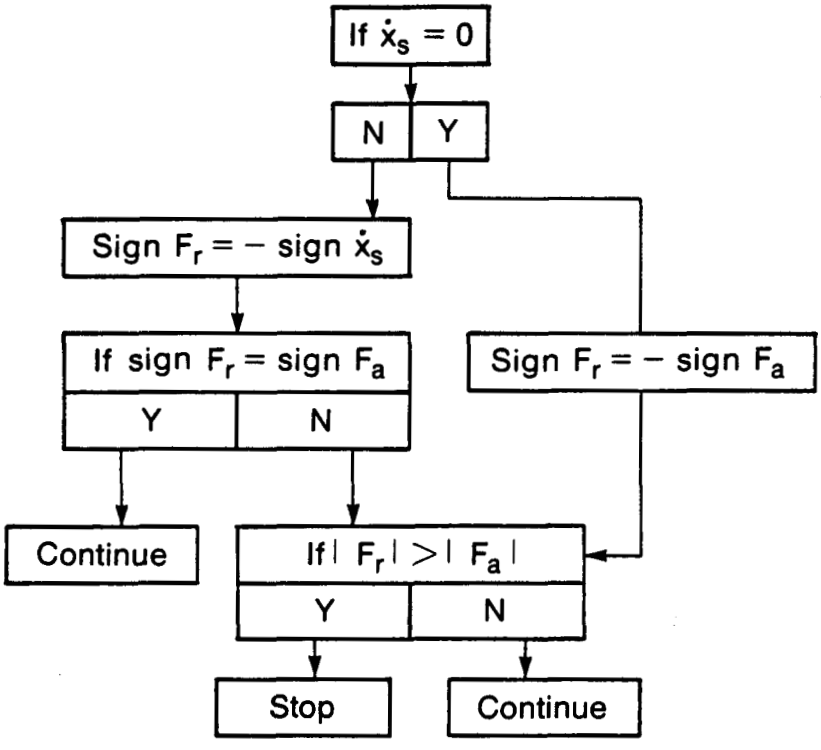

Figure 4-13 Dynamic Response and Friction Algorithm

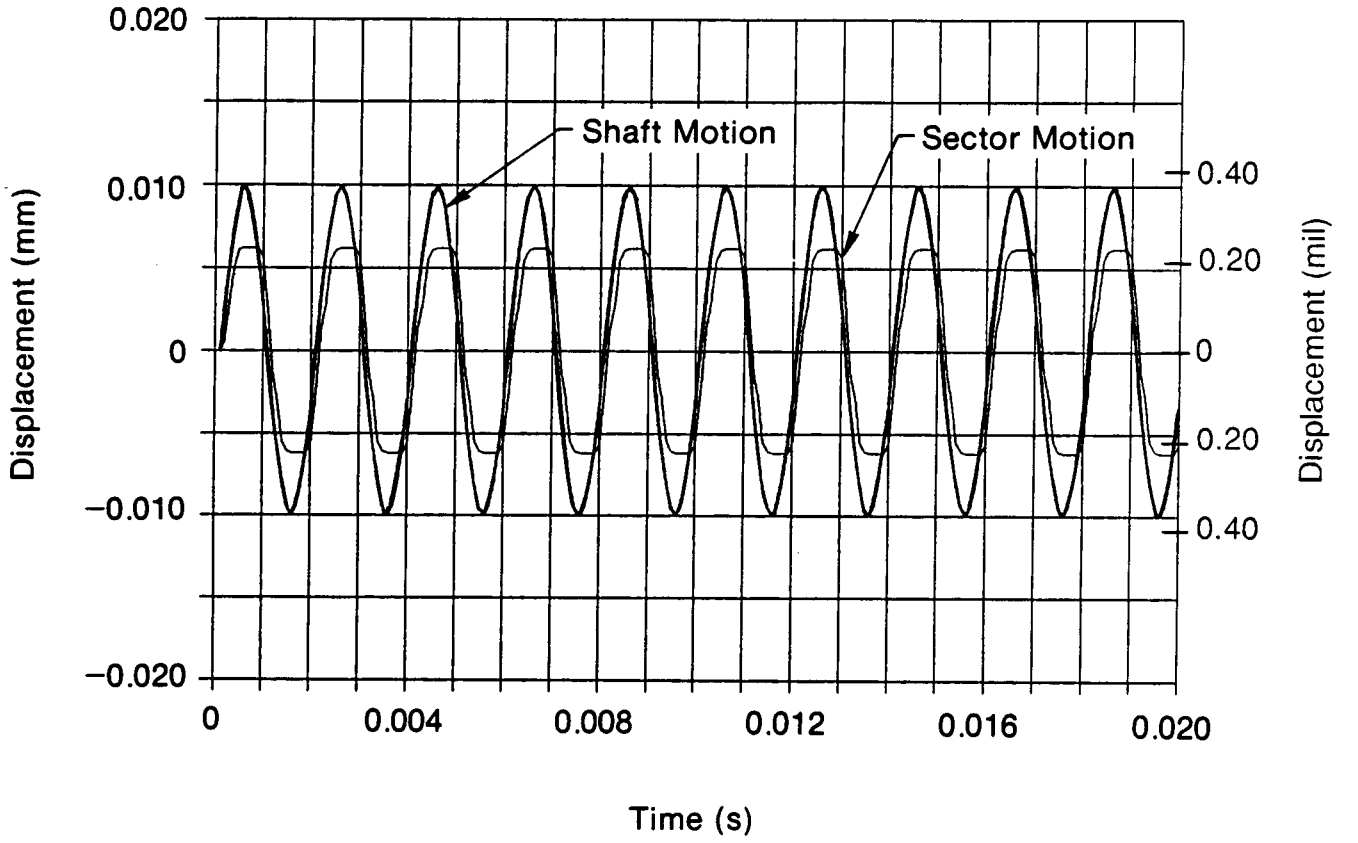

Friction Force = 88.96 N (20 lb)
Shaft Speed = 3142 rad/sec (30,000 rpm)
Shaft Runout = 0.020 mm (0.00079 in.) (peak to peak)

Figure 4-14 Dynamic Response of Seal Sector

DWG NO 771D001 | SH 1 | REV A

REVISIONS				
ZONE	REV	DESCRIPTION	DATE	APPROVED
	A	REDRAWN	15 SEP 1987	

ORIGINAL PAGE IS
OF POOR QUALITY

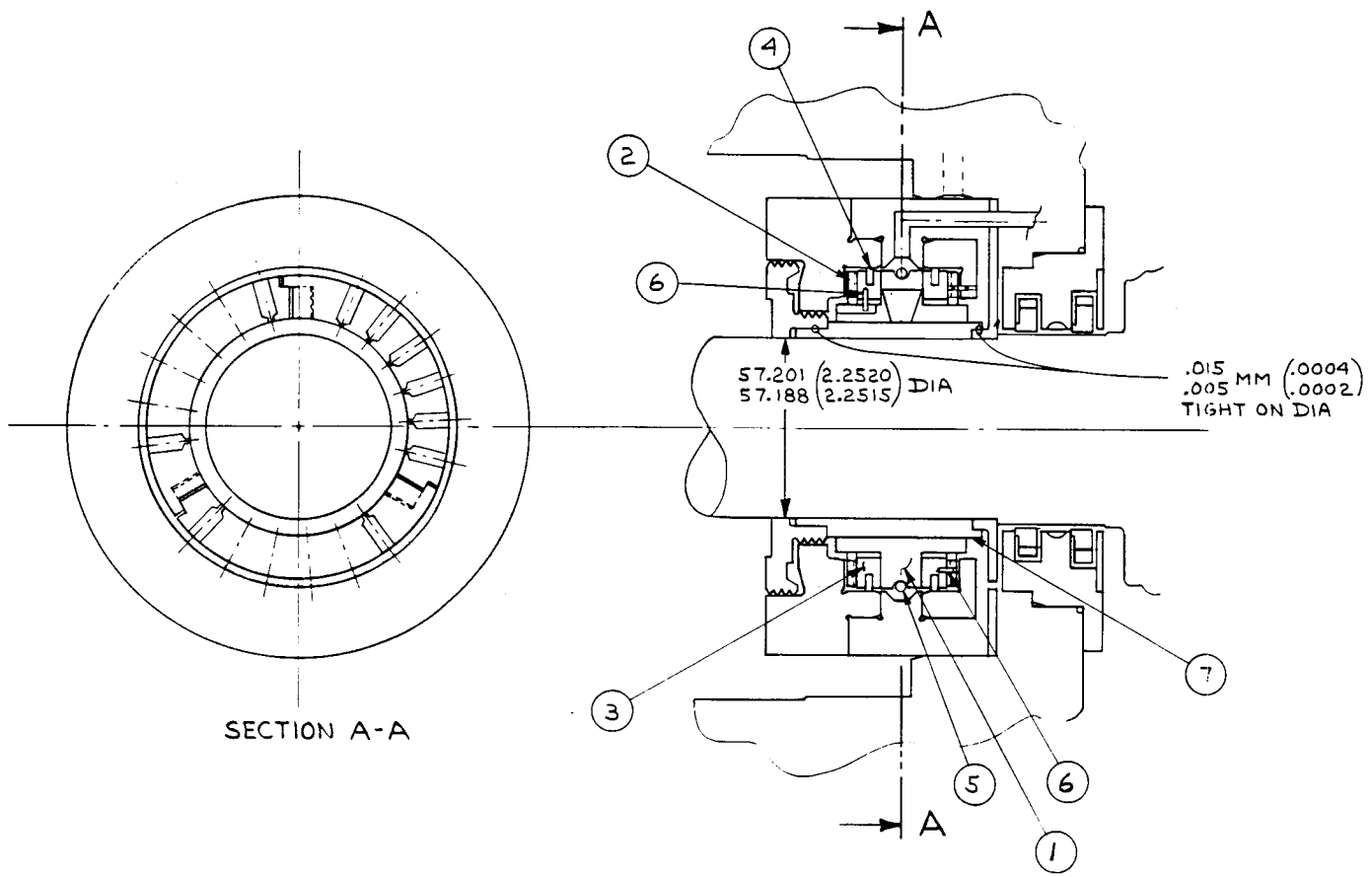

NOTE
ASSEMBLE SO THAT AXIAL SPRING, ITEM 2, HAS
PRELOAD = 2990 N (672 LBS)
SPRING RATE = 17.35×10^6 N/M (99,112 LB/IN)

FOLDOUT FRAME

FOLDOUT FRAME

	1	7	771C015P1	SLEEVE
	5	6	79-012-052-0188	ROLL PIN (1/16 DIA x 3/16 LG) MAT'L: STN. STL. ESNA OR EQ
	1	5	771B008P1	SPRING - GARTER
	2	4	771C007P1	PISTON RING
	2	3	771B006P1	SECONDARY SEAL
	2	2	771C005P1	SPRING
	1	1	771D004P1	SEGMENTED SEAL
			771D001	ASSEMBLY

UNLESS OTHERWISE SPECIFIED
DIMENSIONS ARE IN INCHES
TOLERANCES ON:
DECIMALS: XXX ±, XX ±
FRACTIONS: ±
ANGLES: ±
ALL SURFACES ✓
BREAK SHARP CORNERS AND REMOVE BURRS
GEOMETRIC TOLERANCES PER ANSI Y 14.5
MATERIAL
TREATMENT

COMPANY CLASSIFICATION
PROPRIETARY ☐ NAME-DATE
NON-PROPRIETARY ☐ TITLE

DRAWN H JONES 4/14/87
CHECK
DESIGN
ANALYTICAL
MATERIALS
MFG. ENGR
QUALITY CONTROL 11/21/87
ISSUED

Mechanical Technology incorporated, LATHAM NEW YORK 12110

TITLE
FLOATING RING SEAL
SECTORED-GAS-LUBRICATED

SIZE D | FSCM NO 26741 | DWG NO 771D001 | REV A
SCALE | WT ACT / ALC | SHEET 1 OF 1

BRUNING 40-105 61702-1 D

Figure 4-15 Sectored Seal Assembly

ORIGINAL PAGE IS
OF POOR QUALITY

REVISIONS		SIZE D	771D004	REV.
SYM.	DESCRIPTION	DATE	APPROVAL	

.356 - .406 MM (.014 - .016) DIA. THRU
4.699 - 4.877 MM (.185 - .192) DIA. TO DEPTH SHOWN
6 HOLES PER SEGMENT, 18 HOLES TOTAL
SPACED AS SHOWN

.762 - 1.016 MM
(.030 - .040)

DETAIL "D-8"
(SCALE: 4/1) TYP. 18 PLACES

5 EQ. SP. @ 16° = 80°
(NON- ACCUMULATIVE)

"C-7"

41.375 / 41.275 MM (1.629 / 1.625)

20.725 MM (.816) / 20.625 (.812)

12.751 / 12.738 MM (.5020 / .5015)

6.40 / 6.35 MM (.2510 / .2505)

100.025 MM DIA. / 99.975 (3.938 / 3.936)

68.0686 / 68.0636 MM DIA. (2.6799 / 2.6797)

78.25 / 78.00 MM DIA. (3.080 / 3.071)

95.50 MM DIA. / 95.25 (3.760 / 3.750)

12.7 / 12.5 MM (.500 / .492)

SECTION "C-5"

"C-7"

2.60 / 2.40 MM R (.102 / .094)

"A-7"
"A-4"
"C-5"
17° (REF)
23°
83°
"D-8"
"B-1"
"B-8"

SECTION "C-7"

"C-5"

2.60 / 2.40 MM (.102 / .094)

1.30 / 1.25 MM (.051 / .049)

FULL RADIUS

VIEW "B-8"

2.80 / 2.60 MM (.110 / .102)

(1)

NOTE:
ALL JOINT SURFACES TO HAVE 8 FINISH

ORIGINAL PAGE IS
OF POOR QUALITY

85.20 / 85.00 MM DIA. (3.354 / 3.346)

2.025 / 1.975 MM (.0800 / .0778)

15°
90°

3 GROOVES EQ. SP.
.0122 - .0132 MM (.00048 - .00052) DEEP

FULL R
(TYP.)

3.277 / 3.175 MM (.129 / .125) DIA. X
9.725 / 9.525 MM (.383 / .375) DEEP
3 PLACES EQ. SP.

.0132 / .0122 MM (.00052 / .00048) (REF.)

.245 - .265 MM (.0096 - .0100) DIA. THRU
1.549 - 1.676 (.061 - .066)
DIA. X 2.94 / 2.54 MM (.116 / .100) DEEP

43.70 / 43.50 MM (1.720 / 1.712)

SECTION "B-1"
(SCALE: 4/1) TYP. 3 PLACES

"A-6"

.381 MM R (.015) / .127 (.005)

.1016 / .0508 MM (.004 / .002) RADIUS

10.1600 / 10.1473 MM (.4000 / .3995)

3.2004 / 3.1877 MM (.1260 / .1255)

6.4008 / 6.3754 MM (.2520 / .2510)

"A-6"

SECTION "A-7" (FEMALE JOINT CONSTRUCTION)
(SCALE: 2/1) TYP. 3 PL.

9.5377 MM (.3755) / 9.5250 (.3750)

5.5880 MM (.2200) / 5.5753 (.2195)

SECTION "A-6"

"A-3"

.254 MM R (.010) / .127 (TYP) (.005) RADIUS

10.1727 / 10.1600 MM (.4005 / .4000)

3.1750 / 3.1623 MM (.1250 / .1245)

6.3627 / 6.3500 MM (.2505 / .2500)

"A-3"

SECTION "A-4" (MALE JOINT CONSTRUCTION)
(SCALE: 2/1) TYP. 3 PL

9.5123 / 9.4996 MM (.3745 / .3740)

5.5626 / 5.5499 MM (.2190 / .2185)

.1016 / .0508 MM R (.004 / .002) TYPICAL AT INTERSECTION OF ALL MACHINED SURFACES UNLESS OTHERWISE SPECIFIED

SECTION "A-3"

UNLESS OTHERWISE SPECIFIED DIMENSIONS ARE IN INCHES TOLERANCES ON: DECIMALS XXX : ±.005 XX : ±.01 FRACTIONS : ±1/64 ANGLES : ±0°30' ALL SURFACES 63 √ BREAK SHARP CORNERS AND REMOVE BURRS GEOMETRIC TOLERANCES PER USASI Y 14.5	COMPANY CLASSIFICATION PROPRIETARY ☐ NAME - DATE NON-PROPRIETARY ☐ TITLE
MATERIAL CARBON GRAPHITE C-GPH P-5N	DRAWN B. Bertoncha 2 APR '87 CHECK H. Jones 5/6/87 DESIGN ANALYTICAL MATERIALS APPR. ENGR. MGR. APPROV. W. Phipps 9/4/87 QUALITY CONTROL
TREATMENT	Mechanical Technology Incorporated, Latham, New York 12110 TITLE: SEAL SECTORED SEAL CODE IDENT NO. 26741 SIZE D DWG. NO. 771D004 ISSUED SCALE 1/1 WT. ACT. CALC.

FOLDOUT FRAME 2

Figure 4-16 Sectored Seal Rings

FOLDOUT FRAME

PRECEDING PAGE BLANK NOT FILMED

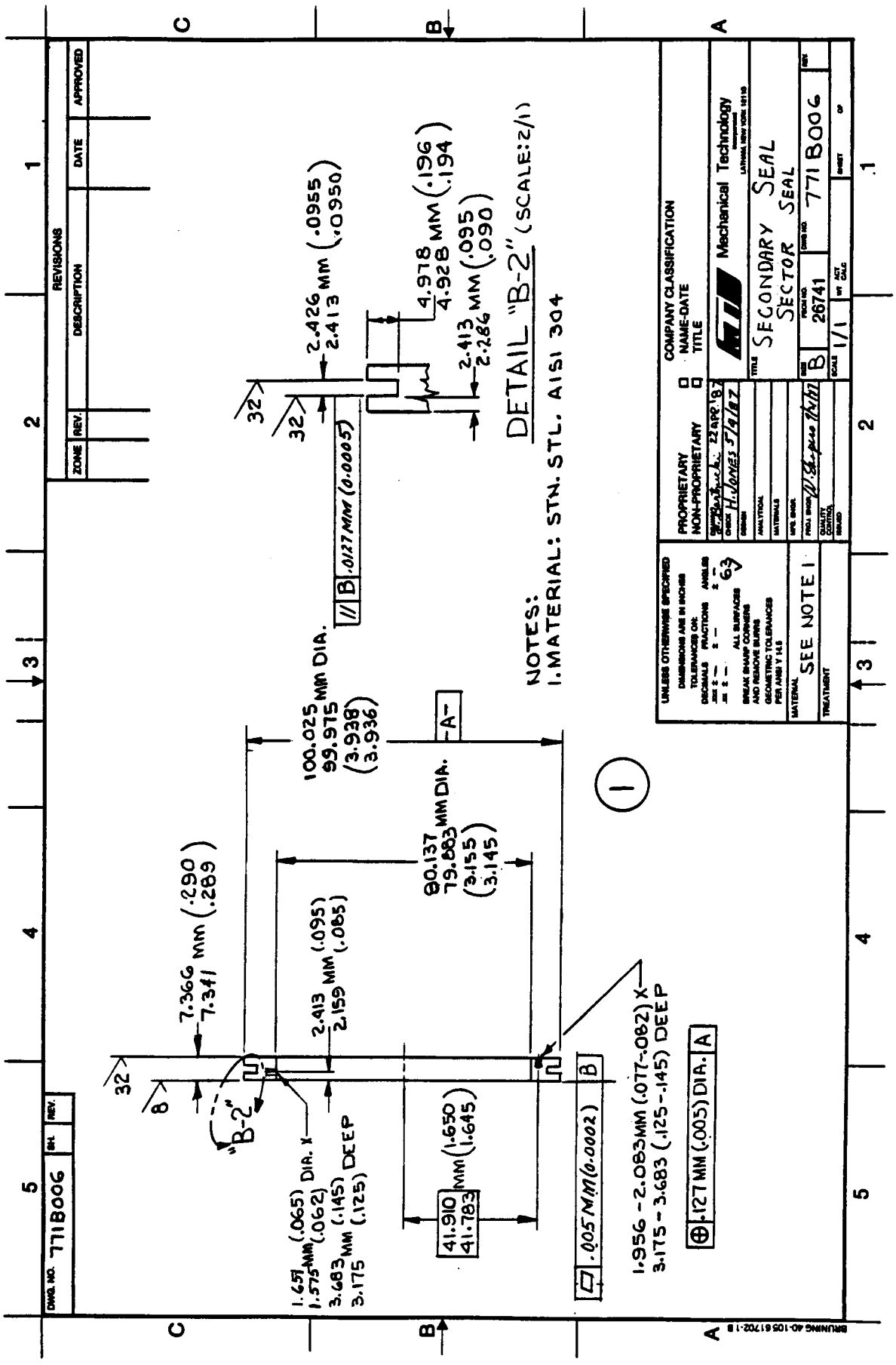

Figure 4-17. Sectored Seal Secondary Preload Ring

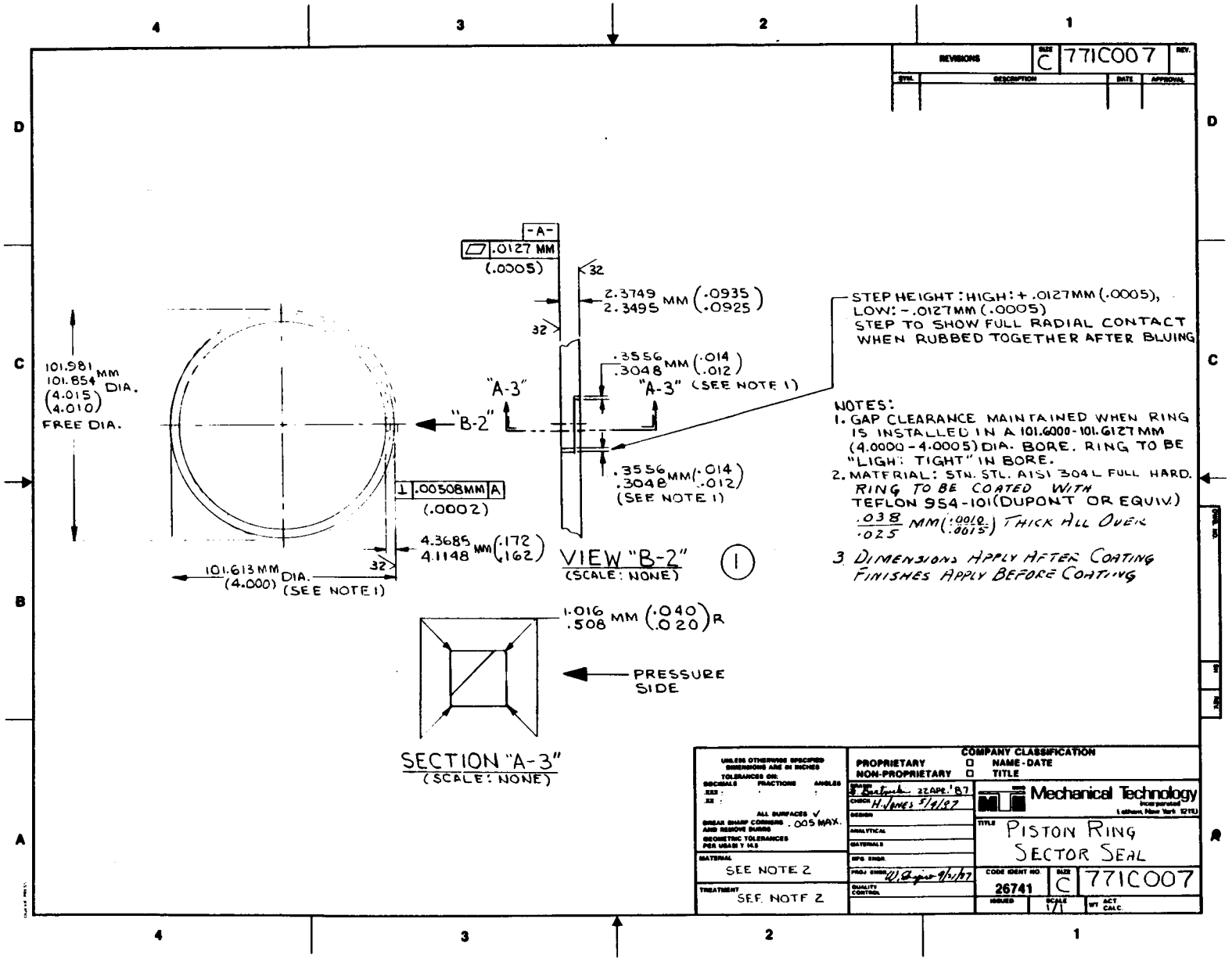

Figure 4-18 Sectored Seal Piston Ring

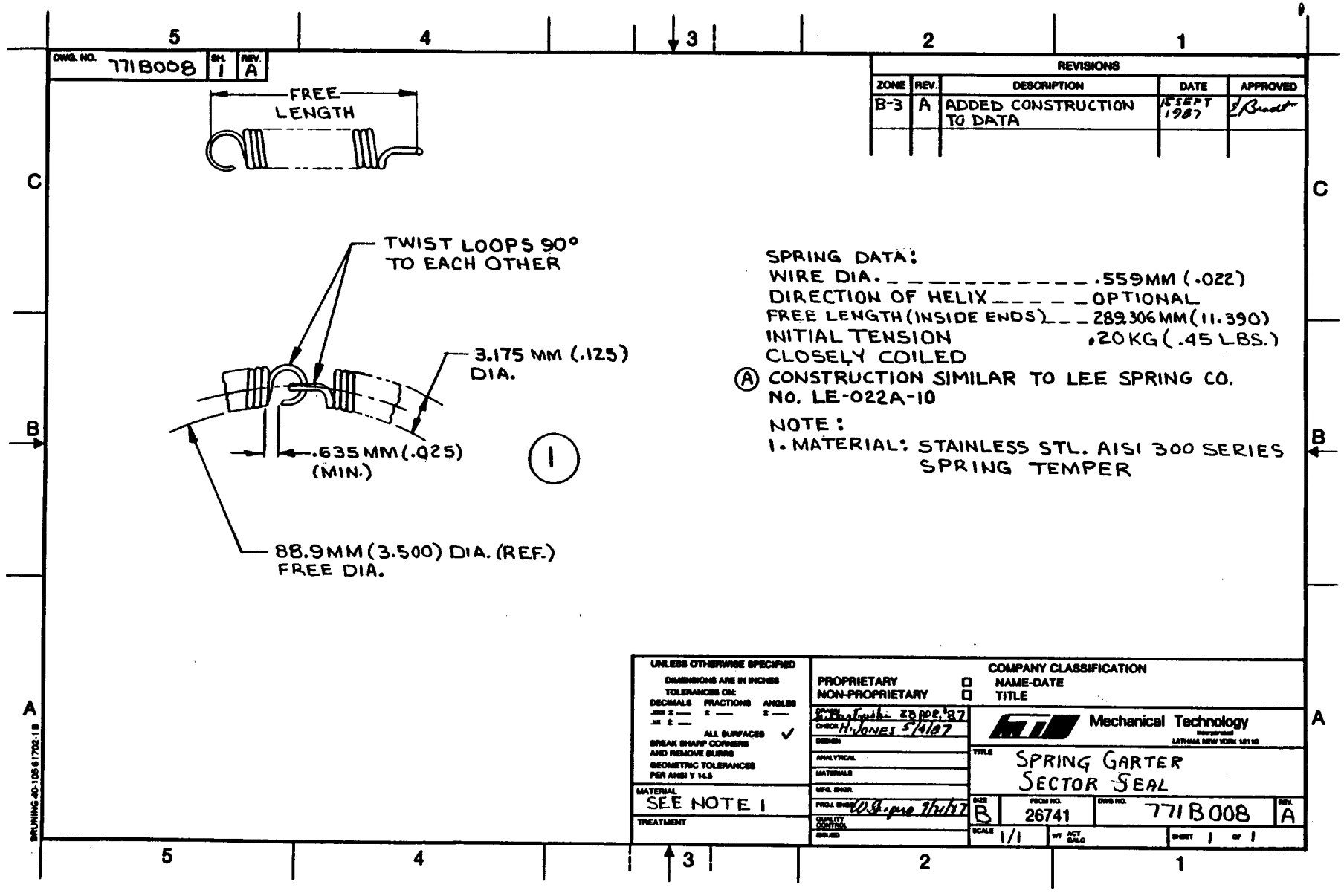

Figure 4-19 Sectored Seal Garter Spring

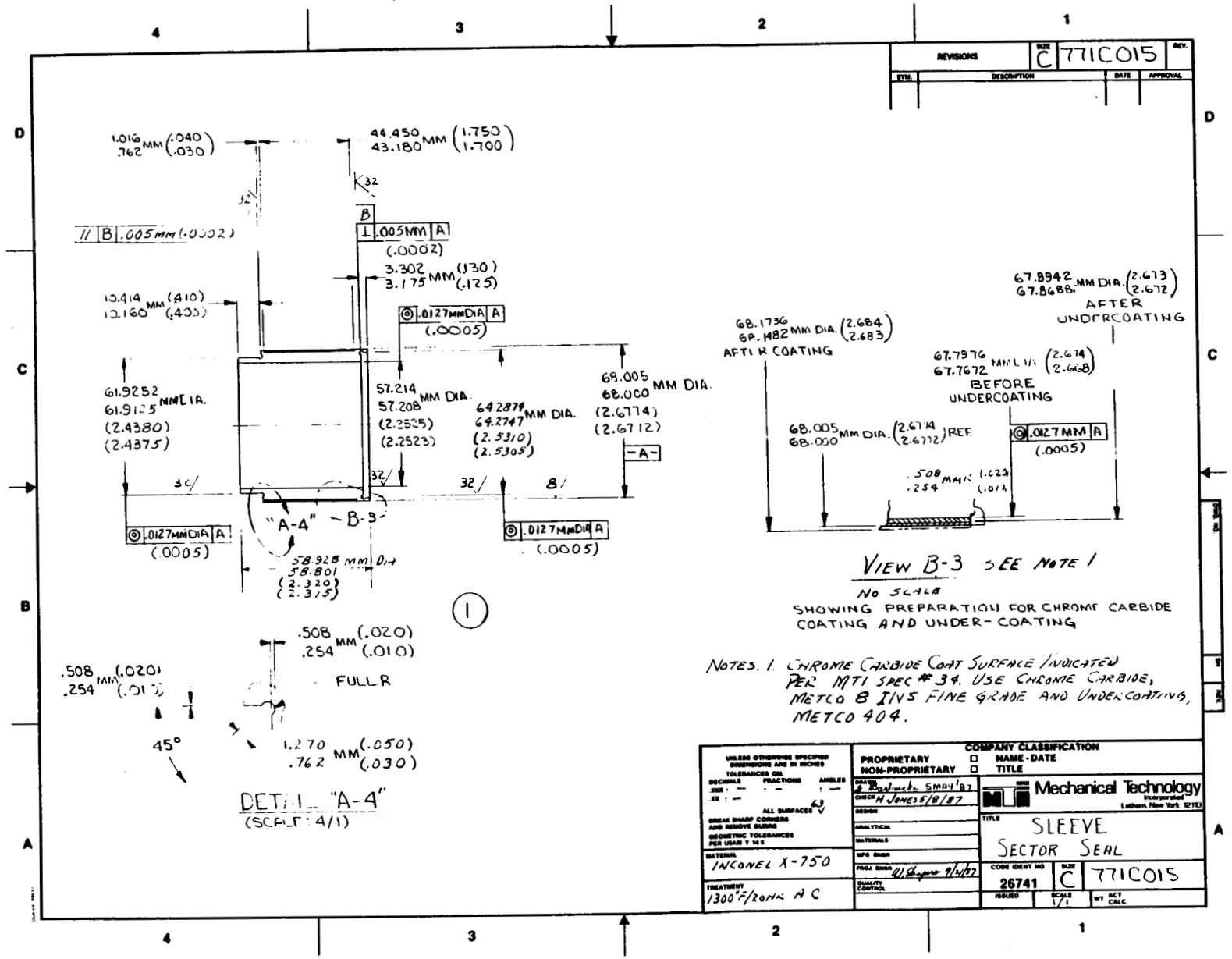

Figure 4-20 Shaft Sleeve

ORIGINAL PAGE IS
OF POOR QUALITY

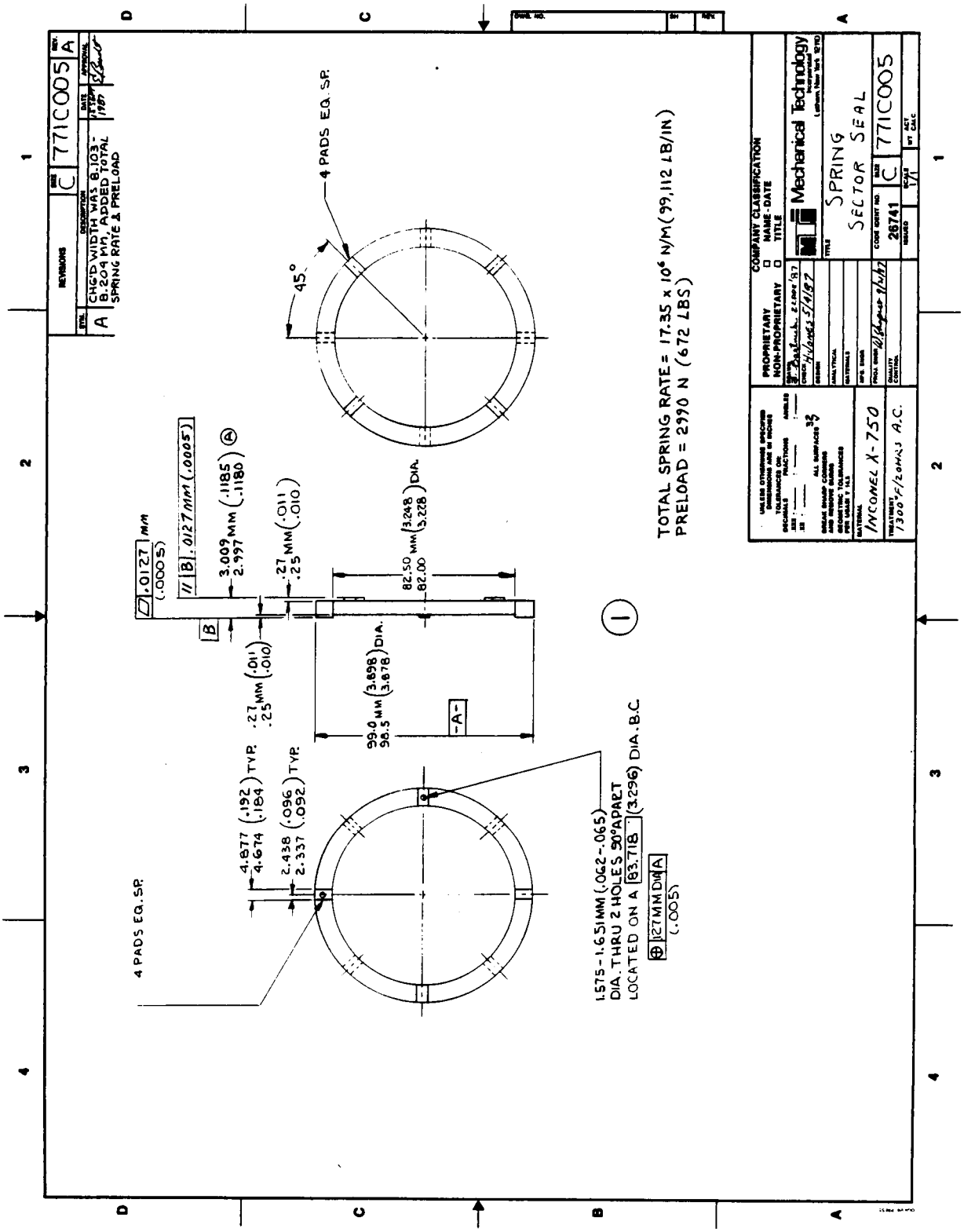

Figure 4-21 Sectored Seal Preload Spring

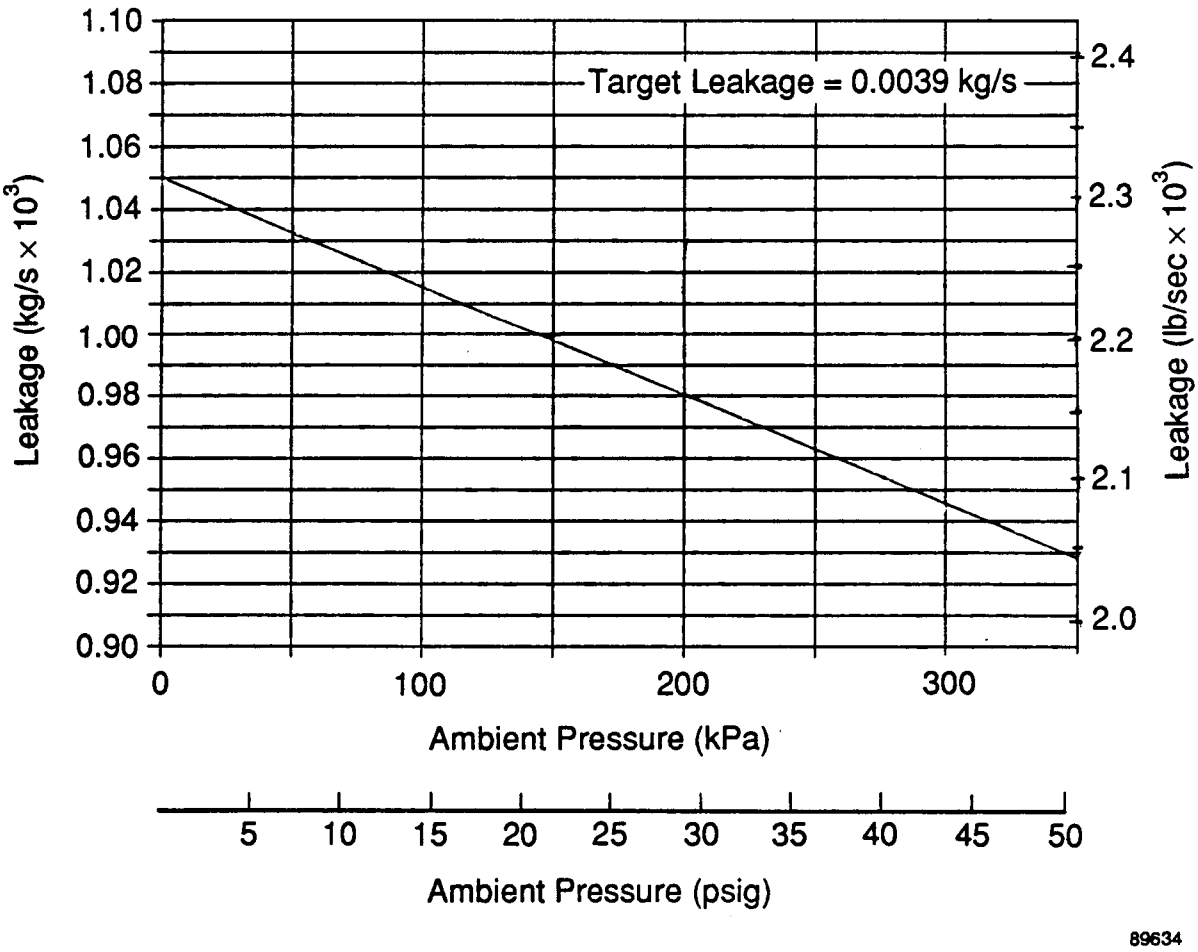

Figure 4-22 Sectored Seal; Total Leakage vs. Ambient Pressure

5.0 FLOATING-RING SEALS

5.1 Configuration and Principle of Operation

Figure 5-1 shows a schematic representation of a helium-buffered, floating-ring seal. The seal consists of two rings that are mounted back-to-back. The helium buffer fluid enters between the rings and forces the rings up against the stationary housing. The buffer fluid leaks in the clearance annulus between the shaft and the seal and prevents ingress of exterior fluid on either side of the floating-ring assembly.

The rings are held in equilibrium by a number of forces as shown in Figure 5-1. A hydraulic pressure closing force, F_C, from the inlet buffer fluid forces the rings up against the housings. This pressure force is balanced part way on the housing sides of the rings by the pressure balance force, F_B. A hydrodynamic force, F_H, is generated by rotation between the shaft and the ring. The net hydrodynamic force is zero when the shaft and rings are in the concentric position. However, when the ring becomes eccentric with respect to the shaft, a hydrodynamic force is built up that opposes the eccentricity. There is also a normal contact force, F_N, acting on the ring at the contact area between the ring and the housing. Generally, F_N is maintained as small as possible to minimize frictional resistance forces. To minimize F_N, F_B should be as large as possible. Therefore, the contact area is small and is located as close to the shaft as is practicable, but with sufficient housing clearance to permit shaft excursions without contact. In addition to the equilibrium forces mentioned above, there is a friction force, F_f, between the seal ring and housing.

5.2 Interface Geometries Considered

Several interface geometries were analyzed and considered for the SSME application. Comparative performance studies were made, and one configuration was selected for detail design. The four basic configurations selected, schematically shown in Figures 5-2 and 5-3, are:

1. Axial taper (AT)
2. Axial step (AS)
3. Rayleigh step, circumferential (RS)
4. Self-energized hydrostatic (SE)

Both the axial taper and axial step geometries were optimized for clearance and length ratios on the basis of stiffness. The Rayleigh-step, circumferential configuration utilized the same geometry as supplied on a prior program [1], since that geometry had already been optimized for step height and step length. Optimization of the self-energized hydrostatic concept was done by a few iterations of the axial position of the recess until satisfactory flow, stiffness, and orifice size were obtained. Practical variations in parameters for the self-energized seal were very limited so that optimization was readily accomplished. All of the optimization studies were accomplished with the computer code GJOURN [7,8].

5.3 Optimization of Axial-Tapered Seal

Optimization studies were conducted at varying values of clearance and pressure differential and at varying ratios of leading to trailing edge clearance and tapered length (LT) to total length (L) (see Figure 5-3); results are indicated in Table 5-1. The performance parameters considered were leakage, stiffness, and stiffness ratio. The stiffness ratio is the cross-coupled stiffness divided by the direct stiffness and is a measure of the stability characteristics of the seal ring. The higher this ratio, the more tendency there is for the ring to whirl.

The third column, LT/L, is the ratio of the tapered region length to the total length of the seal. Three ratios were investigated; 0.25, 0.35, and 0.5. The following columns are the clearance ratios, taper clearance to reference clearance (CT/C) (see Figure 5-3), or the leading to trailing edge clearance ratio of the taper. Three values of clearance ratio were investigated; 2, 4, and 10. Variations in length and clearance ratios were accomplished as a function of the supply pressure and reference clearance. Perusal of these data reveals the following:

- At C = 0.0254 mm (0.001 in.) and P_S = 1379 kPa (200 psig), the flow rates can exceed target values. Since ring seals operate in pairs, total leakage is obtained by doubling the numbers indicated. The target value for a single seal is 1.95×10^{-3} kg/sec (4.3×10^{-3} lb/sec). The calculated numbers either exceed the target or do not provide a sufficient safety margin. Therefore, C = 0.0254 mm (0.001 in.) and P_S = 1379 kPa (200 psig) is a combination that is eliminated on the basis of excessive leakage.

- When stiffness is considered, the C = 0.0254 mm (0.001 in.) and P_S = 689 kPa (100 psig) can be eliminated because of low values. Optimum stiffness occurs when C = 0.0127 mm (0.0005 in.) and P_S = 1379 kPa (200 psig), with a length ratio of 0.5 and a clearance ratio of 2.

- Stiffness ratios above 1.0 should be avoided to prevent destabilizing tendencies. The C = 0.0127 mm (0.0005 in.), P_S = 689 kPa (100 psig) cases are the worst offenders.

From the data produced, the low-clearance, high-pressure condition is best (C = 0.0127 mm (0.0005 in.)), P_S = 1379 kPa (200 psig), with a length ratio of 0.5 and a clearance ratio of 2.0. This was the basic configuration to which further design studies were made.

5.4 Optimization of the Axial-Step Seal

The axial step seal was optimized in a manner similar to the axial taper seal except the step height and step length were the parameters varied in lieu of taper height and length. Results are indicated in Table 5-2. The selective process was identical to that of the axial tapered seal. The optimum geometry incorporated a step height of 0.0127 mm (0.5 mil) and a step length equal to half of the seal length.

5.5 Comparative Steady-State Performance of the Four Types of Ring Seals

The optimization studies discussed above were conducted prior to design, so that the dimensions used for the optimization were not those finally selected. However, the ratios remained the same. The actual dimensions used for all four seals are shown in Figure 5-1.

For captured ring seals, the radial clearance can be expected to vary because of centrifugal and thermal growths. Thus, it was used as the independent parameter for comparing performance of the four types of ring seals that were evaluated. In addition to clearance as an independent parameter, supply and downstream pressures were also varied. The supply pressures considered were 1379 kPa (200 psig) and 689 kPa (100 psig) with downstream pressures of 345 kPa (50 psig) and 0 kPa.

The unbalanced secondary seal (See Figure 5-1) area of the seal ring is 1.757×10^{-4} m^2 (0.272 $in.^2$). At a coefficient of friction of 0.2, the secondary seal radial friction forces are:

24.23 N (5.45 lb) at 689 kPa (100 psi) Supply Pressure
48.46 N (10.89 lb) at 1379 kPa (200 psi) Supply Pressure

Table 5-3 indicates the eccentricity ratio required to overcome the friction force for the various seals as a function of supply pressure and clearance.

Although not all pressure levels were considered for each seal type, the results will not vary much. As the pressure level increases, load capacity increases, as does the friction force to be overcome, so that the eccentricity, ϵ, and minimum film thickness, h_m, will remain about the same. The results indicate that the self-energized hydrostatic seal is the best performer with regard to overcoming friction because it does so with the smallest journal displacement (eccentricity) and largest minimum film thickness. The reason that a 0.0127-mm (0.0005-in.) clearance is not indicated for the self-energized seal is that the hydrostatic pressure ratio is unfavorable for that small a clearance (i.e., the recess pressure approaches the supply pressure degrading stiffness and performance). To produce an acceptable pressure ratio would require an unacceptably small orifice diameter. Thus, the self-energized seal must be designed to operate at clearances of 0.0191 mm (0.8 mil) and above. Load capacity curves for the various types of seals are shown in Figures 5-4 through 5-7.

Several interesting phenomena are indicated by these curves. For the axial taper seal (Figure 5-4), the load capacity does not vary significantly with clearance for the low value of eccentricity ratio. Differentiation occurs after eccentricity ratios of 0.6, where the low clearance seals have higher load capability. For most of the operating range, however, the larger clearance provides the higher minimum film thickness, which is a more significant criterion than eccentricity ratio since it is the film thickness that provides the margin against contact. For the axial step seal (Figure 5-5), the lower clearances have less load capacity at the lower eccentricity ratio and higher load capacity at the higher eccentricity ratios. The general level of load capability is less than that of the axial taper seal. Load capacity of the circumferential Rayleigh-step seal is shown in Figure 5-6. Performance is very sensitive to clearance, and as the clearance increases, performance falls

off rapidly. Since it would be difficult to maintain an optimum clearance ratio throughout the operating range, it would not appear to be a good candidate from the standpoint of load capability. Load capacity of the self-energized seal with a 1379-kPa (200-psig) pressure differential is excellent, as indicated in Figure 5-7.

Further comparative studies were made on the basis of leakage, stiffness, and viscous power loss. These were accomplished at various differential pressures across the seal. The results are indicated in Figures 5-8 through 5-16 as a function of the concentric radial clearance. Examination of these results produces the following conclusions:

- The Rayleigh-step circumferential seal has the highest leakage. Total leakage values will be twice the values shown in the figures because there are two rings to a seal assembly. Even at a pressure differential of 689 kPa (100 psig), leakage is beyond target values.

- The self-energized hydrostatic rings have significantly superior stiffness over the other types of ring seals. However, at a supply pressure of 689 kPa (100 psig), the self-energized hydrostatic seal performance deteriorates rapidly with eccentricity. At a pressure level of 1379 kPa (200 psig), performance is excellent over a wide range of eccentricity and clearance.

- The power loss, as indicated in Figure 5-16, is mostly a function of clearance, surface area, and speed. The effect of pressure level is not significant. The self-energized seal has the highest power loss, although it is not significantly higher than the other types. Also, power loss is not as important a parameter as stiffness or leakage.

On the basis of stiffness and leakage considerations, the self-energized hydrostatic seal is the best performer, with a supply pressure of 1379 kPa (200 psig). It was thus selected for detail design and further analysis.

5.6 Dynamic Analysis of Ring Seals

Dynamic analysis of the self-energized hydrostatic ring seals was accomplished with the computer code RINGDY, which had been supplied to NASA on a proprietary basis, for a previous program [1]. RINGDY is a seal ring dynamics computer code that integrates the equations of motion of the ring in two dimensions. It accounts for both the frictional force between the ring and the housing and the fluid-film force between the ring and the shaft runner. The components of this latter force are interpolated versus eccentricity ratio and attitude angle from a table that is generated by the fluid-film code GJOURN.

A shaft eccentricity or runout of 0.0127 mm (0.0005 in.) was applied (i.e., peak-to-peak amplitudes were 0.0254 mm (0.001 in.). Results are shown in Figures 5-17 and 5-18 for seal radial clearances of 0.0191 mm (0.00075 in.) and 0.0254 mm (0.001 in.), respectively. Shown are orbit plots that indicate the eccentricity ratios (εy and εx) with respect to the clearance circle. The initial condition was the concentric position of the seal ring with respect to the journal.

For the case of C = 0.0191 mm (0.00075 in.), the orbit settles to an eccentricity of approximately 0.37, or 37% of the concentric clearance is consumed in the process of forcing the rings to follow the excursions of the shaft. For the higher clearance case, the orbit is circular with an eccentricity of approximately 0.5. In either case, dynamic response is very acceptable.

5.7 Thermoelastic Distortions of Ring Seals

The boundary conditions for the thermal analyses were taken from Reference [6], which was provided by NASA-LeRC. Figure 5-19, extracted from the referenced report, is a temperature map of the SSME at the turbine end at full power level conditions. The temperature map indicates a very large thermal gradient across the helium seal (946-414°R, ΔT = 532°R, 296°C). These thermal boundary conditions were applied in computing thermoelastic distortions. Thermoelastic distortions of the ring seals were conducted by use of the commercial finite-element program ANSYS.

The mathematical model, including the nodal points, is shown in Figure 5-20. The model consists of the housing surrounding the seal, the carbon rings themselves, the shaft sleeve at the ID of the seals, and the helium gas considered stationary. The housing and sleeve are made from nickel alloy Waspalloy. The temperature boundary conditions are also indicated on the figure. A linear drop was assumed across the housing from high to low temperature. Full pressure of 1379 kPa (200 psig) was applied to the carbon rings at its exterior surfaces, up to the secondary sealing dam. A linear axial pressure drop from 1379 kPa (200 psig) to 0 was assumed at the ID of the carbon rings from the inboard to outboard ends. Temperature and pressure effects were determined independently and then superimposed to obtain total distortions. The most important determination is what happens to the clearance distribution across the seals due to thermal and pressure distortions.

The factors that influence the variation in clearance distribution are:

- Variation in the radial dimension of the shaft sleeve due to centrifugal growth and thermal contraction
- Variation in the seal ring IDs due to temperature and pressure effects.

The temperature distribution across the two ring seals is shown in Figure 5-21. The hot side ring is exposed to large thermal gradients, while the oxygen side ring has only moderate temperature gradients across it. Computed dimensional variations in the ID of the rings and the OD of the sleeves are indicated in Figure 5-22, and the changes in clearance distribution are indicated in Figure 5-23. For both rings, the clearance variation causes a converging wedge in the direction of flow, which is an advantageous factor since it will provide additional load capability. Also note that the clearance in the hot end ring will open substantially more than that of the cold side. Table 5-4 identifies the mean clearances that will result for various room temperature installation clearances. An ideal operating clearance is about 0.0178 mm (0.0007 in.) but because of the converging tapers, an allowable value to 0.0254 mm (0.001 in.) would be acceptable. Because of the large temperature differences between the cold side and hot side rings, which produce different operating clearances, they should not be installed with identical clearances.

The hot side ring needs to have a tighter clearance than the cold side ring. From an examination of Table 5-4, the recommended manufactured (installation) diametral clearances are as follows:

- Cold end, oxygen side seal, diametral clearance: 0.0152 mm ±0.003 mm (0.0006 in. ±0.0001 in.)

- Hot end, hydrogen steam side, diametral clearance: 0.0102 mm ±0.003 mm (0.0004 in. ± 0.0001 in.)

5.8 Ring Seal Design

The general arrangement of the ring seals in the oxidizer pumps is shown in Figure 5-24. The principal constituents are the two opposite hand ring seals, items 1 and 2, which mate up against a housing. The rings are separated by a wave spring, item 3, and by hydraulic pressure. A sleeve, item 5, is attached to the rotating shaft and mates up against the ID of the seal rings. A mounting sleeve, item 4, holds the runner in place on the shaft. MTI designed and detailed items 1 through 5. The housings are similar to those presently employed on the SSME and were not detailed. It is anticipated that the rings will be tested in a separate test facility that will incorporate different housings. As noted on the assembly drawing (Figure 5-24), the surfaces of the housing that mate with the rings should be coated with chrome carbide and have a final surface finish of 0.2 microns (8 μin.). The axial envelope for the ring installation is also indicated on the figure.

The seal rings are shown in Figure 5-25. The rings are made from carbon graphite, P-5N. Four recesses are milled into the interior of the ring to an average depth of 0.0889 mm (0.0035 in.). Orifice restrictors are epoxied into radial holes that individually feed each of the recesses. The secondary seal is composed of a protruding lip at the ID of the ring that mates with the housing. The protrusion is 0.788 mm (0.031 in.) wide. The mating sleeve, item 5 in Figure 5-24, is held in place by a spring mounting sleeve that is shrink fitted to the shaft. The sleeve, in turn, is shrink fitted to the mounting sleeve. The mounting sleeve will compensate for centrifugal and thermal expansions and contractions of the sleeve and maintain appropriate contact with the sleeve at all times. Detail drawings of the ring seal components are included as Figures 5-26 through 5-28.

5.9 General Conclusions Concerning the Ring Seal Design

Comparative performance studies indicated that the self-energized hydrostatic seal is the preferred configuration for the application. It has significantly greater stiffness than the other types with little compromise in flow and power loss.

The supply pressure for the self-energized hydrostatic seal is required to be 1379 kPa (200 psig) to produce an acceptable ratio of recess pressure to supply pressure and to have a reasonable orifice diameter. Anticipated performance of the self-energized hydrostatic seal is indicated in Table 5-5. An average operating clearance of 0.0191 mm (0.0008 in.) is assumed in this tabulation.

To provide proper operating clearances, the ring seals must be installed with very tight clearances. This imposes difficult manufacturing requirements on the ID of the seal rings and the OD of the mating sleeve. Satisfactory performance would occur even if the rings were installed line to line without clearance. Thus, it might be appropriate to match set the rings and sleeve and use the sleeve itself to obtain the final bore dimensions of the rings.

TABLE 5-1

OPTIMIZATION STUDIES - AXIAL TAPERED
(D = 68 mm; L = 20 mm)

P_S (kPa)	C (mm)	LT/L	CT/C 2	CT/C 4	CT/C 10
			Leakage,* kg/sec x 10^3		
1379	0.0254	0.25	1.563	1.686	1.734
		0.35	1.688	1.892	1.989
		0.5	1.936	2.358	2.572
1379	0.0127	0.25	0.1954	0.2108	0.2168
		0.35	0.2111	0.2365	0.2487
		0.5	0.2420	0.2947	0.3215
689	0.0254	0.25	0.4409	0.4756	0.4891
		0.35	0.4762	0.5336	0.5611
		0.5	0.5459	0.6649	0.7253
689	0.0127	0.25	0.05511	0.05945	0.0611
		0.35	0.05953	0.06670	0.0701
		0.5	0.06825	0.08312	0.0906
			Stiffness, N/m x 10^{-6}		
1379	0.0254	0.25	2.915	1.646	0.3305
		0.35	4.001	2.463	0.6299
		0.5	5.925	3.924	0.9325
1379	0.0127	0.25	6.327	3.623	0.9467
		0.35	8.369	5.121	1.406
		0.5	12.1	7.928	1.907
689	0.0254	0.25	1.550	0.8776	0.1895
		0.35	2.111	1.299	0.3366
		0.5	3.112	2.061	0.4910
689	0.0127	0.25	4.003	2.360	0.8945
		0.35	4.893	2.955	0.9407
		0.5	6.684	4.267	1.060

*Target = 1.95×10^{-3}

TABLE 5-1 Continued

PS (kPa)	C (mm)	LT/L	CT/C 2	CT/C 4	CT/C 10
			Stiffness Ratio, K_{xy}/K_{xx}		
1379	0.0254	0.25	0.3444	0.4769	2.138
		0.35	0.2139	0.2352	0.7557
		0.5	0.1158	0.0901	0.2459
1379	0.0127	0.25	1.2641	1.7182	5.9544
		0.35	0.8155	0.9033	2.701
		0.5	0.4526	0.3566	0.9612
689	0.0254	0.25	0.6448	0.8854	3.7821
		0.35	0.4036	0.4436	1.4058
		0.5	0.2197	0.1709	0.4640
689	0.0127	0.25	1.969	2.606	6.229
		0.35	1.378	1.526	4.0023
		0.5	0.8118	0.6583	1.7160

TABLE 5-2

OPTIMIZATION STUDIES - AXIAL STEP
(D = 68 mm; L = 20 mm)

P_S (kPa)	C (mm)	LT/L	CT/C 1.5	CT/C 2.0	CT/C 2.5
			Leakage,* kg/sec x 1000		
1379	0.0254	0.25	1.585	1.672	1.705
		0.35	1.733	1.882	1.942
		0.5	2.015	2.322	2.455
1379	0.0127	0.25	0.1981	0.2090	0.2131
		0.35	0.2166	0.2353	0.2427
		0.5	0.2519	0.2902	0.3068
689	0.0254	0.25	0.4470	0.4715	0.4809
		0.35	0.4887	0.5309	0.5478
		0.5	0.5683	0.6548	0.6924
689	0.0127	0.25	0.05587	0.05893	0.0601
		0.35	0.06109	0.06637	0.0684
		0.5	0.07104	0.08185	0.0865
			Stiffness, N/m x 10^{-6}		
1379	0.0254	0.25	3.177	2.188	1.390
		0.35	4.592	3.309	2.136
		0.5	6.816	5.376	3.602
1379	0.0127	0.25	6.83	4.73	3.106
		0.35	9.544	6.835	4.463
		0.5	13.910	10.870	7.299
689	0.0254	0.25	1.686	1.163	0.7431
		0.35	2.421	1.745	1.128
		0.5	3.581	2.825	1.894
689	0.0127	0.25	4.241	2.972	2.069
		0.35	5.499	3.886	2.585
		0.5	7.669	5.863	3.931

*Target = 1.95×10^{-3}

TABLE 5-2 Continued

			CT/C		
PS (kPa)	C (mm)	LT/L	1.5	2.0	2.5
			Stiffness Ratio, K_{xx}/K_{xy}		
1379	0.0254	0.25	0.3125	0.3765	0.5480
		0.35	0.1869	0.1926	0.2586
		0.5	0.1071	0.0849	0.0955
1379	0.0127	0.25	1.158	1.3888	1.9569
		0.35	0.7174	0.7446	0.9892
		0.5	0.4187	0.3355	0.3774
689	0.0254	0.25	0.5864	0.7052	1.02
		0.35	0.353	0.363	0.4871
		0.5	0.2032	0.1610	0.1808
689	0.0127	0.25	1.8401	2.184	2.904
		0.35	1.231	1.297	1.692
		0.5	0.7527	0.6184	0.6965

TABLE 5-3

ECCENTRICITY RATIO AND MINIMUM FILM THICKNESS
TO OVERCOME SECONDARY SEAL FRICTION FORCES

Seal Type	P_S kPa (psi)	C mm (mil)	ε	h_m mm (mil)
AT	689 (100)	0.0127 (0.5) 0.0191 (0.75) 0.0254 (1.0)	0.48 0.51 0.53	0.0066 (0.26) 0.0094 (0.37) 0.0119 (0.47)
AS	689 (100)	0.0127 (0.5) 0.0191 (0.75) 0.0254 (1.0)	0.52 0.57 0.61	0.0061 (0.24) 0.0082 (0.32) 0.0099 (0.39)
RS	689 (100)	0.0127 (0.5) 0.0191 (0.75) 0.0254 (1.0)	0.50 0.72 0.84	0.0064 (0.25) 0.0053 (0.21) 0.0041 (0.16)
SE	1379 (200)	0.0191 (0.75) 0.0254 (1.0)	0.23 0.41	0.0147 (0.58) 0.0150(0.59)

TABLE 5-4

RING SEAL RADIAL CLEARANCE

Installation (Room Temperature)						
mm mils	0.0051 0.2	0.0076 0.3	0.0102 0.4	0.0127 0.5	0.0152 0.6	0.0178 0.7
Operating (Cold End)						
mm mils	0.0152 0.6	0.0178 0.7	0.0203 0.8	0.0229 0.9	0.0254 1.0	0.0279 1.1
Operating (Hot End)						
mm mils	0.0279 1.1	0.0305 1.2	0.0330 1.3	0.0356 1.4	0.0381 1.5	0.0406 1.6

TABLE 5-5

SELF-ENERGIZED HYDROSTATIC RING SEAL
PERFORMANCE AND GEOMETRICAL PARAMETERS

Mean Operating Clearance, mm (in.)	0.0191 (0.0008)
Buffer Pressure, kPa (psig)	1379 (200)
Ambient Pressure, kPa (psig)	0 (0)
Wall Friction, N (lb)	48 (10.79)
Eccentricity Ratio to Overcome Wall Friction	0.24
Leakage, Two Rings (ΔP = 1379 kPa), kg/s (lb/sec)	2.8×10^{-3} (6.17×10^{-3})
Stiffness, N/m (lb/in.)	10×10^{6} (5.71×10^{4})
Power Loss, Two Rings, W (hp)	56 (0.075)

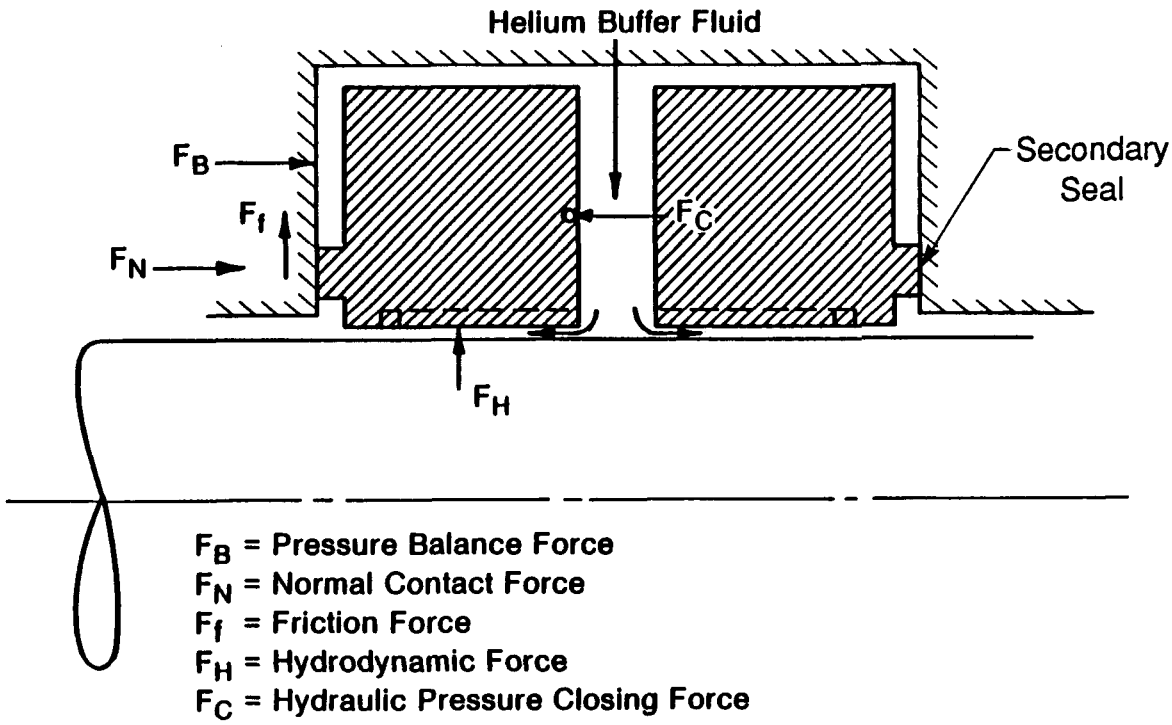

Figure 5-1 General Arrangement of Floating Ring Seals

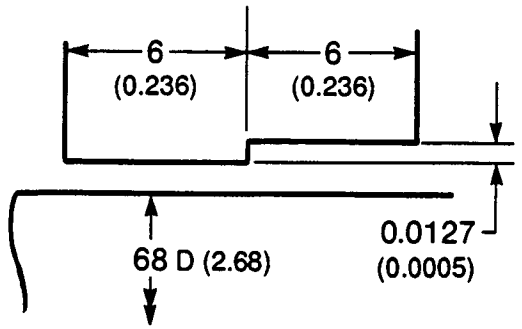

1. Axial Step (AS)

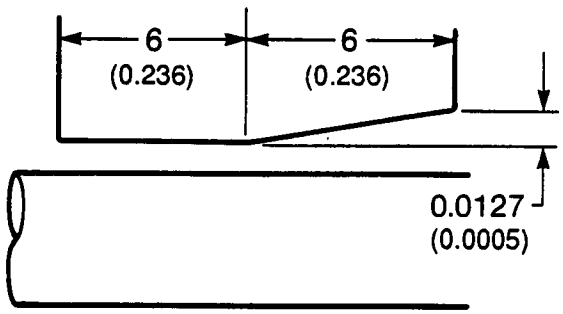

2. Axial Tapered (AT)

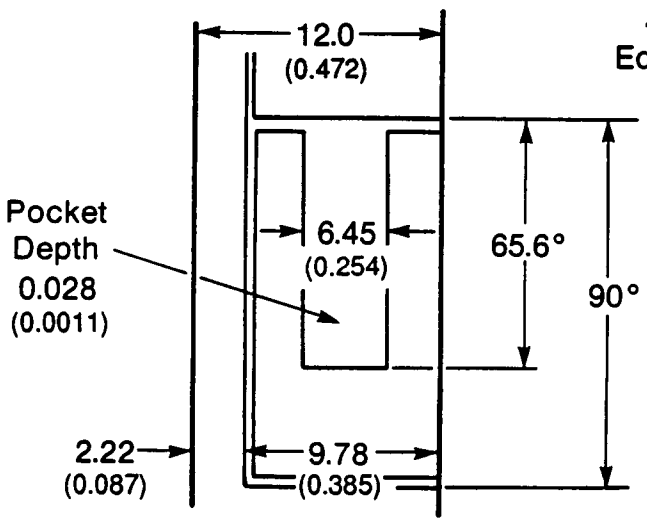

3. Rayleigh Step (RS)

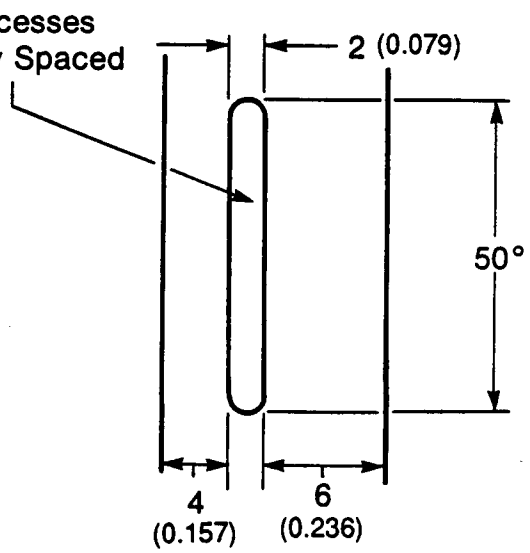

4. Self-Energized Hydrostatic (SE)

Dimensions in mm (in.)

Figure 5-2 Floating Ring Seal Interface Geometries

1. Optimization Axial Step Seal

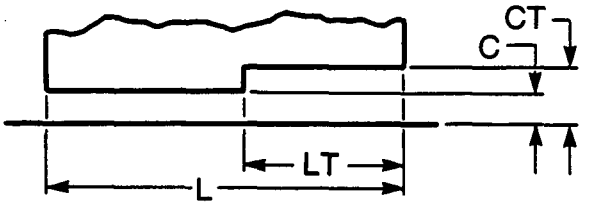

CT/C	LT/L
1.5	0.25
2.0	0.35
2.5	0.50

2. Optimization Axial Tapered Seal

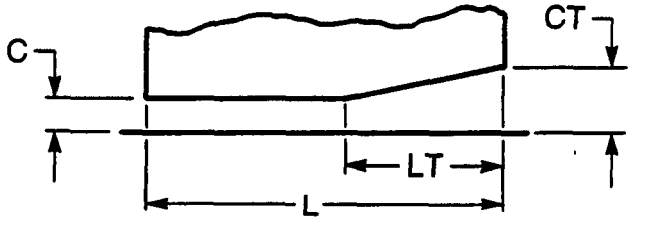

CT/C	LT/L
2.0	0.25
4.0	0.35
10.0	0.50

3. Use Optimized Valules from Reference 1 Rayleigh Step Seal

4. Optimization Self-Energized Hydrostatic Seal
   - P_s = 689 kPa (100 psig), 1379 kPa (200 psig)
   - Orifice Location
   - Orifice Size

CT = Tapered Clearance
C = Reference Clearance
LT = Tapered Length
L = Length

872557

Figure 5-3 Initial Optimization Studies, Floating Ring Seals

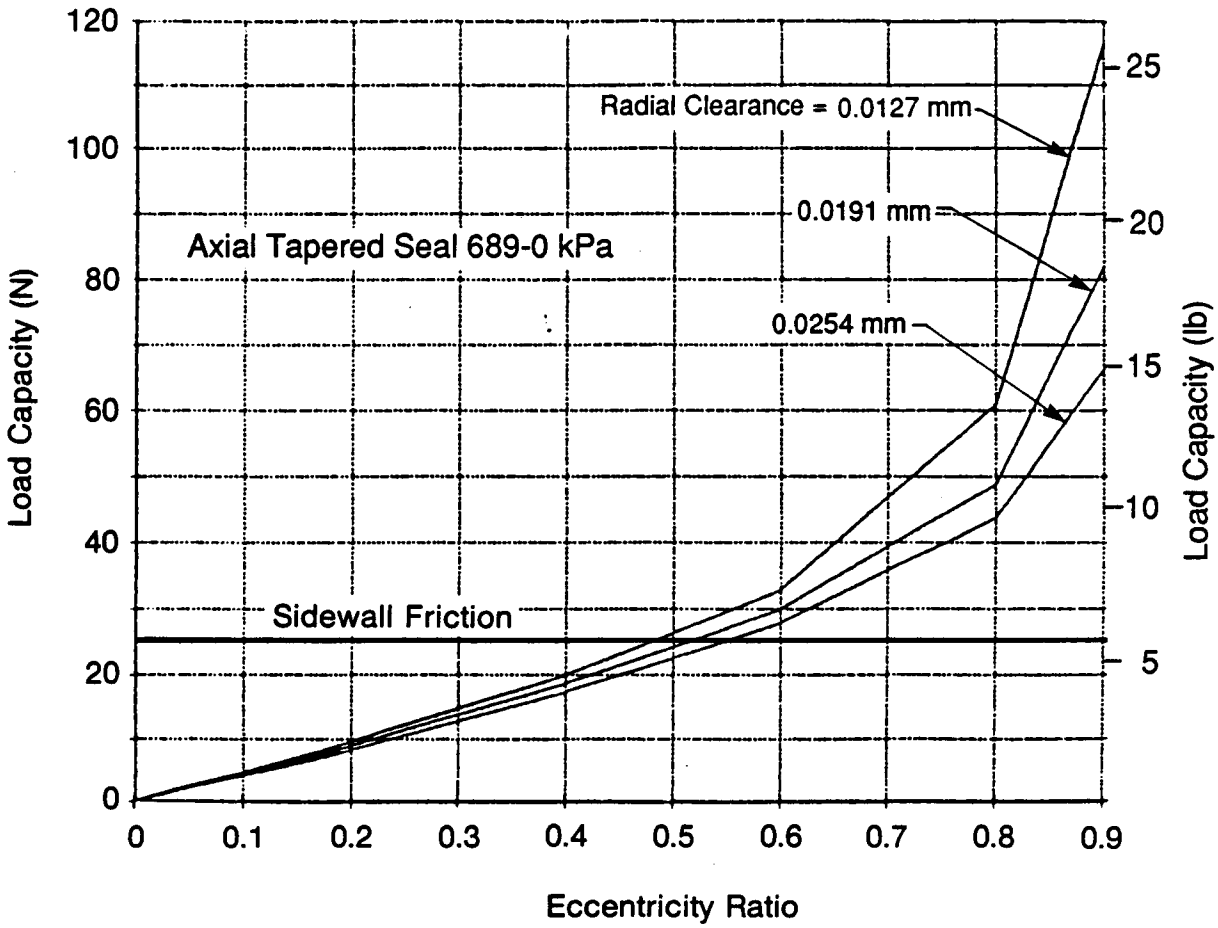

Figure 5-4 Load Capacity vs. Eccentricity Ratio, Axial Tapered Seal

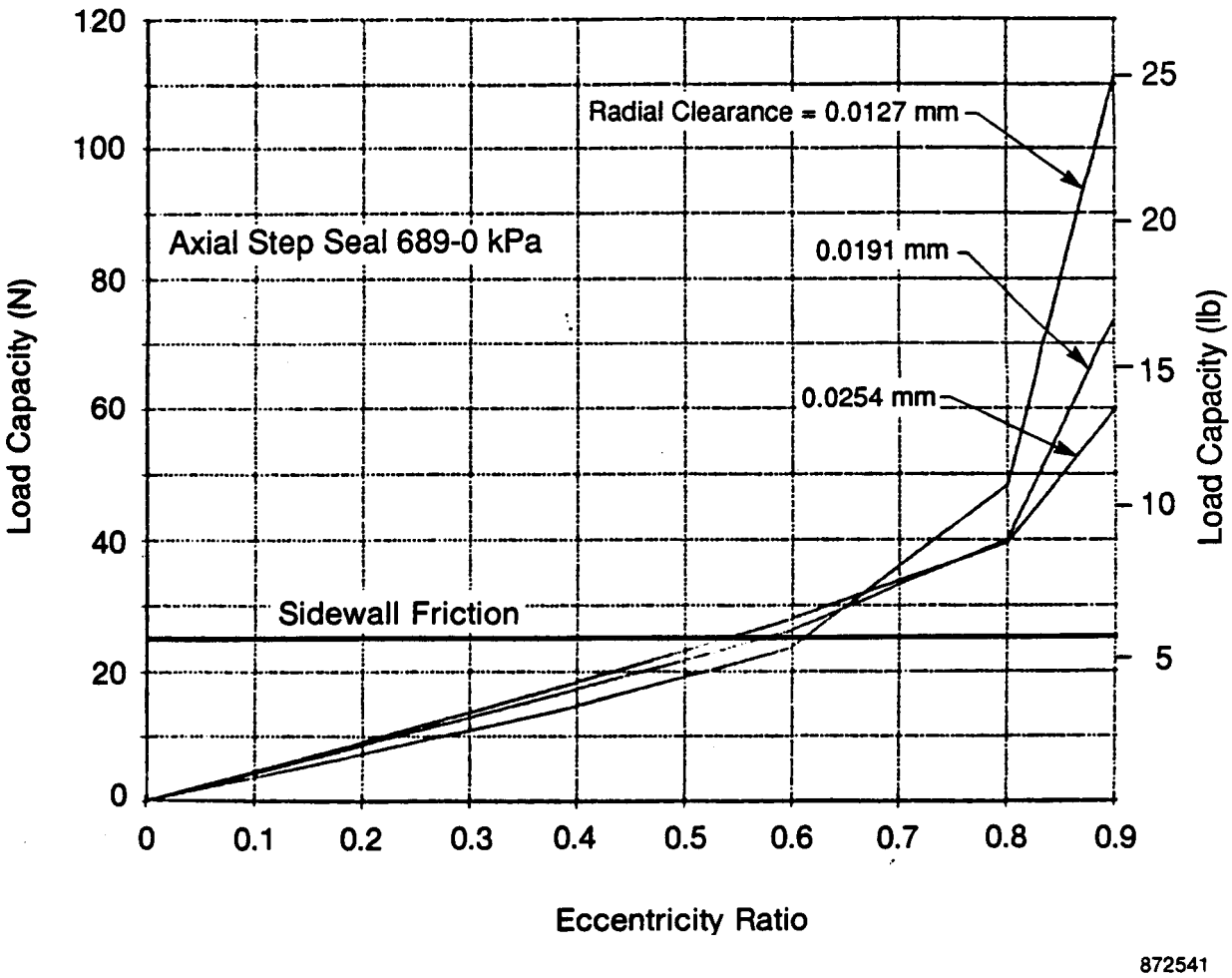

Figure 5-5 Load Capacity vs. Eccentricity Ratio, Axial Step Seal

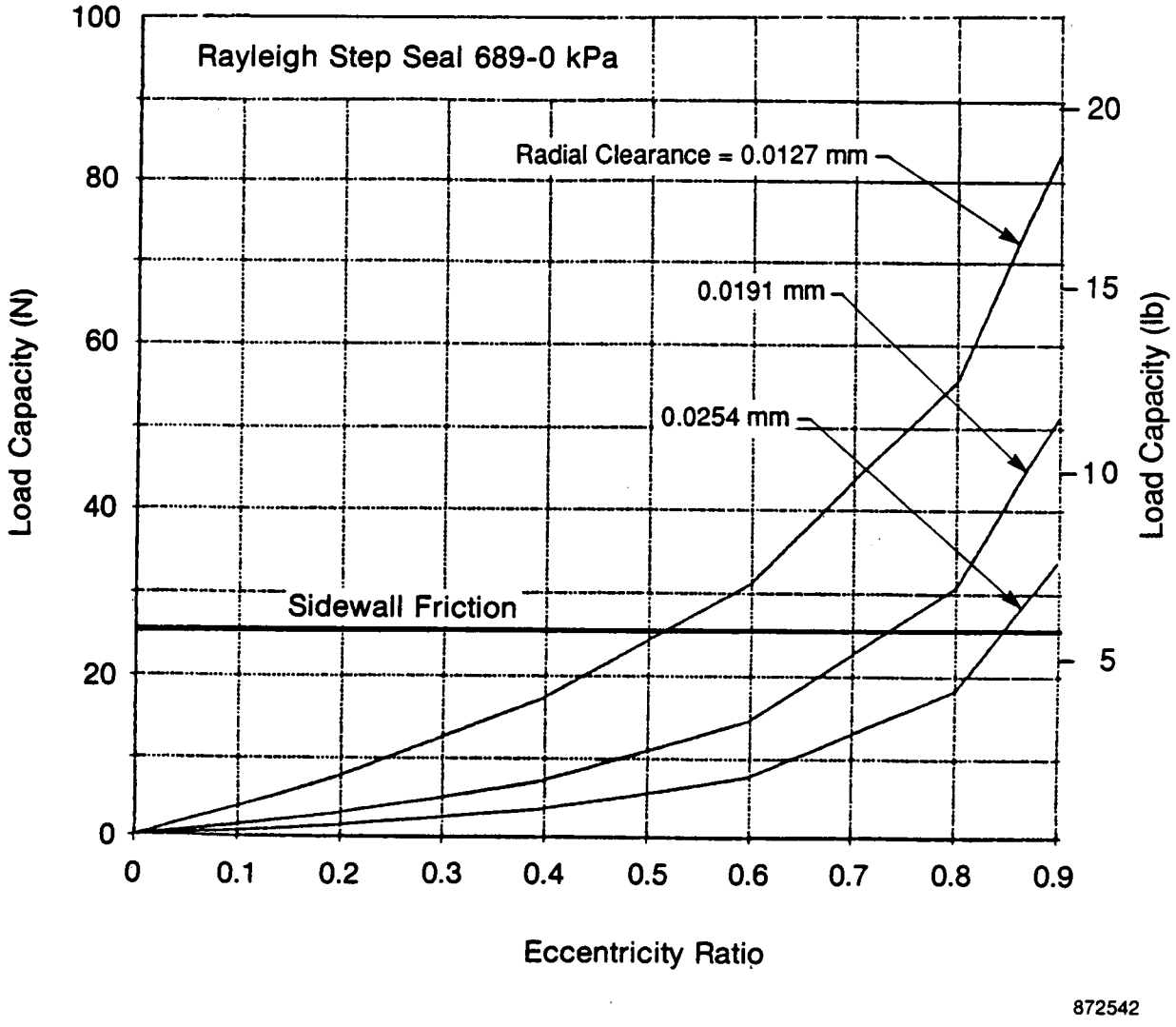

Figure 5-6 Load Capacity vs. Eccentricity Ratio, Rayleigh Step Seal

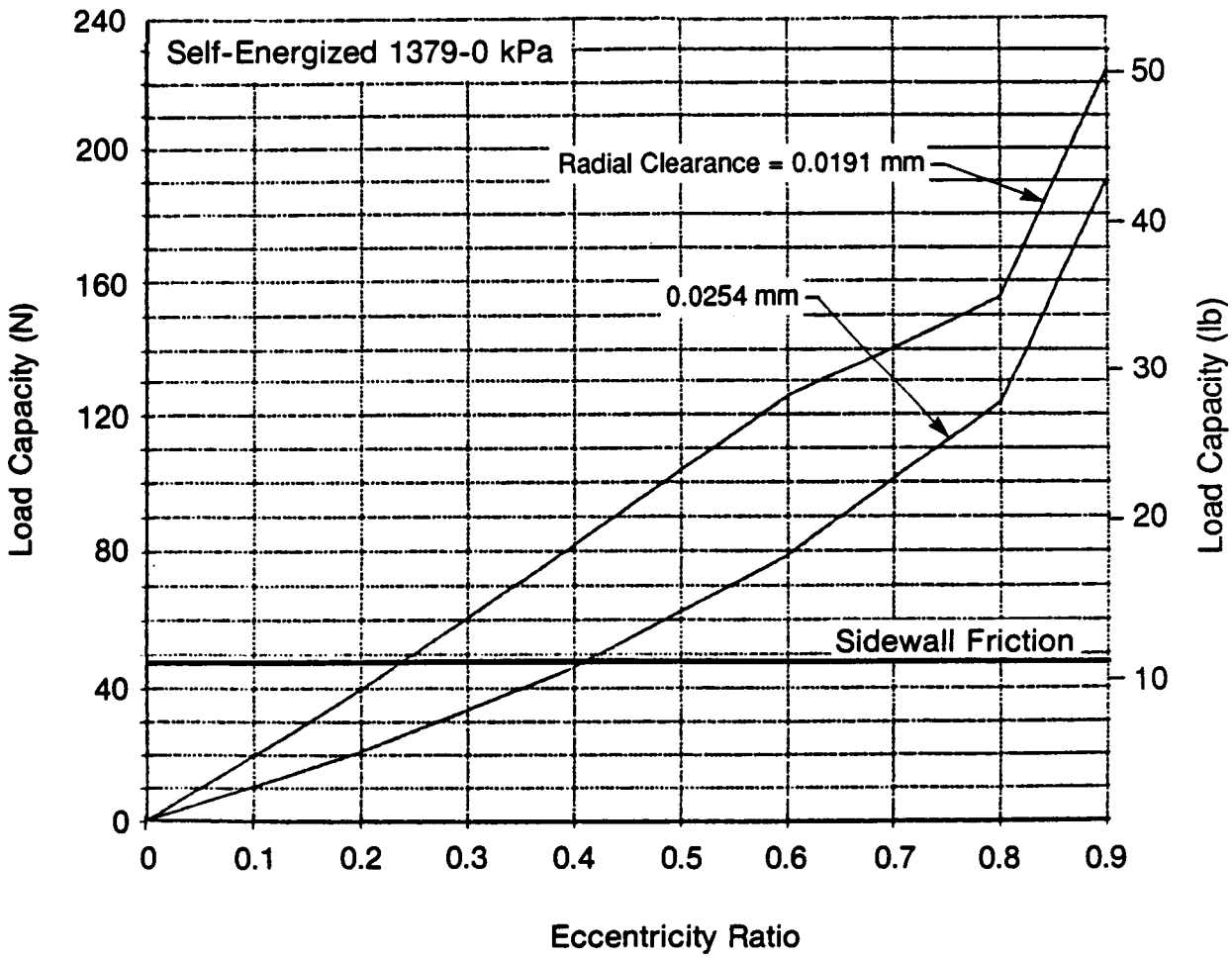

Figure 5-7 Load Capacity vs. Eccentricity Ratio, Self-Energized Hydrostatic Seal

872543

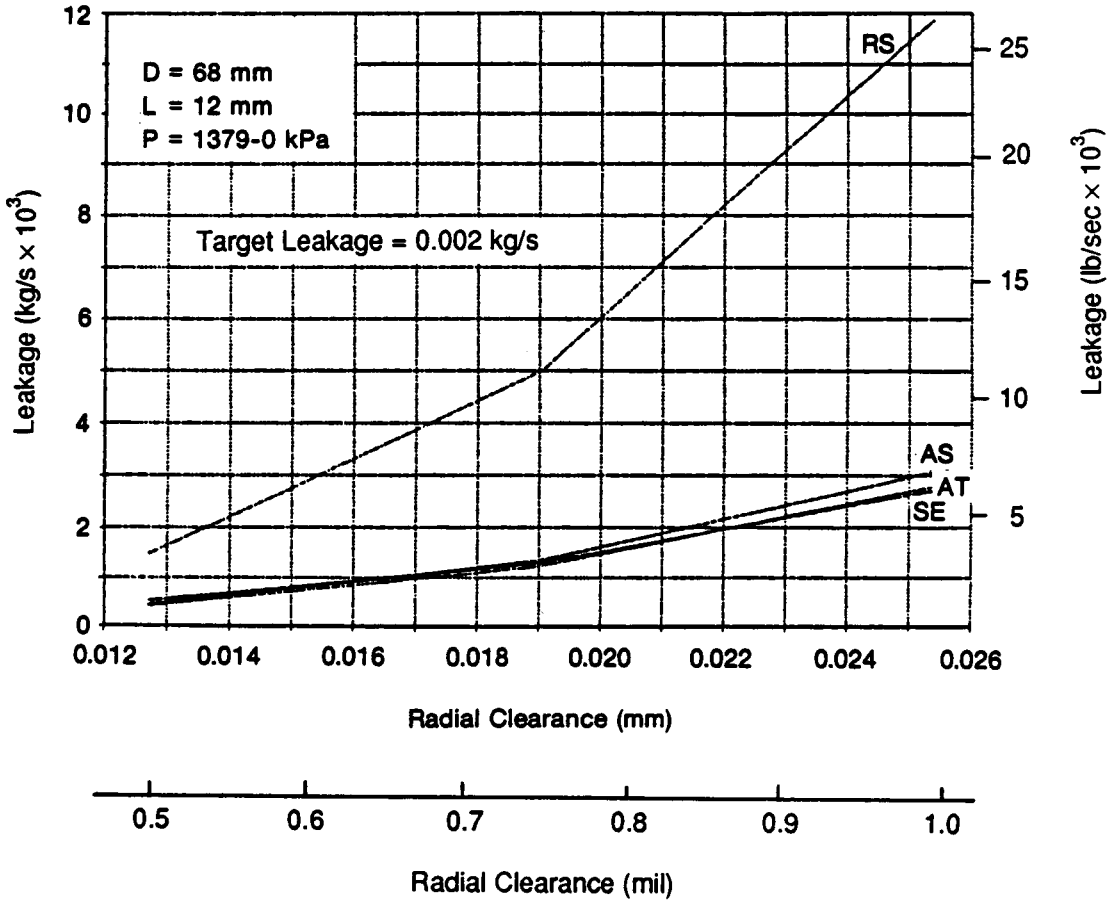

Figure 5-8 Ring Seal Comparative Performance (Single Ring); Leakage vs. Radial Clearance (ΔP = 1379 kPa)

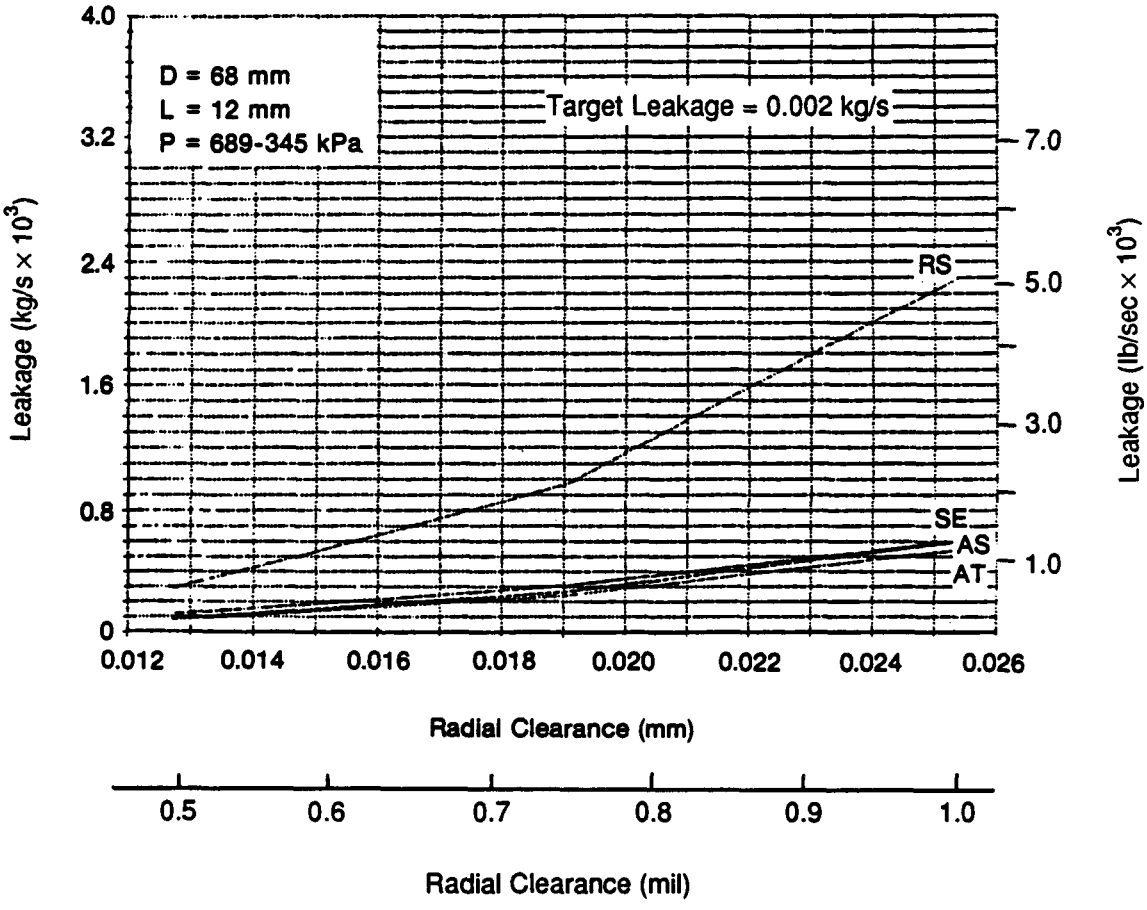

Figure 5-9 Ring Seal Comparative Performance (Single Ring); Leakage vs. Radial Clearance (ΔP = 345 kPa)

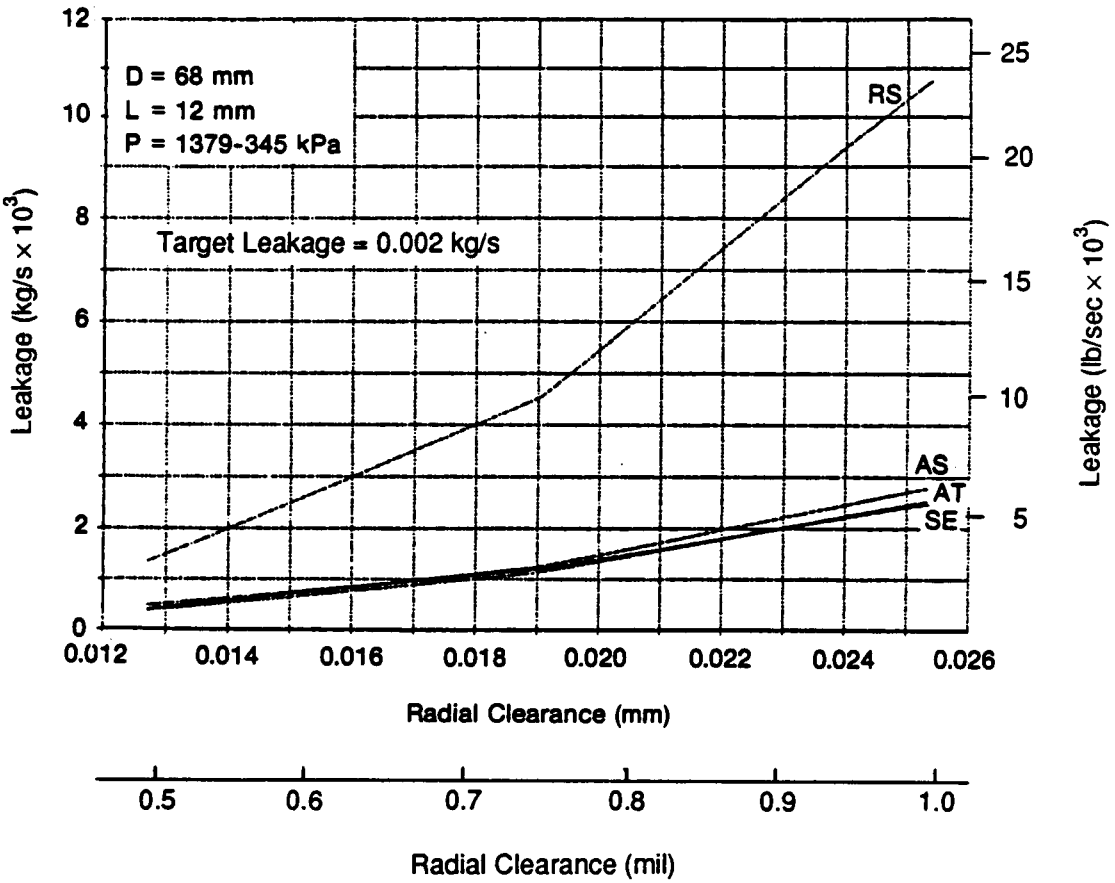

Figure 5-10 Ring Seal Comparative Performance (Single Ring); Leakage vs. Radial Clearance (ΔP = 1034 kPa)

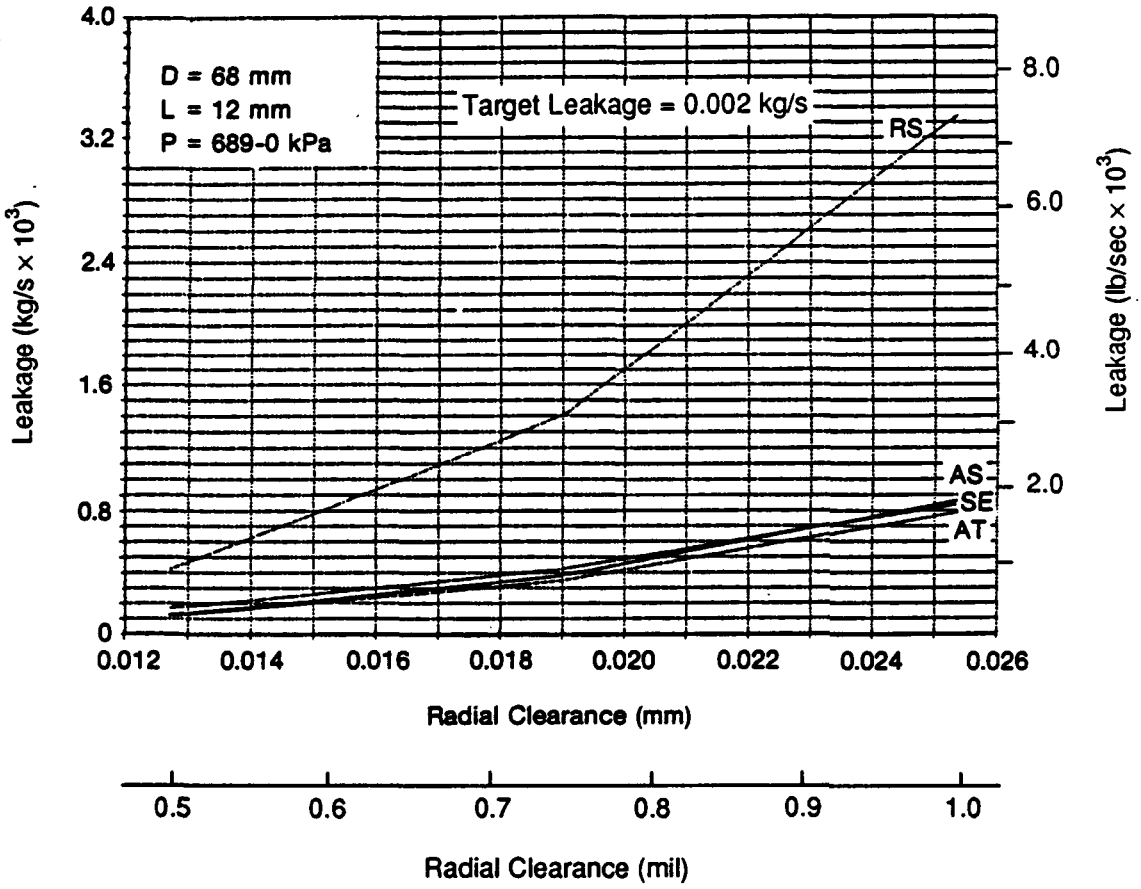

872547

Figure 5-11 Ring Seal Comparative Performance (Single Ring); Leakage vs. Radial Clearance (ΔP = 689 kPa)

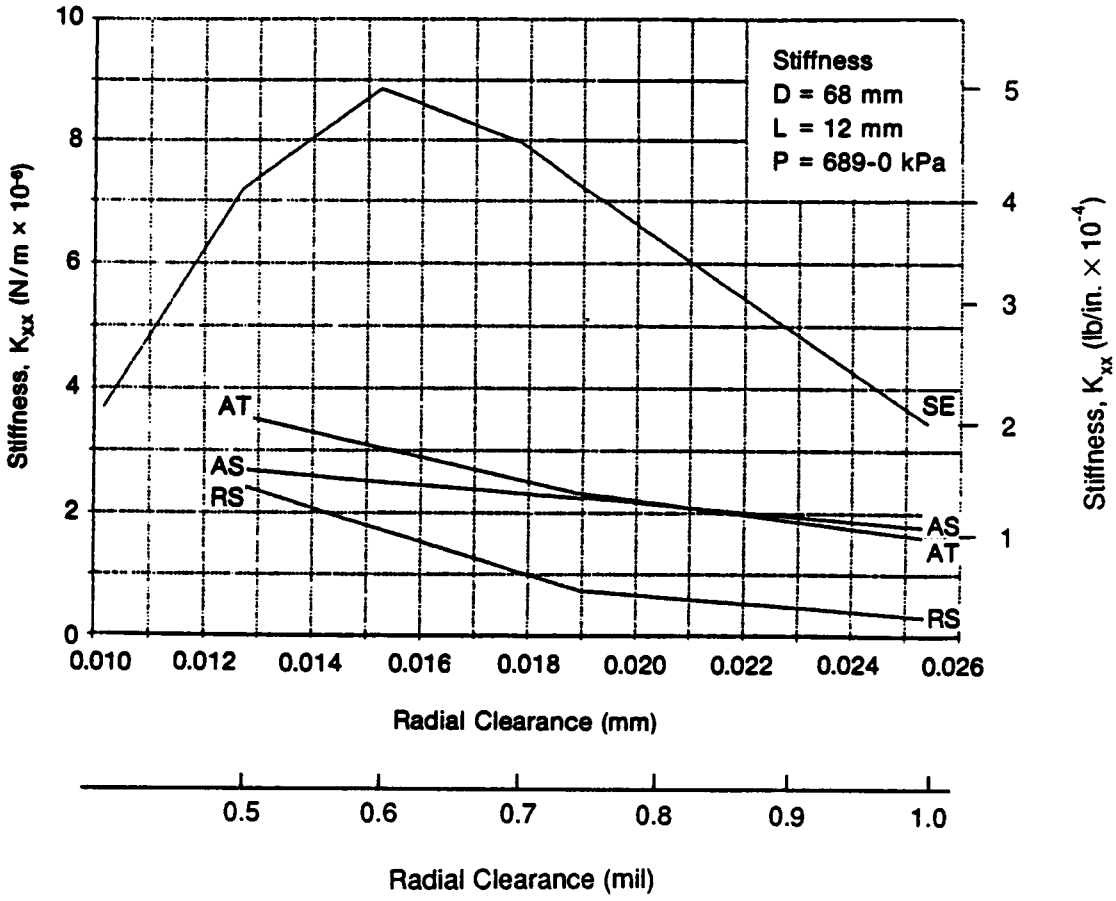

Figure 5-12 Ring Seal Comparative Performance; Stiffness vs. Radial Clearance (ΔP = 689 kPa)

872549

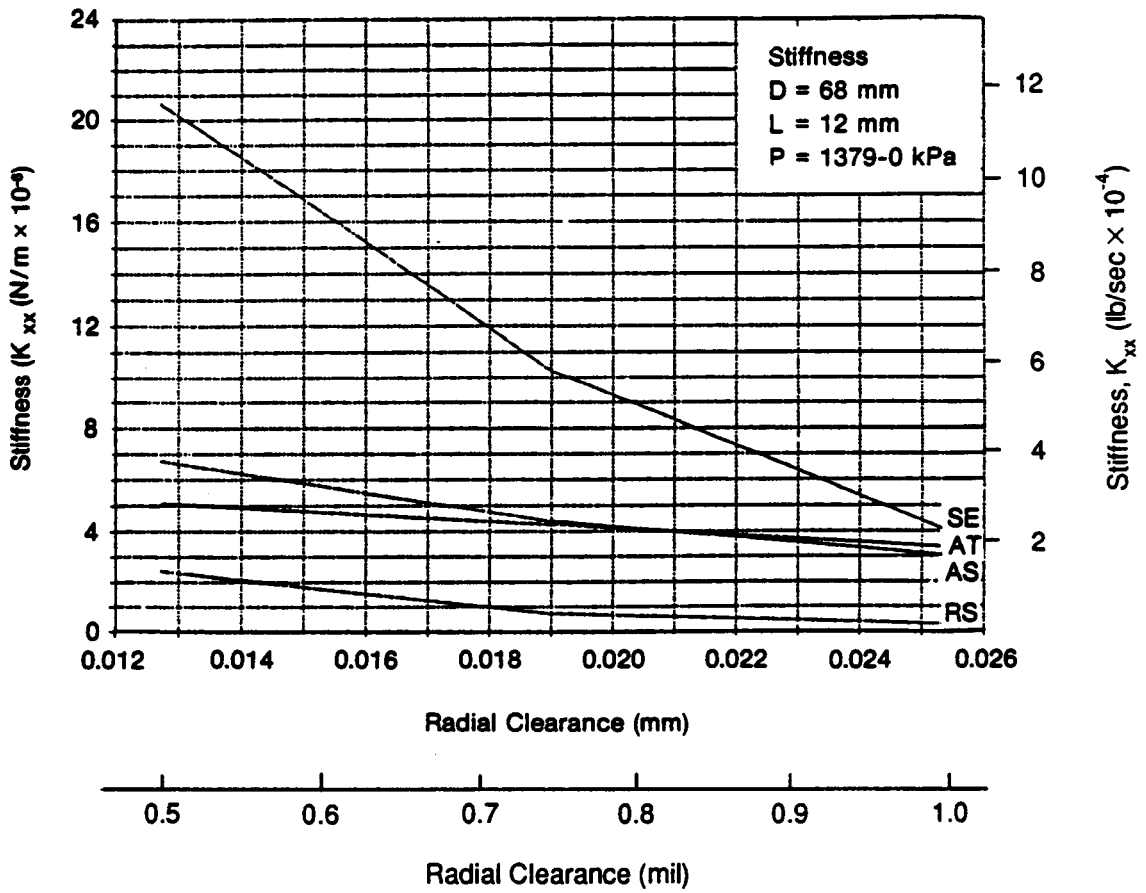

872550

Figure 5-13 Ring Seal Comparative Performance; Stiffness vs. Radial Clearance (ΔP - 1379 kPa)

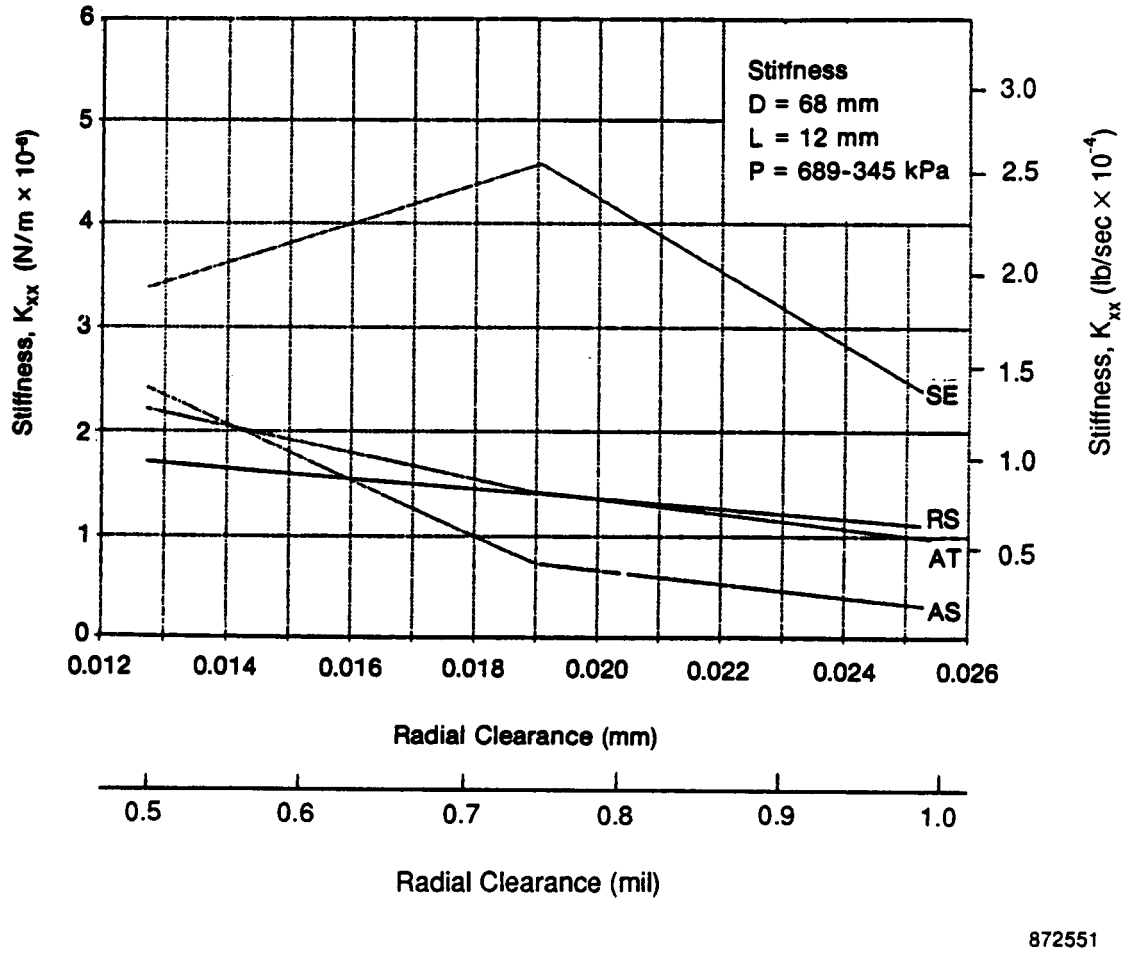

Figure 5-14 Ring Seal Comparative Performance; Stiffness vs. Radial Clearance (ΔP = 345 kPa)

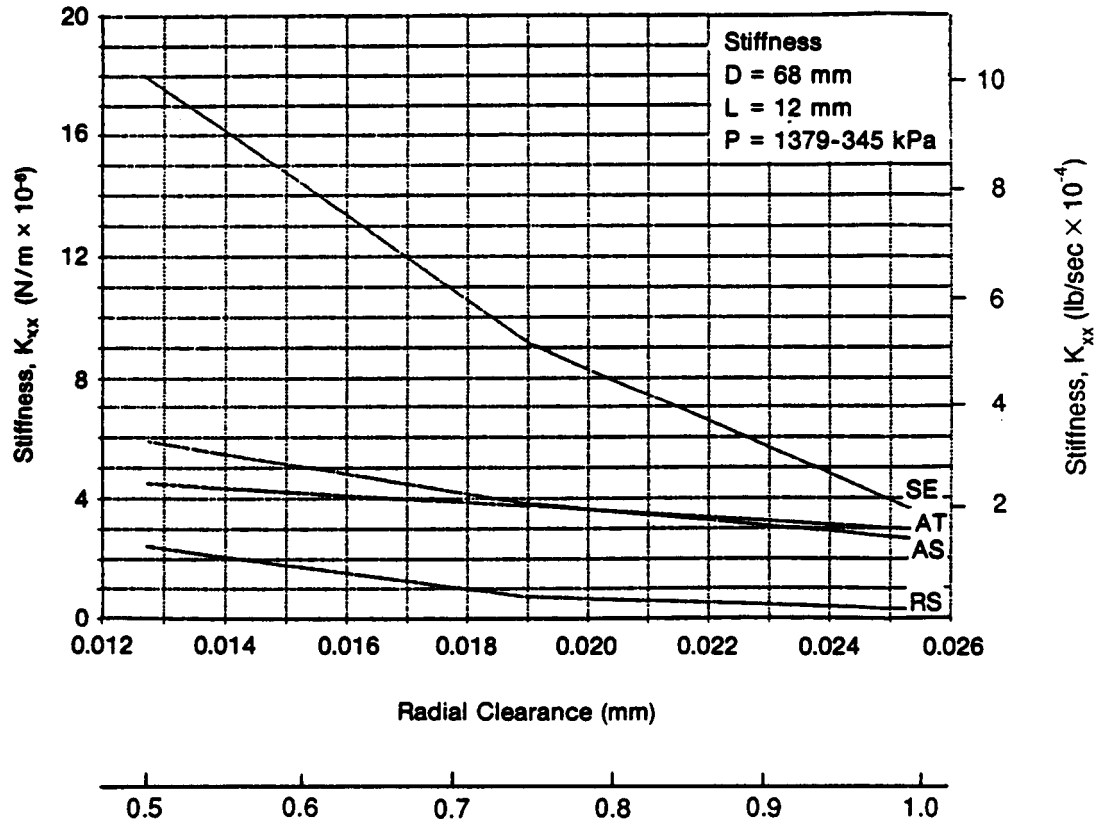

Figure 5-15 Ring Seal Comparative Performance; Stiffness vs. Radial Clearance (ΔP = 1034 kPa)

872553

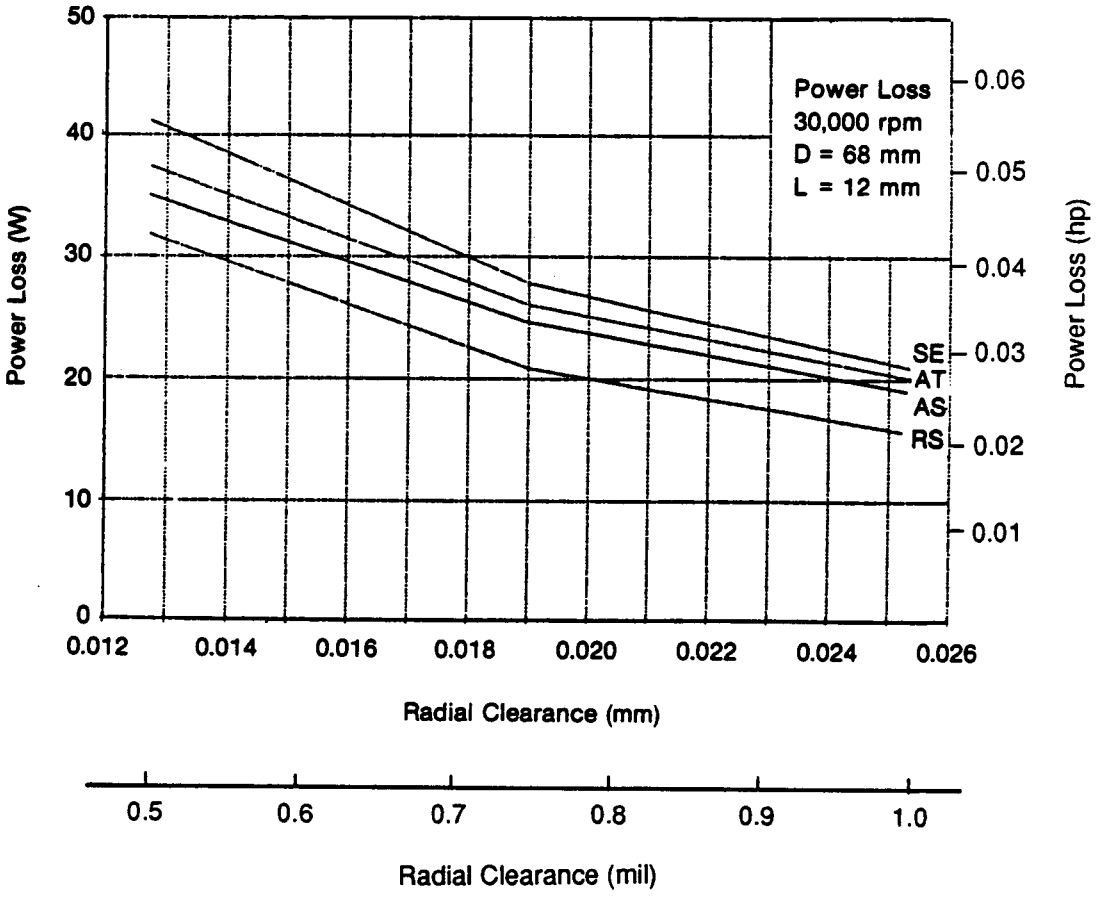

Figure 5-16 Ring Seal Comparative Performance (Single Ring); Power Loss vs. Radial Clearance

- Radial Clearance = 0.0191 mm (0.00075 in.)
- Supply Pressure = 1379 kPa (200 psig)
- Shaft Eccentricity = 0.0127 mm (0.0005 in.)
- Friction Coefficient = 0.2
- Shaft Speed = 3142 rad/s (30,000 rpm)

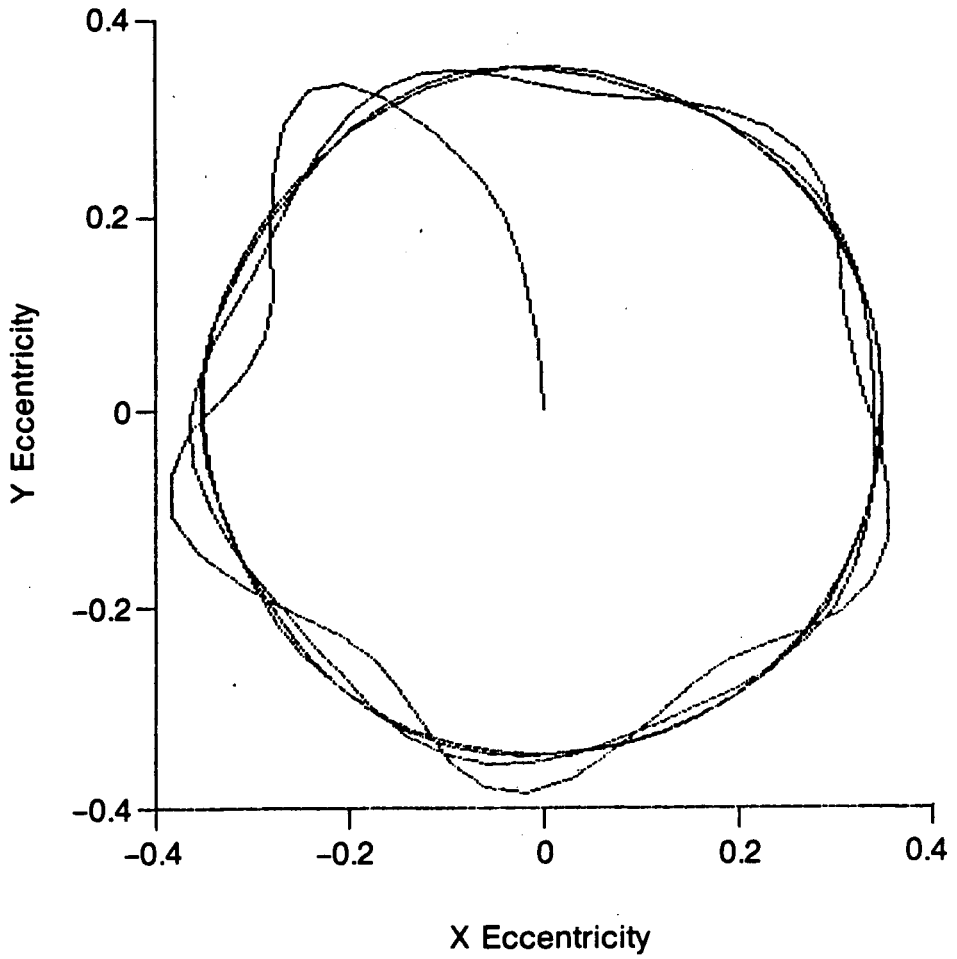

Figure 5-17 Dynamic Response of Self-Energized Hydrostatic Seal Ring (C = 0.0191 mm)

- Radial Clearance = 0.0254 mm (0.001 in.)
- Supply Pressure = 1379 kPa (200 psig)
- Shaft Eccentricity = 0.0127 mm (0.0005 in.)
- Friction Coefficient = 0.2
- Shaft Speed = 3142 rad/s (30,000 rpm)

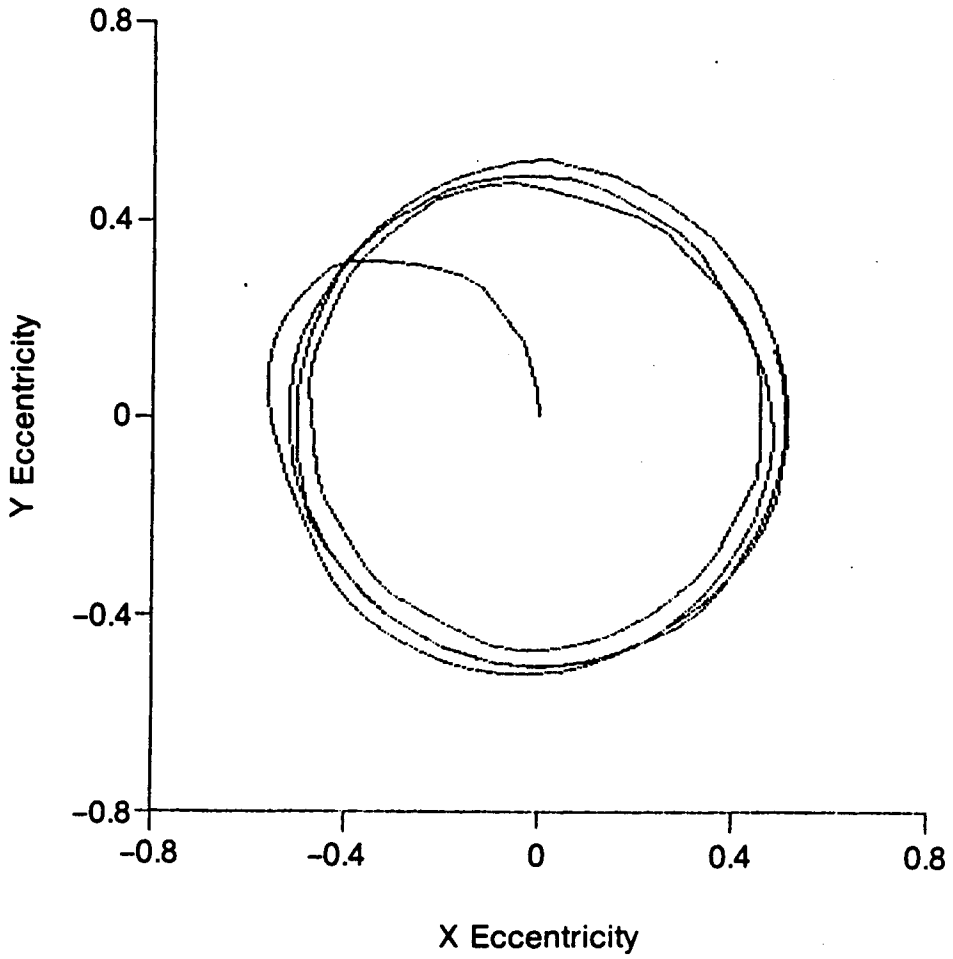

Figure 5-18 Dynamic Response of Self-Energized Hydrostatic Seal Ring (C = 0.0254 mm)

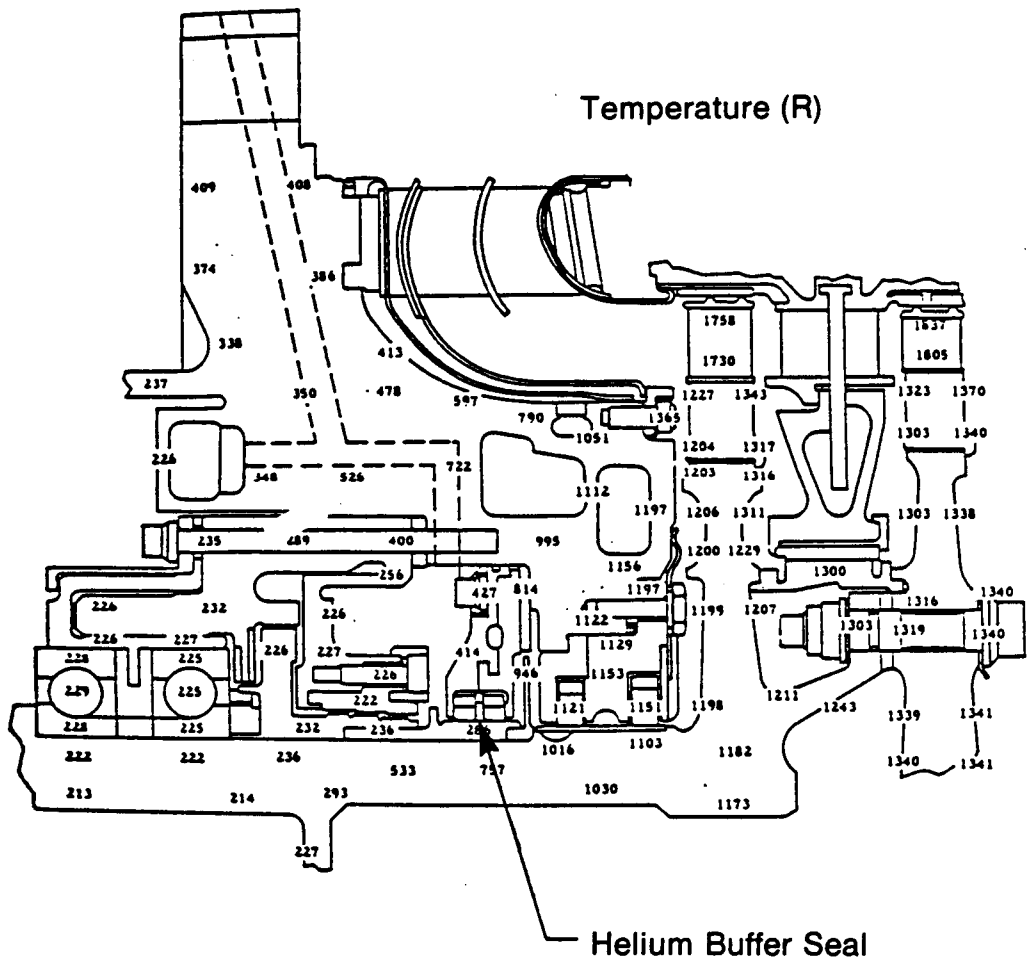

Figure 5-19 HPOTP Turbine Temperature Distribution at Full Power Level

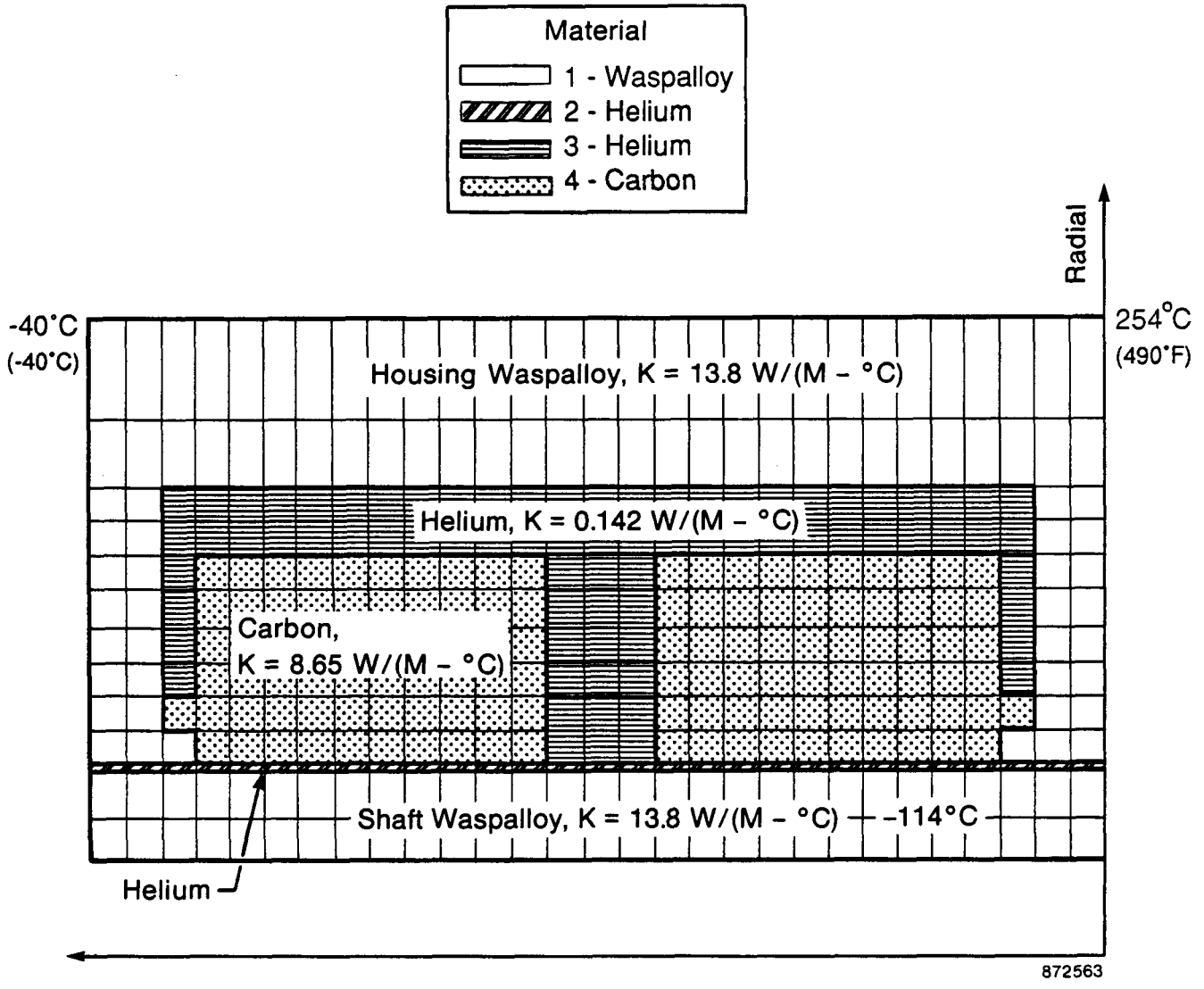

Figure 5-20 Mathematical Model for the Ring Seal Thermal Analysis

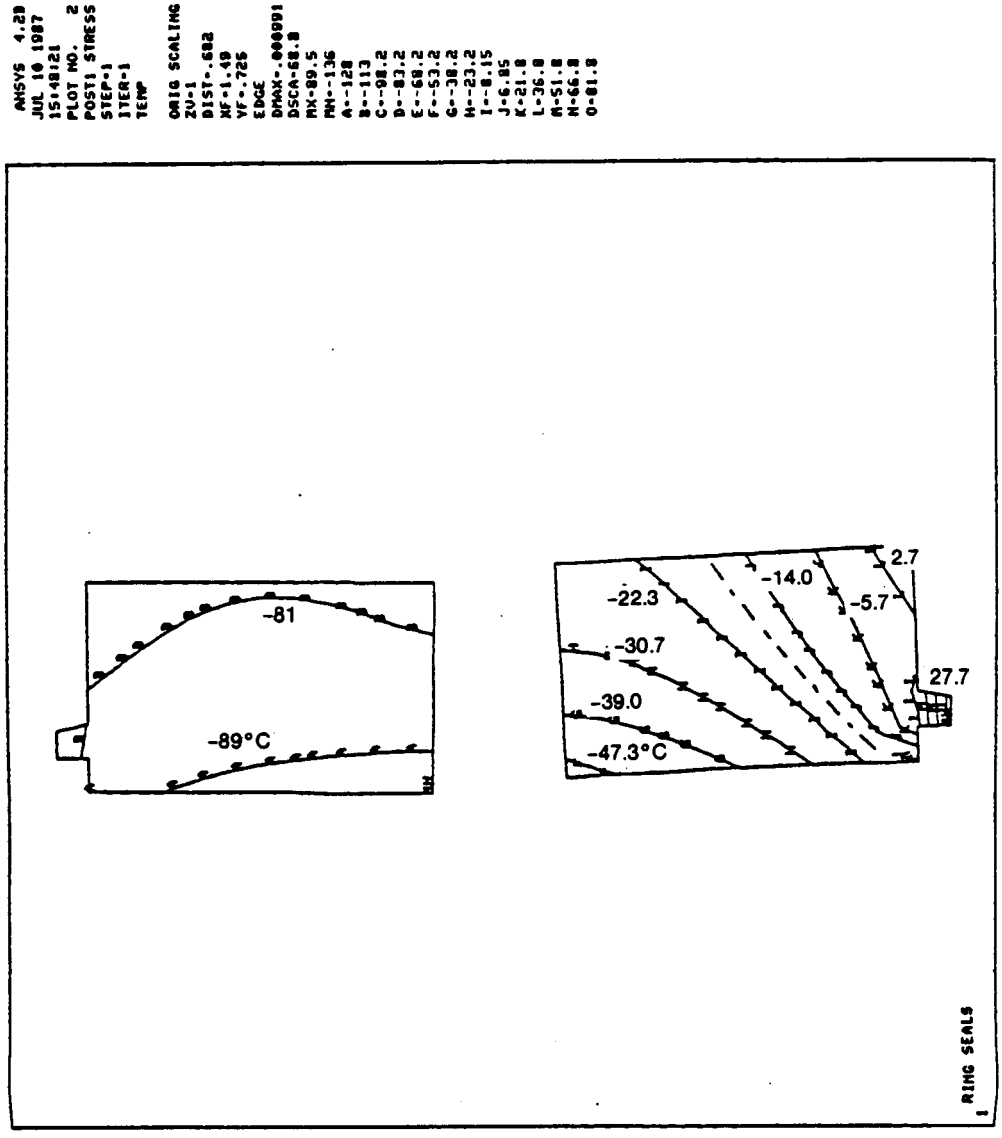

Figure 5-21 Ring Seal Temperature Distributions

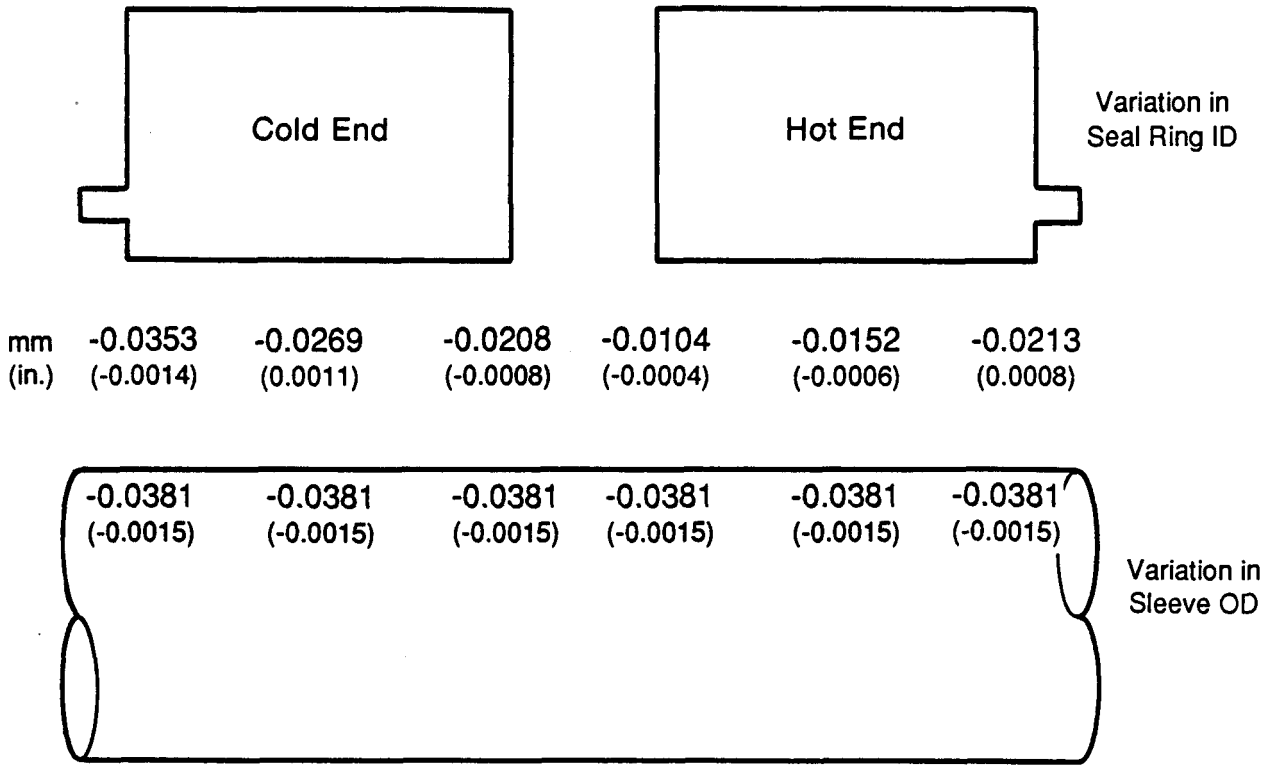

Figure 5-22 Ring Seal Distortions

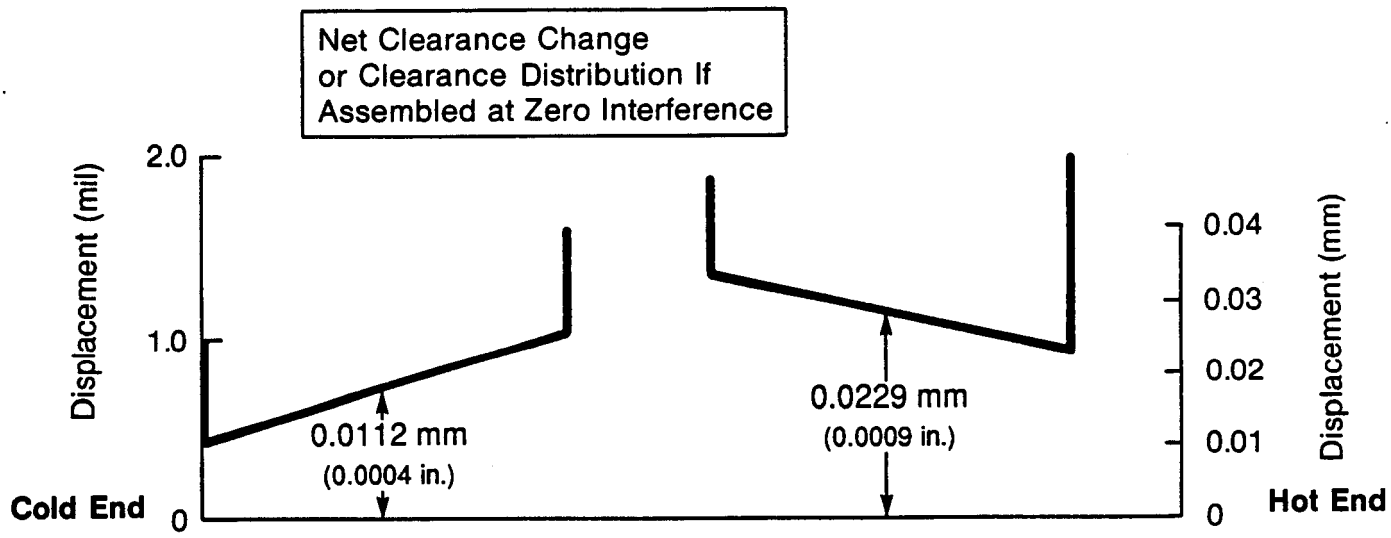

Figure 5-23 Ring Seals; Distorted Clearance Distributions

872528

REVISIONS		SIZE D	771D002	REV.
SYM.	DESCRIPTION		DATE	APPROVAL

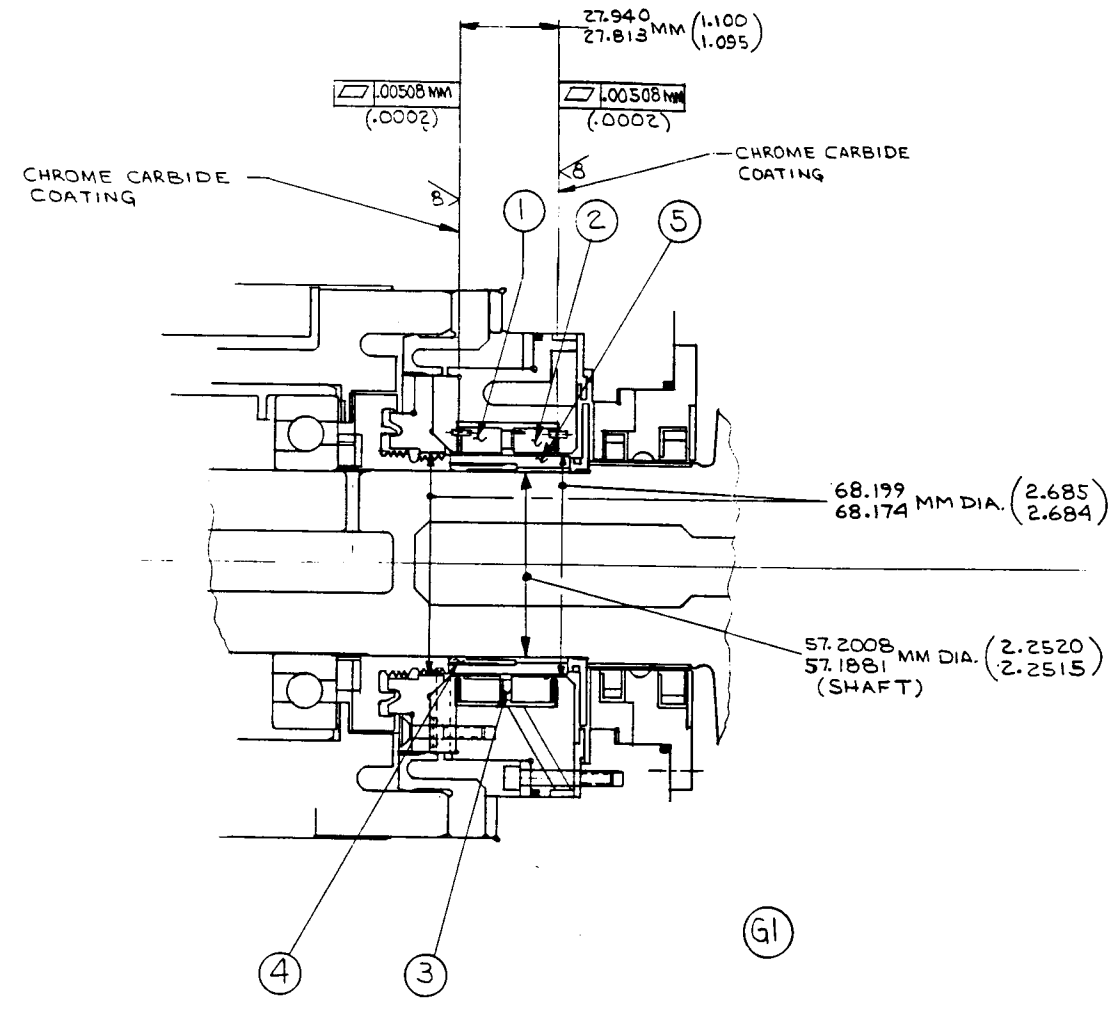

HELIUM PURGE SEAL FLOATING RING
TURBINE GAS SEAL

	1	5	771C009 P1	RING SEAL-SLEEVE
	1	4	771B010 P1	RING SEAL-MOUNTING SLEEVE
	1	3	771B014 P1	RING SEAL-WAVE SPRING
	1	2	771D013 G2	RING SEAL -SEAL
	1	1	771D013 G1	RING SEAL- SEAL
			771 D002 G1	ASSEMBLY
		PART NO.		DESCRIPTION

UNLESS OTHERWISE SPECIFIED DIMENSIONS ARE IN INCHES
TOLERANCES ON:
DECIMALS .XXX ± .XX ± FRACTIONS ± ANGLES ±
ALL SURFACES ✓
BREAK SHARP CORNERS AND REMOVE BURRS
GEOMETRIC TOLERANCES PER USASI Y 14.5
MATERIAL
TREATMENT

COMPANY CLASSIFICATION
PROPRIETARY ☐ NAME-DATE
NON-PROPRIETARY ☐ TITLE

DRAWN H.JONES 6/6/86
CHECK H. JONES 5/11/87
DESIGN
ANALYTICAL
MATERIALS
MFG. ENGR.
PROJ. MGR. W.Simpson 9/11/87
QUALITY CONTROL

Mechanical Technology Incorporated
Latham, New York 12110

TITLE
RING SEAL ASSEMBLY
OXIDIZER TURBOPUMP

CODE IDENT NO. 26741 | SIZE D | 771D002
ISSUED | SCALE FULL | WT. | ACT. CALC.

87TR72

ORIGINAL PAGE IS
OF POOR QUALITY

ORIGINAL PAGE IS
OF POOR QUALITY

Figure 5-24 Ring Seal Assembly, Oxidizer Turbopump

FOLDOUT FRAME

FOLDOUT FRAME

REVISIONS		SIZE D	771D013	REV. A
SYM.	DESCRIPTION	DATE	APPROVAL	
A	ADDED SECOND RING SEAL PT 2 AND GROUP 2.	1/25/87 1987		

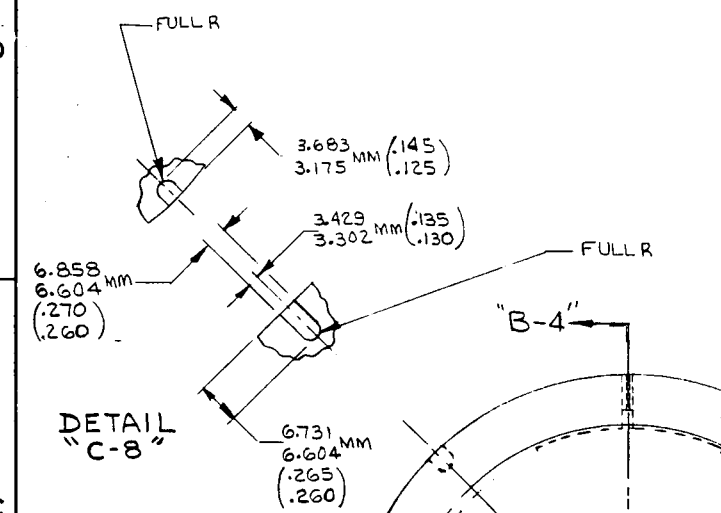

DETAIL "C-8"

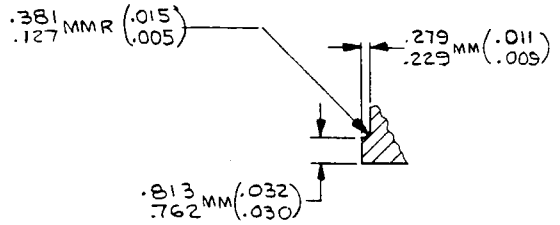

DETAIL "D-5"
(SCALE: 10/1)

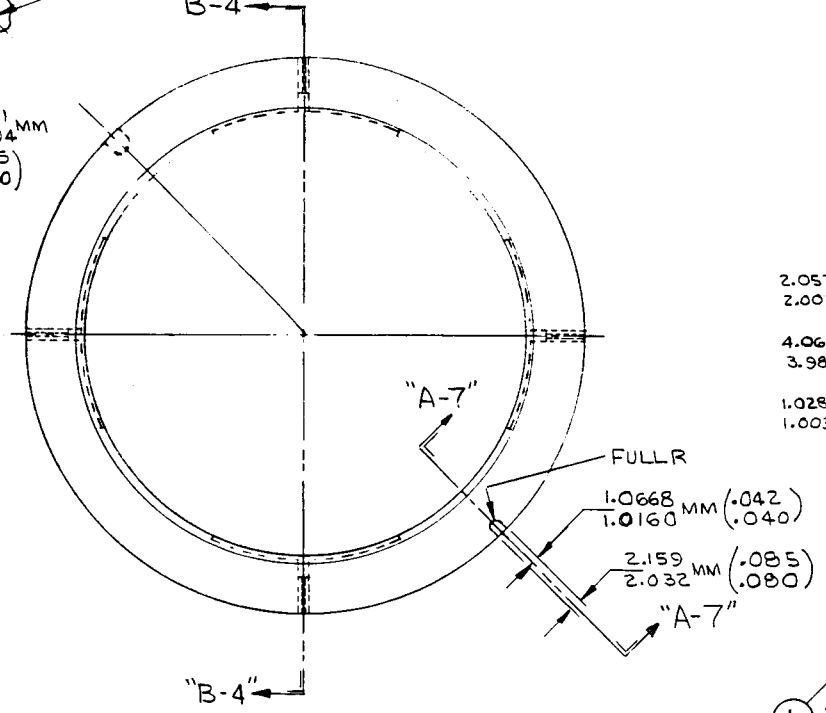

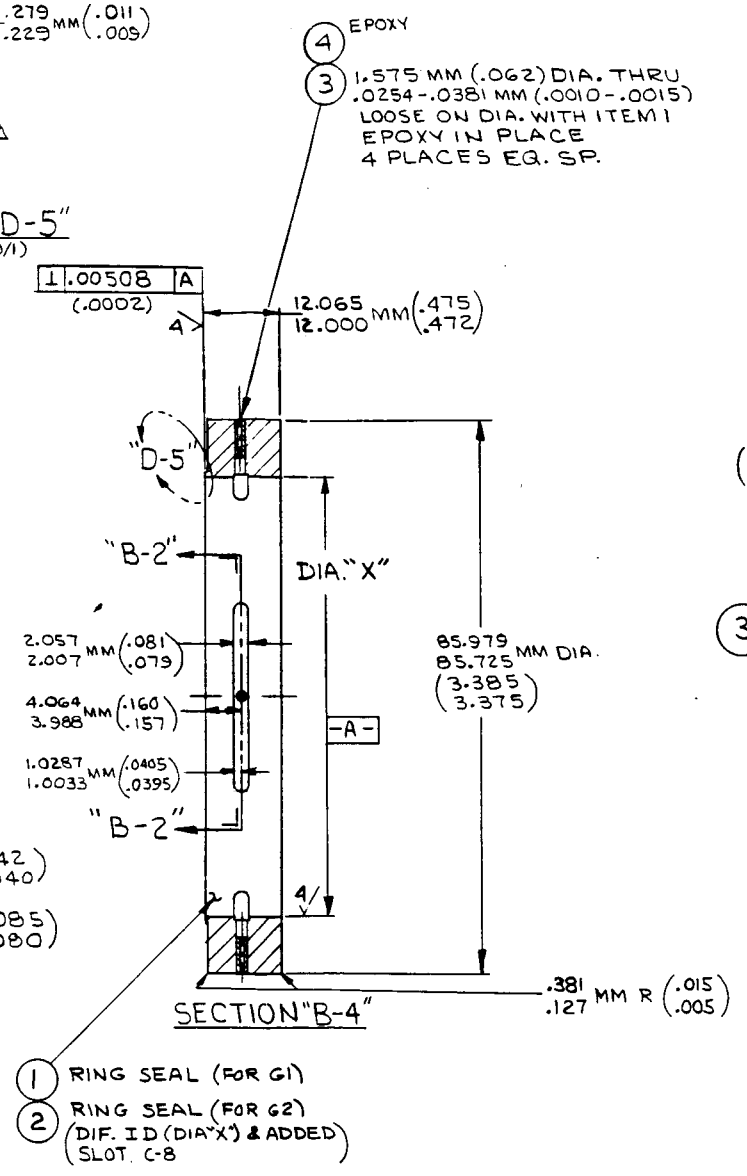

SECTION "B-4"

1 RING SEAL (FOR G1)

2 RING SEAL (FOR G2) (DIF. I D (DIA "X") & ADDED SLOT. C-8

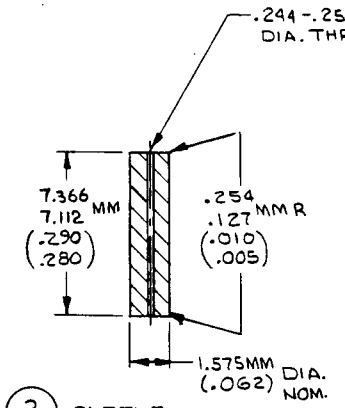

3 SLEEVE

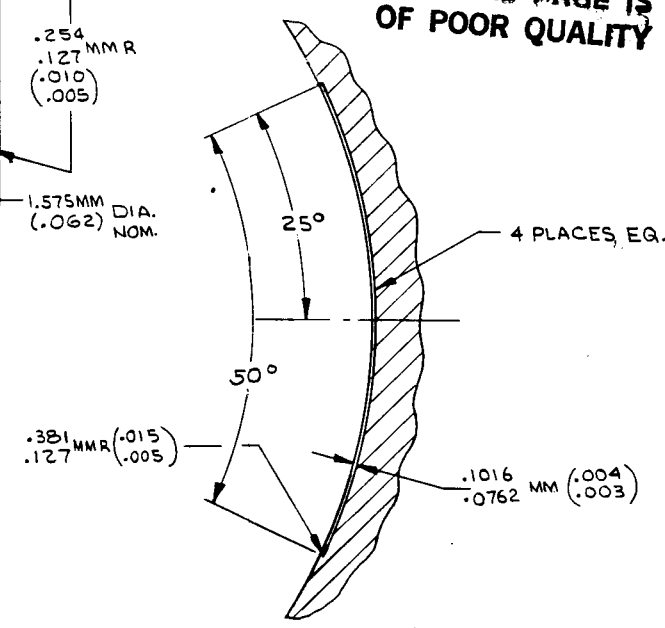

SECTION "B-2"
(SCALE: 10/1)

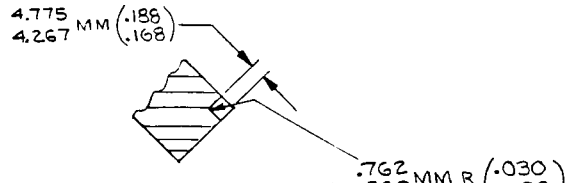

SECTION "A-7"

PART NO.	DIA "X"	SLOT DETAIL C-8
1	68.0182 / 68.0152 MM (2.6779 / 2.6778)	OMIT
2	68.0132 / 68.0102 MM (2.6777 / 2.6776)	AS SHOWN IN DETAIL C-8

G1

G2 PT 2 REPLACES PT 1 OTHERWISE SAME AS G1

AR	AR	4		EPOXY - TORR SEAL (VARIAN PRODUCTS DIV)
4	4	3	771D013P3	SLEEVE-MAT'L: CARPENTER C-42
1	-	2	771D013P2	RING SEAL-MAT'L: CARBON GRAPHITE C-GPH P-5N
-	1	1	771D013P1	RING SEAL-MAT'L: CARBON GRAPHITE C-GPH P-5N
				DESCRIPTION

UNLESS OTHERWISE SPECIFIED DIMENSIONS ARE IN INCHES
TOLERANCES ON: DECIMALS .XXX ± — .XX ± — FRACTIONS ± — ANGLES ±0°30'
ALL SURFACES 63
BREAK SHARP CORNERS AND REMOVE BURRS
GEOMETRIC TOLERANCES PER USASI Y 14.5
MATERIAL SEE PART NO'S.
TREATMENT

COMPANY CLASSIFICATION
PROPRIETARY ☐ NAME - DATE
NON-PROPRIETARY ☐ TITLE

DRAWN E. Bandzuchi 27APR'87
CHECK H. JONES 5/11/87
DESIGN
ANALYTICAL
MATERIALS
APPD. ENGR.
PROJ. APPROVAL M. Cooper 5/11/87
QUALITY CONTROL

Mechanical Technology Incorporated, Latham, New York 12110

TITLE: RING SEAL SEAL

CODE IDENT NO. 26741 | SIZE D | 771D013
ISSUED | SCALE 2/1 | WT. ACT. CALC.

87TR72

ORIGINAL PAGE IS OF POOR QUALITY

ORIGINAL PAGE IS OF POOR QUALITY

PRECEDING PAGE BLANK NOT FILMED

Figure 5-25 Ring Seal; Seal

FOLDOUT FRAME

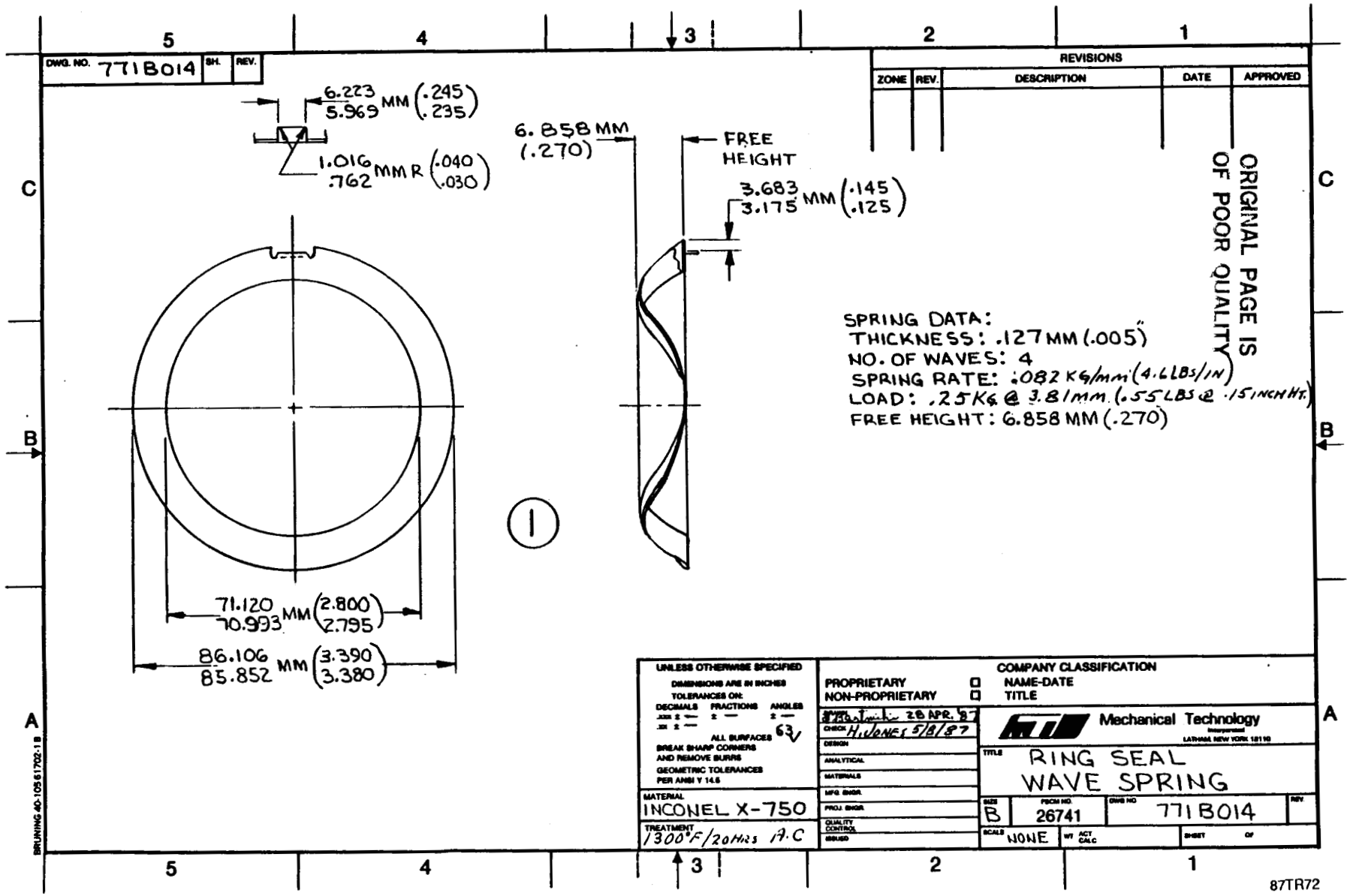

Figure 5-26 Ring Seal; Wave Spring

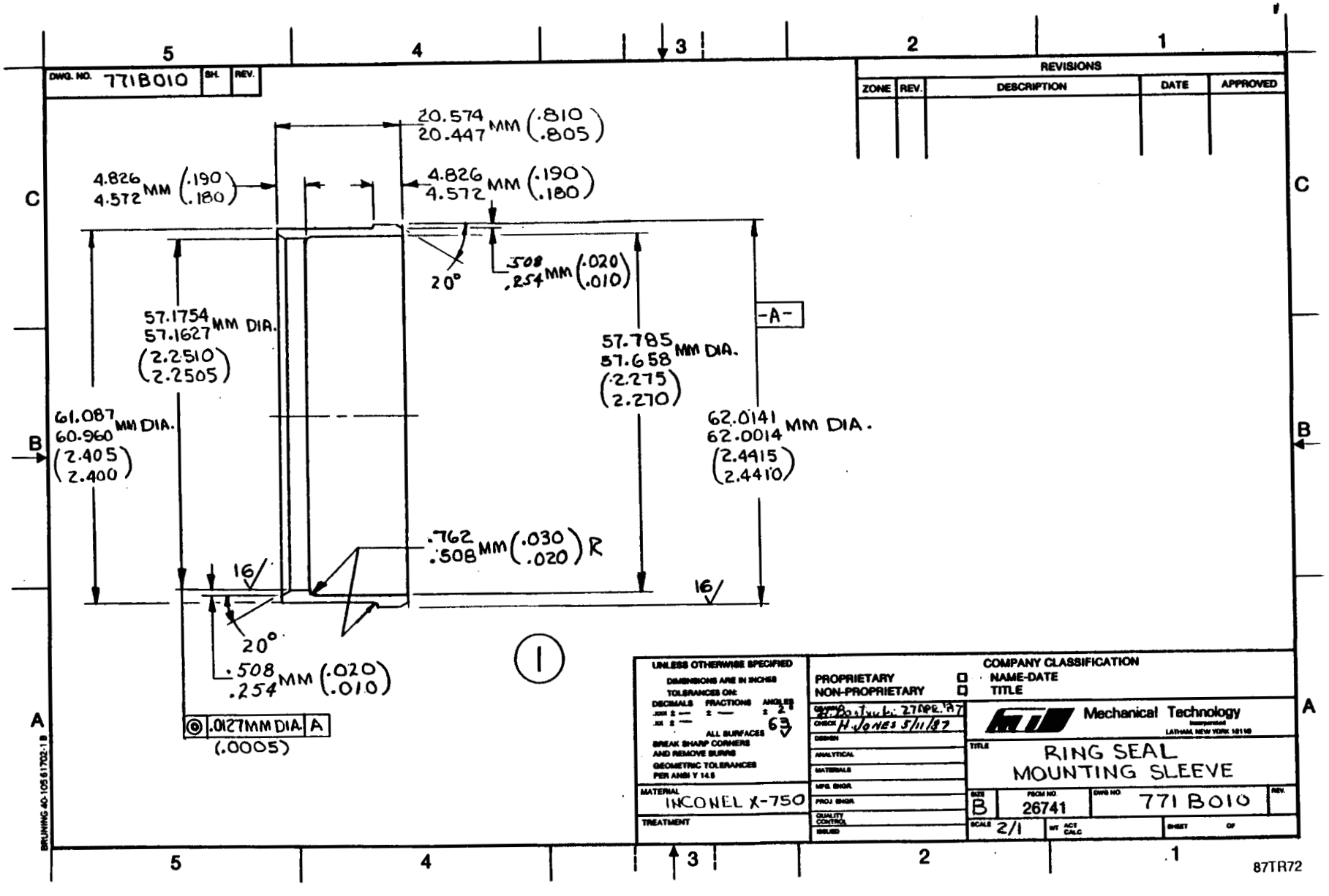

Figure 5-27 Ring Seal; Mounting Sleeve

ORIGINAL PAGE IS
OF POOR QUALITY

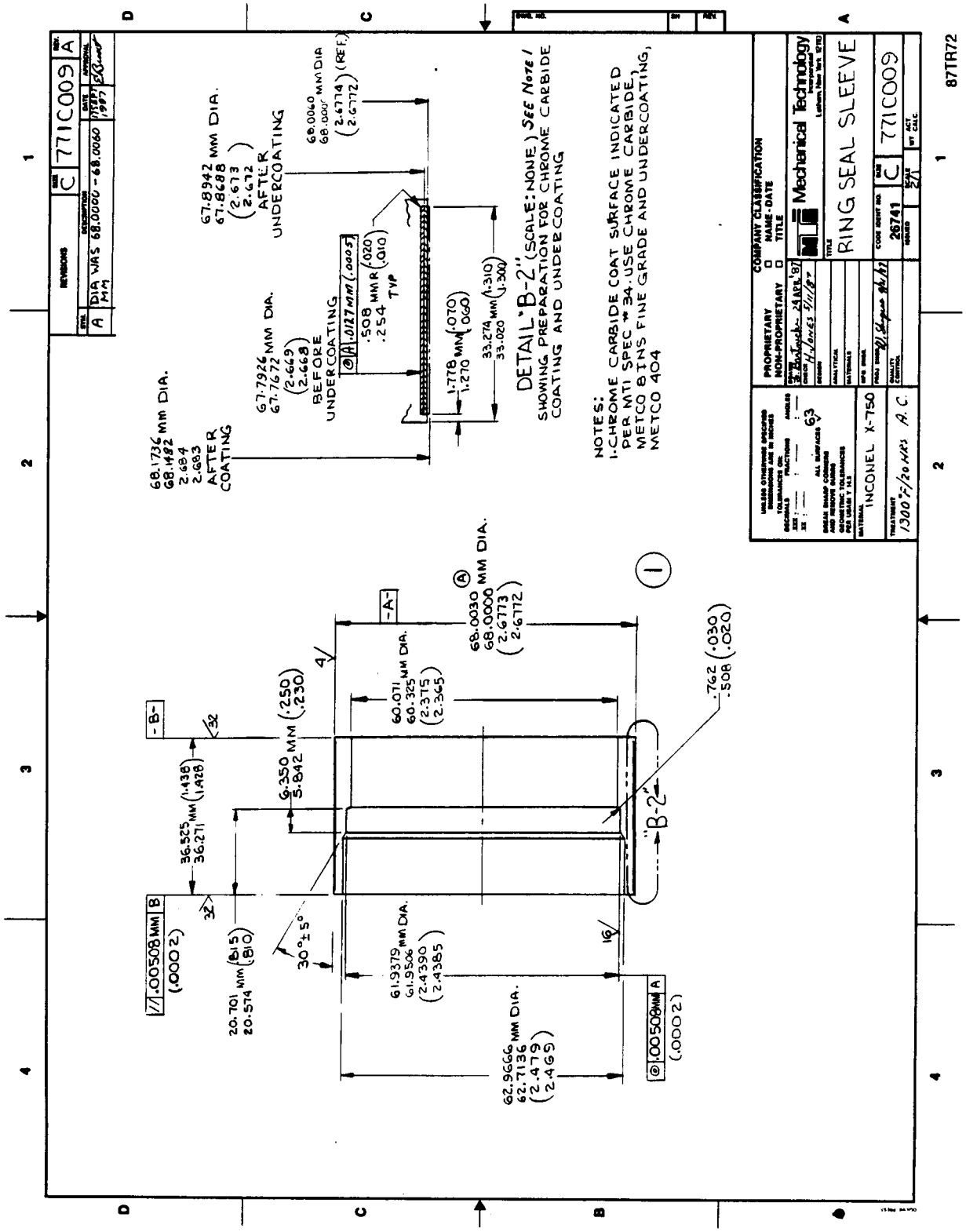

Figure 5-28 Ring Seal; Sleeve

6.0 BUFFERED FLUID-FILM FACE SEALS

The helium buffer seal may also consist of two opposed fluid-film face seals mating against a single collar. An assembly view of the face seals installed in the LOX pump is shown in Figure 6-1. Helium buffer gas is introduced at the OD of the seals and flows through the clearance space between the seal ring and rotating collar to the ambients on either side of the seal rings.

6.1 Comparative Studies

Four types of face seal configurations were examined. These were radial tapered (RT), radial step (RS), self-energized hydrostatic (SE), and spiral groove (SG). All but the spiral groove are shown in Figure 6-2.

For purposes of conducting comparative parametric studies, preliminary layouts were completed and the following dimensions selected:

Outside diameter = 96 mm (3.78 in.)
Inside diameter = 70 mm (2.76 in.)
Secondary seal diameter = 76.70 mm (3.02 in.)

Note that these dimensions were subsequently altered, after the seal type was selected, and detail design was initiated.

Information for the spiral groove seal was derived from the computer code SPIRALP. Optimization parameters were determined by examining performance at the various pressure differentials involved and selecting the geometry that best suited the operating spectrum. Table 6-1 quantifies the parameters used, which are shown in Figure 6-3.

The closing force on the seal is a function of both the buffer pressure and the ambient pressure in accordance with the following equation:

$$F_C = P_S(\pi/4)\,[(OD)^2 - (SD)^2] + P_a(\pi/4)\,[(SD)^2 - (ID)^2] \qquad (6\text{-}1)$$

where

F_C = Closing force
OD = Outside seal diameter
ID = Inside seal diameter
SD = Secondary seal diameter
P_S = Buffer supply pressure
P_a = Ambient downstream pressure

The resulting closing forces are indicated on Table 6-2. Figure 6-4 shows load capacity as a function of film thickness for the four seals involved at a buffer supply pressure of 689 kPa (100 psi). For each type of seal there are two load curves corresponding to the two different ambient pressures. The two curves for a particular type seal are joined by a vertical arrowed line with the seal type indentifier label. Superimposed on these curves are the closing force lines for the two ambient pressures. The intersection of the closing force line with the opening load curve represents a seal position to satisfy axial load equilibrium. For the range of film thicknesses indicated, neither the radial taper nor the radial step configurations are in equilibrium for the

two ambient pressure conditions (i.e., unacceptably large or small clearances occur over the operating range of ambient pressures). The problem is related to the changes in opening load that occur because of a variation in the downstream or ambient pressure, coupled with poor stiffness characteristics of these seals (i.e., flat load vs. film thickness curves). On Figures 6-4 and 6-5. the operating positions are at the following points:

Point	Description
1	SG Seal, P_a = 345 kPa (50 psi)
2	SG Seal, P_a = 0 kPa (0 psi)
3	SE Seal, P_a = 0 kPa (0 psi)
4	SE Seal, P_a = 345 kPa (50 psi)

Similar information was produced at a buffer fluid pressure of 1379 kPa (200 psi). Results are shown in Figure 6-5. The radial step and radial taper seals are confronted with the same problem as those that occurred at the lower pressure; namely, that unacceptably large clearance variations occur as a function of the pressure differential across the seal. The self-energized hydrostatic seal configuration, however, can satisfy the closing load over a limited and acceptable operating film thickness range. The spiral groove seal produces very good performance. Additional performance curves for leakage and stiffness are indicated on Figures 6-6 through 6-13.

The radial step and radial taper seals were eliminated because of poor stiffness characteristics and unacceptable clearance variations to accommodate the extremities in ambient pressures.

Table 6-3 shows comparative performance of the two remaining candidates, the spiral groove and the self-energized hydrostatic. The spiral groove operates at larger film thicknesses, which is an advantage because it provides a greater safeguard against contact. The leakage, however, for the spiral-groove seal is significantly larger than for the self-energized hydrostatic. It was decided to proceed with further evaluation of both seals. Although the spiral-groove seal can operate at 689 kPa (100 psig), the stiffness characteristics at this pressure are approximately half of those at the higher buffer pressure of 1379 kPa (200 psig). Film stiffness is important to keep the surfaces separated. Therefore, it was decided to proceed with both candidate seals at a buffer pressure of 1379 kPa (200 psig).

6.2 Final Configurations and Steady-State Performance of Selected Seals

Further layouts of the face seals were made. It was determined that the ODs could be increased, as well as the secondary seal radii, to provide greater wall thickness and structural rigidity. For the comparative studies, the wall thickness was 3.35 mm (0.132 in.), which was considered only marginally acceptable. To maintain operating clearances in an appropriate range, the seal face ID was undercut as shown in Figure 6-14. This effectively reduces the closing load at the high ambient pressure condition to permit operation at higher film thickness. The principal dimensions for the self-energized hydrostatic seal are identified in Table 6-4, and the information for the spiral-groove seal is presented in Table 6-5. These dimensions were determined through optimization studies.

Figure 6-15 shows load capacity vs film thickness for the self-energized seal and the spiral-groove seal for the two extremes of ambient pressure. Superimposed are the closing force lines, and as before, the intersection of the closing force with the film force represents operating points. On Figures 6-15 through 6-19, the identifying numerals are:

Point	Description
1	SE Seal, P_a = 345 kPa (50 psi)
2	SE Seal, P_a = 0 kPa (0 psi)
3	SG Seal, P_a = 345 kPa (50 psi)
4	SG Seal, P_a = 0 kPa (0 psi)

Figures 6-16 through 6-18 are performance curves for flow, stiffness, and power loss, respectively. Figure 6-19 shows recess pressure curves that apply to the self-energized hydrostatic seal only. Important comparative performance information of the two final configurations is tabulated on Table 6-6.

The performance of the two seals are very comparable. The self-energized seal operates at larger film thickness than the spiral-groove seal with slightly less leakage at an ambient pressure of 345 kPa (50 psi) and equal leakage at an ambient of 0 kPa (0 psi). Its only disadvantage is that it has slightly higher viscous power loss. The film thickness of the spiral-groove seal is marginal, and for this reason, it was decided to consummate a design for the self-energized seal. The spiral-groove seal's film thickness could be increased by reducing the interface ID, and it is believed that a very viable configuration could be produced, but based on the constraints imposed to accomplish the comparison, the self-energized seal was selected for final design.

6.3 Face Seal Dynamics

The dynamics of the face seal were examined with the computer code FACEDY. The geometry of the design, subsequently described, was inputted into the program. The cases examined were at the high ambient pressure condition. This is the worst condition with respect to dynamic response because the film thickness is less than at 0 kPa (0 psi) ambient condition. Fluid-film stiffness characteristics were obtained from the steady-state computer output (see Figure 6-17 and Table 6-6), as generated from the computer code GFACE. The stiffnesses used in the analysis were as follows:

Axial Stiffness = 84.0×10^6 N/m (479.6×10^3 lb/in.)
Angular Stiffness = 49.2×10^3 N-m/rad (435.4×10^3 lb-in./rad)

The principal variables are the shaft displacements and frequencies and the coefficient of friction of the secondary seal piston ring. Four dynamic cases were considered where displacements and friction were varied. These are summarized in Table 6-7. Other seal parameters produced by the code are indicated on Table 6-8.

For Case 2, the shaft was given vibration displacements of 0.0076 mm (0.0003 in.) and angular vibrations of 0.0003 radians about orthogonal axes normal to the axis of shaft rotation. All displacements, translatory and angular, were applied at a synchronous frequency of 3142 rad/s (30,000 rpm). This combination of axial and angular movement causes a total seal ring half peak-to-peak displacement at the outer diameter of the rotating collar of

0.0238 mm (0.0009 in.), which is significantly greater than the axial equilibrium clearance of 0.0127 mm (0.0005 in.). Results of this dynamic analysis are shown on Figures 6-20 through 6-27. Figures 6-20 shows the axial displacement of the seal ring in response to the shaft excitations. The curve is actually the axial shaft vibration superimposed upon the seal ring response. The seal ring and seal runner (shaft) are in perfect unison, indicative of excellent tracking characteristics in the axial mode. Angular displacements are shown on Figures 6-21 and 6-22. For the angular modes, there is a clear distinction between the forcing function from the shaft and the response of the seal ring. Frictional resistance is inhibiting the amplitude of the seal ring to be slightly less than the collar, and the response lags behind by a visible phase shift. The midpoint axial film thickness is shown on Figure 6-23. The film thickness vibrates about the equilibrium position, 0.0127 mm (0.0005 in.), with a peak-to-peak amplitude of about 0.00051 mm (0.0002 in.), which is slightly less than the prescribed shaft motion. The minimum film thickness, which is the more important parameter, is shown on Figure 6-24. The film thickness has a minimum value close to 0.00025 mm (0.0001 in.), which would be close to the minimum acceptable for a seal of this size and speed.

Friction forces and moments, which are produced by the secondary seal, are shown on Figures 6-25 through 6-27. The axial friction has a maximum value of 316 N (71 lb), and the friction moments peak at approximately 9 N-m (80 lb-in.).

Referring back to Table 6-7, Case 3 was identical to Case 2 except shaft translations were increased to 0.0102 mm (0.0004 in.), and angular rotations increased to 0.0004 radians. These amplitudes are semi-peak-to-peak values. The secondary seal friction coefficient remained the same. For this situation, the seal ring did not track the excursions of the runner and contact occurred. For Case 4, the large amplitudes were retained, but the coefficient of friction of the secondary seal was reduced from 0.2 to 0.1, which is a reasonable value for the Teflon-coated piston ring. The seal ring tracked very well for this case.

Figures 6-28 through 6-34 show the results of Case 4. Note that the angular displacements, Figures 6-29 and 6-30 are tracking the shaft collar very well; much better than in Case 2, which had lower vibration amplitudes but higher friction. The minimum film thickness, shown on Figure 6-31, is significantly better than for Case 2. The minimum film thickness is 0.0085 mm (0.00033 in.), which is a respectable value. Friction forces and moments are shown on Figures 6-32 through 6-34. Note that they are approximately half of those for Case 2, because the friction coefficient was halved.

The following conclusions are made as a result of the dynamic studies of the face seal:

- The seal has satisfactory tracking capability. Rotor excursions of 0.0152 mm (0.0006) peak-to-peak amplitudes and total indicated misalignment runouts of 0.0324 mm (0.0013 in.) measured at the OD of the runner can be safely handled. Thus, the total peak-to-peak excursions at the runner OD are 0.0476 mm (0.0018 in.). These values exceed the specification of vibration amplitudes of 0.0137 mm (0.0005 in.) peak to peak.

- Minimizing the coefficient of friction has a very beneficial effect. A coefficient of friction of 0.1 would enable tracking rotor excursions of 0.0204-mm (0.0008-in.) peak-to-peak amplitudes and misalignment runout of 0.0008 radians peak to peak, measured at the OD of the seal face.

6.4 Face Seal Thermoelastic Distortions

The overall face seal model and boundary conditions for the thermal analysis are shown in Figure 6-35. The fluid helium was considered stationary, and heat transfer across it was strictly by conduction. This assumption was considered valid because of the low flow velocity and small film thickness and heat conduction path involved. Two separate analyses were conducted: 1) a thermal analysis to establish the temperature distribution and thermal distortion, and 2) a pressure analysis to determine distortions and stresses due to the pressure boundary conditions. The two analyses were then superimposed to determine total distortions.

The temperature distributions for the housing, seal rings, and runner are shown in Figures 6-36, 6-37, and 6-38, respectively. As indicated in Figure 6-37, the gradient across the high-temperature seal ring is very large. Across the low-temperature seal ring, the gradient is very small.

Thermal deformations are indicated in Figures 6-39, 6-40, and 6-41 for the runner, seal rings and housing, respectively. The high-temperature seal ring is subject to considerable thermal distortion, as indicated in Figure 6-39. The distortion produces a divergent clearance distribution of a magnitude significantly greater than the designed operating clearance of 0.0127 mm (0.0005 in.)

Furthermore, distortions of the carbon rings due to pressures on the seal ring surfaces are also unfavorable. These are shown in Figure 6-42. The pressure distortions can be reduced by increasing the thickness of the seal ring flange region. An attempt was also made to increase the length of the seal to provide a greater pressure moment that would oppose the cantilevered bending of the seal ring. As indicated in Figure 6-43, an increase in length of approximately 2.5 mm (0.098 in.) reduces the deformation by 27%. A summary of the deformations is indicated in Table 6-9.

The deformations produce a divergent clearance distribution in the direction of flow, which is detrimental to performance. Also, since the design operating clearance is 0.0127 mm (0.0005 in.), the deformation of the H_2 side ring of 0.0495 mm (0.0019 in.) is well beyond an acceptable value. Pressure distortions were reduced by thickening the flange region of the seal ring, but the major contributor to the deformation is the thermal boundary conditions. It is concluded that a buffer face seal is not feasible unless the thermal gradient across the helium buffer seal is significantly reduced.

6.5 Face Seal Design

The design of the face seal is shown in Figure 6-1 and in Figures 6-44 through 6-48. The assembly is shown in Figure 6-1. The face seals were inserted in the available SSME envelope with alterations made to housings and sleeves to accommodate the face seal configuration. Details of the main seal components

were completed by MTI. Housings and sleeves were not detailed since original seals would not be installed in the SSME pump but a NASA seal tester that would require different housings and sleeves.

The seal rings, Figure 6-44, are made from carbon graphite P-5N and the appropriate dimensions are shown in the figure. The ODs of the seal rings are greater than the designed seal OD because the rotating collar diameter is smaller and governs the effective OD of the seal. P-5N carbon graphite was selected because it is commonly used in cryogenic pump seals; a major attribute of this material is its structural integrity and ability to withstand high-speed rubs. The carbon's light weight is advantageous for dynamic tracking, and carbon materials have superior rub characteristics. The mating material on the face seal runner is chrome carbide and is shown in Figure 6-45. The secondary seal is a split piston ring, as shown in Figure 6-46. The material is stainless steel that is Teflon coated to reduce Coulomb friction. A wavy-washer-type closing spring has been designed to maintain closure when helium pressure is not applied and to prevent excessive face opening. The spring has been designed to apply a preload of 111.2 N (25 lb) with a spring rate of approximately 17,512 N/m (100 lb/in.). The spring configuration is shown in Figure 6-47. As shown on the assembly (Figure 6-1), an expandable sleeve is inserted underneath the rotating collar. The sleeve is shrunk onto the shaft, and the collar is shrunk onto the sleeve, which preloads the central portion of the sleeve. Thus, the sleeve remains in contact with the collar as its ID expands due to centrifugal force. The sleeve is shown in Figure 6-48.

6.6 General Conclusions Concerning the Face Seal Design

Comparative studies indicate that the self-energized hydrostatic configuration is superior to the other types considered because it can accommodate the required variation in downstream pressures without excessive clearance changes. A buffer pressure of 1379 kPa (200 psi) is required for proper operation of the seal. Predicted performance at design conditions is indicated in Table 6-10.

Thermoelastic studies indicate that excessive and detrimental distortions will occur in the hydrogen side seal ring. A divergent clearance distribution in the direction of flow is produced to a degree that would incapacitate operation. The problem is due to the very large temperature gradient (239°C, 430°F) that occurs across the seal ring

The seal rings are capable of tracking nutations and translations of the rotating collar provided misalignment is held to 0.0006 radians peak to peak and vibrations are held to within 0.0152 mm (0.0006 in.) peak to peak. This tracking capability is considered excellent and is due to the high stiffness of the film.

TABLE 6-1

SPIRAL GROOVE PARAMETERS

Inside Radius, mm (in.)	35 (1.378)
Radius at Groove Dam Interface, mm (in.)	37.6 (1.480)
Outside Radius, mm (in.)	48.0 (1.89)
Film Thickness, mm (in.)	0.0191 (0.0008)
Groove Depth, mm (in.)	0.038 (0.0015)
Groove Angle, deg	28
Land/Groove Ratio	1.65
Shaft Speed, rad/s (rpm)	3142 (30,000)
Fluid Viscosity, Pa-s (lb-sec/in.)	2×10^{-5} (2.9×10^{-9})

TABLE 6-2

COMPARATIVE STUDY FACE SEAL CLOSING FORCES

P_S	P_a	F_C
kPa (psi)	kPa (psi)	N (lb)
689 (100)	0	1804 (406)
689 (100)	345 (50)	2069 (465)
1379 (200)	0	3610 (812)
1379 (200)	345 (50)	3876 (871)

TABLE 6-3

COMPARATIVE PERFORMANCE BETWEEN SELF-ENERGIZED HYDROSTATIC AND SPIRAL-GROOVE SEALS

		h		Q		K	
P_S	P_a	SG	SE	SG	SE	SG	SE
kPa (psi)	kPa (psi)	mm (in.)		kg/s x 10^{-3} (lb/s x 10^{-3})		N/m x 10^{-6} (lb/in. x 10^{-4})	
689 (100)	0	0.0238 (0.00094)	0.0155 (0.0006)	0.87 (1.92)	0.30 (0.66)	10.0 (5.7)	18.0 (1.0)
689 (100)	345 (50)	0.0178 (0.0007)	0.0110 (0.0004)	0.5 (1.1)	0.08 (0.18)	15.4 (8.8)	8.5 (0.5)
1379 (200)	0	0.0208 (0.0008)	0.0136 (0.0005)	3.1 (6.8)	0.68 (1.50)	29.0 (16.5)	48.0 (27.4)
1379 (200)	345 (50)	0.0203 (0.0008)	0.0106 (0.0004)	2.6 (6.4)	0.22 (0.48)	27.0 (15.4)	45.0 (25.7)

P_S = Supply Pressure
P_a = Ambient Pressure
h = Film Thickness
Q = Single Side Leakage
K = Axial Stiffness
SG = Spiral-Groove Seal
SE = Self-Energized Hydrostatic Seal

C-2

TABLE 6-4

DIMENSIONS AND SETUP OF SELF-ENERGIZED HYDROSTATIC FACE SEAL

Outside Diameter, mm (in.)	108	(4.25)
Recess Diameter, mm (in.)	88	(3.46)
Secondary Seal Diameter, mm (in.)	84	(3.31)
Inside Diameter of Hydrostatic Face, mm (in.)	76	(2.99)
Inside Diameter of Seal, mm (in.)	70	(2.76)
Recess Width - 4 Equally Spaced 54° Circumferential Recesses, mm (in.)	2	(0.078)
Orifice Diameter, mm (in.)	0.381	(0.015)

TABLE 6-5

DIMENSIONS OF SPIRAL-GROOVE FACE SEAL

Outside Diameter, mm (in.)	108	(4.25)
Secondary Seal Diameter, mm (in.)	84	(3.31)
Inside Diameter of Seal Interface, mm (in.)	81.0	(3.19)
Inside Diameter of Seal, mm (in.)	70	(2.76)
Diameter of Groove-Dam Interface, mm (in.)	85.9	(3.38)
Groove Depth, mm (in.)	0.0445	(0.00176)
Groove Angle (deg)	27.9	
Land-to-Groove Ratio	2.34	
Inward Pumping		

TABLE 6-6

SPIRAL-GROOVE AND SELF-ENERGIZED HYDROSTATIC FACE SEAL PERFORMANCE

Type	P_a kPa (psi)	h mm (in.)	W N (lb)	Q kg/s (lb/s)	K N/m x 10^{-6} (lb/in. x 10^{-4})	PL W (hp)
SE	345 (50)	0.0118 (0.0005)	5336 (1200)	0.00035 (0.00077)	84 (47.9)	149 (0.2)
SE	0	0.0141 (0.0006)	4991 (1122)	0.0007 (0.0015)	80 (45.6)	130 (0.17)
SG	345 (50)	0.0091 (0.0004)	5336 (1200)	0.00045 (0.0010)	82 (46.8)	130 (0.17)
SG	0	0.0098 (0.0004)	4991 (1122)	0.0007 (0.0015)	86.5 (49.4)	118 (0.16)

P_S = Supply Pressure: 1379 kPa (200 psi)
N = 3142 rad/s (30,000 rpm)
μ = 2×10^{-5} Pa-s (2.9×10^{-9} lb-s/in.^{2})
SE = Self-Energized Hydrostatic Seal
SG = Spiral-Groove Seal
P_a = Ambient Pressure
h = Film Thickness
W = Equilibrium Load
Q = Single Side Leakage
K = Stiffness
PL = Viscous Power Loss

TABLE 6-7

SUMMARY OF FACE SEAL DYNAMIC CASES

	Case			
	1	2	3	4
x-Displacement (mm)	0.0051	0.0076	0.0102	0.0102
y-Displacement (mm)	0.0051	0.0076	0.0102	0.0102
z-Displacement (mm)	0.0051	0.0076	0.0102	0.0102
a-Displacement (rad)	0.0002	0.0003	0.0004	0.0004
B-Displacement (rad)	0.0002	0.0003	0.0004	0.0004
Frequency (rad/s)	3142	3142	3142	3142
Coefficient of Friction	0.2	0.2	0.2	0.1
Result	Tracks	Tracks	Contact	Tracks

Fluid-Film Axial Stiffness = 84.0×10^6 N/m (479.6×10^3 lb/in.)
Fluid-Film Angular Stiffness = 49.2×10^3 N-m/rad (435.4×10^3 lb-in/.rad)
Equilibrium Film Thickness (h_o) = 0.0127 mm (0.0005 in.)
Buffer Fluid Pressure = 1379 kPa (200 psig)
Ambient Pressure = 345 kPa (50 psig)

0.0051 mm = 0.0002 in.
0.0076 mm = 0.0003 in.
0.0102 mm = 0.0004 in.
3142 rad/s = 30,000 rpm

TABLE 6-8

OTHER SEAL PARAMETERS

Mass of Seal Ring, kg (lb)	0.13	(0.286)
Distance from Seal Face to CG, mm (in.)	6.37	(0.251)
Polar Moment of Inertia, kg-m^2 (lb-$in.^2$)	2.71×10^{-4}	(0.9252)
Transverse Moment of Inertia, kg-m^2 (lb-$in.^2$)	1.38×10^{-4}	(0.4713)
Closing Area, m^2 ($in.^2$)	3.643×10^{-3}	(5.65)
Hydraulic Closing Force, N (lb)	5331	(1200)
Interface Area, m^2 ($in.^2$)	4.625×10^{-3}	(7.17)
Secondary Seal Preload Friction, N (lb)	315.92	(71.02)

TABLE 6-9

SUMMARY OF SEAL RING DEFORMATIONS

	LOX Side Seal Ring mm (in.)	H2 Side Seal Ring mm (in.)
Temperature Deformation	0.0041 (0.0002)	0.0406 (0.0016)
Pressure Deformation	0.0089 (0.0004)	0.0089 (0.0004)
Total Deformation	0.0130 (0.0005)	0.0495 (0.0019)

TABLE 6-10

PREDICTED PERFORMANCE OF SELF-ENERGIZED FACE SEAL

	Ambient Pressure			
	0 kPa	(0) (psig)	345 kPa	(50) (psig)
Supply Pressure, kPa (psi)	1379	(200)	1379	(200)
Recess Pressure, kPa (psi)	1144	(166)	1245	(181)
Film Thickness, mm (in.)	0.0141	(0.0006)	0.0118	(0.0005)
Leakage, Two Rings, kg/s (lb/sec)	0.0014	(0.003)	0.0007	(0.0015)
Axial Stiffness, $N/m \times 10^{-6}$ ($lb/in. \times 10^{-4}$)	80	(45.6)	84	(47.9)
Power Loss, Two Rings, W (hp)	260	(0.34)	298	(0.40)

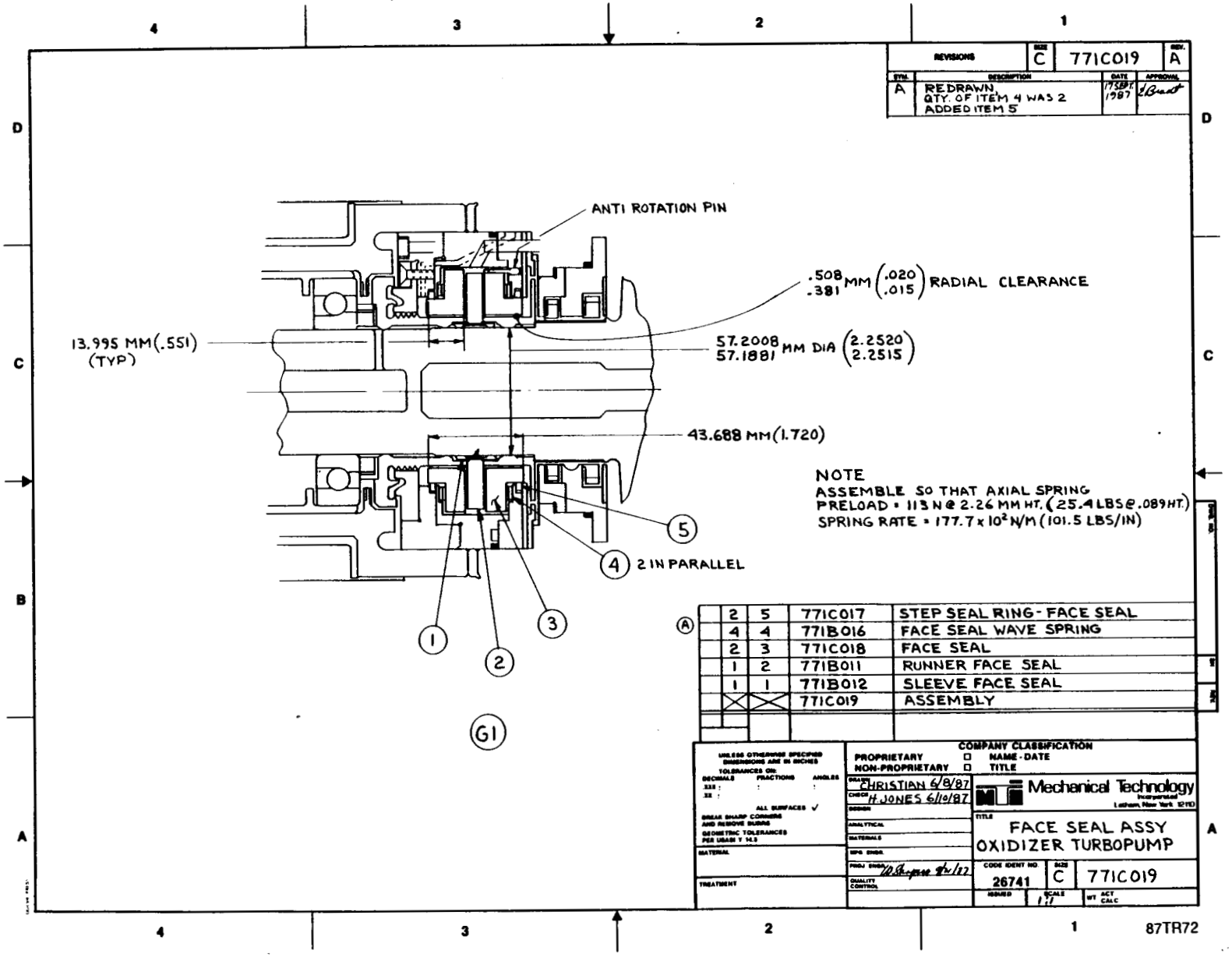

Figure 6-1. Face Seal Assembly

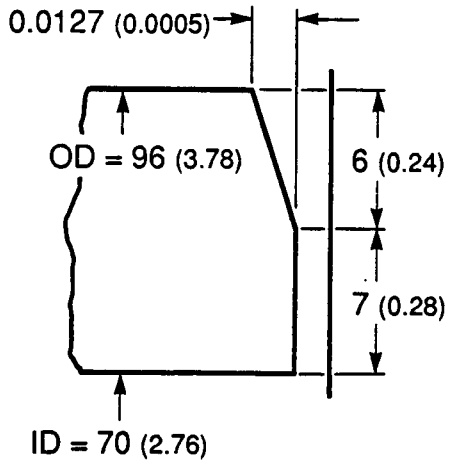

1. Radial Tapered (RT)

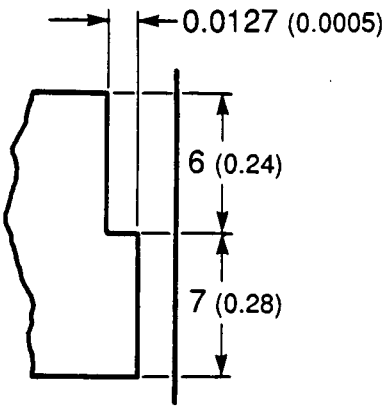

2. Radial Step (RS)

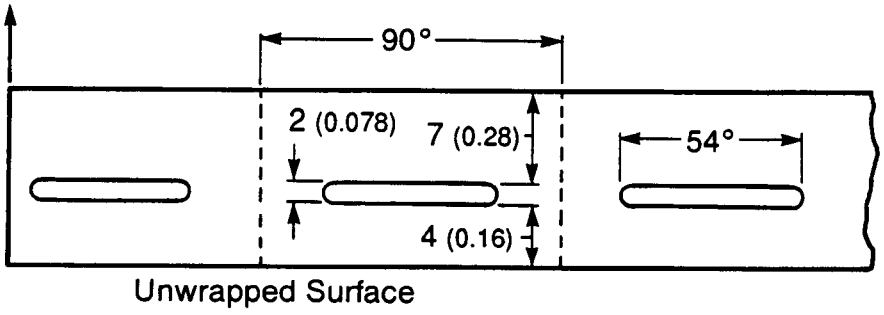

3. Self-Energized Hydrostatic

All dimensions in mm (in.)
unless otherwise specified

872529

Figure 6-2 Face Seal Configurations

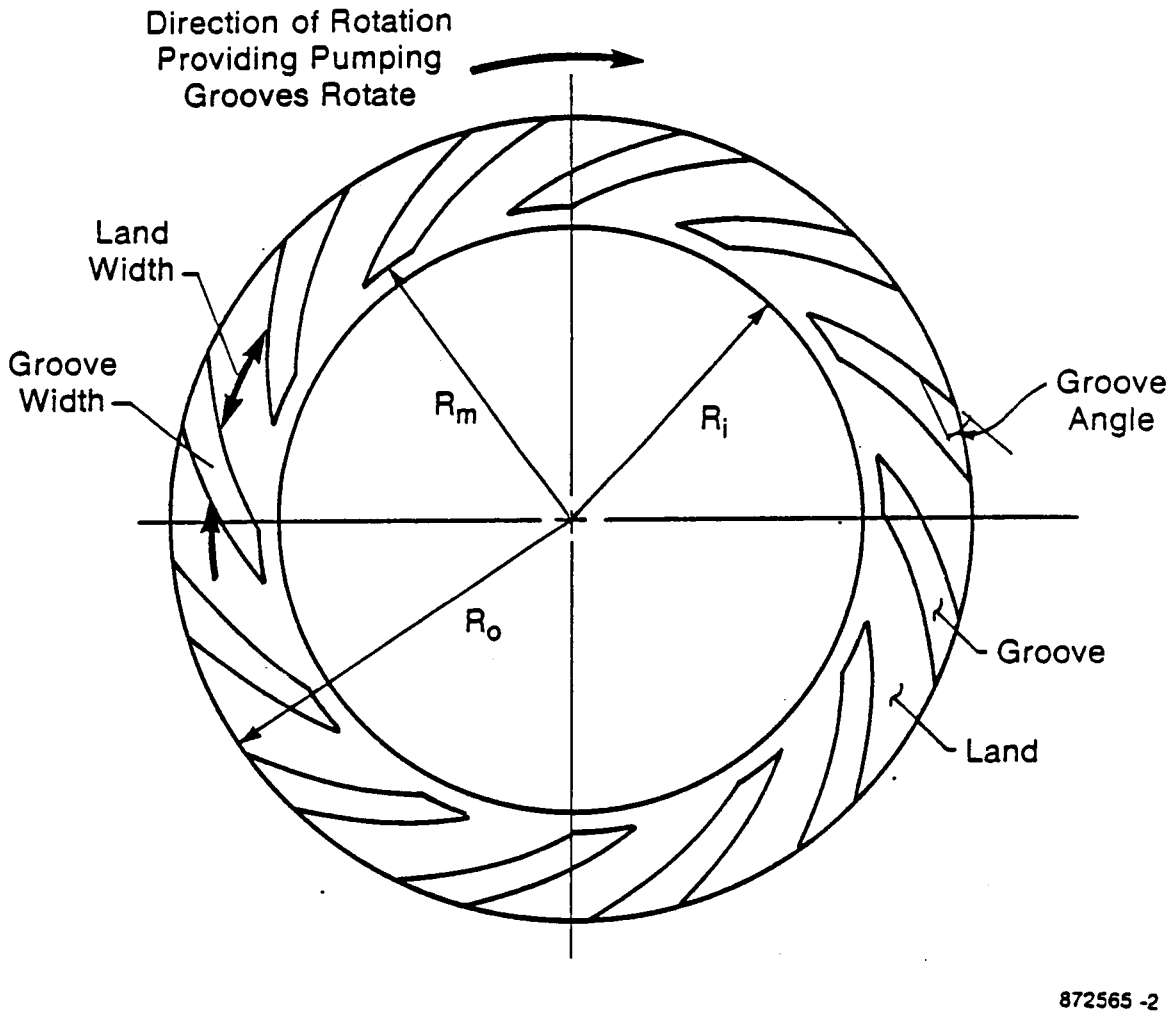

Figure 6-3 Spiral Groove Parameters

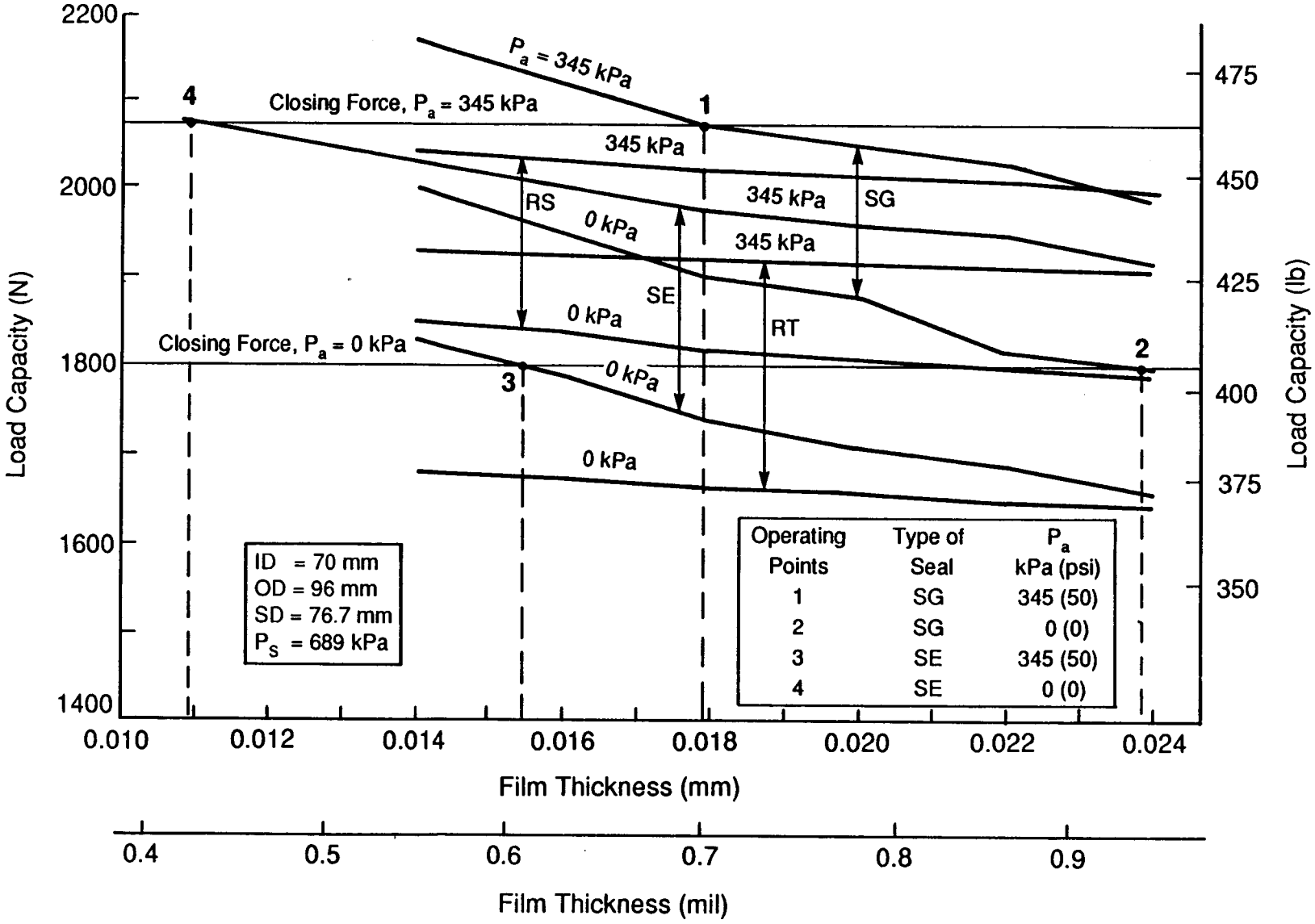

Figure 6-4 Face Seal Clearance Variation (P_S = 689 kPa)

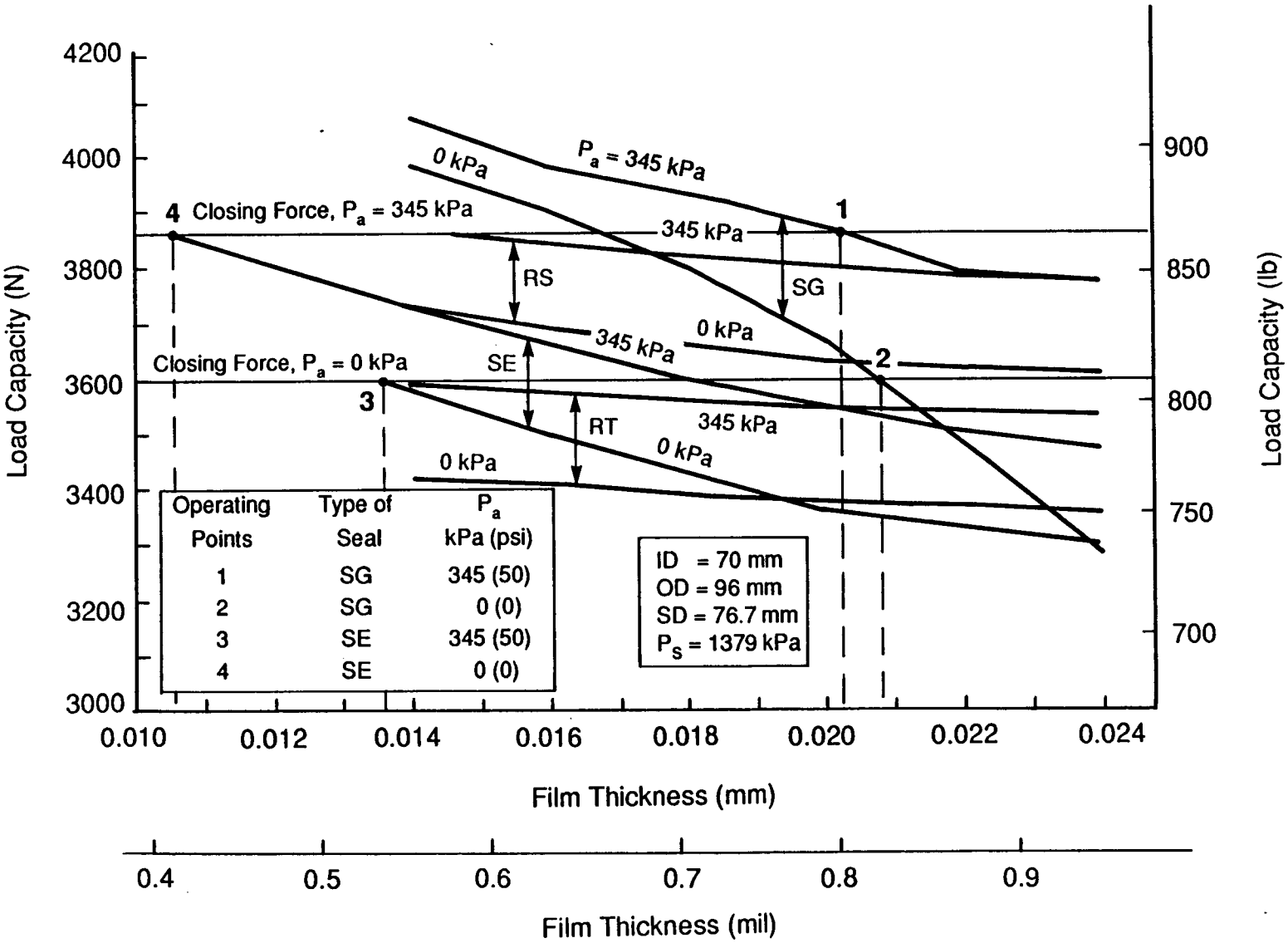

Figure 6-5 Face Seal Clearance Variation (P_s = 1379 kPa)

89678

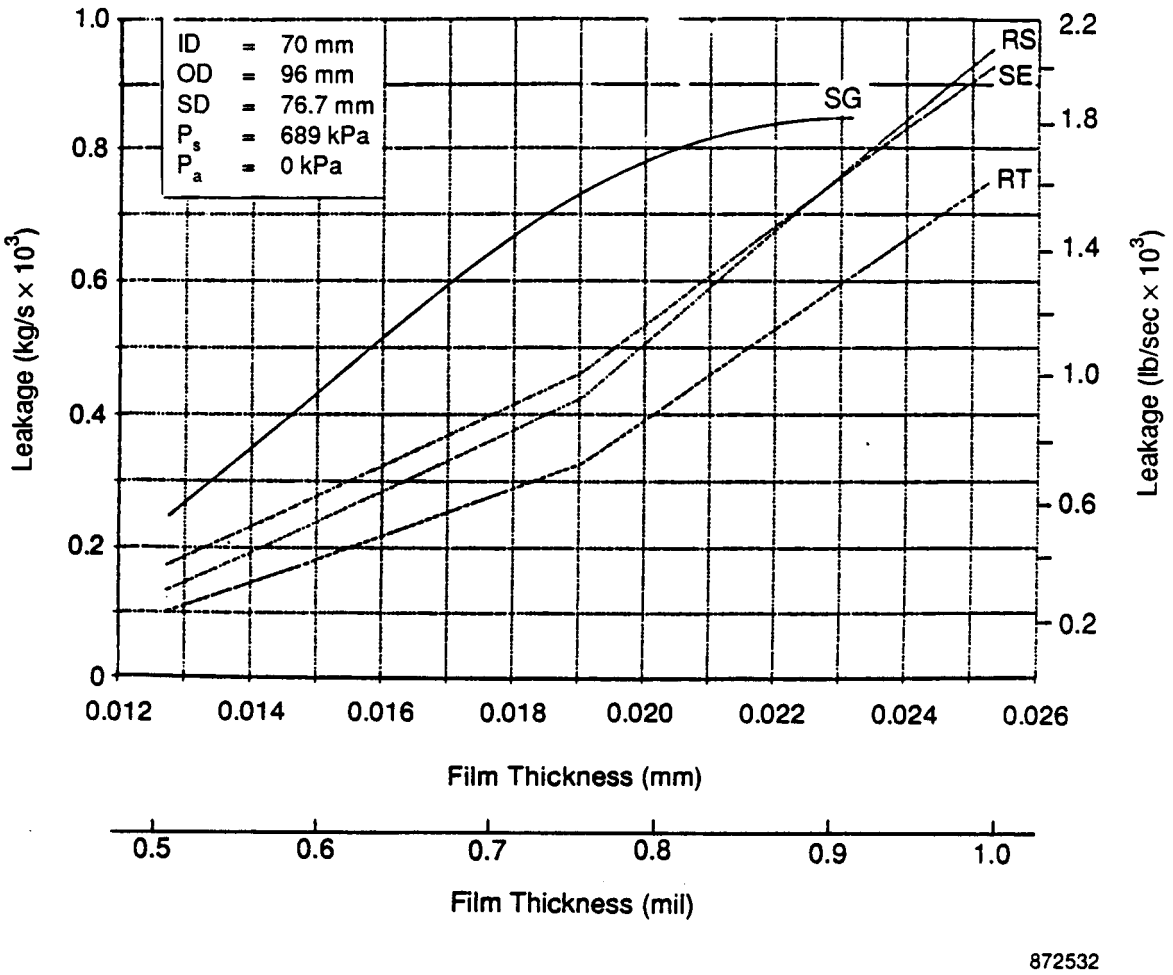

Figure 6-6 Face Seal Comparative Performance; Leakage vs. Film Thickness (P_s = 689 kPa, P_a = 0 kPa)

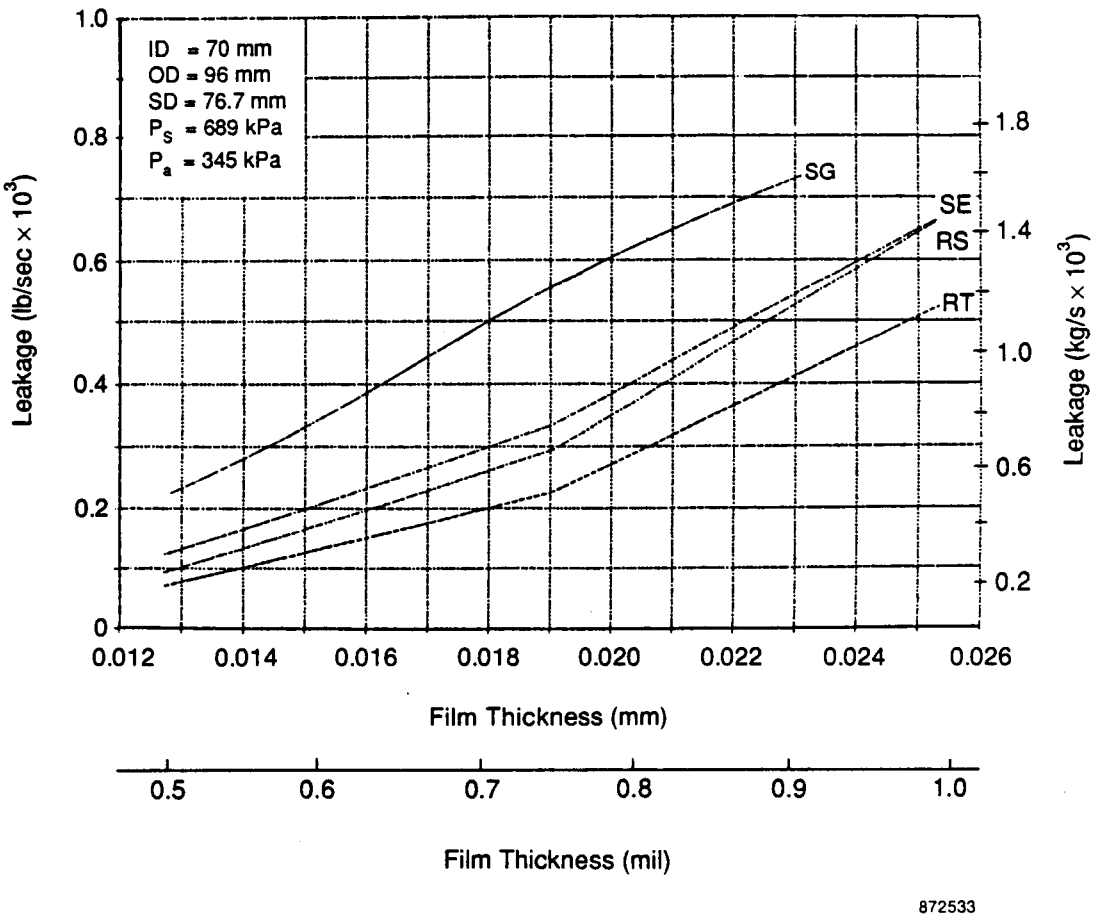

Figure 6-7 Face Seal Comparative Performance; Leakage vs. Film Thickness (P_s = 689 kPa; P_a = 345 kPa)

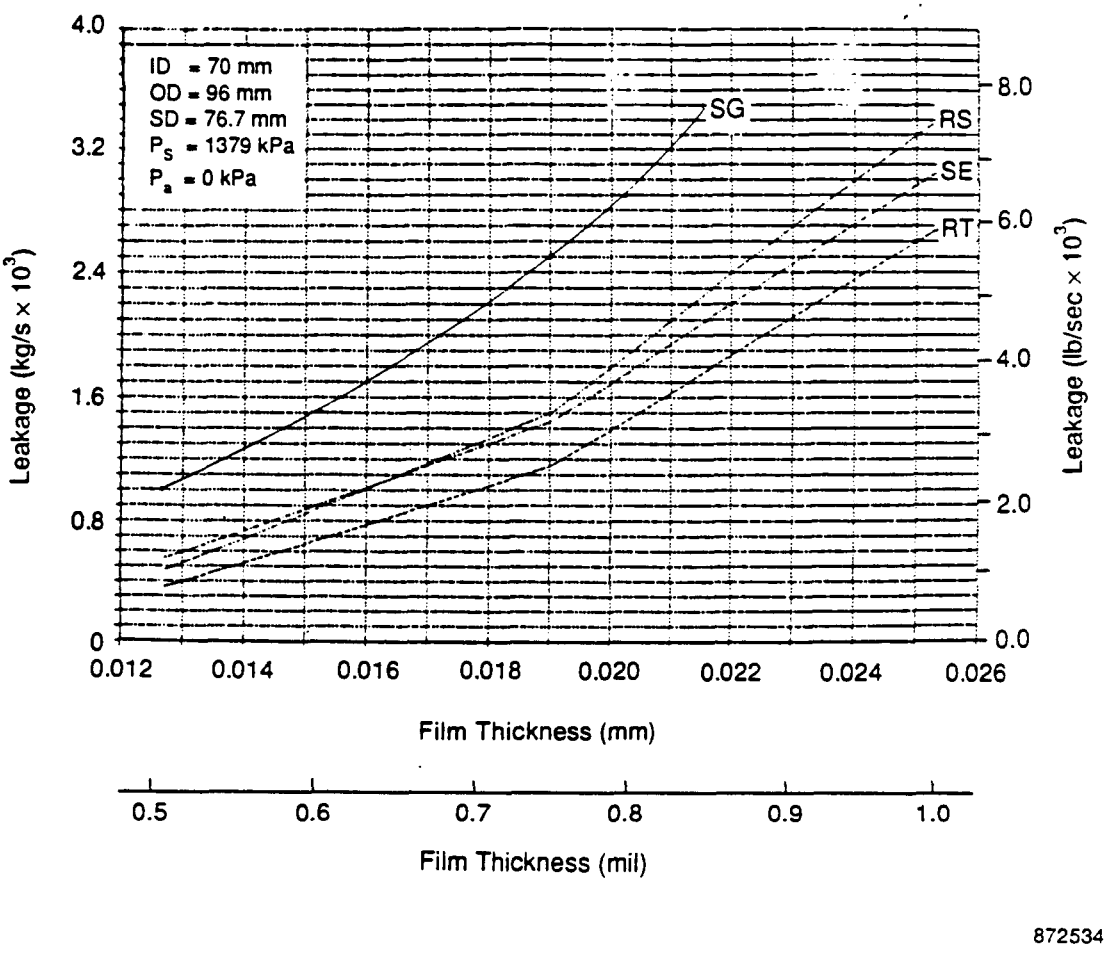

Figure 6-8 Face Seal Comparative Performance; Leakage vs. Film Thickness (P_s = 1379 kPa; P_a = 0 kPa)

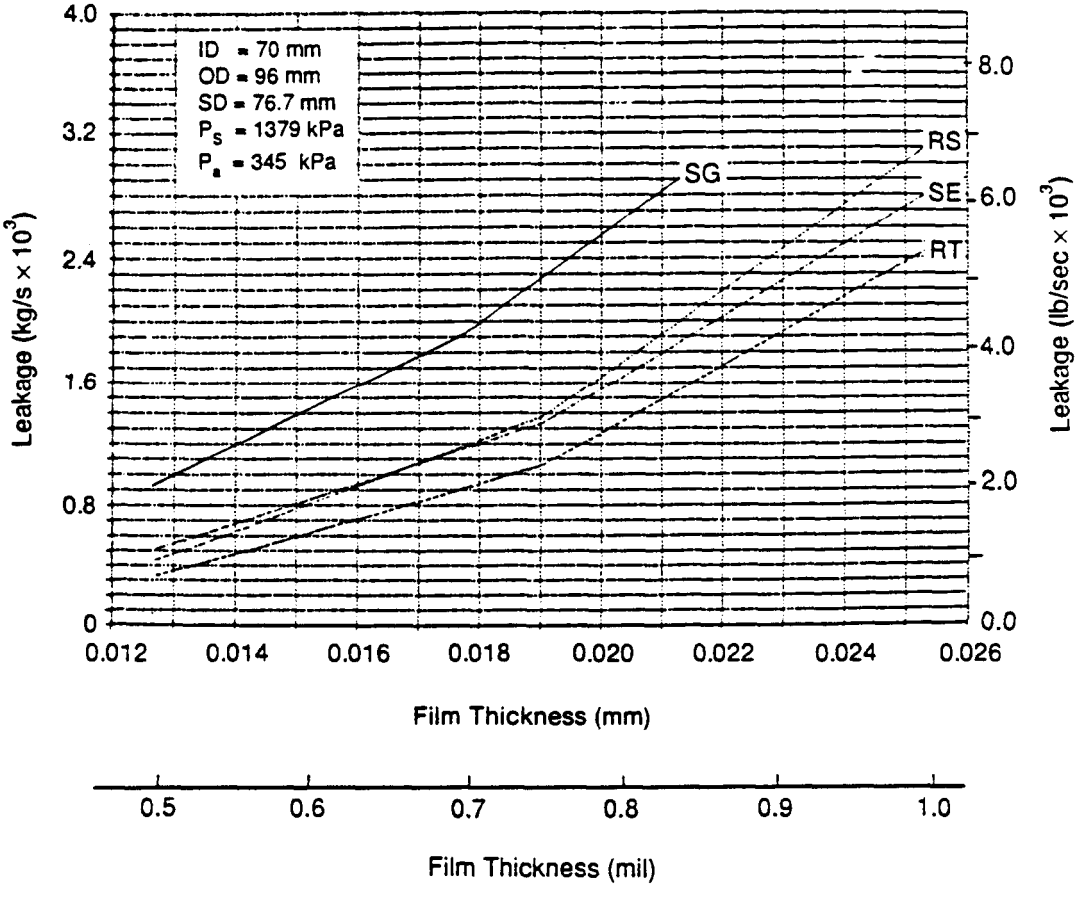

Figure 6-9 Face Seal Comparative Performance; Leakage vs. Film Thickness (P_s = 1379 kPa; P_a = 345 kPa)

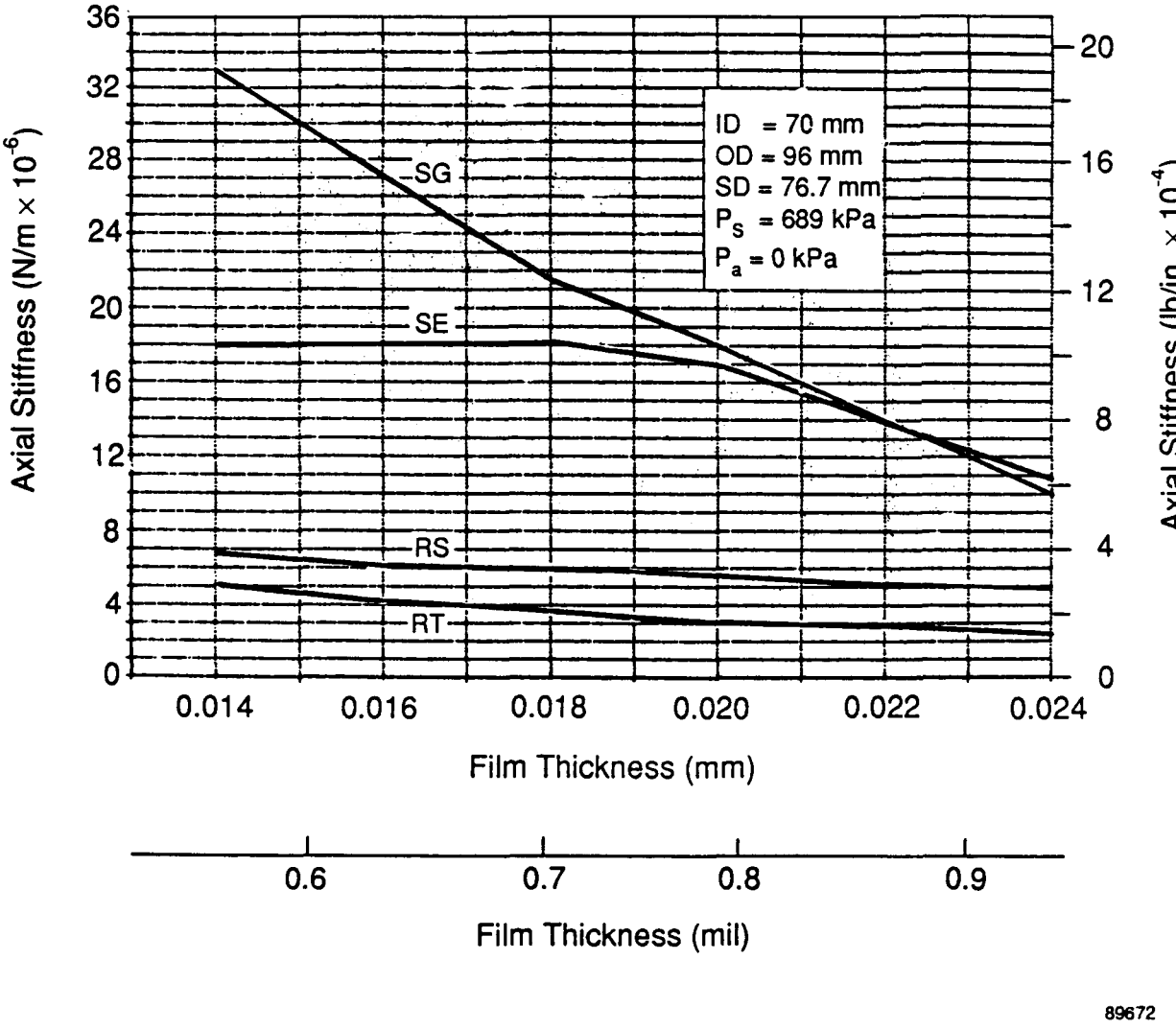

Figure 6-10 Face Seal Comparative Performance; Stiffness vs. Film Thickness (P_s = 689 kPa; P_a = 0 kPa)

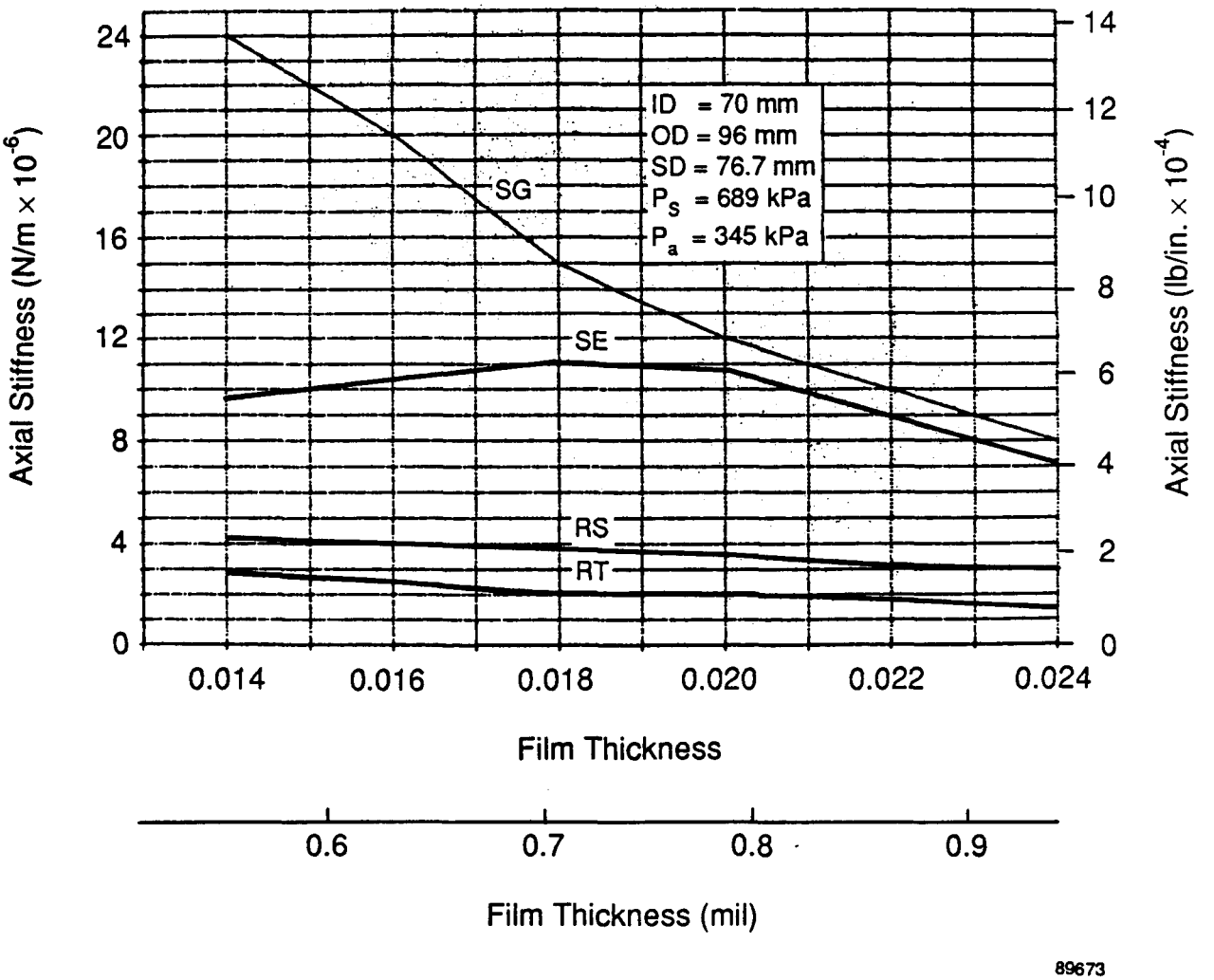

Figure 6-11 Face Seal Comparative Performance; Stiffness vs. Film Thickness (P_s = 689 kPa; P_a = 456 kPa)

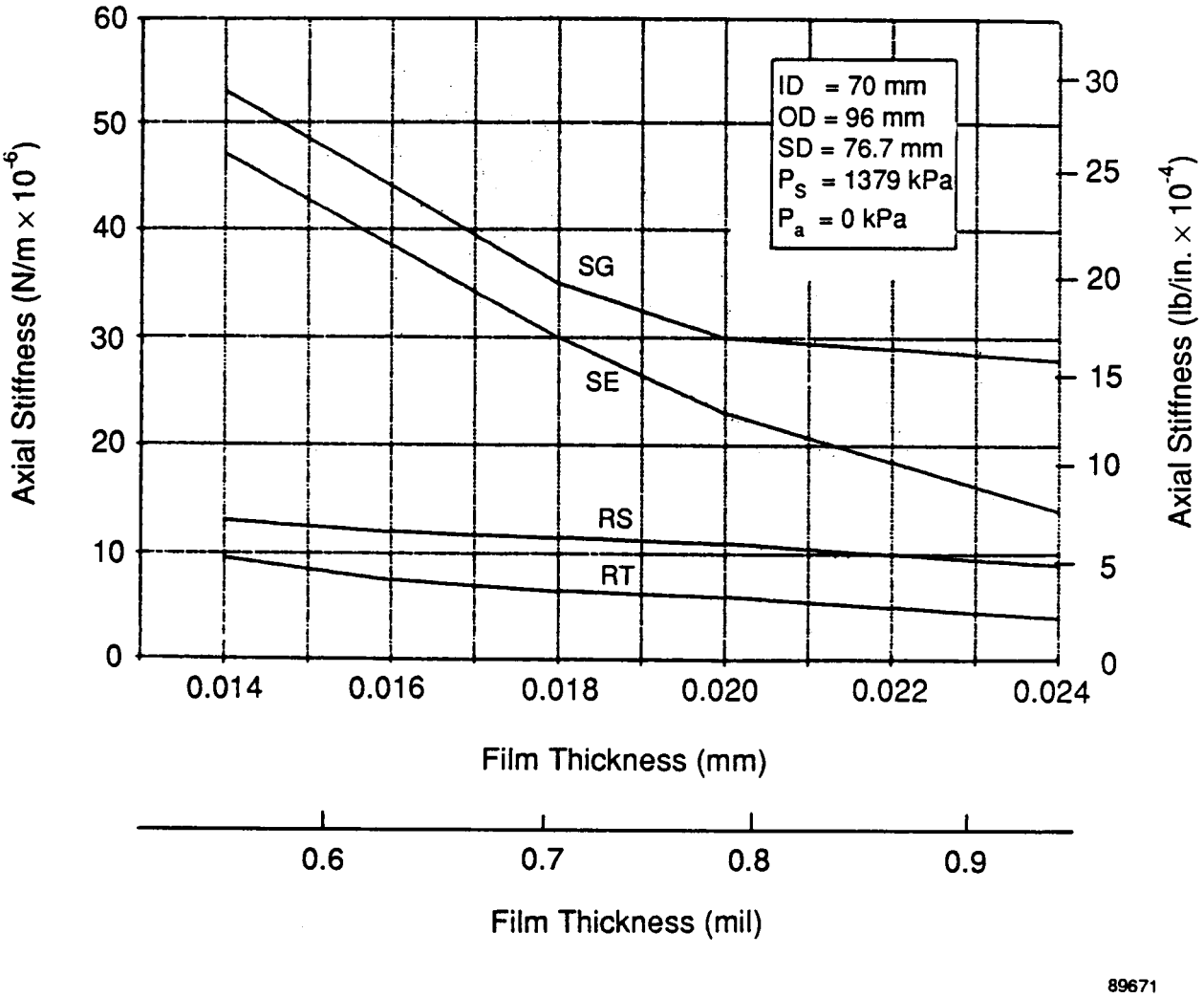

Figure 6-12 Face Seal Comparative Performance; Stiffness vs. Film Thickness (P_s = 1379 kPa; P_a = 0 kPa)

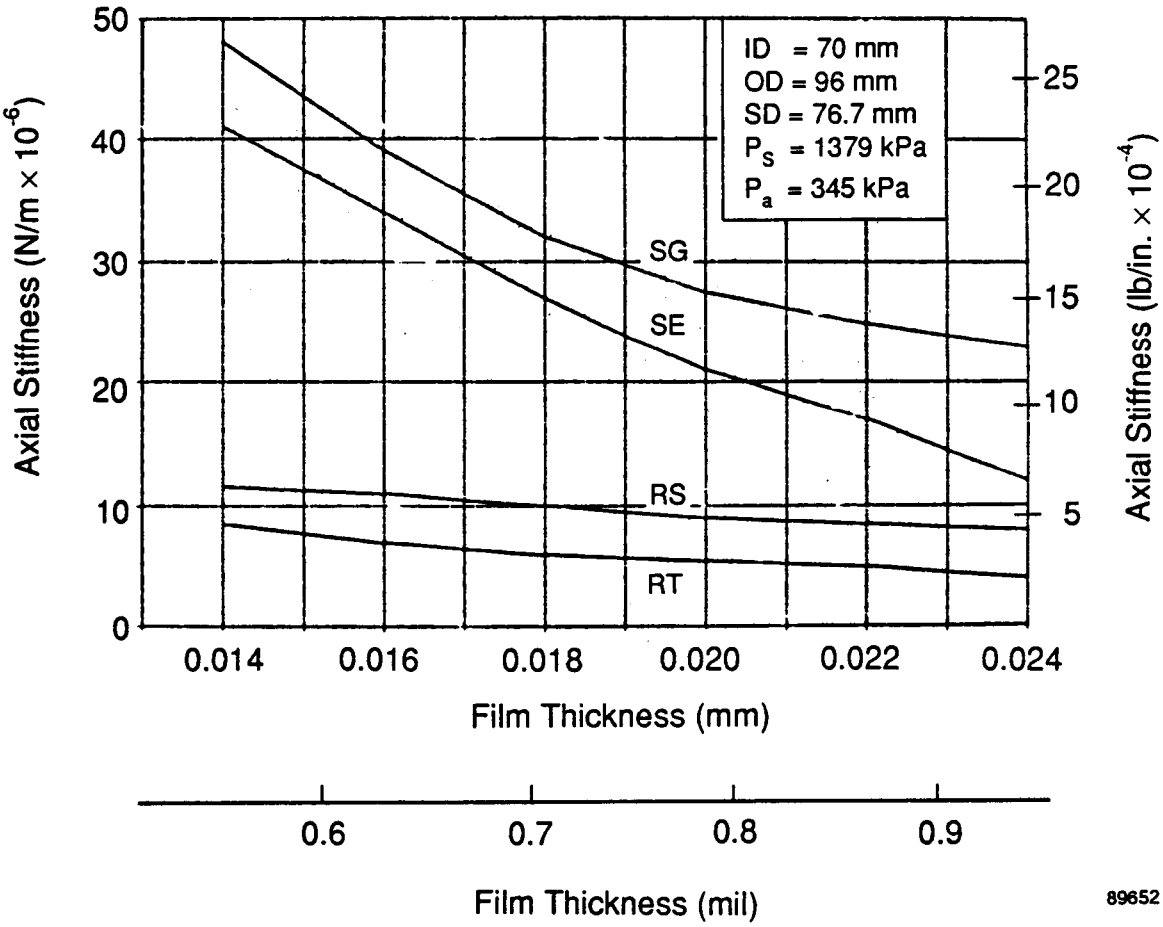

Figure 6-13 Face Seal Comparative Performance; Stiffness vs. Film Thickness (P_s = 1379 kPa; P_a = 345 kPa)

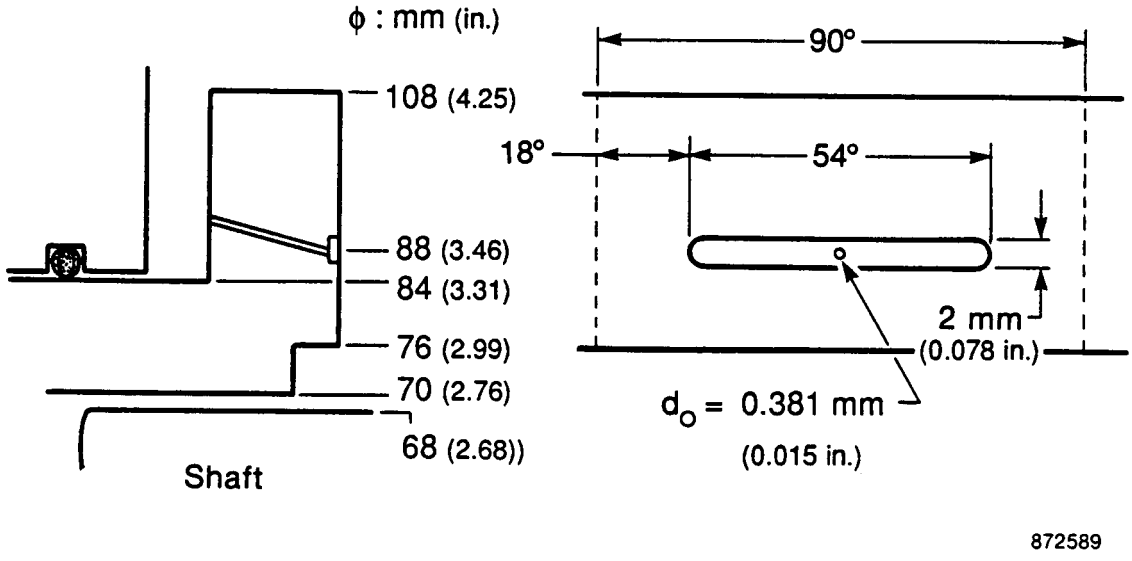

Figure 6-14 Self-Energized Hydrostatic Face Seal Final Dimensions

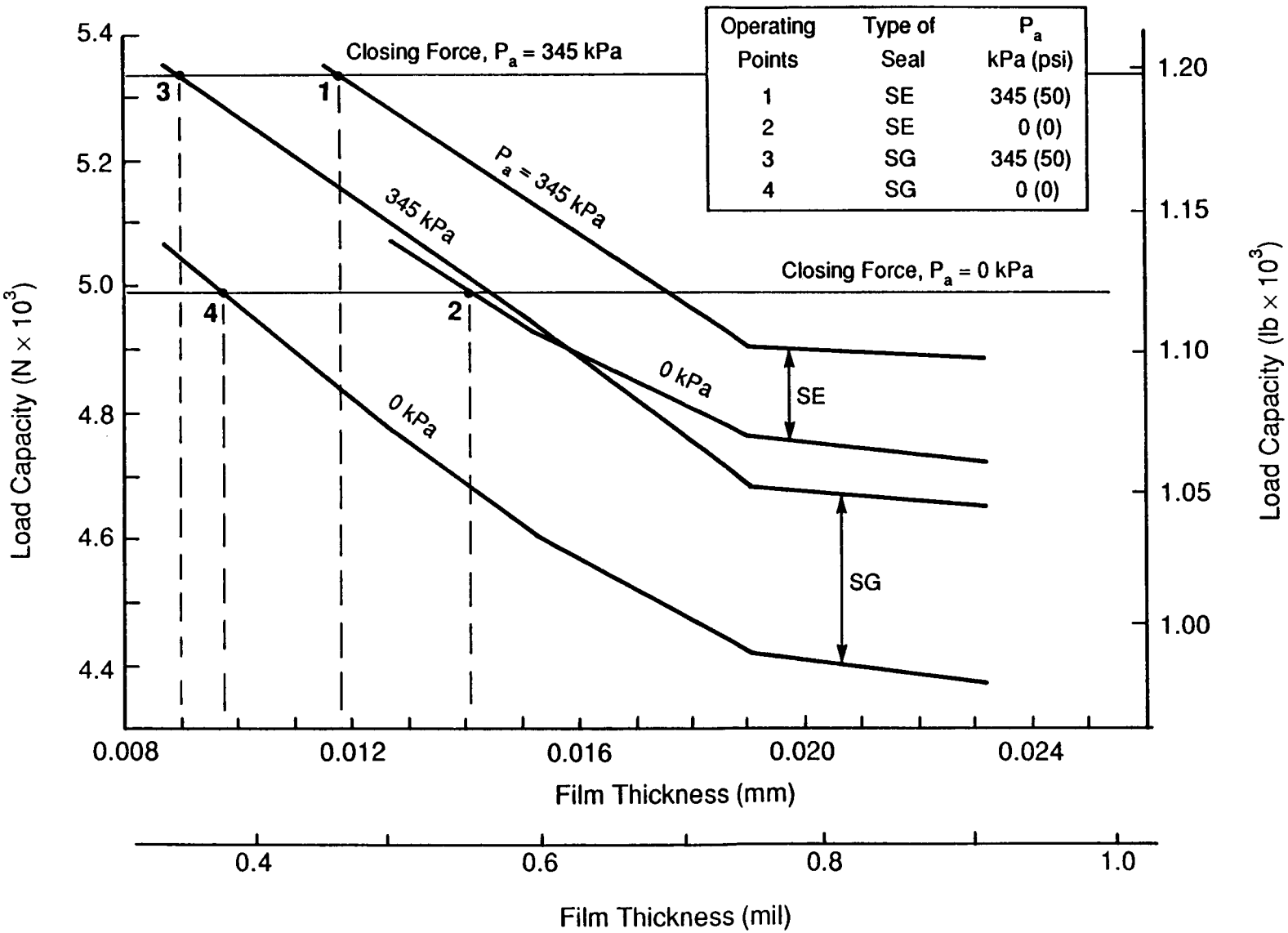

Figure 6-15 Face Seal Performance, Load vs. Film Thickness

89679

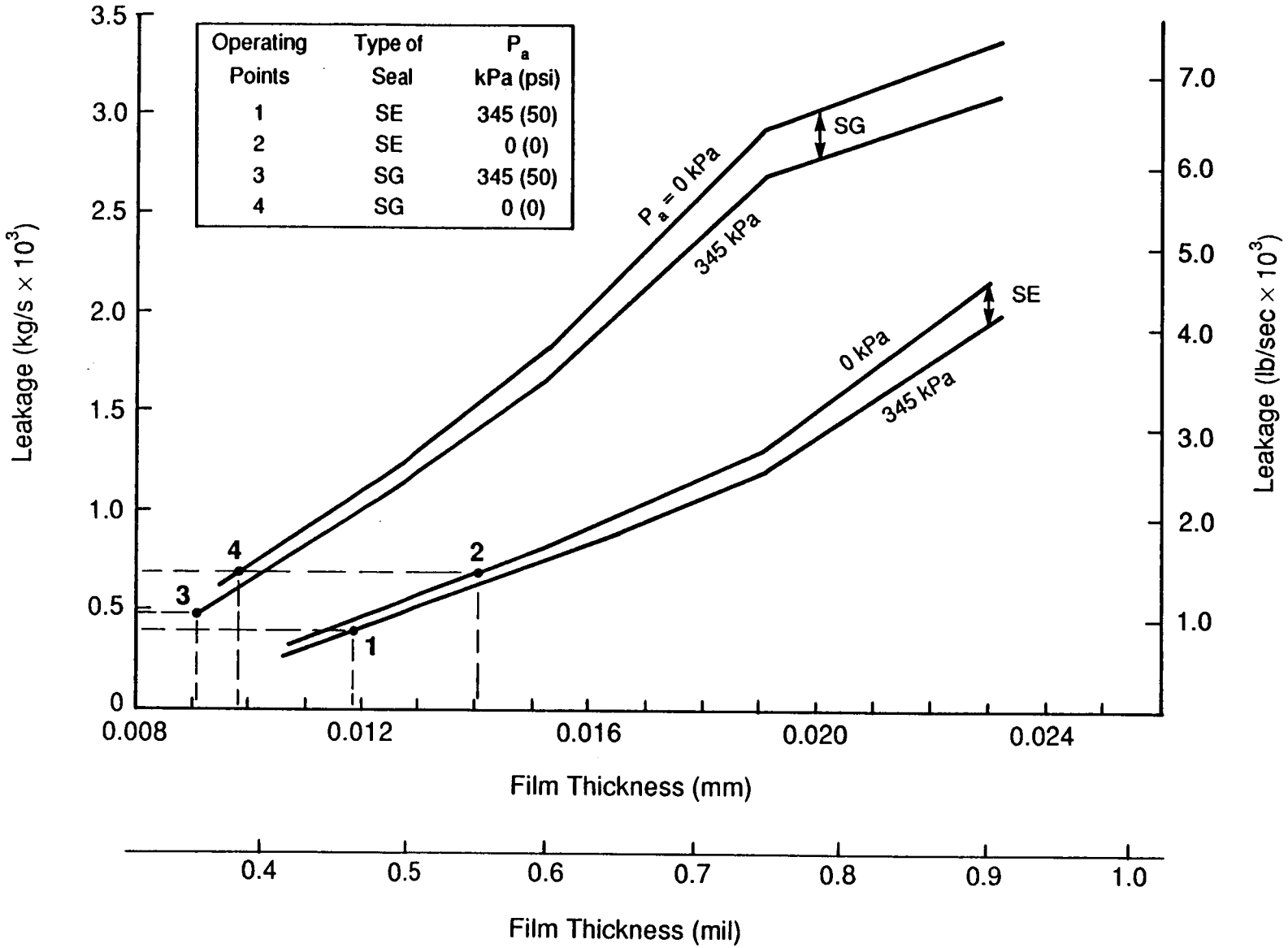

Figure 6-16 Face Seal Performance, Single Side Leakage vs. Film Thickness

89681

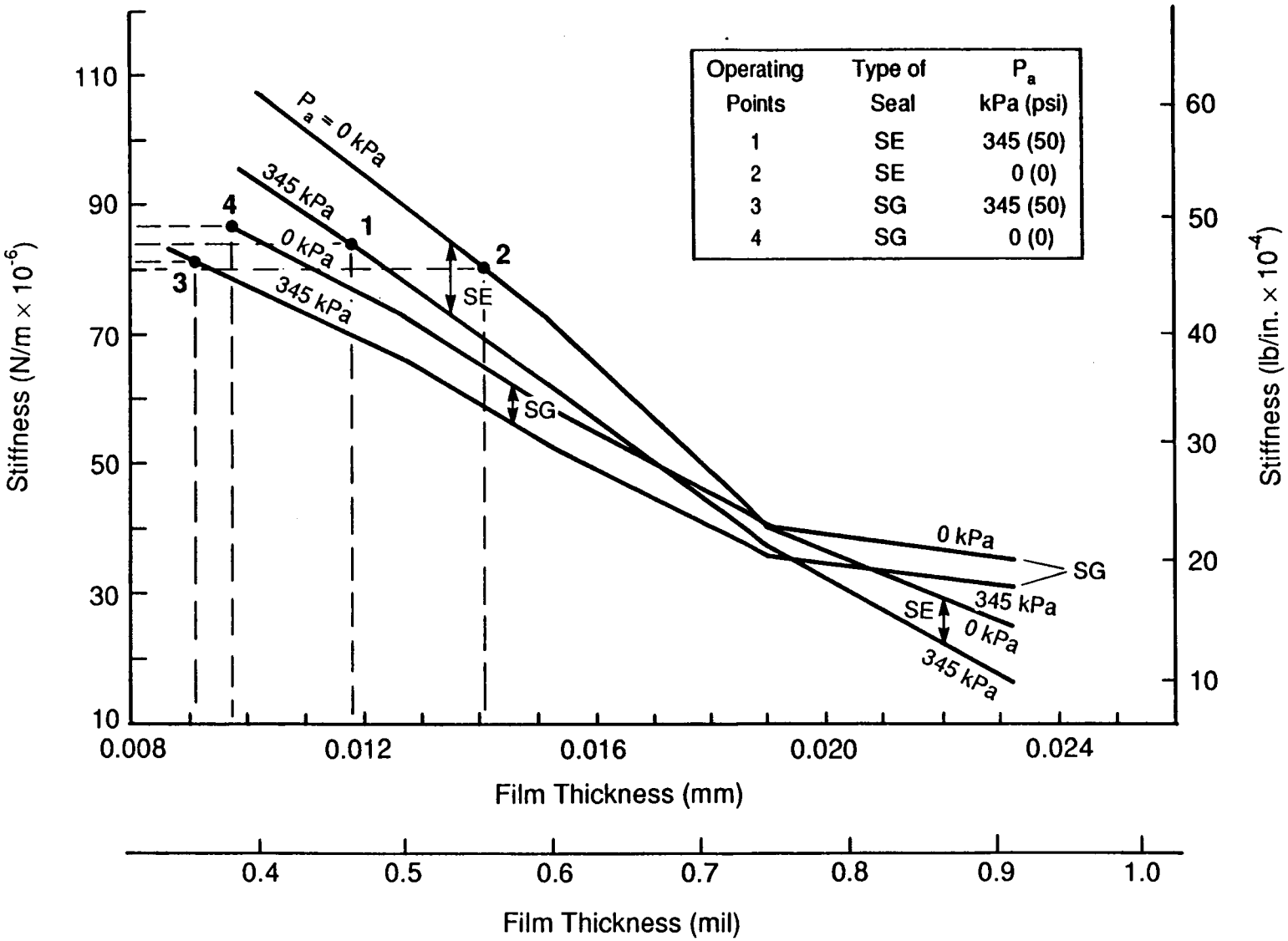

Figure 6-17 Face Seal Performance, Stiffness vs. Film Thickness

89680

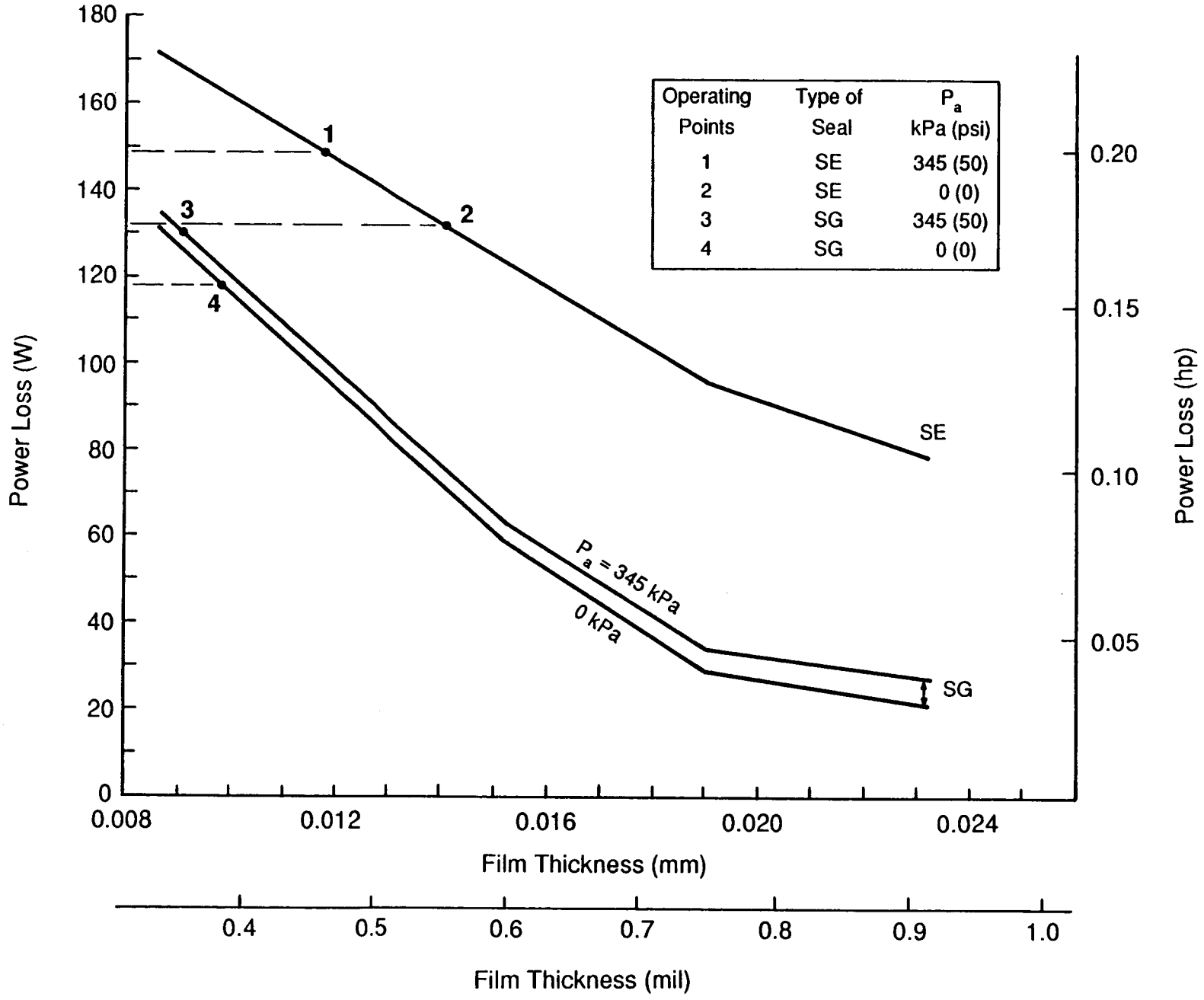

Figure 6-18 Face Seal Performance, Power Loss vs. Film Thickness

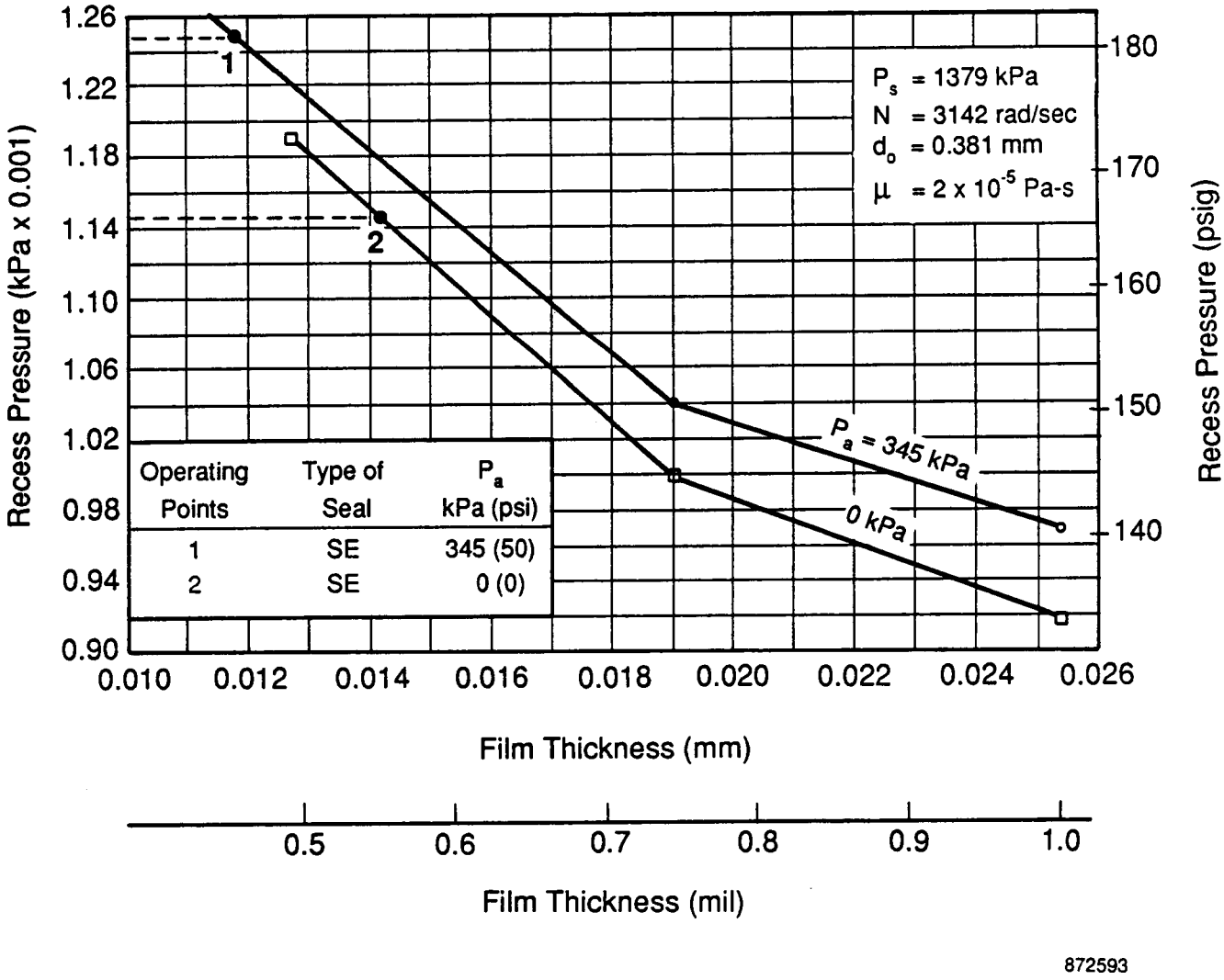

Figure 6-19 Self-Energized Face Seal; Recess Pressure vs. Clearance

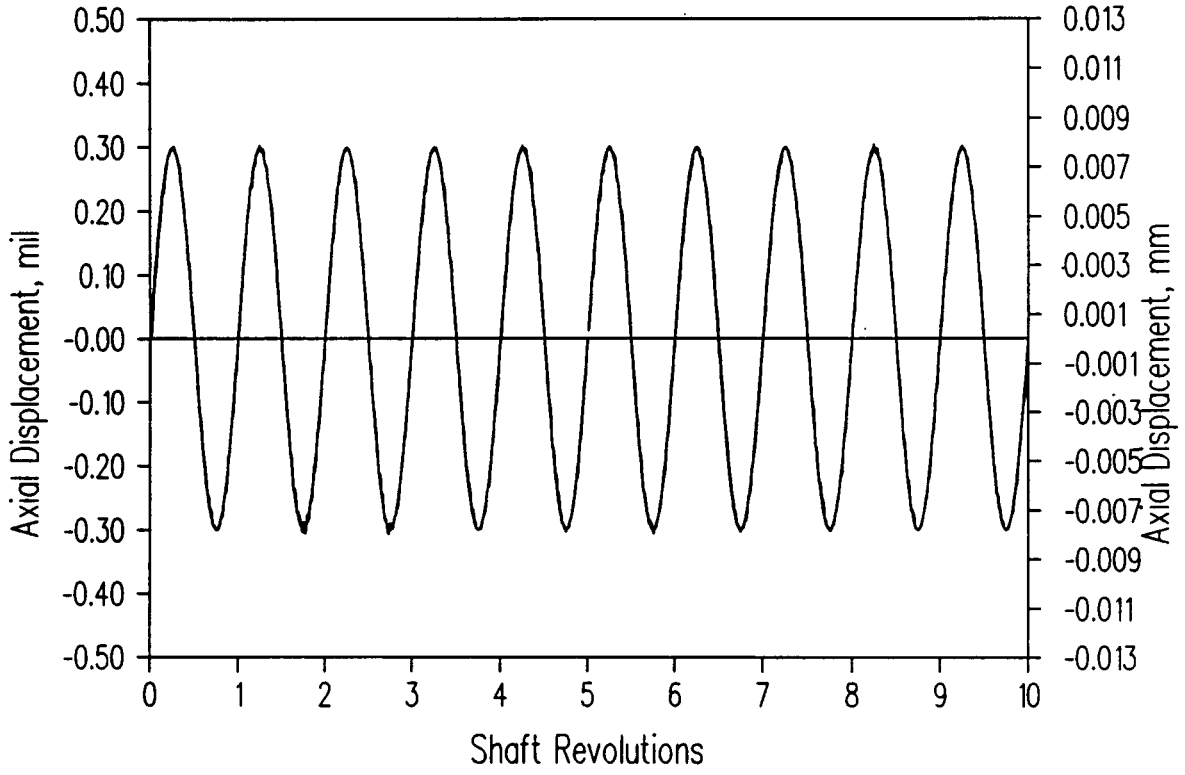

Figure 6-20 Axial Displacement vs. Shaft Revolutions, Case 2

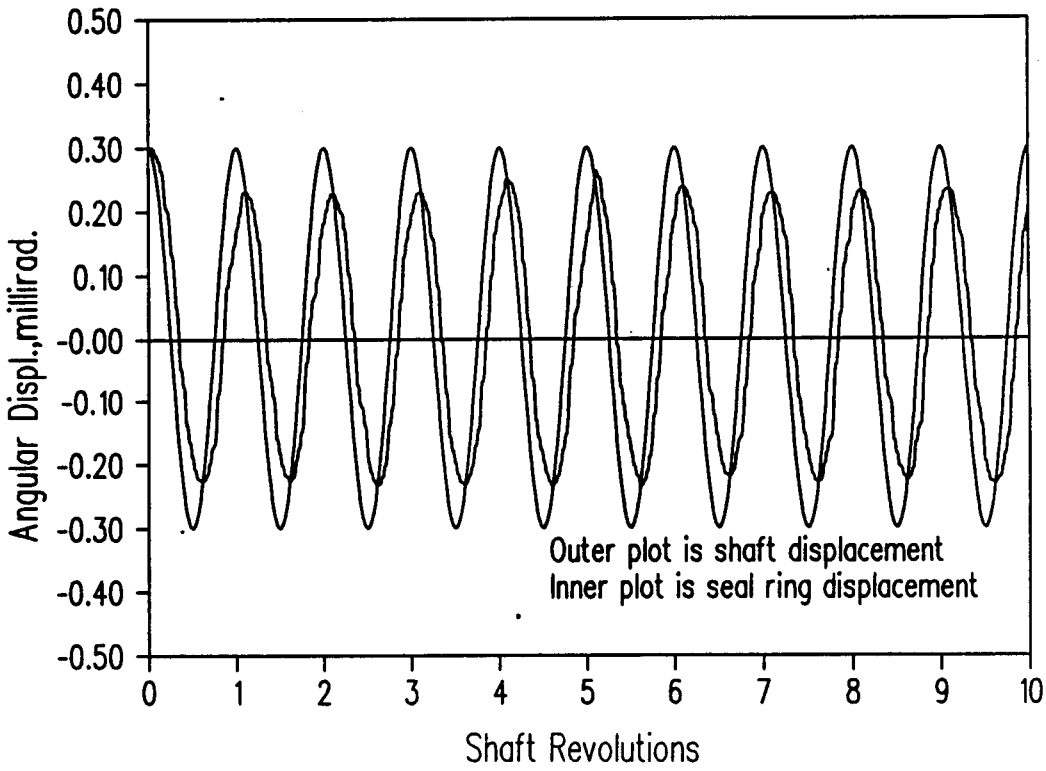

Figure 6-21 Angular Displacement about X-Axis vs. Shaft Revolutions, Case 2

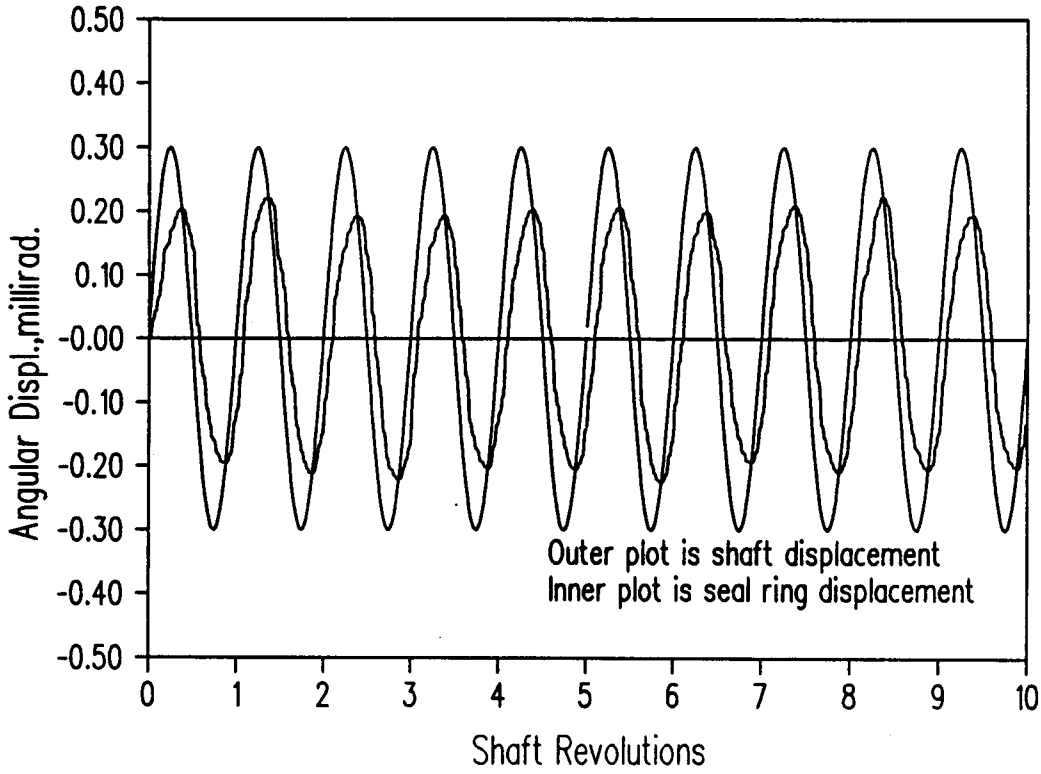

Figure 6-22 Angular Displacement about Y-Axis vs. Shaft Revolutions, Case 2

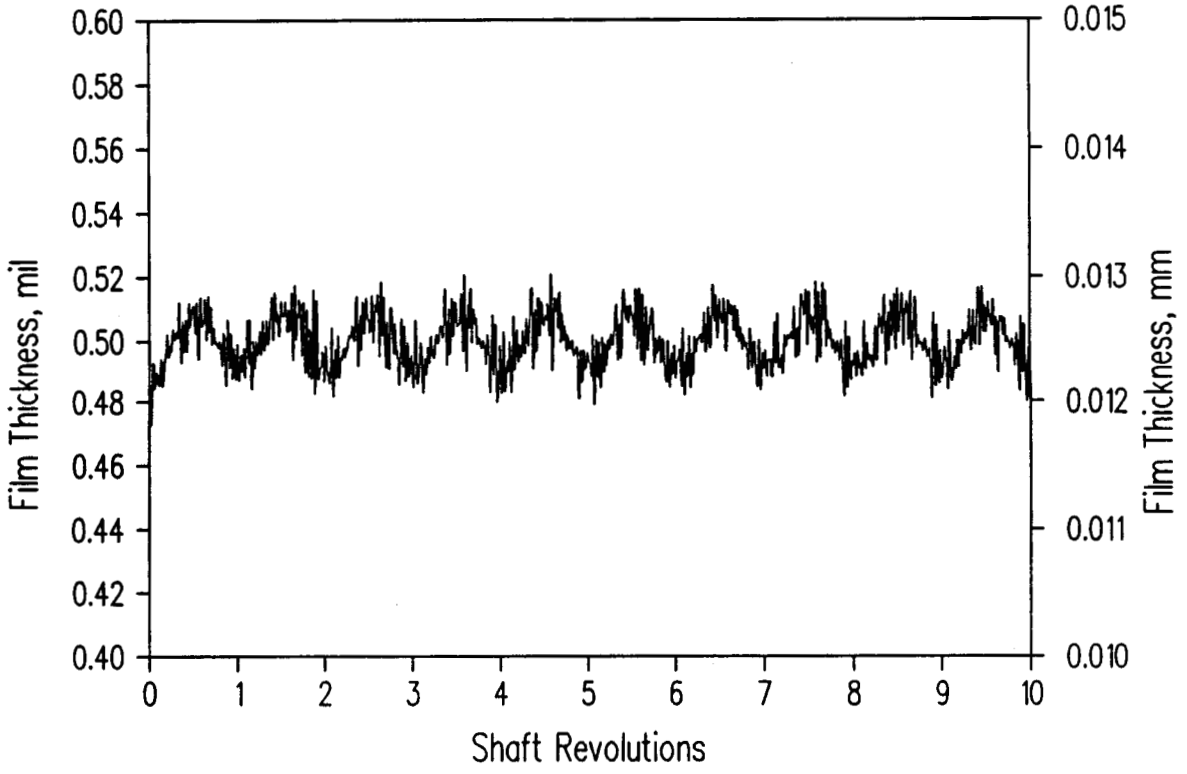

Figure 6-23 Midpoint Film Thickness vs. Shaft Revolutions, Case 2

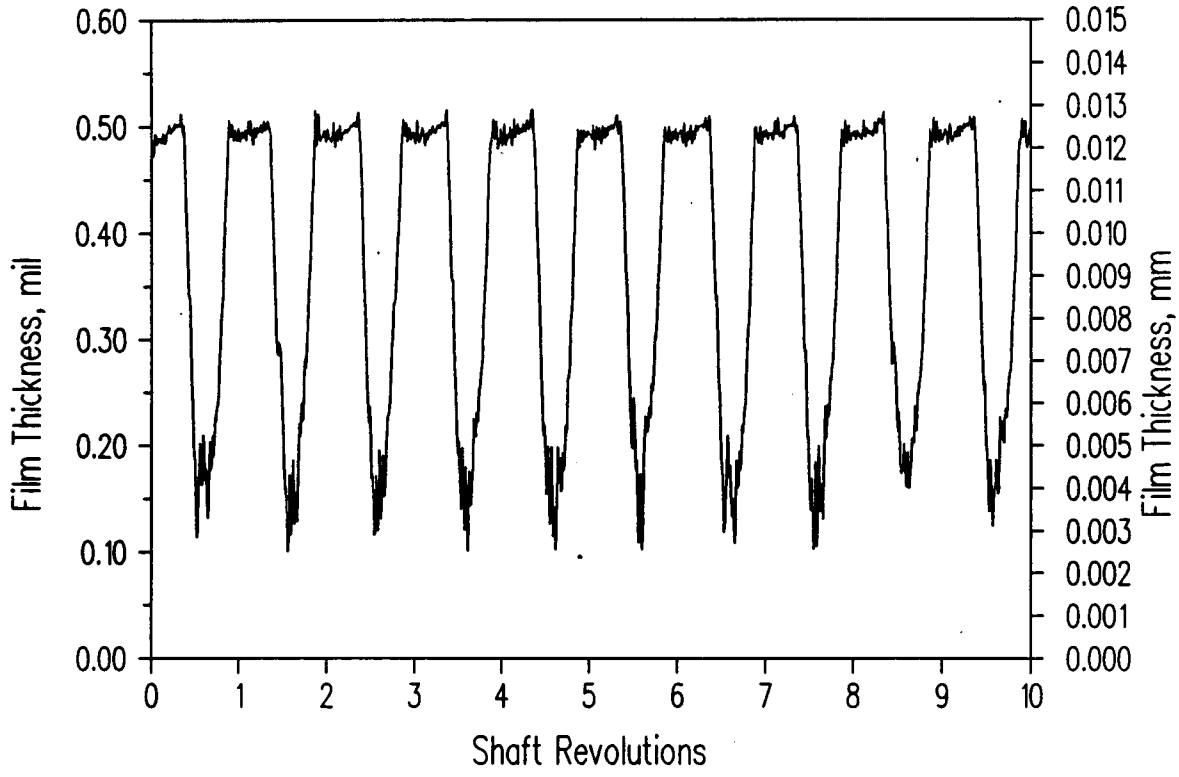

Figure 6-24 Minimum Film Thickness vs. Shaft Revolutions, Case 2

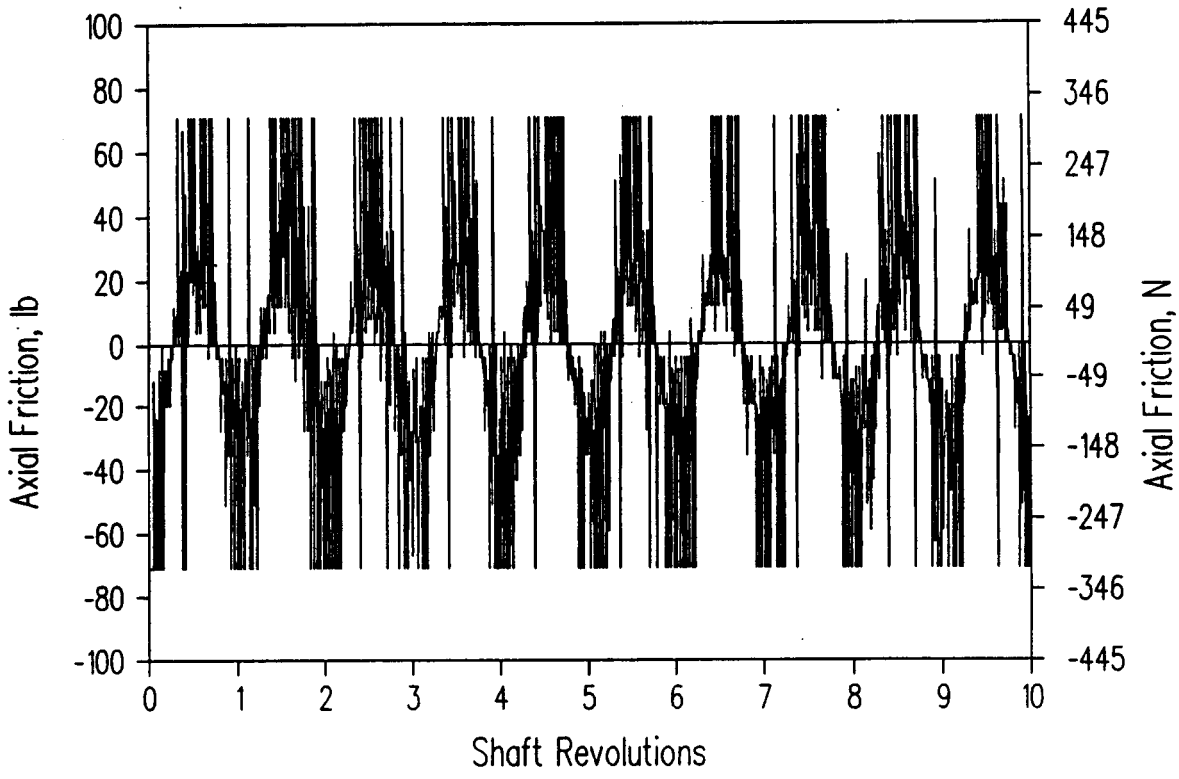

Figure 6-25 Axial Friction vs. Shaft Revolutions, Case 2

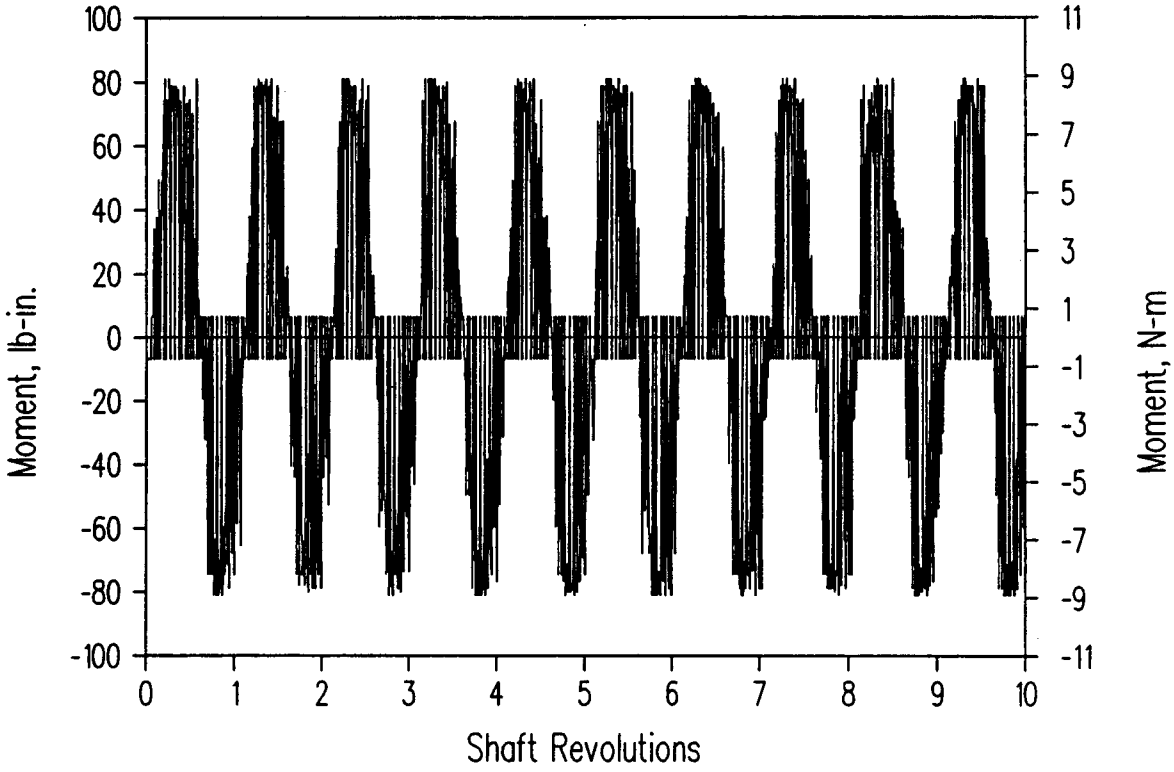

Figure 6-26 Friction Moment about X-Axis vs. Shaft Revolutions, Case 2

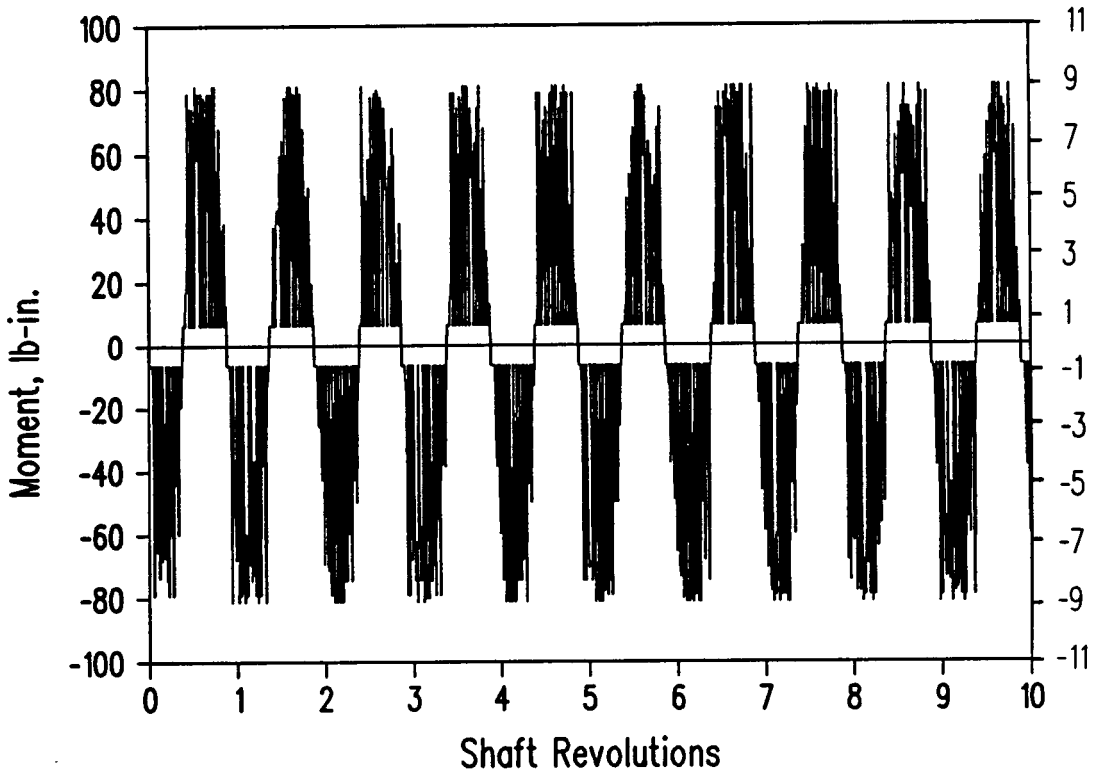

Figure 6-27 Friction Moment about Y-Axis vs. Shaft Revolutions, Case 2

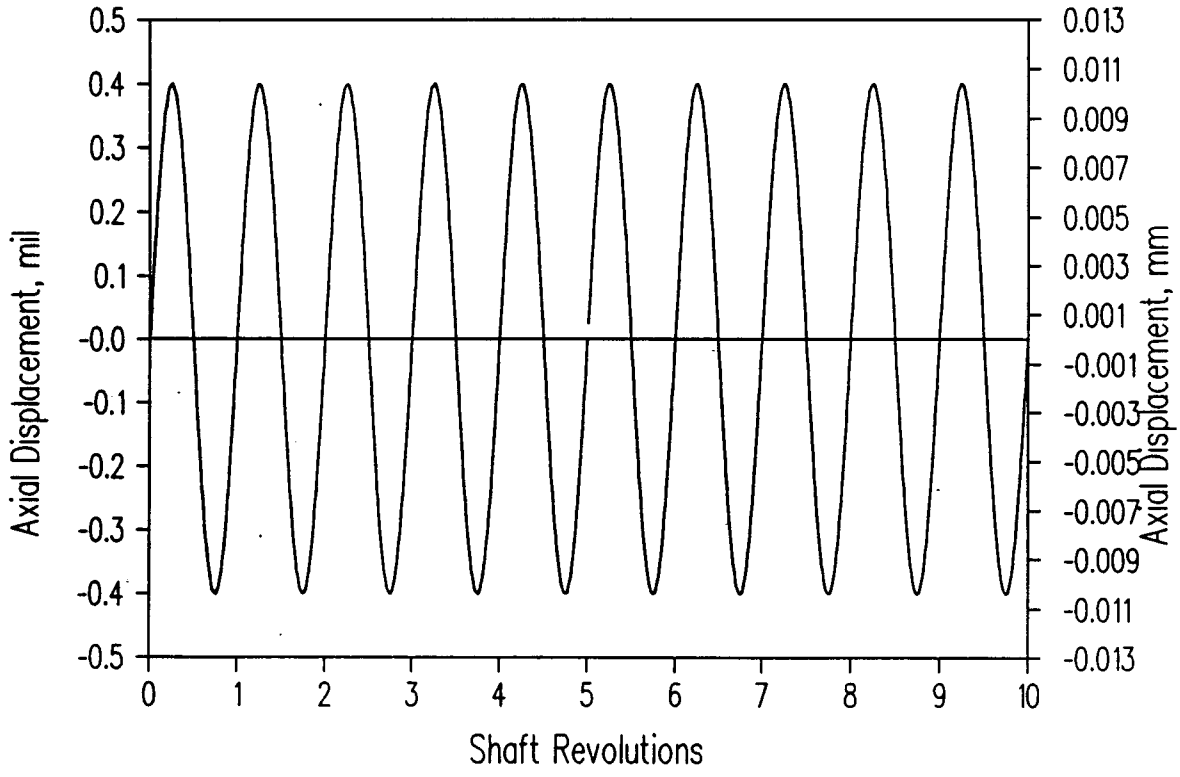

Figure 6-28 Axial Displacement vs. Shaft Revolutions, Case 5

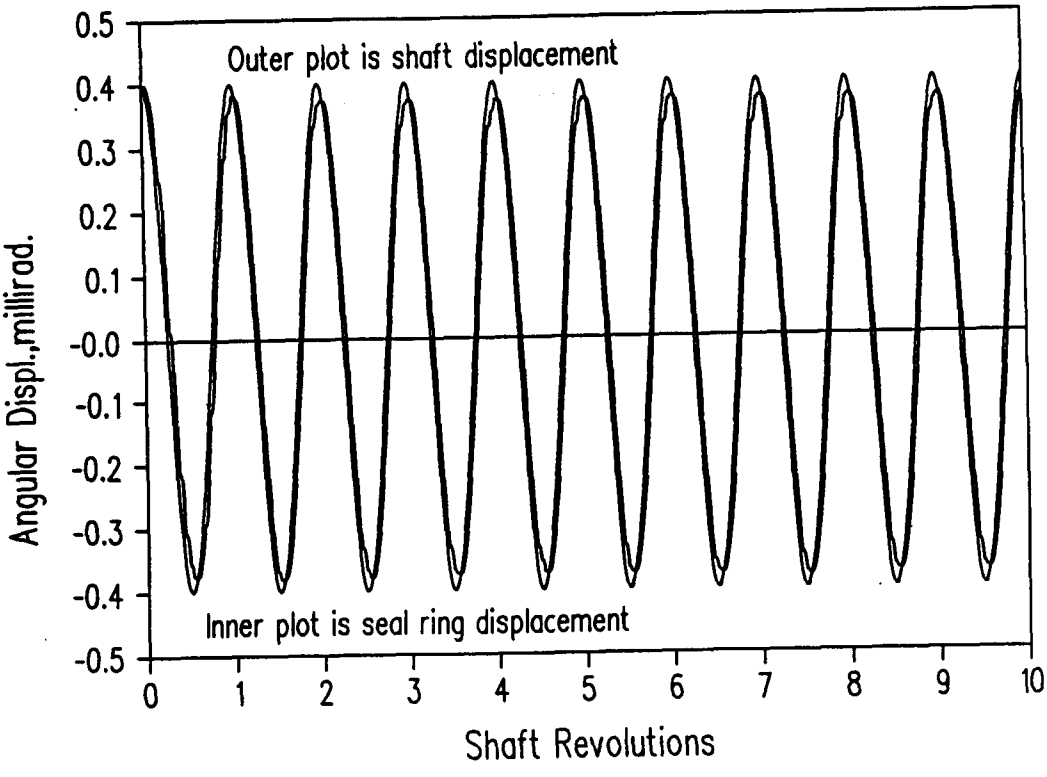

Figure 6-29 Angular Displacement about X-Axis vs. Shaft Revolutions, Case 5

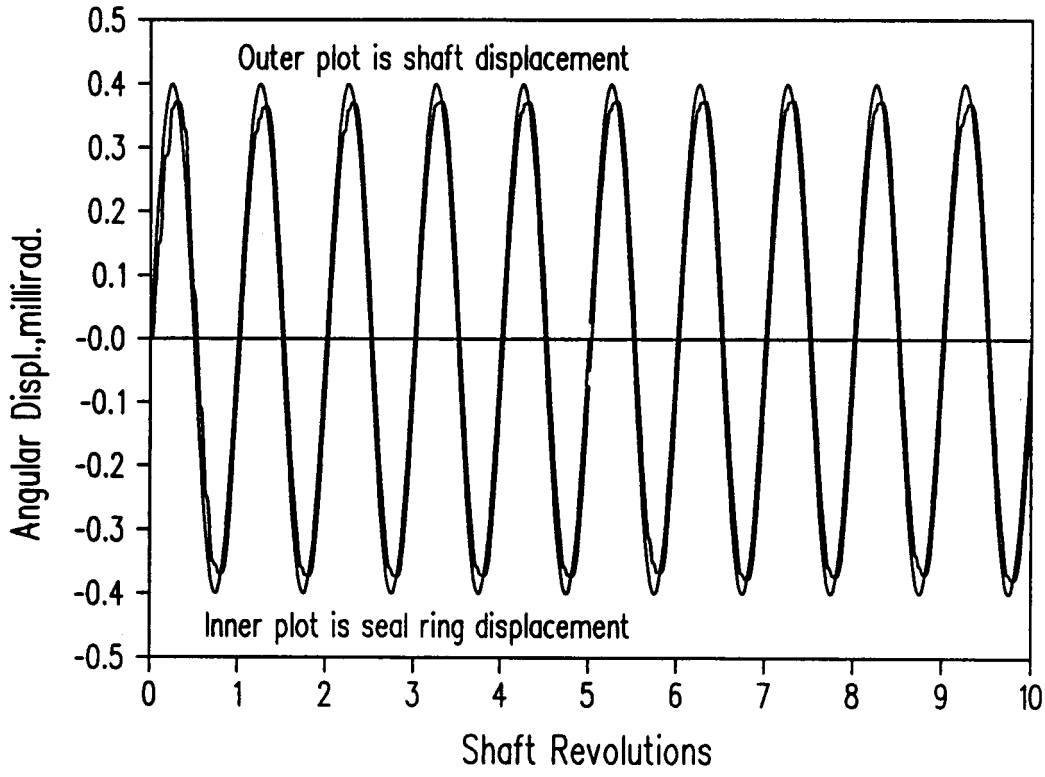

Figure 6-30 Angular Displacement about Y-Axis vs. Shaft Revolutions, Case 5

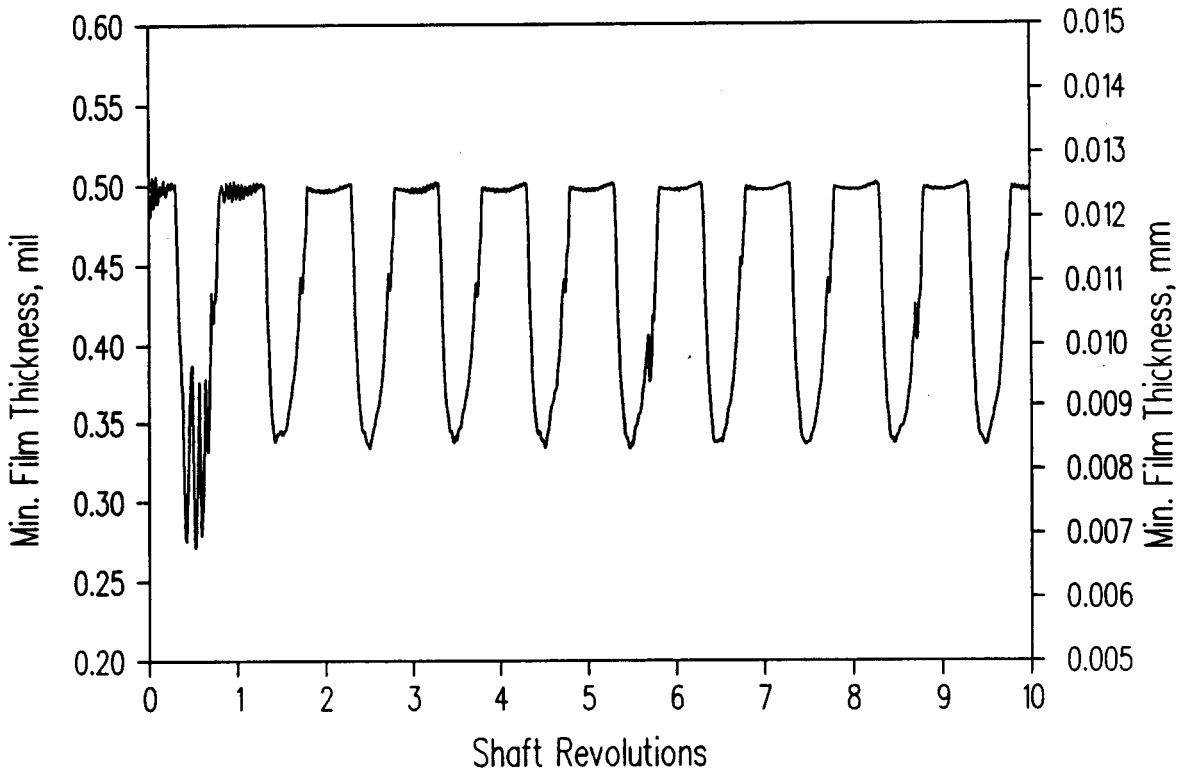

Figure 6-31 Minimum Film Thickness vs. Shaft Revolutions, Case 5

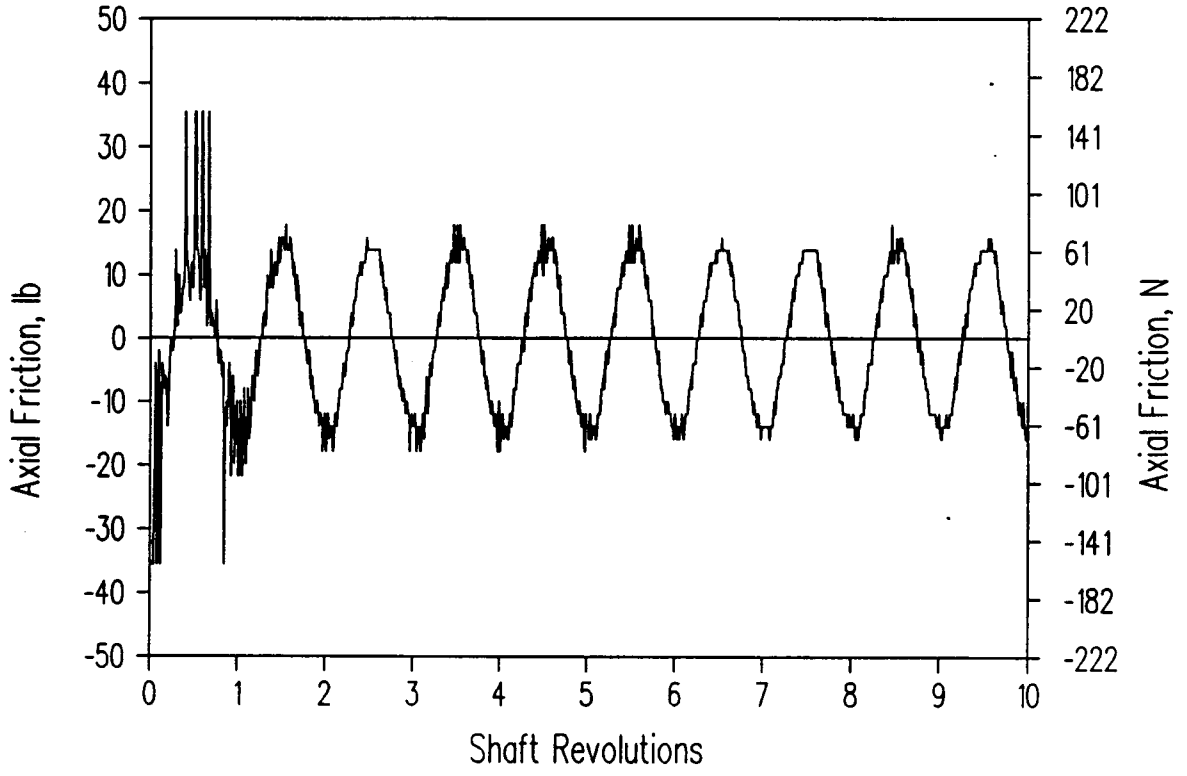

Figure 6-32 Axial Friction vs. Shaft Revolutions, Case 5

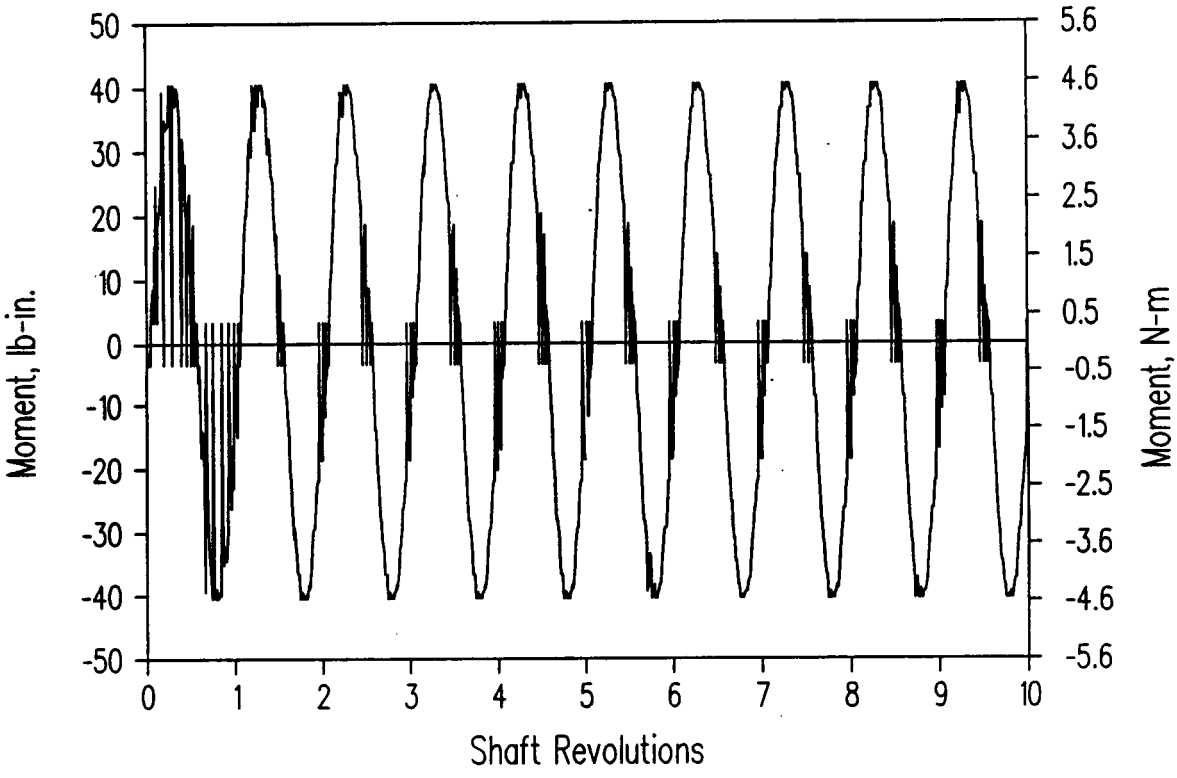

Figure 6-33 Friction Moment about X-Axis vs. Shaft Revolutions, Case 5

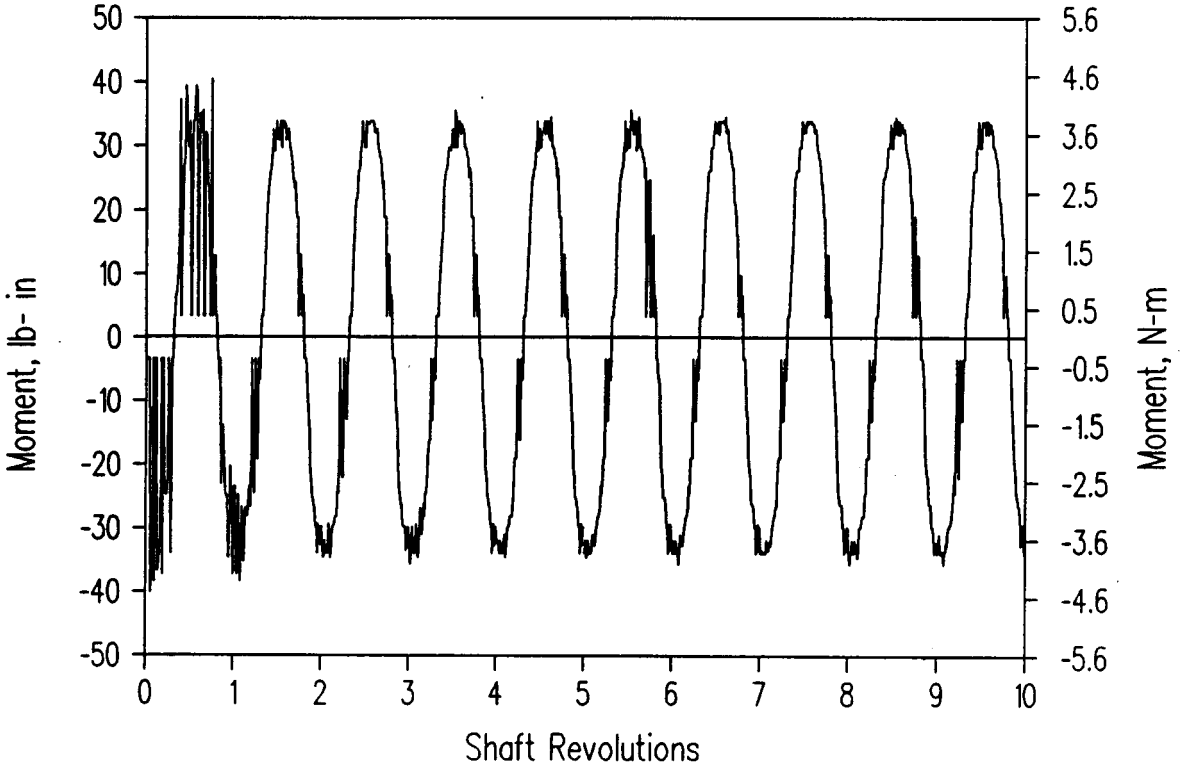

Figure 6-34 Friction Moment about Y-Axis vs. Shaft Revolutions, Case 5

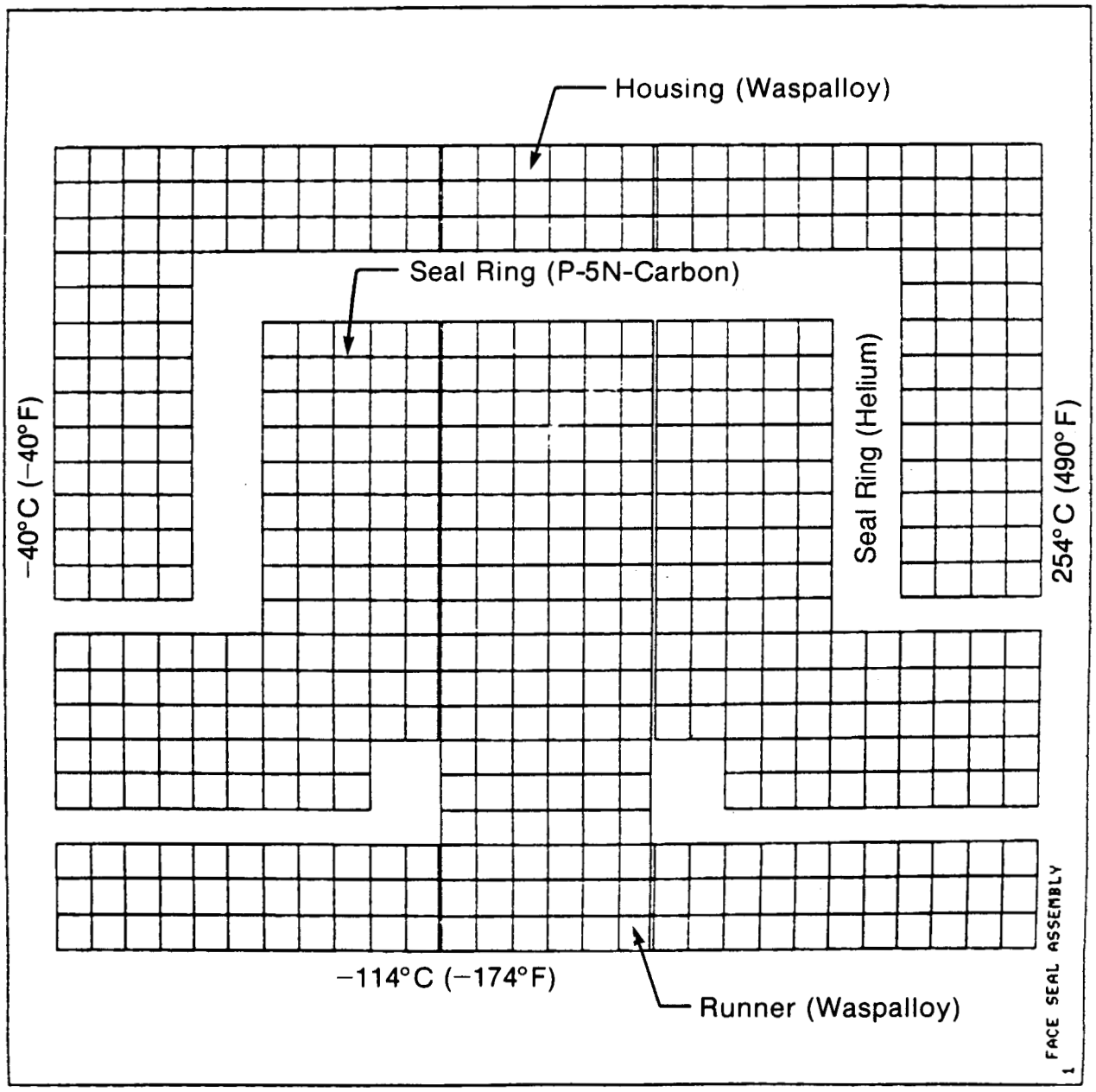

Figure 6-35 Face Seal Thermal Model

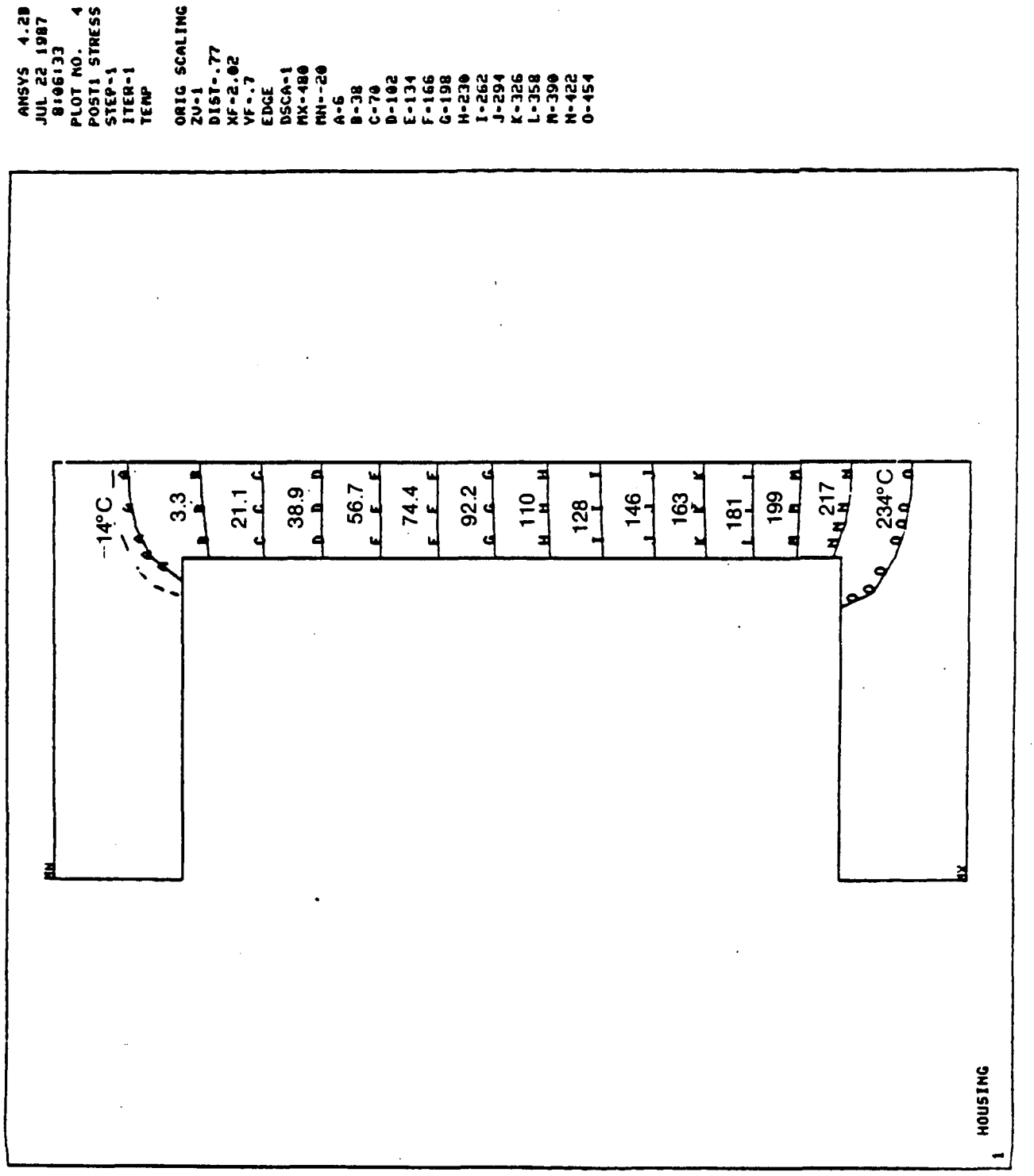

Figure 6-36 Face Seal Housing Temperature Distribution

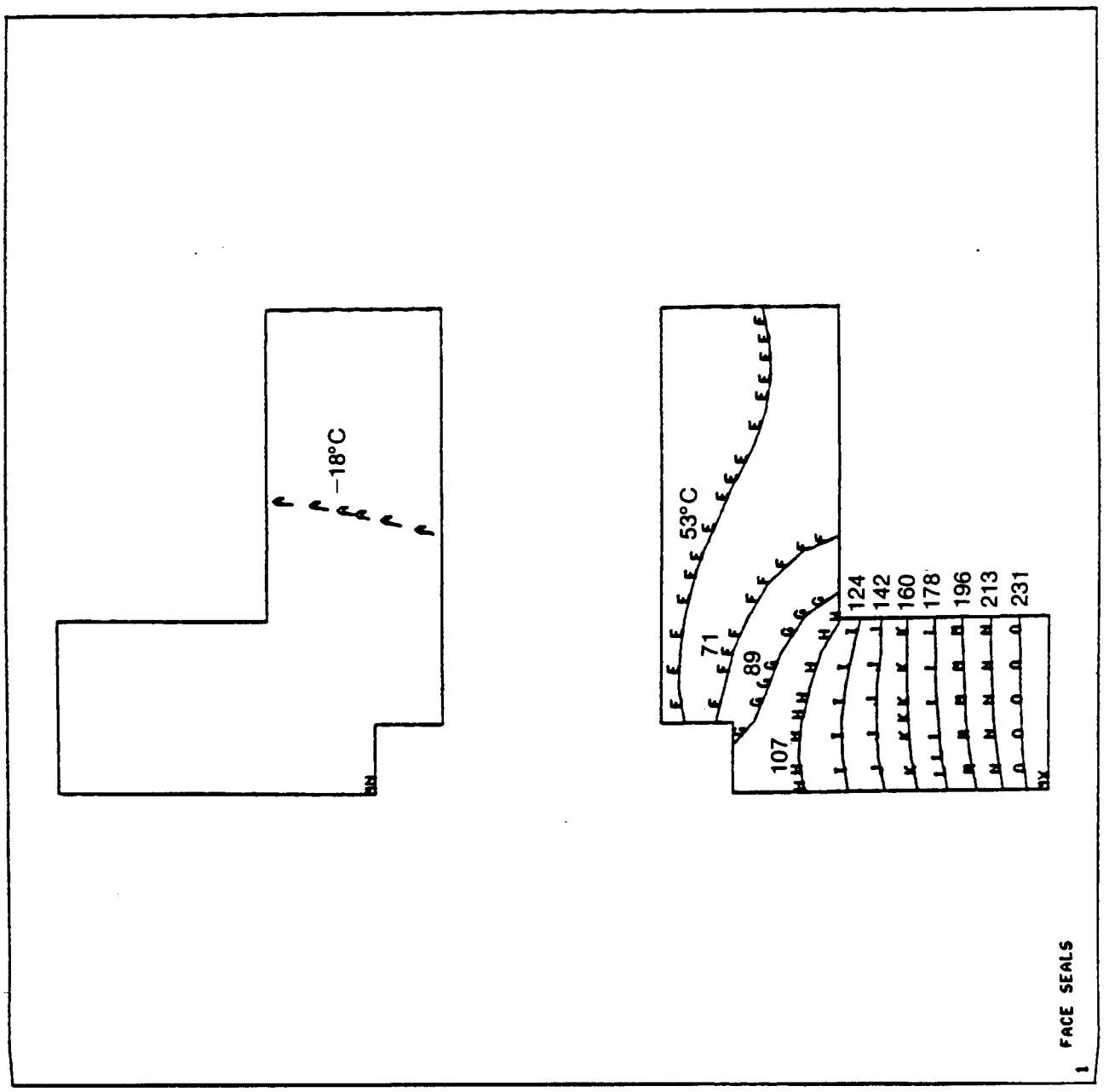

Figure 6-37 Face Seal Temperature Distribution

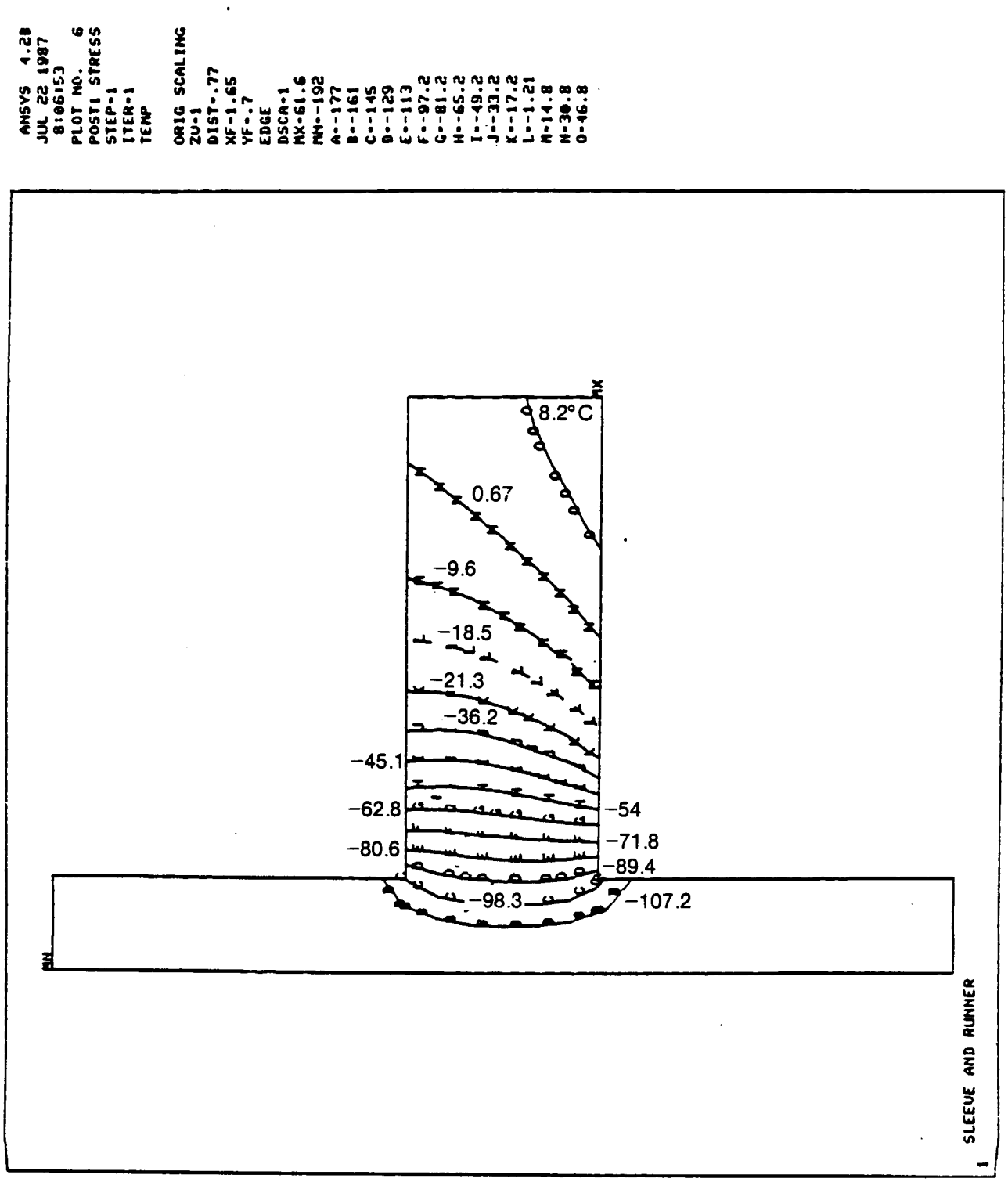

Figure 6-38 Face Seal Runner Temperature Distribution

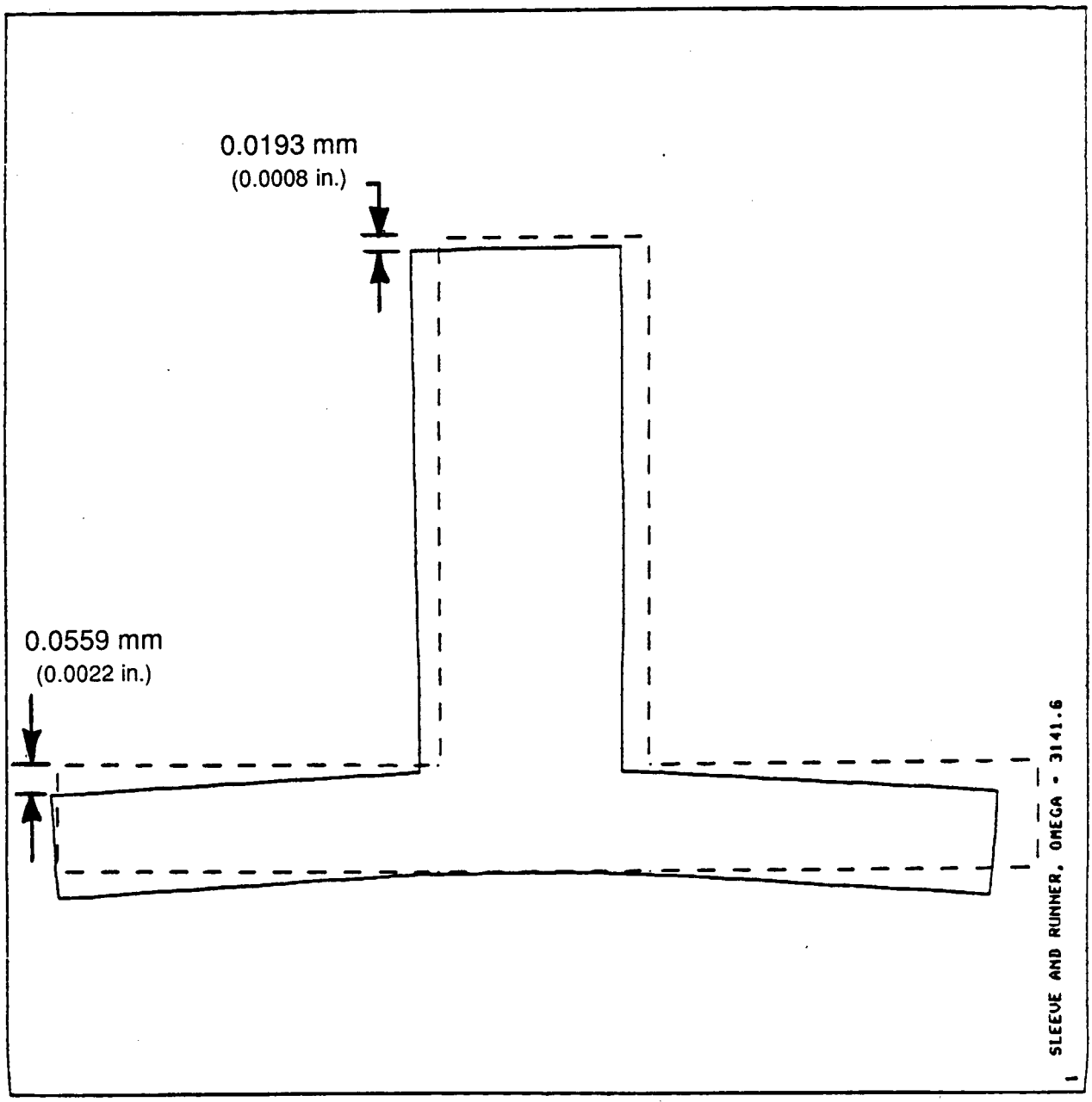

Figure 6-39 Face Seal Thermal Deformation of Runner

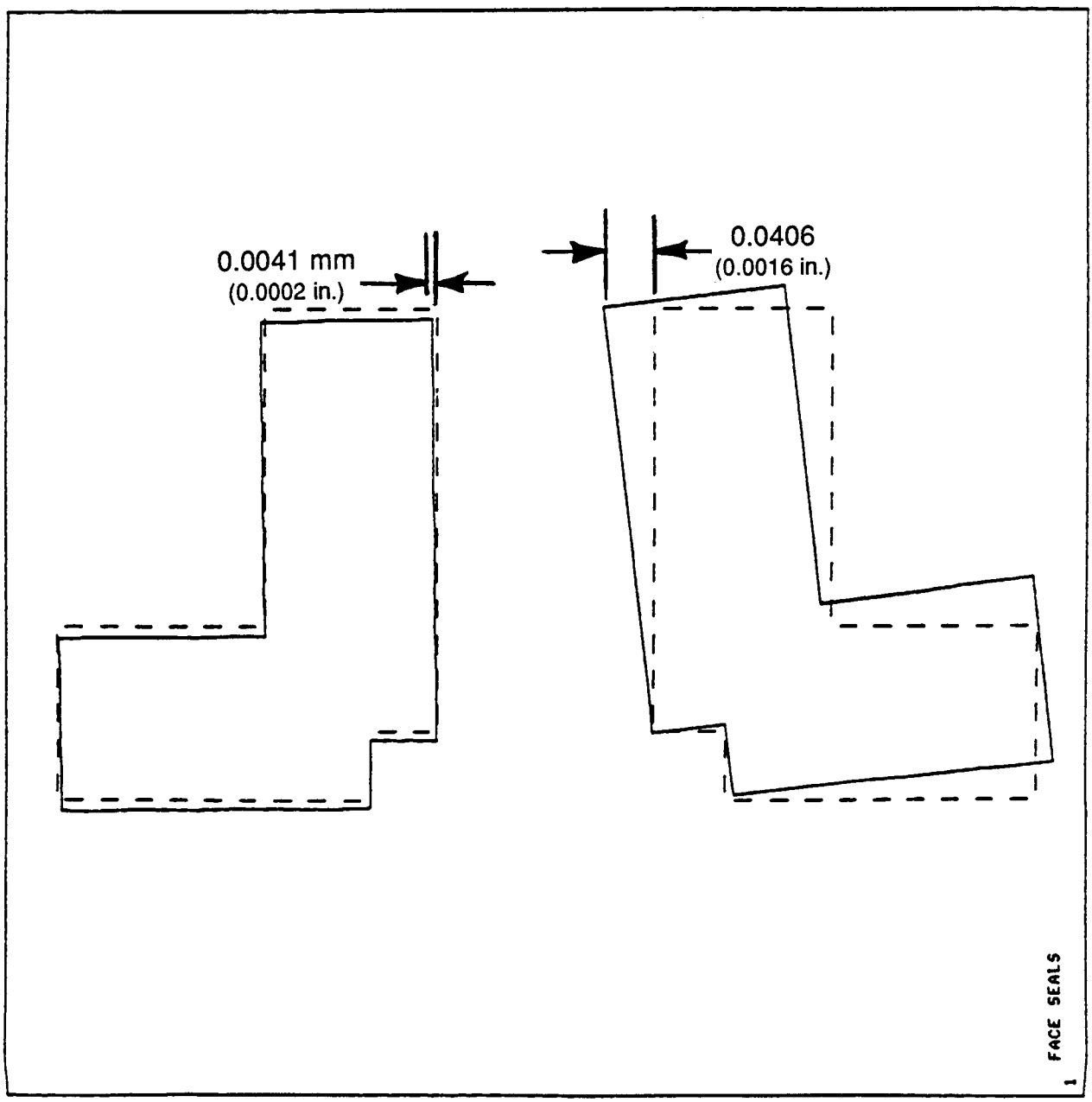

Figure 6-40 Face Seal Thermal Deformation of Seal Rings

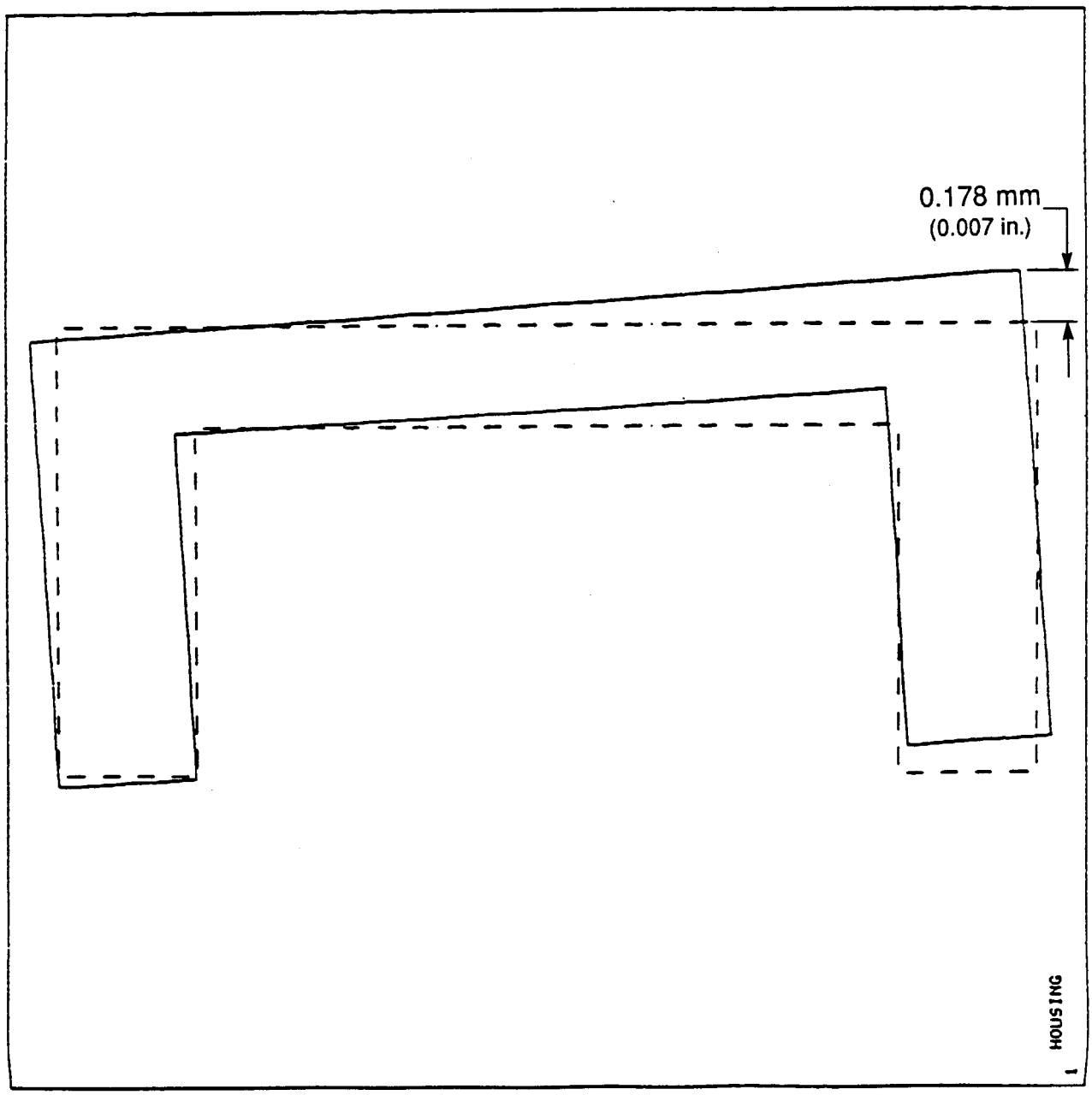

Figure 6-41 Face Seal Thermal Deformation of Housing

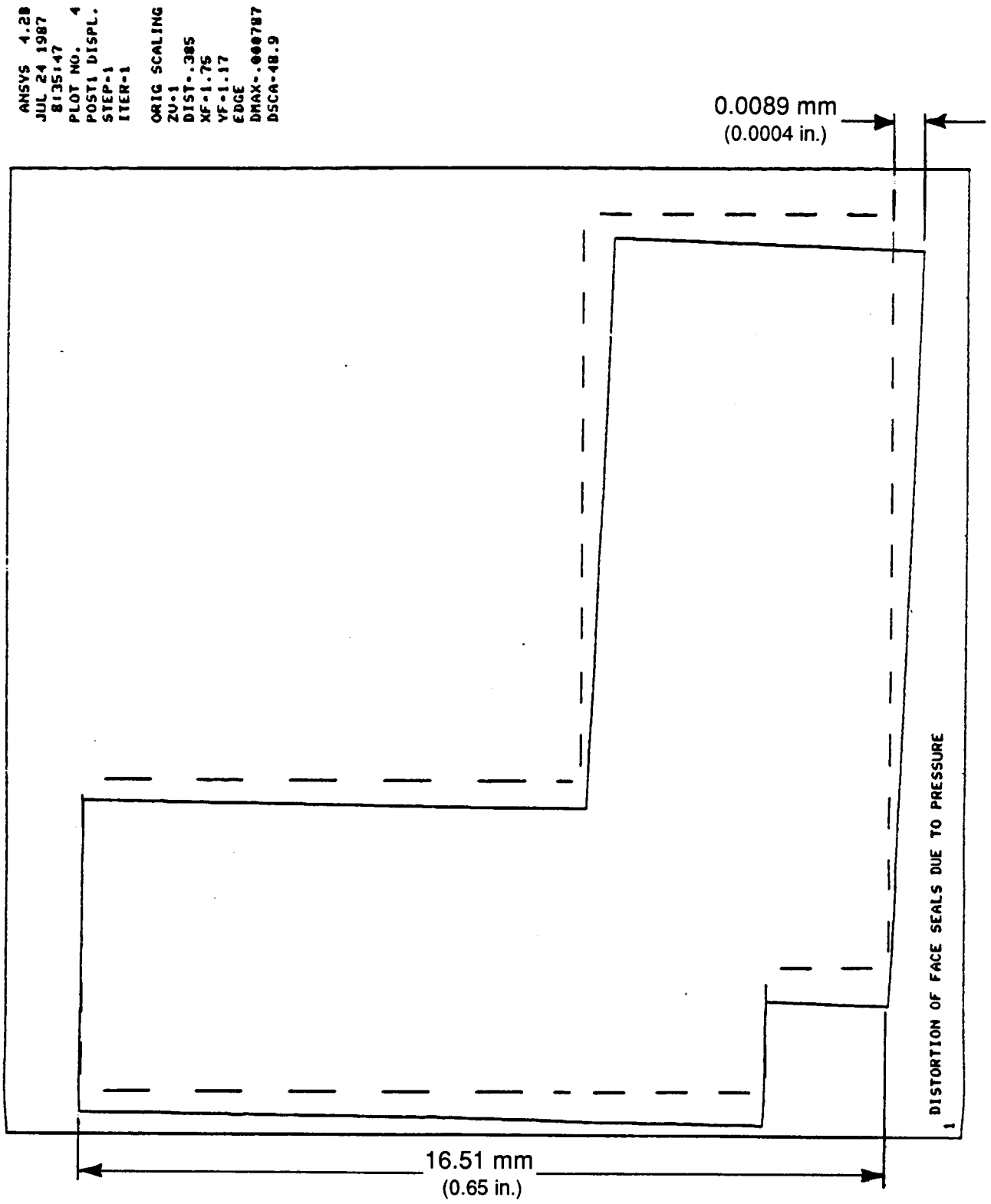

Figure 6-42 Face Seal; Pressure Distortion of Seal Ring

872526

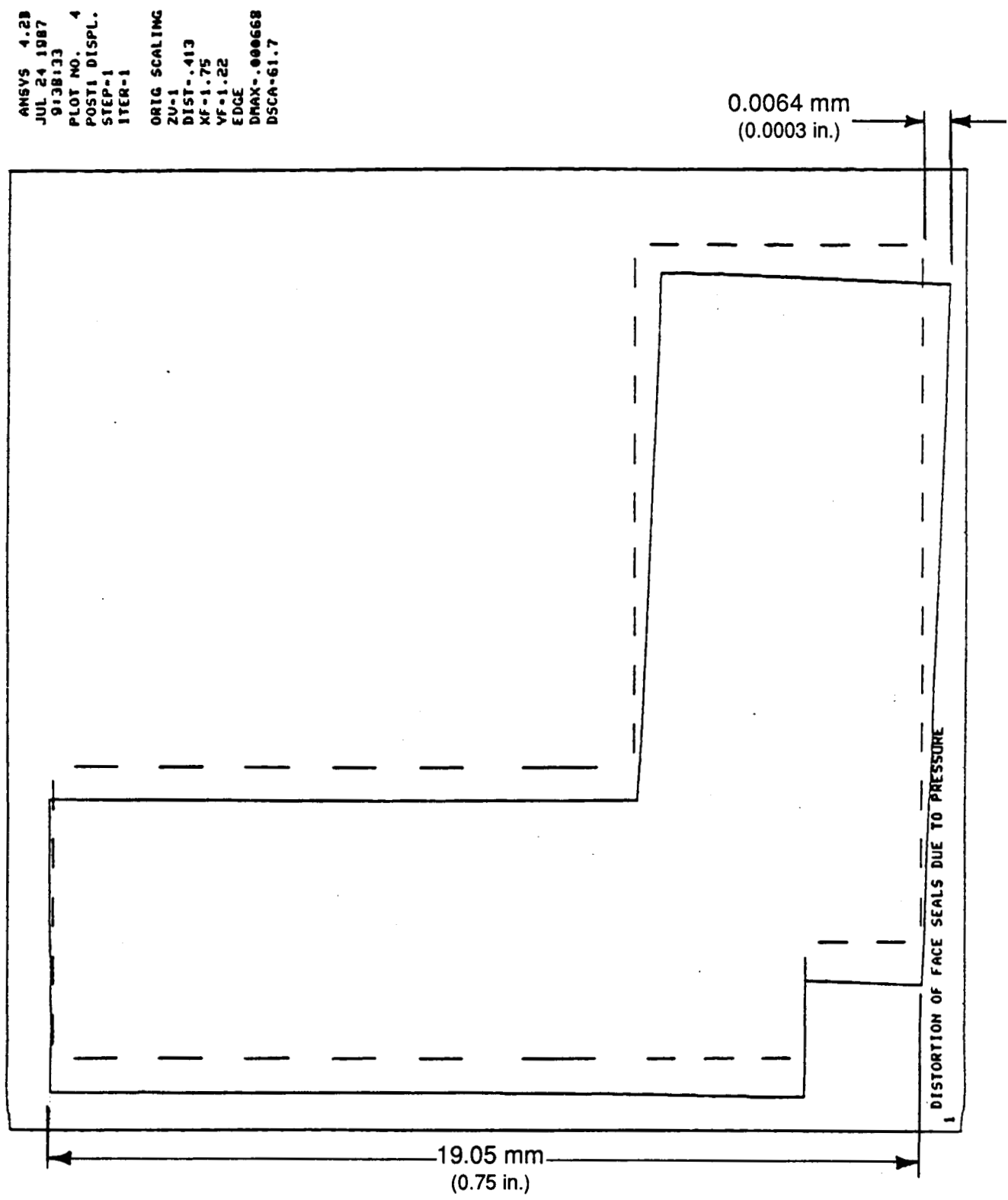

Figure 6-43 Face Seal; Pressure Distortion of Elongated Ring

ORIGINAL PAGE IS
OF POOR QUALITY

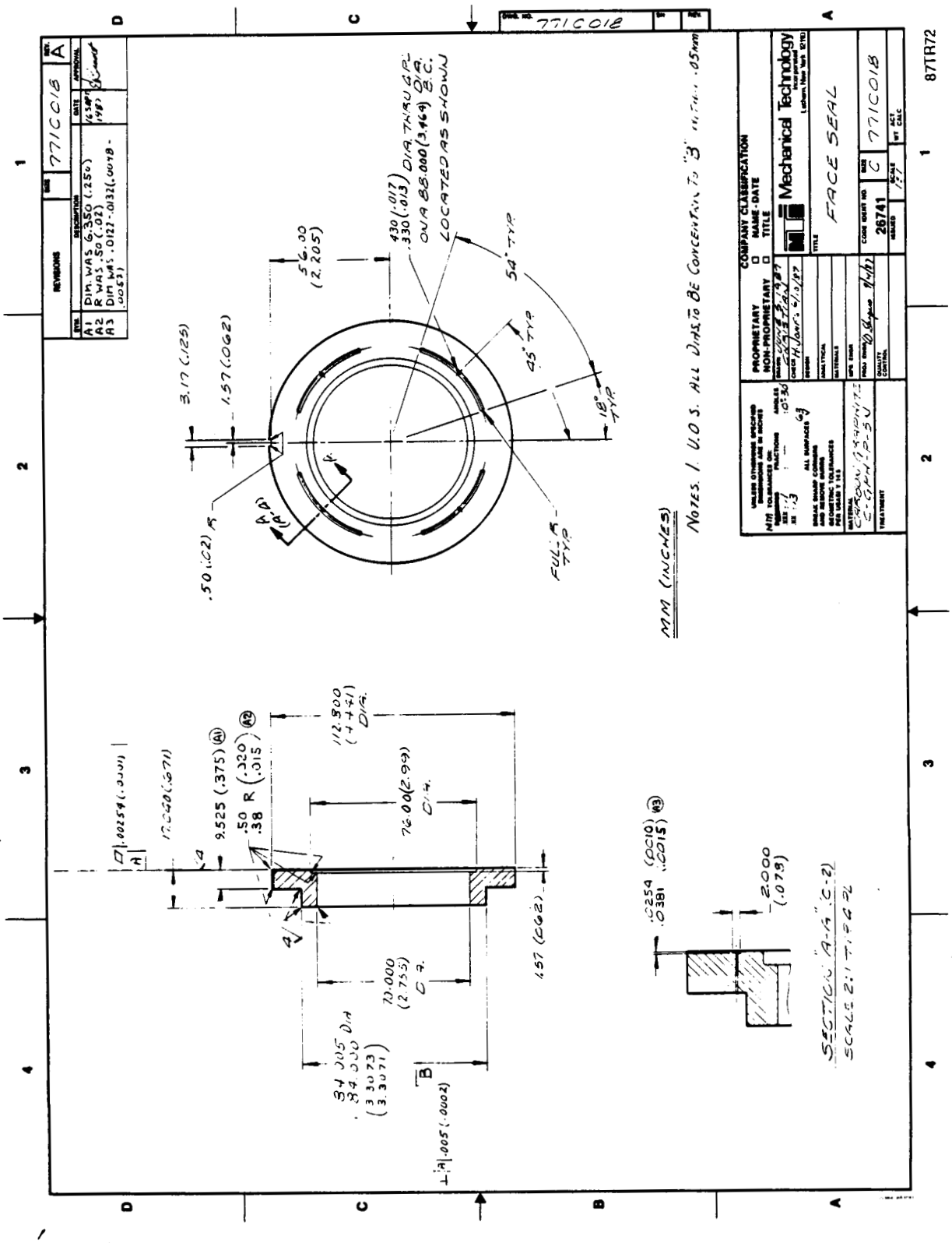

Figure 6-44 Face Seal Ring

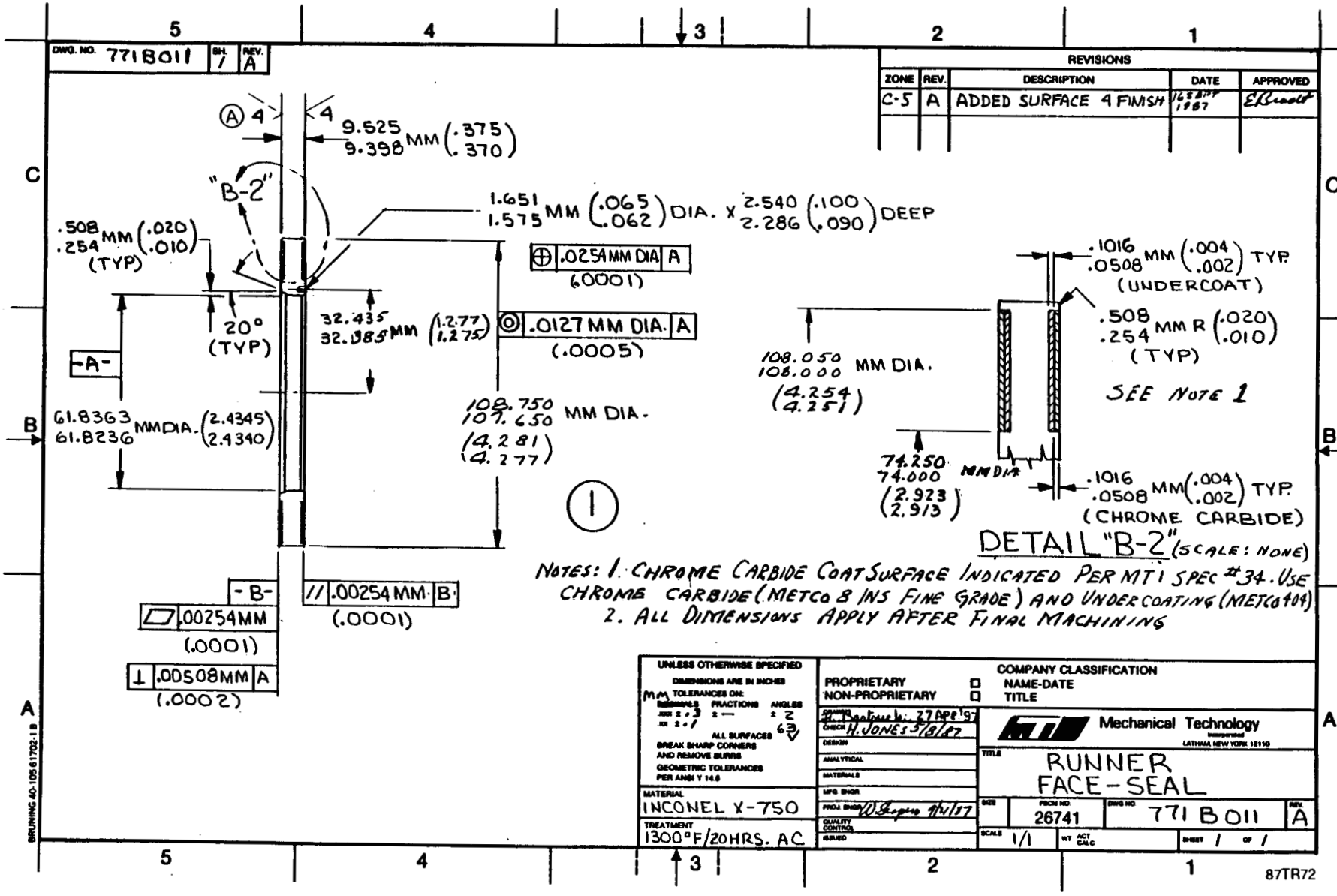

Figure 6-45 Face Seal Runner

ORIGINAL PAGE IS
OF POOR QUALITY

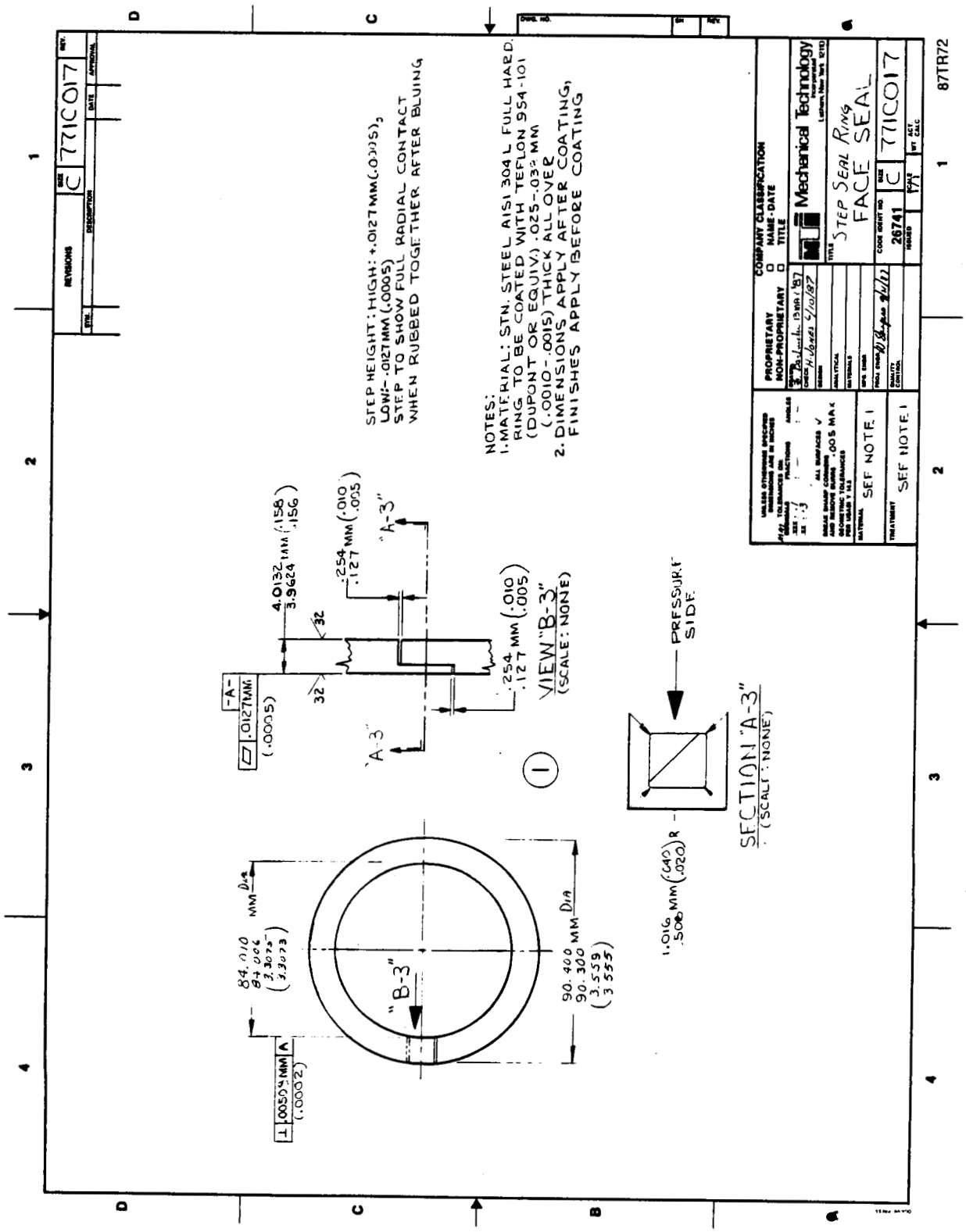

Figure 6-46 Face Seal Piston Ring

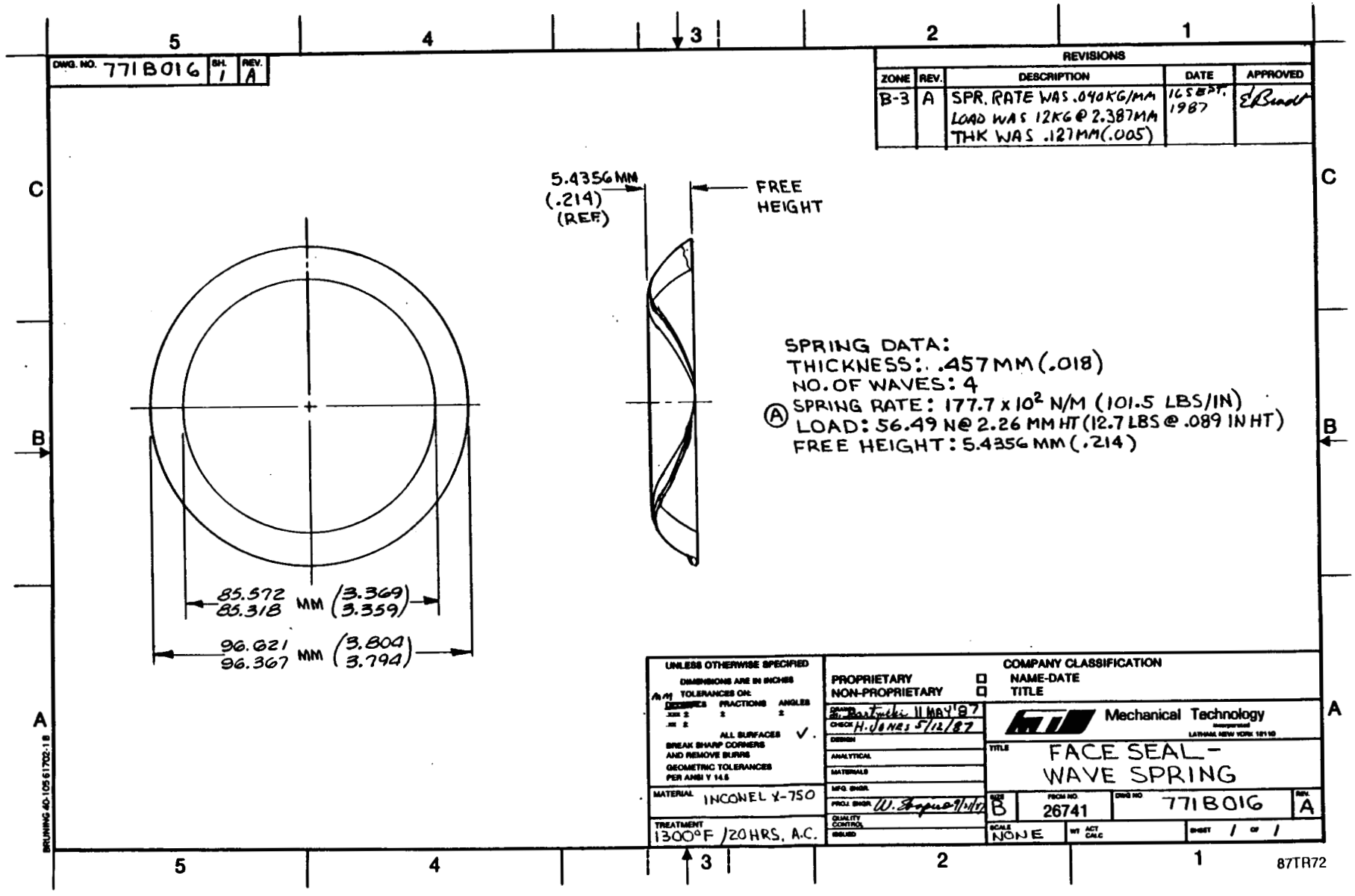

Figure 6.47 Face Seal Wave Spring

ORIGINAL PAGE IS
OF POOR QUALITY

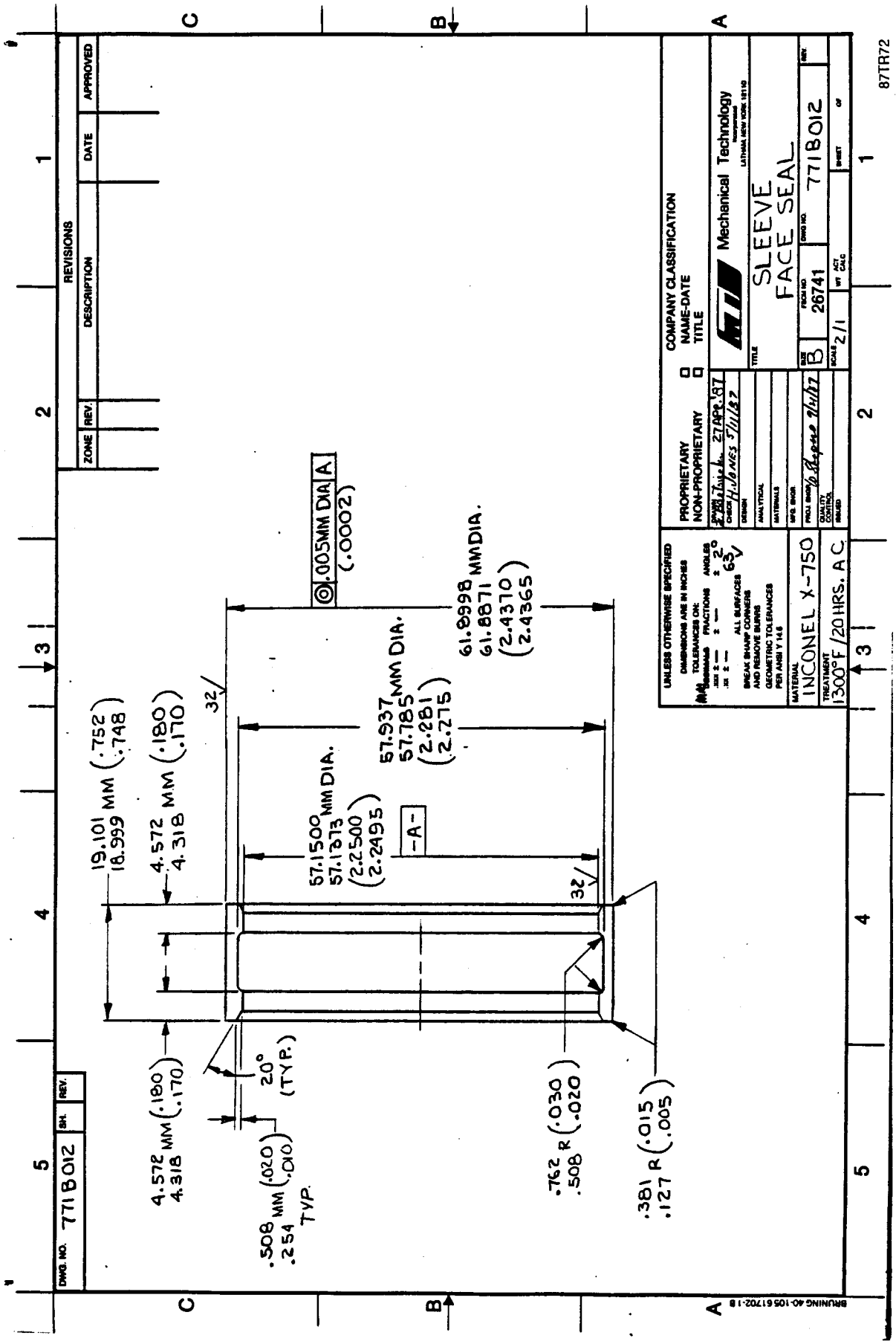

Figure 6-48 Face Seal Runner Sleeve

7.0 DESCRIPTION OF COMPUTER CODES

A brief description of the computer codes supplied to NASA under this program are presented in this section.

7.1 GJOURN [7,8]

The program GJOURN was designed to produce steady-state performance of a variety of cylindrical gas bearing and seal configurations. Figure 7-1 shows the solid ring configurations that the program handles. It also can analyze a sectored seal. Additional capabilities include:

- Variable grid definition
- Misalignment
- Determining journal position as a function of load and load direction or determining load and load direction as a function of journal position
- Known pressure or periodic boundary conditions
- Treating externally pressurized bearings with inherent or recess orifice compensation; recesses or holes can be arbitrarily located.

The output consists of:

- The clearance distribution (numerical and plotted format)
- The pressure distribution (numerical and plotted format)
- Eccentricity
- Eccentricity angle
- Load
- Load angle
- Power loss
- Leakage
- Cross-coupled stiffness coefficients.

7.2 GFACE [9,10]

The program GFACE was designed to produce steady-state performance of a variety of thrust gas bearing and face seal configurations. Figure 7-2 shows the configurations that the program handles. Capabilities include:

- Variable grid definition
- Misalignment
- Known pressure or periodic boundary conditions
- External pressurization with inherent or recess orifice compensation; recesses or holes can be arbitrarily located.

The output consists of:

- The clearance distribution (numerical and plotted format)
- The pressure distribution (numerical and plotted format)
- Load
- Righting moment
- Power loss
- Leakage
- Cross-coupled stiffness coefficients.

7.3 FACEDY [11,12]

The computer code FACEDY establishes the response of fluid-film face seals, as shown in Figure 7-3, to external forcing functions. Capabilities of the code include:

- Determination of the response of the seal ring in five degrees of freedom to shaft vibrations in as many as five degrees of freedom. These degrees of freedom are:
  - x_s = seal ring displacement in x direction
  - y_s = seal ring displacement in y direction
  - z_s = seal ring displacement in z direction
  - β_s = seal ring rotation about x-x axis
  - α_s = seal ring rotation about y-y axis
- Coulomb friction is accounted for in the secondary piston ring seal
- Pressure pulsations are included as an option.

The fluid-film characteristics are inserted as cross-coupled stiffness and damping coefficients which are inserted as input to the program. The other input quantities include:

- Geometric and physical parameters
- Operating conditions
- Shaft speed
- Pressure to be sealed
- Coefficient of friction of secondary seal
- Fluid viscosity
- Time-step and number of time steps
- Shaft vibration amplitudes and frequencies.

Output includes:

- Seal ring mass
- Distance to center of gravity
- Polar and transverse moments of inertia
- Hydraulic closing area
- Hydraulic closing force
- Interface preload
- Secondary seal preload friction
- Initial film thickness or interference.

The following is produced in plotted format as a function of time or shaft revolutions:

- x-displacement of seal ring and shaft
- y-displacement of seal ring and shaft
- z-displacement of seal ring and shaft
- α-displacement of seal ring and shaft
- β-displacement of seal ring and shaft
- Central film thickness
- Minimum film thickness
- x-friction force

- y-friction force
- z-friction force
- Friction moment about x-axis
- Friction moment about y-axis.

7.4 SPIRALP [13,14]

Computer code SPIRALP is used for determining steady-state performance of gas-lubricated, spiral-groove bearings and seals. Figure 6-3 depicts an inward-pumping, spiral-groove seal and identifies significant geometry.

The SPIRALP code has been especially designed for user-friendly operation on a PC and uses a display panel menu for input generation. In addition to providing steady-state performance, SPIRALP includes an option for determining the optimum geometry to satisfy a given set of operating conditions.

The input and output for sample problem no. 1 are shown on Figure 7-4. The panel input is shown at the top and the output at the bottom. When the code is applied with the instruction SPIRALP, the input menu will appear on the screen. The variables are then inserted to suit the problem. If a variable is unknown and is to be determined by the optimization option of the code, a best-guess value is inserted.

The sealing land depth is the difference in height between the spiral-groove land and the sealing land. Usually, there is no difference, and this variable equals 0.

The variables that can be optimized include:

- Groove angle, ALPHA
- Land-to-groove ratio, GAMMA
- Groove depth, GD
- Radius at the groove dam interface, RM.

The number of these variables to be optimized is indicated by the number given in the optimum number input row, e.g., a number 4 indicates that all four variables will be optimized, while a number 1 indicates that only the groove angle will be optimized. A minus sign in front of the optimization input number means that the previous case pressure distribution will be applied as an initial guess to increase accuracy.

Accuracy numbers can also be applied for calculating the pressure distribution and the optimization parameters. An increasing number means increasing accuracy but will require a longer running time to satisfy convergence. A value of zero is generally used for optimization problems, since higher numbers can often produce numerical instabilities.

A plot of the spiral-groove geometry can also be achieved by activating the last variable in the input column. The number of grooves to be plotted are specified, and the grooves can be displayed on the screen via the F10 key or plotted via the F7 to F9 keys, the higher number function key indicating a higher print density but slower printout. The function of keys F1 through F4 are as follows:

- F1 - Execute the problem with the input tabulated
- F2 - Load a different input file and provide the name as prompted
- F3 - Return to the DOS system
- F4 - Save the input file with an optional file name as prompted.

This sample problem, shown on Figure 7-4, is an optimization problem of an inward-pumping, spiral-groove gas seal.

The output includes the steady-state performance and optimization parameters. The load capacity in pounds appears first, followed by the leakage flow through the seal. The leakage appears as a negative number because it is a net inflow into the spiral-groove region. The flow is in units of $in.^3/sec$, at pressure PO, which is the lower pressure on either side of the spiral-groove region. The stiffness is the axial stiffness of the fluid-film in lb/in. The power loss is the viscous dissipation given in horsepower. The temperature output is the temperature rise of the fluid from viscous dissipation as it travels through the spiral groove and dam regions.

The optimum geometric parameters follow. If an optimization problem is run, i.e., OPTIM. NO. > 0, then the output geomeric quantities would not equal those supplied as input. If OPTIM. NO. = 0, these quantities would be identical to the input quantities. For sample problem no. 1, the optimum groove angle is 16.608°, while the best-guess quantity was 28°. Similar variations occur between the input and output for the other geometric parameters. The input and optimized quantities for sample problem no. 1 are listed below.

Parameter	Input	Optimized
Groove Angle, ALPHA (°)	28.0	16.608
Land-to-Groove Ratio, GAMMA	1.65	2.123
Groove Depth, GD, (in.)	0.0015	0.00162
Dam Radius, RM, (in.)	1.48	1.4796

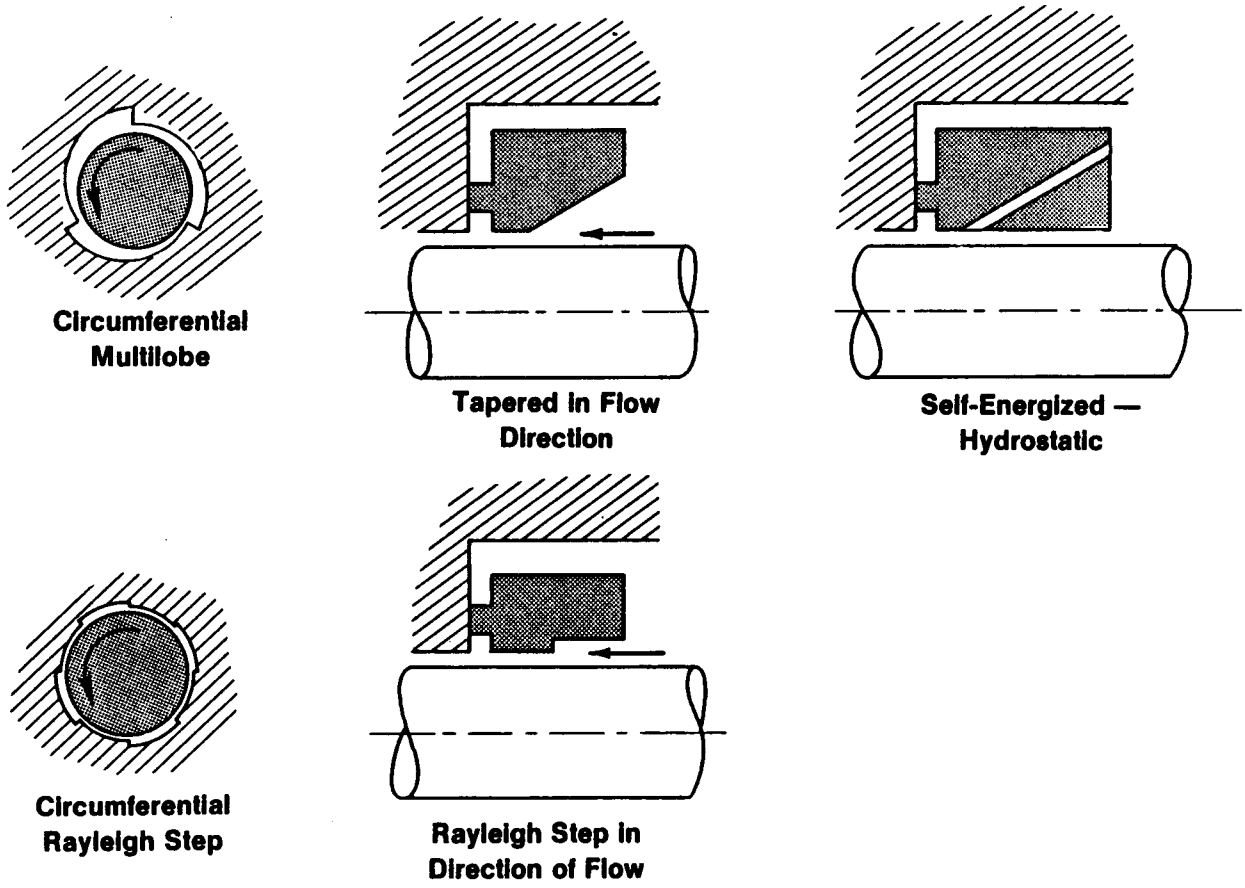

Figure 7-1. Leakage Path Geometries (Floating Ring)

852165

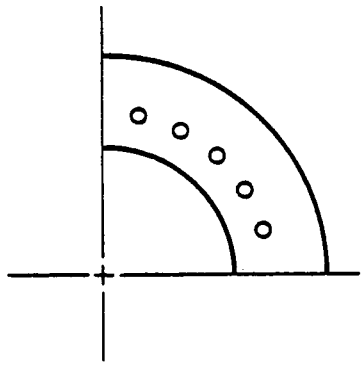

Hydrostatic

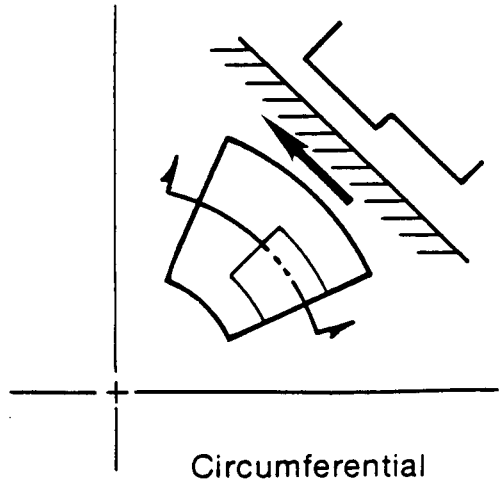

Circumferential
Rayleigh Step

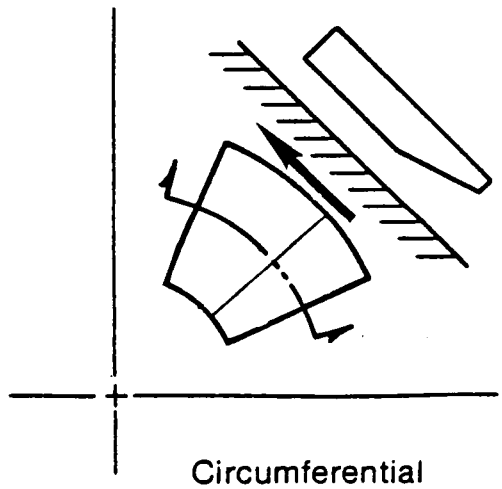

Circumferential
Tapered Land

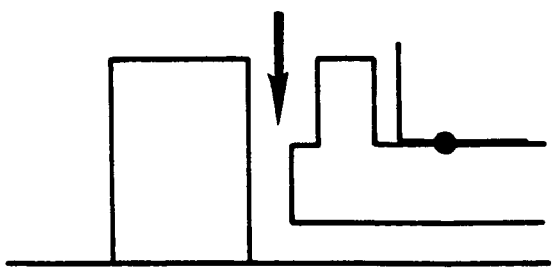

Radial Rayleigh Step

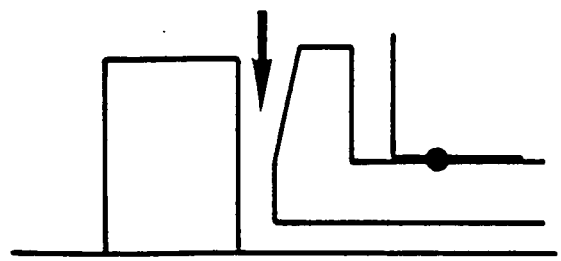

Radial Tapered Land

Figure 7-2. Face Seal Configurations

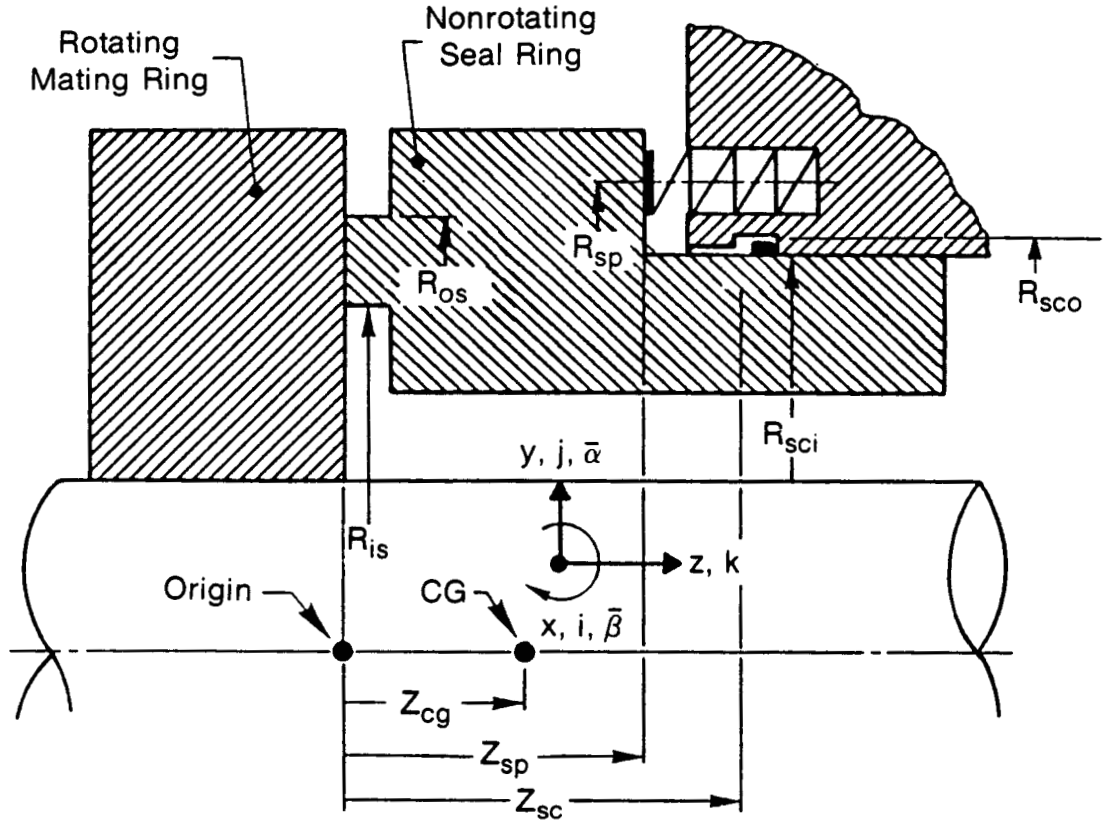

Figure 7-3. Fluid-Film Face Seal Dynamic Parameters

831834-2

```
1.378              INSIDE RADIUS (IN)
1.48               RADIUS AT GROOVE-DAM INTERFACE, RM (IN)
1.89               OUTSIDE RADIUS (IN)
.0005              FILM THICKNESS OVER LAND BETWEEN GROOVES (IN)
.0015              GROOVE DEPTH, GD (IN)
0                  SEALING LAND DEPTH (IN)
28.0               GROOVE ANGLE, ALPHA (DEGREES)
1.65               CIRCUMFERENTIAL EXTENT OF LAND TO GROOVE RATIO, GAMMA
15.                INSIDE PRESSURE (PSIA)
215.               OUTSIDE PRESSURE (PSIA)
30000.             SPEED (RPM)
2.9E-09            VISCOSITY (LB-SEC/IN**2)
.0739              DENSITY * SP. HEAT, AT P0=MIN(PIN,POUT) (PSI/DEGF)
-1                 PUMPING DIRECTION, 1 FOR OUTWARD PUMPING -1 FOR INWARD
1                  GROOVE LOCATION 1 FOR GROOVES OUTSIDE, 0 FOR INSIDE
4                  OPTIM. NO., NOPT, 1-ALPHA, 2-GAMMA, 3-GD, 4-RM INCLUSIVE
0                  PRESSURE ACCURACY FLAG 0 - 10 FOR INCREASING ACCURACY
0                  OPTIMIZATION ACC. FLAG 0,1,2,3,4 FOR INCREASING ACCURACY
12                 NUMBER OF GROOVES FOR PLOTTING (F10 SCREEN, F7-F9 PRINTER)



F1=>EXECUTE          F2=>FILE LOAD          F3=>QUIT          F4=>FILE SAVE

       8.53531E+02 LOAD (LB)
      -2.66581E+02 FLOW (IN**3/SEC @  P0)
       3.30204E+05 STIFFNESS (LB/IN)
       6.72480E-02 POWER LOSS (HP)
       2.25294E+01 TEMPERATURE (DEGF)
       1.66084E+01 OPTIMUM GROOVE ANGLE IF NOPT > 0 (DEGREES)
       2.12317E+00 OPTIMUM VALUE OF LAND TO GROOVE RATIO IF NOPT > 1
       1.62129E-03 OPTIMUM GROOVE DEPTH IF NOPT > 2 (IN)
       1.47962E+00 OPTIMUM VALUE OF RM IF NOPT = 4 (IN)
       1.37793E+01 RUNNING TIME (SEC)



========> Strike Enter To Return
```

Figure 7-4 SPIRALP, Sample Problem No. 1

8.0 REFERENCES

1. Shapiro, W., and R. Hamm. "Seal Technology for Liquid Oxygen (LOX) Turbopumps." NASA CR-174866, MTI 85TR20, November 1985.

2. Rockwell International Corporation. "Seal, Intermediate - Oxidizer, High-Pressure Turbopump." Procurement Specification RC1084, June 1975.

3. NASA/Lewis Research Center. "Advanced Floating Helium Purge Seals for Liquid Oxygen Turbopumps." NASA/LeRC Contract NAS3-24645, September 1985.

4. Artiles, A., W. Shapiro, and H. F. Jones. "Design Analysis of Rayleigh-Step, Floating-Ring Seals." ASLE Transactions, Vol. 27, No. 4, October 1984, pp. 321-331.

5. Hamm, R., and W. Shapiro. "Testing of Helium Buffered, Raleigh-Step, Floating-Ring Seals." Lubrication Engineering, Vol 43, No. 5, May 1987, pp. 376-383.

6. Anderson, P. G. et al. "Fluid Flow Analysis of the SSME High-Pressure Oxidizer Turbopump Operating at Full Power Level." Lockhead Missles and Space Company, Inc. Report LMSC-HREC-TR-D698083, for NASA/MSFC, August 1980.

7. Shapiro, W., and C. Lee. "Gas-Lubricated Journal Bearings and Seals (GJOURN)." Program Users Manual, MTI 86TR48 Report, September 1986.

8. Shapiro, W., and C. Lee. "Gas-Lubricated Journal Bearings and Seals (GJOURN)." Program Documentation Manual, MTI 86TR49 Report, September 1986.

9. Shapiro, W., and C. Lee. "Gas-Lubricated Thrust Bearings and Seals (GFACE)." Program Users Manual, MTI 87TR30 Report, March 1987.

10. Shapiro, W., and C. Lee. "Gas-Lubricated Thrust Bearings and Fluid-Film Face Seals (GFACE)." Program Documentation Manual, MTI 87TR28 Report, March 1987.

11. Shapiro, W., and C. Lee. "Dynamics of Fluid-Film Face Seals (FACEDY)." Program User's Manual, MTI 87TR26 Report, February 1987.

12. Shapiro, W., and C. Lee. "Dynamics of Fluid-Film Face Seals (FACEDY)." Program Documentation Manual, MTI 87TR5 Report, January 1987.

13. "Computer Code SPIRALP for Gas-Lubricated, Spiral-Groove Bearings and Seals." Volume I - User's Manual, MTI 88TM2, February 1988.

14. "Computer Code SPIRALP for Gas-Lubricated, Spiral-Groove Bearings and Seals." Volume II - Computer Program Documentation, February 1988.

APPENDIX A

APPLICATION OF CHROME-CARBIDE COATINGS TO THE SURFACES OF BEARINGS AND SHAFTS

Issued by _____

Date _____

Revised _____

Date _____

Specification No. 34 Approved by _____

APPLICATION OF CHROME CARBIDE COATINGS TO THE SURFACES OF BEARINGS AND SHAFTS

1.0 ACKNOWLEDGMENT

Vendor shall mention this specification number and its revision number in all quotations and when acknowledging purchase orders.

2.0 PURPOSE

To provide a procedure for the application of a surface layer of chrome carbide to bearing parts. Also to provide a procedure for the application of an undercoating (prior to application of chrome carbide) for the purposes of improving chrome carbide adhesion or for providing the base material with improved corrosion resistance.

It should be noted that extremely high-density coatings are not mandatory for this purpose. Similarly, a high-gloss surface finish is not mandatory after finish grinding or lapping the coating.

3.0 EQUIPMENT

A specially constructed torch or gun which imparts an extremely high velocity and high temperature to a suitable carrier gas in which the powdered coating material is suspended. The carrier gas used shall be argon.

4.0 PROCESS

Two suitable processes for the satisfactory deposition of chrome carbide coatings have been developed by vendors. These processes are generally described as the "plasma flame spray" process and the "detonation" process. Either process may be used unless the detail drawing of the part states otherwise.

5.0 COATING AND UNDERCOATING MATERIALS

Shall be indicated on the detail drawing by name, e.g., chrome carbide coating, nickel or nickel chrome or molybdenum undercoating. The identity of the materials shall be determined by the vendors powder or coating number in accordance with the following tabulation:

	Coating	Undercoating		
Vendor	Chrome-Carbide 25% NI-CR	Nickel Aluminide	Nickel Chrome	Molybdenum
Linde Division of Union Carbide	LC-1	- - -	LC-8	LM-6
Metco Inc.	8 INS	404	43C	63

The minimum bond strength between the chrome carbide and the base material or between the chrome carbide coating, the undercoating and the base material shall be 1600 PSI as determined by the bond strength test (Para. 11).

6.0 BASE MATERIAL

Prior to coating the parts should be, as far as is possible, in the finished machined condition. All heat treatment shall be performed prior to coating.

When practicable, any acid or alkali cleaning and electroplating shall precede coating. If these processes are to be performed after coating, the coating shall be suitably masked to prevent contact with the solutions involved.

If temperature sensitive materials are to be coated, it should be anticipated that surface temperatures up to 350°F will be produced by the coating process. Where this temperature might present problems, this shall be noted on the drawing.

7.0 MACHINING PRIOR TO COATING

7.1 All Parts

The chrome carbide coating and undercoating, when specified, shall only be applied to those areas designated on the drawing. Any such overspray areas shall have the same machining preparations as the required coating areas.

On the areas which are to be coated with chrome carbide, the part should be machined undersize on external surfaces, or oversize on internal surfaces, by an amount which will leave a chrome carbide thickness of .001/.003 inches (see Para. 7.4) after finish machining. If a metallic undercoat is to be used, then an additional .001/.002 inches shall be allowed for the thickness of this undercoat, unless otherwise specified on the drawing.

Where possible, the coating should be applied in a recess bounded by the base material. This prevents the possibility of chipping the otherwise exposed edges of the coating.

All sharp corners in the areas to be coated shall be broken with a .015/.020 radius unless otherwise specified.

7.2 Shafts

The length of the coating, and where specified the length of the undercoating, shall be at least 1/8 inch longer than the bearing so that the coating on the shaft protrudes by 1/16 inches beyond each end of the bearing. This will ensure that the bearing cannot contact any uncoated portion of the shaft.

7.3 Bearings

The chrome carbide coating and, where specified, the undercoating will only be applied to the load bearing surface.

It should be noted that the minimum angle which can be used between the nozzle of the equipment and the part to be coated is 45 degrees. Therefore, it is not possible to coat an internal surface in one setup if the length to diameter ratio (L/D) exceeds 1. Turning the part around and applying the coating from the opposite end is necessary for larger L/D ratios.

7.4 Bearings with Grooved Patterns

The chrome carbide coating shall be sprayed through a metal template such that the buildup of chrome carbide forms the land portion of the grooved pattern. The bottom of the groove is, therefore, the surface of either the base material or, where specified, the undercoat. The finished thickness of the chrome carbide coating will not necessarily conform with the previously established thickness of the finished coating. For these parts the thickness of the finished machined coating shall be equal to the groove depth as quoted on the drawing. Machining allowances before coating shall therefore be based on groove depth and, when specified, the thickness of the undercoating.

It is not possible with this technique to produce a groove with a 90 degree sharp-cornered edge. The groove shall have after-finish machining, a sharp edge with an inclination less than 45 degrees to a plane vertical to the bearing surface, unless otherwise stated.

7.5 Bearings with Orifice Holes

Bearings with orifice holes in the surface shall have a ridge or a boss of parent metal around each orifice hole. The parent metal around the holes can be machined into the bearing or sprayed on the bearing using a template. The ridge or boss should be approximately twice the diameter of the orifice hole. When the final dimensions of the bearing are achieved, chrome carbide coating must not be adjacent to the orifice holes.

The orifice holes are to be machined after coating and final grinding.

8.0 TEMPLATES FOR GROOVED PATTERNS

Templates shall be prepared by photo-etching cold rolled 300 series stainless steel sheet .010/.020 inches thick. The photo etching shall be performed from one side of the template only. The etching shall be performed from the side of the template which will be placed against the part during the application of the chrome carbide.

A suitable fixture shall be used to hold the part and the template in the required position, to within the accuracy specified, during the coating process.

The profile of the finished template shall correspond to the bottom of the grooves and have an accuracy in accordance with the tolerances given for the grooves on the finished part. The dimensions of the profile of the grooves in the chrome carbide as applied shall be finished dimensions.

If, for the bearing with orifice holes, the parent metal bosses or ridges are sprayed on the bearing surface, the template can be machined in .010" thick 300 series stainless steel.

9.0 COATING PROCEDURE

Actual coating of the parts shall be performed as soon as practicable after the surface preparation (Para. 9.1, 9.1 and 9.3) preferably within two hours.

9.1 All parts shall be thoroughly cleaned free from dust, grit, oil grease and other foreign materials by vapor degreasing or by washing thoroughly in petroleum solvent and drying.

9.2 All the surfaces to be coated shall be abrasive blasted with No. 16-24 aluminum oxide grit at 80-100 psi to produce a roughened surface which will promote adhesion of the coating. A minimum surface roughness after blasting of 63 microinches, AA, is recommended. The grit shall be changed at frequent intervals to maintain a sharp cutting action.

When the parts require grooves formed by the chrome carbide coating, the abrasive blasting shall be performed before the attachment of the template which is used to form the outline of the required grooved pattern. The same sequence is required when the parent metal bosses or ridges are sprayed on the bearings with orifice holes.

Masking shall be used to protect surfaces which are not to be coated. This masking can be done with adhesive-backed tape, shim stock metal shielding or any other appropriate method. Any orifices in the surface shall be plugged with suitable sized wire to prevent grit from penetrating these holes. Larger holes shall be protected with rubber plugs or other suitable material.

9.3 After abrasive blasting, and before chrome carbide coating or undercoating, all temperature sensitive masking materials shall be removed and replaced with metal shim stock or metal shields if these are required to protect finished surfaces. Any holes or orifices will be plugged with graphite or other suitable material to prevent bridging during the coating operation.

9.4 Dry, free-flowing coating and, where specified, undercoating shall be deposited on the designated surfaces in strict accordance with the vendor's process operation sheet.

The thickness of the deposited undercoating shall be .001/.002 inches, unless otherwise specified on the drawing. The thickness of the deposited chrome carbide shall be at least twice as thick as the final thickness of the coating after finish machining. When parts require grooves formed by the chrome carbide coating, the part shall have the undercoating applied before the grooving template is attached. The grooving template shall be mechanically attached to the part by means of a fixture so as to leave a clearance of .004/.006 between the template and the part. The side of the template from which the pattern was etched shall be placed against the part to be coated.

The temperature of the part being coated shall be maintained so as not to exceed 350 degrees F.

10.0 FINISH MACHINING OF COATINGS

The bearing surfaces shall be ground, and where necessary, lapped to drawing dimensions and tolerances. The surface finish shall be 8 RMS unless otherwise specified on the drawing. All sharp protruding edges of the coating shall be broken with a .020/.030 radius. It is extremely important that proper machining techniques be used to finish the coating. These techniques are described in "Finishing of Flame Plated Parts", copyright 1956 by Union Carbide Corporation and used by Linde Air Products Division.

11.0 BOND STRENGTH

A representative bond strength specimen, machined to the dimension shown in Figure 2 and prepared and tested in accordance with 11.1, 11.2, and 11.3, shall have a bond strength not less than that specified in Paragraph 5.0.

11.1 The portion of the test specimen which is to be coated shall be manufactured from the same material as the part which it represents. The mating part of the specimen may be manufactured from any suitable material. For identification purposes the mating part of the specimen shall be slotted on the 23/32 diameter.

11.2 The designated surface of the test specimen shall be prepared in accordance with Paragraphs 9.1 and 9.2, and coated and undercoated when specified, in accordance with Paragraph 9.4. The preparation and coating of the specimen and the parts which it represents shall be performed at the same time and with the same equipment and settings.

11.3 The coating shall be ground until the chrome carbide is .001/.003 inches thick. After grinding, the specimen shall be cleaned by vapor degreasing or by rinsing thoroughly in petroleum solvent and drying.

Join and align the test specimen to a clean, dry and grit blasted mating specimen, using Minnesota Mining and Manufacturing Epoxy Cement EC2186.

Care should be taken to avoid the entrapment of air bubbles. Excess adhesive shall be removed from the vicinity of the joint before curing in a circulating air oven for one hour at 350 F $\pm$ 20.

The specimens should be pulled on a tensile tested at a rate of .028 inches/minute.

If the bond fails to meet the minimum requirements because fracture occurs at the coating epoxy interface, the test shall be considered invalid and shall be repeated. When a control sample is tested (i.e., plain, prepared, uncoated specimens joined with epoxy cement), the bond strength shall not be less than 10,000 psi.

12.0 QUALITY

The coating, and when specified, the undercoating, shall be adherent to the base material and shall have a uniform surface free from blistering, spalling, chipping, flaking, cracking or other objectionable imperfections. The coating shall, when finished machined, clean up over the whole of the specified area to be coated when the finished coating thickness is .001/.003 inches. The finished surface of the coating shall be free from metallic or other inclusions foreign to the coating material.

13.0 CONTROL

Control of quality and control of shipments shall be in accordance with the latest issue of MTI Quality Control Manual or as otherwise directed.

14.0 TOLERANCES

The tolerances at the boundaries of the areas designated to be coated shall be defined on the drawing of the part. Tolerances on the thicknesses of the coating shall be as stated in the relevant paragraphs of this specification unless otherwise stated on the drawing of the part.

15.0 APPROVAL

15.1 Coating shall be performed only by sources approved by MTI Engineering Department.

15.2 Operation sheets covering all details of the coating process for each part shall be submitted by the vendor to MTI Engineering Department for approval. Figure 1 shows a typical operation sheet. Use of format shown in Figure 1 is not mandatory, provided all applicable information shown thereon is reported. Vendor may supplement operation sheets by use of sketches, marked drawings, or notes when necessary.

15.3 To assure adequate performance characteristics, vendor's methods of grinding and/or lapping coating (if grinding and/or lapping is performed) shall be approved by purchaser before parts for production use are supplied, unless such approval be waived.

15.4 Vendor shall use the same coating material, equipment, manufacturing procedures, processes, and methods of inspection for production parts as for approved sample parts. If it is found necessary to make any change which could unfavorably affect any characteristics of the coating, vendor shall submit revised operation sheets to MTI Engineering Department prior to incorporating such change.

16.0 REJECTIONS

Coated parts not conforming to this specification or to authorized modifications will be subject to rejection.

Issued by _____

Date _____

Revised _____

Date _____

Specification No. 34 (continued)

Approved by _____

FIGURE 1

PLASMA SPRAY PROCESS OPERATION SHEET

PART NO._____PART NAME_____PLASMA SPRAY COMPANY NAME_____

SPRAYING SCHEDULE NO._____ SHEET ____OF____SHEETS

SPRAY IN ACCORDANCE WITH MTI SPEC. 34.

GUN TYPE_____GUN MODEL NO._____

PREPARATION

METHOD OF CLEANING_____
MASKING INFORMATION_____
FIXTURING TYPE_____
GRIT TYPE AND SIZE_____ GRIT BLAST PSI_____
NOZZLE TO WORK DISTANCE_____

SPRAY EQUIPMENT SUPPLEMENTS

NOZZLE (ANODE) TYPE NO._____
NOZZLE (CATHODE) TYPE NO._____
TYPE OF GAS USED (1)_____
TYPE OF GAS USED (2)_____
NOZZLE ORIFICE SIZE_____

ARC GAS SETTINGS

REGULATOR (1) P.S.I._____ ± _____
REGULATOR (2) P.S.I._____ ± _____
CONSOLE P.S.I._____ ± _____
CONSOLE FLOW C.F.H.
GAS (1)_____
GAS (2)_____

POWER

VOLTAGE D.C. OPEN CIRCUIT___ ± ____
VOLTAGE D.C. OPERATING ____ ± _____
AMPERES D.C. OPERATING_____ ± _____
POWER CONTROL SETTING:
START____ ± ____RUN_____ ± _____

COATING MATERIAL

SPEC. NO._____

PART MATERIAL_____

TEST PIECE MATERIAL

CUP & BEND_____
BOND_____

POWDER FEEDER
TYPE_____MACHINE NO._____
TYPE OF CARRIER GAS_____
REGULATOR P.S.I._____ ± ____CONSOLE PSI__ ± __
FLOW CM__ ± __C.F.H.___ ± _____
VENTURI SETTING:
FLUSH___TURNS IN____ TURNS OUT_____
FEED WORM PITCH_____
R.P.M._____ ± _____ SPEED IND._____ ± ____
VIBRATOR ON____ OFF____ SETTING___ ± _____
FEEDER HOSE TO GUN:
DIAMETER I.D._____LENGTH_____

COATING DATA

POWDER INJECTION PORT
FRONT_____
REAR_____
GUN TO WORK DISTANCE IN. _____ ± _____
PART R.P.M._____ ± ____SURFACE FT./MIN.__ ± __
COATING THICKNESS
AS SPRAYED _____
AFTER FINISHING_____
PREHEAT TEMP_____
SPRAY TIME (PERCYCLE)_____ ± _____
COOL TIME (PER CYCLE)_____ ± _____
METHOD OF COOLING_____
AIR_____GAS_____
FORCED_____STATIC_____
TOTAL NO. OF CYCLES (SPRAY + COOL)_____

NOTES, SKETCHES, ETC.

Issued by _____

Date _____

Revised _____

Date _____

Approved by _____

Specification No. 34 (continued)

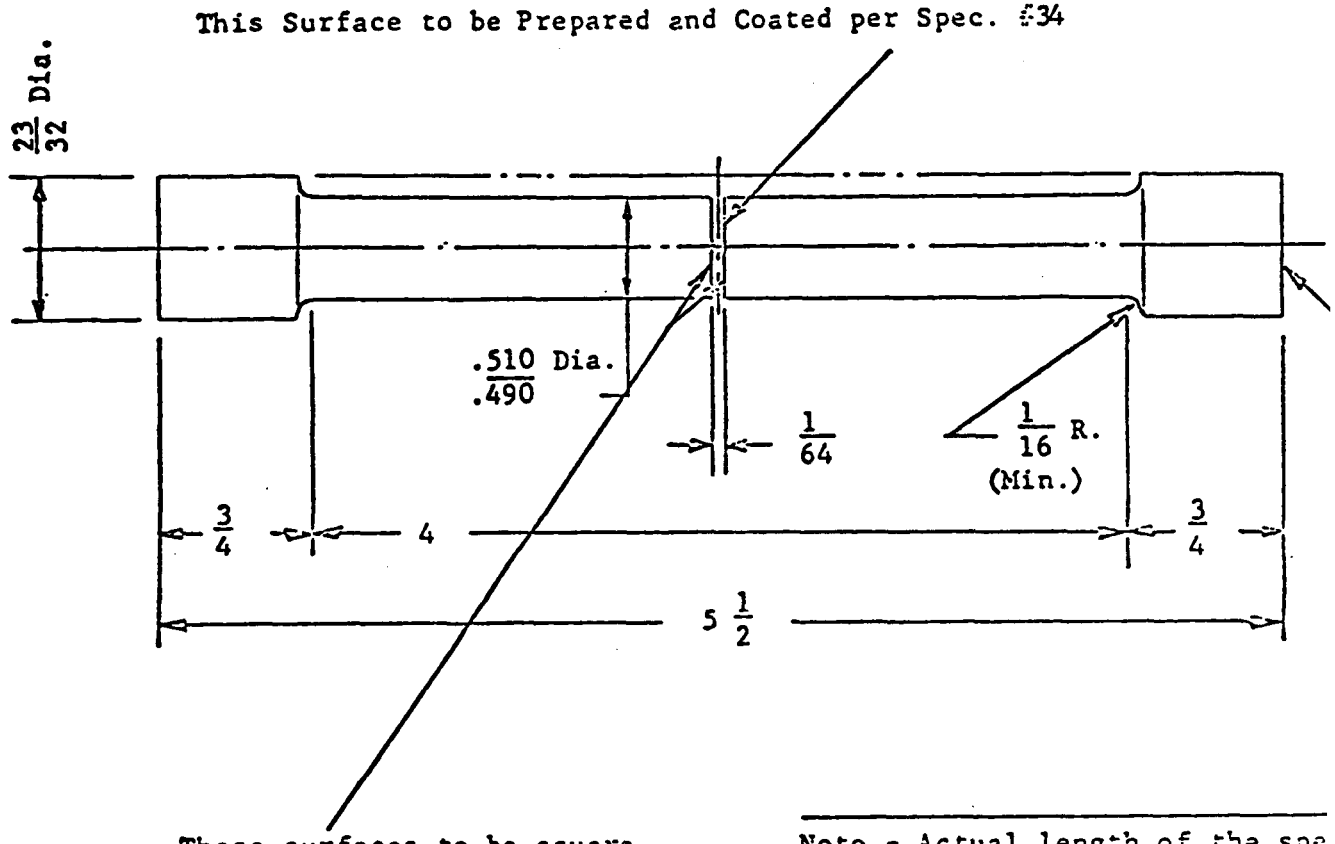

Note - Actual length of the spe
which is to be coated, t
measured within .0001 an
recorded on end of speci

Fig. 2 Bond Strength Specimen

ORIGINAL PAGE IS
OF POOR QUALITY